'Exploration of Self-Assembly in Short Peptides for the Development of Useful Functional Materials'

Submitted by

Payel Dowari

Registration No.: 166122039

Department of Chemistry
Indian Institute of Technology Guwahati
Guwahati, Assam-781039
India

A thesis submitted for the partial fulfilment of the requirements of the degree of

Doctor of Philosophy
In
Chemistry

IIT Guwahati, January, 2022

Declaration

I hereby declare that all the matters embodied in the thesis result from the experiments and investigations performed by me in the Department of Chemistry, Indian Institute of Technology, Guwahati, India, under the supervision of Prof. Debapratim Das. In keeping with the general practice of reporting scientific observations, due acknowledgements have been made wherever the work described is based on the findings of the other investigators.

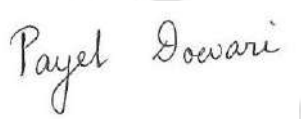

(**Payel Dowari**)

भारतीय प्रौद्योगिकी संस्थान गुवाहाटी

INDIAN INSTITUTE OF TECHNOLOGY GUWAHATI

Dr. Debapratim Das

Professor

Department of Chemistry

Ph: + 91 361 258 3301

Fax: + 91 361 258 2349

E-mail: ddas@iitg.ac.in

To Who It May Concern

This is to certify that the thesis entitled as 'Exploration of Self-Assembly in Short Peptides for the Development of Useful Functional Materials' submitted by Ms. Payel Dowari (Roll No. 166122039) for award of PhD degree to IIT Guwahati, is absolutely based on her own research work and that neither this thesis nor any part of it has been submitted for any degree/diploma or academic award anywhere.

(Prof. Debapratim Das)

Acknowledgements

The thesis is the last milestone of my PhD journey. Indeed, it is the most crucial academic documentation of my scientific activities. These endeavours only became prosperous by the immense support and encouragement from numerous people, including my lab mates, friends, family, and well-wishers. I hereby take the privilege to express my gratitude to one and all who had extended their helping hands several times to help in take a step closer to my destination.

To begin with, I would like to express my heartfelt gratitude to my supervisor, Prof. Debapratim Das, for giving me the opportunity to work under his supervision. His inspiration, guidance and scientific assistance has smoothened my journey throughout the time. Apart from being a successful academician and teacher, he is an amazing person to be with from whom I have gathered knowledge in many instances.

I was fortunate to have my doctoral committee members: Prof. Bhubaneswar Mandal (Chairperson), Prof. A.S. Achalkumar and Dr. Kalyan Raidongia to access my doctoral work time to time. At different periods, their helpful scientific suggestions and insightful thoughts have helped me in exploring the scientific ideas for my research.

It has been an absolute pleasure to work with my seniors, Dr. Sahnawaz Ahmed, Dr. Nilotpal Singha and Dr. Bapan Pramanik, who were the pillars of the lab during my initial years. I am also thankful to Dr. Shubhajit Ghosh and Dr. Tanur Sinha for their support and encouragement during their presence. A big thanks also goes to my batchmate, Mr. Basab Kanti Das for his enormous cooperation in various experiments. Besides seniors, I must mention my juniors especially, Mr. Saurav Das and Mr. Sumit Chowdhuri, Mr. Priyam Das, Ms. Tanushree Das, Mr. Malay Kumar Baroi and Ms. Ritvika Khushwaha for their timely assistances and scientific contributions in my projects. My special thanks also go to my friends Pranjal, Batie, Raktim, Anjali, Sachin and Doli for their generous help at different instances.

I would like to express my sincere thanks to our collaborators, Prof. Oren Scherman and Prof. Anindita Ukil for their assistance for my different projects.

I extend my sincere acknowledgements to all the members and technical staff of my department and C.I.F. for their direct or indirect help. I am immensely helpful to IIT Guwahati for providing the

doctoral fellowship with consistency and the opportunity to be a part of India's one of the finest educational institutes.

Last but not least, I have got ample motivation and assistance from my family members to focus on my research carrier entirely.

Abstract

The thesis on 'Exploration of Self-Assembly in Short Peptides for the Development of Useful Functional Materials' deals with the design of novel short peptides, studying their self-assembly behaviour with the different non-covalent interactions, and exploring their possible applications in the field of peptide-based functional materials.

Chapter 1 is a brief introduction on peptide-based nanomaterials and their various applications with sufficient literature review.

Chapter 2 describes the development of a thixotropic hydrogel using the self-aggregation of a peptide amphiphile.

Chapter 3 describes the successful utilization of the technique of peptide coassembly for the formulation of a functional peptide hydrogel for aiming localized drug-delivery through receptor mediated cellular internalization mechanisms.

Chapter 4 deals in development of a multi-stimuli responsive cross-linked peptide polymer using different cross-linking methodologies, for attaining size-tunability property and controlled cell-proliferation.

Chapter 5 deals in development of an artificial hydrolase. The work involves systematic design and immobilization of a hydrolase-like short peptide amphiphile on silica surfaces for enhancement of extent of catalysis, improvement of catalyst stability and increased stereoselectivity, compared to the micellar aggregates.

ABBREVIATIONS

1.	ECM:	Extracellular matrix
2.	Tyr (Y):	Tyrosine
3.	Phe (F):	Phenylalanine
4.	Gly (G):	Glycine
5.	Lys (K):	Lysine
6.	Cys (C):	Cysteine
7.	Arg (R):	Arginine
8.	Asp (D):	Aspartic acid
9.	Ser (S):	Serine
10.	Pro (P):	Proline
11.	Val (V):	Valine
12.	His (H):	Histidine
13.	Glu (E):	Glutamic acid
14.	HBTU:	N,N,N′,N′-Tetramethyl-O-(1H-benzotriazol-1-yl)uronium hexafluorophosphate
15.	DIPEA:	Diisopropyl ethylamine
16.	HRP:	Horseradish peroxidase
17.	TFA:	Trifluoroacetic acid
18.	TES:	Triethylsilane
19.	ACN:	Acetonitrile
20.	DMF:	Dimethyl formamide
21.	DMSO:	Dimethyl sulfoxide
22.	HPLC:	High Performance Liquid Chromatography
23.	DCM:	Dichloromethane
24.	DTT:	Dithiothreitol
25.	CD:	Circular dichroism
26.	DLS:	Dynamic light scattering
27.	BSA:	Bovine serum albumin
28.	FESEM:	Field Emission Scanning Electron Microscopy
29.	FETEM:	Field Emission Transmission Electron Microscopy
30.	GABA:	γ-Amino butyric acid
31.	PA:	Peptide amphiphile
32.	NMR:	Nuclear Magnetic Resonance
33.	FTIR:	Fourier Transform Infrared Spectroscopy
34.	CMC:	Critical micellar concentration
35.	$PhSiH_3$:	Phenylsilane
36.	BET:	Brunauer–Emmett–Teller
37.	TEOS:	Tetraethyl orthosilicate
38.	APTES:	3-Aminopropyltriethoxysilane
39.	5Acl:	Dipentaerythritol hexaacrylate
40.	SiNP:	Silica nanoparticles
41.	MGC:	Minimum gelation concentration
42.	TGA:	Thermogravimetric analysis
43.	PNP:	p-Nitrophenol
44.	PNPA:	p-Nitrophenyl acetate
45.	PNPP:	p-Nitrophenyl propionate

46.	PNPB:	p-Nitrophenyl butanoate
47.	PNPH:	p-Nitrophenyl hexanoate
48.	GDL:	Gluconolactone
49.	HFIP:	Hexafluoro-2-propanol
50.	NaOD:	Sodium deuteroxide
51.	FRET:	Förster Resonance Energy Transfer
52.	NaOMe:	Sodium methoxide
53.	TLC:	Thin layer chromatography
54.	NaOH:	Sodium hydroxide
55.	NOESY:	Nuclear Overhauser Effect Spectroscopy
56.	MALDI:	Matrix-assisted Laser Desorption Ionization
57.	UV-Vis:	Ultraviolet-Visible spectroscopy
58.	FI:	Fluorescence spectroscopy
59.	LVR:	Linear viscosity region
60.	Nap:	Naphthalene
61.	G':	Storge modulus
62.	G":	Loss modulus
63.	CV lipase:	Chromobacterium viscosum lipase
64.	MeOH:	Methanol
65.	EtOH:	Ethanol
66.	TOF:	Time of flight
67.	AFM:	Atomic force microscopy
68.	wt. %:	(Wieght/Volume) %
69.	RPMI:	Roswell Park Memorial Institute (cell-culture media)
70.	HCl:	Hydrochloric acid
71.	Ac_2O:	Acetic anhydride
72.	Na_2SO_4:	Sodium sulfate
73.	Boc_2O:	Di-tert-butyl dicarbonate
74.	CB[8]:	Cucurbit[8]uril
75.	ITC:	Isothermal titration calorimetry
76.	DAPI:	4',6-diamidino-2-phenylindole
77.	HEPES:	4-(2-hydroxyethyl)-1-piperazineethanesulfonic acid

CONTENTS **Page Nos.**

Chapter 1: Introduction

1.1 Prelude

'Molecular self-assembly', as the name suggests, is the well-defined organization of molecules to form well-defined structures without any external assistance. Self-assembly phenomenon is an equilibrium driven process which arranges components spontaneously, balancing between enthalpic and entropic interactions, to develop thermodynamically stable (or metastable) molecular architectures. Nature has performed countless iterations with its primitive components through self-assembly to evolve with fascinating complex systems with central importance. A living cell is an example of highest level of its sophistication. Formation of lipid-membranes, genetic materials, vesicles, organelles, proteins, ion-pumps and an ocean of useful molecular nanomachines have resulted from repeated selection and evolution of molecular components.

Self-assembly can be of two types: static and dynamic. As we know that assembly mechanism is an exothermic process, that is, the components spontaneously organize to attain energetically stable structures. Such assembly is called 'static' assembly. However, some assembly pathways are endothermic and needs energy ingestion. Such systems form metastable intermediate which dissipates energy to form more stable structures. Therefore, such systems have the potential of self-modification and during its course, provides energy to another up-hill reaction in a series cascade, hence the name 'living polymerization' or dynamic self-assembly. Static assembly is unquestionably important in various material applications, but major functioning systems are mostly based on the dynamic, out-of-equilibrium systems. A living cell, for example, uses static assembly to construct lipid bilayers to attain a well-defined shape and rigidity. On the other hand, it uses dynamic assembly to perform all the functions that keep the cell living. With scrutiny, it can be found that enzymatic cascades, oscillating reactions uses out-of-equilibrium assembly. Self-assembly is the best available strategy to design and construct artificial nanomachineries sidestepping critical synthetic reaction methodologies and harsh reaction conditions. It uses non-covalent interactions which are reversible under simple chemical and physical stimulations, like thermal, mechanical, chemical, electrical stimuli. Such stimuli-responsive nanomaterials have become immensely useful in modern applications. Supramolecular structures can be formed from various types of components, organic, inorganic and their combinations.

1.2 Peptide self-assembly

Study of peptide self-assembly has been a major focus of modern research in biological and medical concerns. The surge for finding novel and unique peptide building blocks was initiated

with the first serendipitous discovery of self-assembling short peptide sequence, EAK16 in 1990s.[1] Naturally occurring proteins vividly portray the role of different peptide secondary interactions to govern the structural and functional character of the proteins. Protein sequences are an outcome of eons of evolution, but it is nowadays universally accepted that all proteins can be made to form β-sheet amyloids under certain chemical constrains. In-fact, diseases like Alzheimer's, Type II diabetes, and human calcitonin hormone linked to medullary thyroid carcinoma are all results of protein amyloid formations. Therefore, a de-structured protein may cause diseases resulting from protein misfolding. In modern days, proteins also utilize intramolecular folded β-strands which could mimic molecular architectures of intra-strand β-sheets formed by ancient short peptides. Therefore, it is necessary to understand the underlying mechanisms driving to peptide self-assembly. To this end, examination of short peptides and their assembly have become a key to unveil the complex biological systems.[2, 3] Research in the field of peptide self-assembly has undergone huge progress in the past few decades. From numerous reports, it is evident that peptides can form a wide variance of morphologies and complex nano-architectures by combination of non-covalent interactions.[4] However, it is of anticipation that ancestral peptides were simple-structured and formed unadorned simpler morphologies rather than complex ones.[5] Most knowledge of peptide self-assembly at the molecular level is accomplished from microscopic structure information established from protein amyloids. Due to their biocompatibility, structural and functional diversity, peptide-based materials find extensive use in biomedicine, biomarkers and biosensors, drug-delivery, and tissue-engineering. Peptide self-assembly leads to various morphologies like micelles, vesicles, sheets, fibres, rods, and tubes, and cross-linked polymers. Sometimes these morphologies undergo hierarchical assembly process to form hydrogels. Reckoning to the diverse morphologies of peptides, scientists developed versatile building blocks, like dipeptides, amphiphilic peptides, ionic peptides, cyclic peptides, block co-polypeptides, aromatic peptides, peptide coassemblies, and peptide-heterosystem conjugates to modulate the self-assembly for divergent material applications.

1.2.1 Driving forces for self-assembly

Supramolecular self-assembly is the most confident road that connects the pool of monomers to the diverse realms of complex materials. The pillar of self-assembly stands on weak non-covalent associations. Electrostatic interactions, hydrophobic interactions, π-π interactions, hydrogen bonding, ion coordination, host-guest interactions, charge-transfer interactions and van der

Waals' interactions are the recognized weak interactions known to hold fast the supramolecular architectures, as summarized in Figure 1.1.

In relevance to peptide assembly, electrostatic interactions involve both attractive and repulsive forces between charged residues from amino acids. Solvent interactions play a vital role in tuning the nature and extent of electrostatic interactions which holds crucial in the self-assembly mechanisms. For example, positive amino acid residues decorated on the surface of self-assembled peptide fibres were utilized to bind sulphonates of Alexa-488 dye which helped in super resolution imaging of supramolecular structures.[6]

Hydrophobic interaction is one of the most important factors leading to association and aggregation, mainly in aqueous or hydrophilic environments. Self-assembled materials arising from hydrophobic interactions, especially amphiphilic molecules build a hydrophobic core allow entrapment of organic drugs, yet keeping the whole system water soluble. Sometimes, colocalization of hydrophobic components within hydrophobic compartments allow organic reactions to be carried out in aqueous medium. Amphiphilic systems are therefore very important for persistence of hydrophobic entities in hydrophilic milieu.[7] The self-assembly of amphiphilic peptides could be readily accomplished through microphase separation driven by thermodynamics because of the coexistence of polar and nonpolar regions inside the peptide sequences. For example, the cationic lipidated peptides which assemble into micellar structures in aqueous conditions show antibacterial activities.[8]

The organization of aromatic residues in hydrophobic interactions is less organized than in π-π stacking interactions. The π-π stacking can drive directional assembly in peptides containing aromatic residues. π-π interactions can give rise to more robust self-assembly in water because of limited aqueous solubility, and in organic solvents like toluene and TFA. The dipeptide, FF is a classic example of assembly due to π-π interactions which generates diverse spectra of nanostructures utilized in different applications.[9] A cut-short peptide segment from a protein sometimes fails to conserve its secondary structure in absence of the restrictions imparted by the protein. An added aromatic-aromatic interaction can organize the molecules and provide a protein-like restrictive environment to reconstruct the secondary motif of the peptide segment.[10]

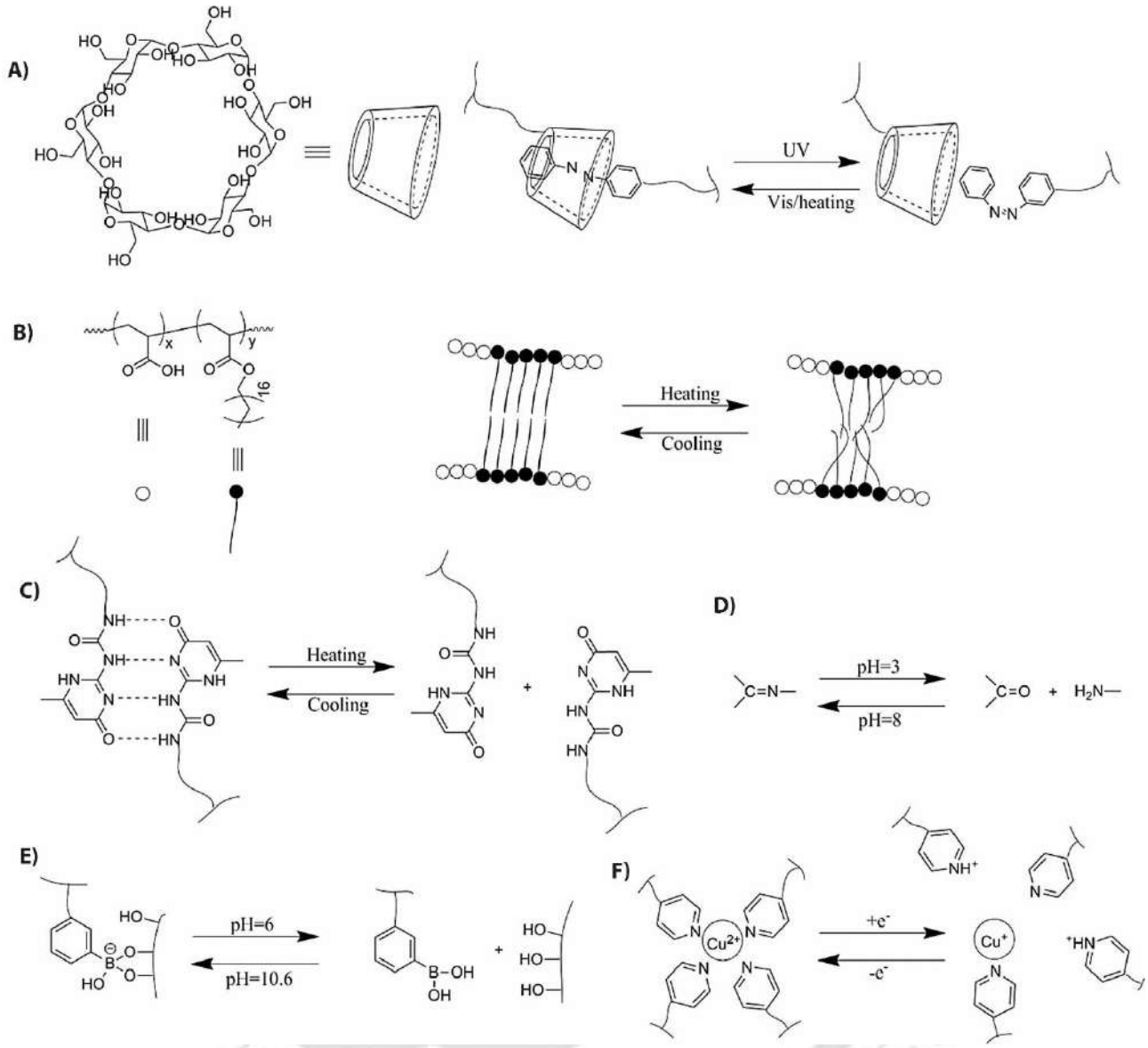

Figure 1.1 Various supramolecular interactions. Pictorial representation of (A) Host-guest interactions, and (B) Hydrophobic interactions, (C) Hydrogen-bonding interactions, (D), (E) Dynamic covalent bonding, and (F) Chelate complex formation.[11]

Hydrogen-bonding is a widely occurring phenomena in peptides and proteins which form secondary conformations for peptide stability and protein folding. Hydrogen bond is an attractive force acting between a hydrogen atom (connected to an electronegative atom; the donor centre) and another electronegative atom with free electron pairs (hydrogen bond acceptor centre). Hydrogen-bonding is omnipresent in peptide assembly. In peptide self-assembly, hydrogen bonding assists in creating a hydrophilic environment within molecules and with water to stabilize the assembly.[12] For example, molecular arrangement in cyclic peptides lead to directional hydrogen bonding to form nanotubes which are applicable as transport channels.[13] A triblock polypeptide containing two terminal hydroxyproline PPII helical sequences connected with a

central uncharged hydrophilic serine-leucine stretch formed linear aggregation due to backbone hydrogen bonding to form pH and ionic strength dependent hydrogel.[14] Some important secondary conformations attained by peptides are shown in Figure 1.2.

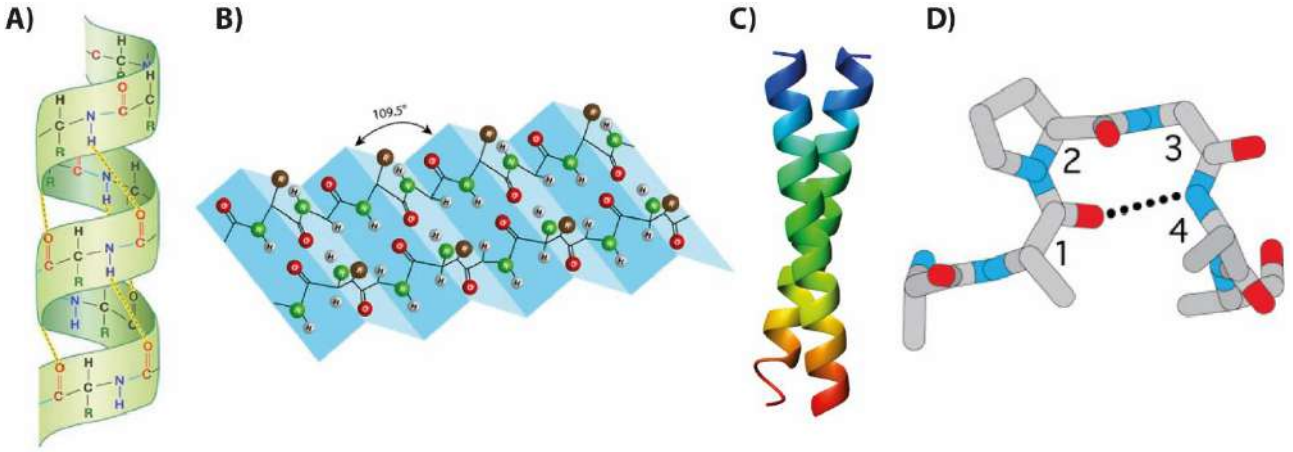

Figure 1.2 Peptide secondary structures. Diagrammatic representations of (A) α-helix, (B) β-sheet, (C) Coiled-coil, and (D) β-turn.

Host-guest chemistry is another important and well recognized non-bonding interaction popular in the area of synthetic soft materials. Host is a macrocyclic organic molecule that affords a hollow cavity with a distinct dimension. Guests are small organic molecules, portions of a molecule or ions which get incorporated within the guest cavity by the aid of electrostatic attractions or hydrophobic interactions. Pictorial representation of some hosts, guests and a common host-guest complex is shown in Figure 1.3. Calixarenes, cyclodextrins and cucurbiturils are the most widespread hosts under scrutiny. Water soluble hosts (cyclodextrins and cucurbiturils) are much extensively applied in biological purposes.[15] By the help of host-guest complexation, two different molecules, or distant segments within a same molecular entity can be brought in close proximity to behave as a single unit. This allows a specific organized state. Applying a stimulus (like strain, or another guest molecule) can break the supramolecular system to revert to a different organized state. Therefore, this concept is widely used to develop stimuli-responsive functional materials.[16] Host cavities can act as a haven for hydrophobic drugs facilitating its easy delivery. Confinement of chromophore molecules within host cavities exhibit differential photophysical properties than the unbound state. This concept is used for sensing purposes, disease diagnosis and therapy.[17]

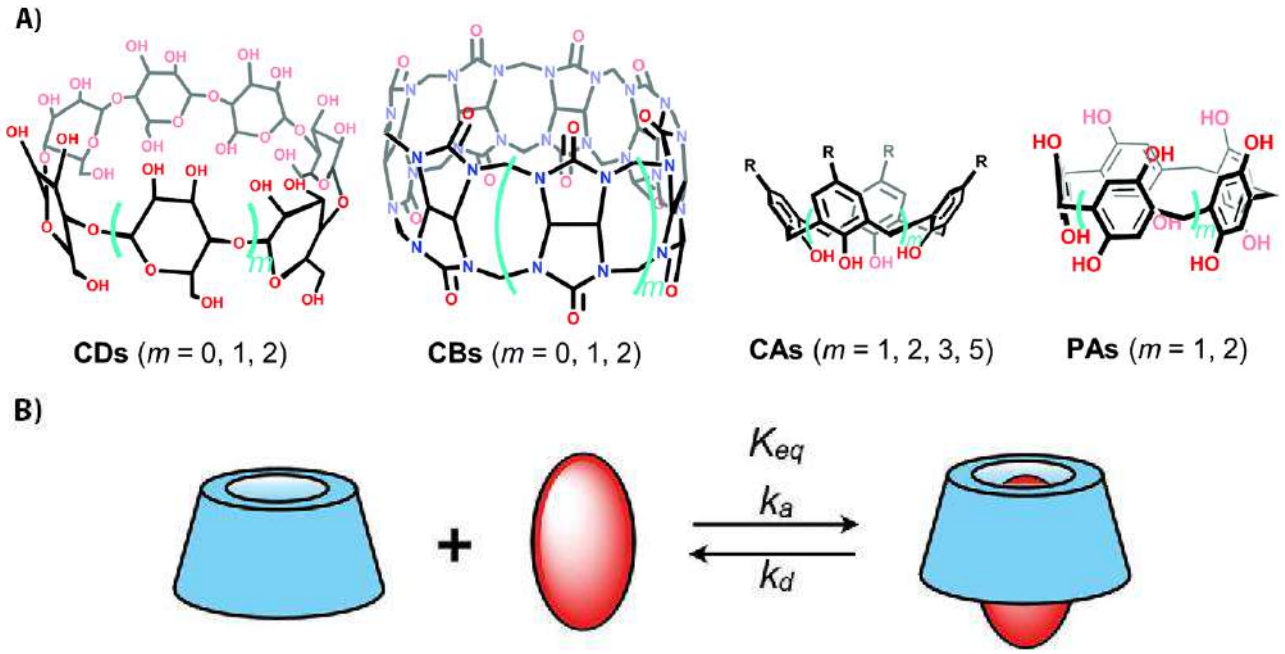

Figure 1.3 (A) Molecular structures of different supramolecular hosts, and (B) Pictorial representation of a supramolecular host-guest complex.

1.3 Peptide-based soft materials

Nanomaterials have captivated the technology world with its varied usances. Richard Feynman has rightly said in his remarkable speech in 1959, "There's plenty of room at the bottoms". Every material to be shaped is determined by the selected components and the associated environmental co-factors. Also, a set of components can form various end-products depending on the different synthetic processing set for their formation. Self-assembly can yield materials extended in any dimensions, 0D, 1D, 2D and 3D. Over the past few decades, extensive research has been devoted to the fabrication and development of nano biomaterials through exploration of peptide self-assembly. Development of peptide-based soft materials have grown enormously due to its low fabrication cost, biocompatibility, functional diversity and tunability and varied applications.[18-23] are developed by scrupulous engineering of monomer peptide building blocks which undergo spontaneous self-assembly coordinated by various non-covalent interactions: hydrogen bonding,[24-26] hydrophobic interactions,[27, 28] π-π interactions,[29] ionic interactions and van-der Waals' interactions are a few instances.

1.3.1 Peptide hydrogels

Peptide hydrogels are shaped from the 3D entanglement of fibres to form a hydrophilic network which can arrest the whole aqueous solvent within the self-assembled structure. The fact that hydrogels can restrict bulk solvent has been exploited for drug entrapment, controlled drug-

release applications, cellular entrapment and tissue engineering platforms. The self-assembled fibres are obtained through constructive supramolecular associations like α-helices, β-sheets, coiled-coils, vesicles, micelles, ribbons, tapes and tubes.[30-33] These sub-morphologies undergo reorganization and/or hierarchical supramolecular associations under various chemical and physical conditions to form fibrous structures to build the resultant gel framework.[34, 35] Short peptide hydrogels have earned attention of researchers because of their simplistic synthetic protocols, uncomplicated functionalization techniques and excellent tunability properties. Design and research of peptide hydrogels comprise hydrogelators which fall under the following major categories: peptide amphiphiles, ultrashort peptides, coassembled peptidic systems. The trigger for hydrogel formation can be set through various parameters, like pH, temperature, mechanical forces, redox properties, light, ultrasound, addition of salts, addition of metal ions, enzymatic reaction or a chemical reaction.[1, 34, 36] An important functional aspect that is necessary in development of soft materials is stimuli-responsiveness. Smart hydrogels are produced by structural modulations of the designed hydrogelators where hydrogel properties can be tuned as a function of various stimuli.

1.3.1.1 Hydrogels from peptide amphiphiles

The process of self-assembly in peptide amphiphiles is based on congregative effect of three structural domains: hydrophobic segment that induces the self-association in aqueous medium, charged amino acids for efficient water solubility and a peptide backbone for intermolecular hydrogen-bonding. Amphiphilic peptides are constructed through a distinct amphipathic arrangement of hydrophobic and hydrophilic amino acids. Schneider et al. reported a series of peptide hydrogelators based on valine and lysine residues where the polar and apolar amino acids were arranged in an alternative fashion along the length of the peptide sequence. Two such amphiphilic segments were connected with a central D-pro L-pro dyad. Inter-segment hydrogen bonding and hydrophobic interactions between the valine residues forms a stable secondary β-hairpin structure. In basic pH, lysine residues participate in inter-strand hydrogen bonding to form a β-sheet structure which results in formation of a pH-responsive hydrogel.[37, 38] Another type of amphiphilic peptides were studied by Deming where a stretch of hydrophobic amino acids, like $(val)_n$, $(leu)_n$ were attached to a stretch of polyelectrolyte forming hydrophilic amino acid sequences, $(glu)_n$ or $(lys)_n$ formed crystalline β-sheets and α-helices respectively.[39, 40] Metal induced synthesis helped in control of polypeptide chain length and these block polypeptides

formed thermostable hydrogels at concentrations above 0.25 wt. % in deionized water. Helicity induced gelation made these peptides unique in the fact that aggregation and material properties could be tuned by controlling the polypeptide sequence without much effect on the gelation concentrations. Hydrophilic-lipophilic balance (HLB) was found to be crucial factor for self-assembly. Change in length of hydrophilic stretch did not affect the assembly behaviour whereas decrease in the hydrophobic segment hindered the polypeptides to attain aggregating structures. These gels recovered 80-90% of mechanical strength within 10 s, and were also stable in presence or absence of salts. These hydrogels could be used as tissue regeneration scaffolds.[41]

Zhang's group has investigated another class of ionic self-complementary peptides termed 'molecular lego'. Study of such systems began with the discovery of Z-DNA binding protein which contains a 16-aa sequence AEAEAKAKAEAEAKAK (EAK16). This peptide forms membrane-like structures. Self-assembly into nanofibrils and hierarchical nanofiber formation occurs when the total charge of the peptides reaches zero. This is determined by the ionic strength and pH of the solution. Another designed peptide RADARADARADARADA (RADA16-I) showed similar properties with charge distribution +-+-+-. Hydrogel derived from a variant, RARADADARARADADA (RADA16-II) with charge distribution of ++--++-- was found to entrap >99.5% of water. This peptide projects reassembly properties from α to β structures and have been used in tissue repair and regenerative medicine.[42]

Design of lipid chain conjugated peptides have been acquired from the natural membrane proteins like the post-translational modified Ras-superfamily proteins. Usually, the signal transduction proteins have been modified by biological processes to get adhered to the cellular membranes for proper functioning.[43] These peptides can be composed of a lipid chain attached to a single amino acid or a stretch of di- or tripeptides to constitute the polar head group. These type of amphiphiles form micelles or bilayer structure in a concentration dependent fashion. At a higher concentration, these morphologies form the basis of hierarchical aggregations to form nanofibers. Stupp and co-workers have showcased a classic example of a peptide amphiphile which contains five different functional domains. A N-terminal alkyl chain segment for hydrophobic interactions, connected with a central short cysteine stretch for redox assisted self-assembly. A phosphorylated serine was associated in calcium mineralization, whereas a cell-adhering segment manifested the functional cross-linked peptide hydrogel as a mimic for collagen fibres in bone.[44]. Length of alkyl chain plays an important role in tuning the rigidity of the nanoassemblies. For example, surface-binding of heme was accelerated in case of kinetically

trapped rigid fibres formed by long chain lipidated peptide, compared to thin and dynamic fibres of shorter chain lipidated peptide.[45] Amino acid sequence in constitutional isomers of a peptide directs the type of articulated 1D-nanostructures. Actually, the interactions occurring at a molecular level are reflected in the macroscopic architechture.[46] A novel peptide amphiphile C_{16}KTTβAH, which was derived from 'matrixyl' lipopeptides C_{16}KTTKS, containing the bioactive β-alanine-histidine dipeptide segment was found to form long tapes and hydrogels in different aqueous media. Change in concentration and nature of the aqueous media allowed room for hydrogel strength modulations. These hydrogels express exceptional stiffness compared to previously reported β-sheet peptide-based materials (**Figure 1.4**).[47]

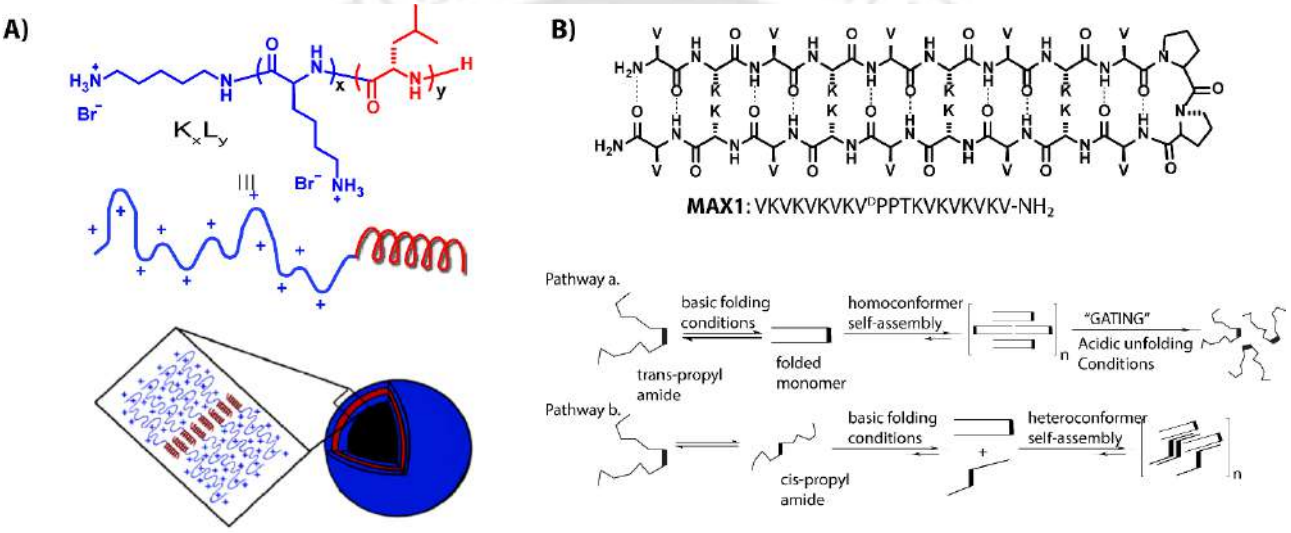

Figure 1.4 (A) Schematic drawing showing proposed self-assembly of $K_{60}L_{20}$ into vesicles, and (B) Sequence and proposed β-hairpin structure of MAX1. Valine at position 9 strongly enforces a *trans*-prolyl amide bond geometry favouring hairpin formation prior to self-assembly (pathway a). A cis geometry undergoes mixed self-assembly with correctly folded hairpins (pathway b).

1.3.1.2 Ultrashort peptide hydrogels

The smallest peptide hydrogel ever reported is a cinnamoyl protected phenylalanine. Xu and co-workers have further investigated the gelation of Fmoc-protected single amino acids. All these hydrogelators were triggered by basification to form hydrogels.[48] Janmey *et al.* first noticed that Fmoc-derivatives of some dipeptides formed hydrogels. The key driving force for hydrogelation was aromatic interactions.[49] Later, Gazit *et al.* had done extensive research in diphenylalanine peptide hydrogelators, where π-π interactions of phenylalanine residues and hydrogen-bonding of the amide backbone was held responsible for self-assembly.[50] Fmoc-Phe-Phe-OH formed very rigid hydrogels and therefore it has been extensively applied in technological applications.[51] Recently, ultrashort peptides are emerging as a cost-effective cell-culture scaffolds. FFV sequence

is one of such sequences. The problem is that stability of all L-peptide falls at stake with proteases, and all-D peptide does not allow cell growth. However, a peptide with mixed D- and L-amino acids was found to allow cell culture on the generated hydrogel matrix structure.[52] Ulijn and co-workers have reported many Fmoc-protected dipeptide hydrogelators. Adams and co-workers have studied a series of naphthalene containing dipeptides for hydrogelation.[53] Similarly, Banerjee et al. have reported some tripeptide hydrogels portraying various useful applications.[54] Another important area of short peptide hydrogel research is derived from the amyloid fibrils. Investigation of amyloid self-assembly behaviour is of pathological relevance and hence amyloid peptides based soft materials are used in nanomedicines. 'KLVFF' has been screened as the smallest assembling unit from the full amyloid protein.[55] These are known to form β-sheet fibrils resulting in hydrogels at higher concentrations.[56] Many variants of this mother sequence have been reported by different research groups which has been of enormous assistance in understanding the basis of self-assembly and design of smart materials with significant applications.[57] In the search of the minimalistic building block that self-assembles to form ordered structures, several metabolites, including amino acids and nucleic bases were found to form fibrillar "amyloid-like" assemblies.[58] Phenylalanine monomers were shown to assemble into amyloid-like fibrils and self-healing hydrogels with extremely high storage moduli, unusual for non-covalent self-assembled hydrogels.[59,60] Due to simplicity of the building blocks, these materials are used in the biomaterial industry. An unusual water insoluble property of a pyrene conjugated Lys-Cys dipeptide hydrogel was serendipitously observed. The π-π stacking between the pyrene groups led to formation of densely entangled nanofibrous structures. The strong propensity of stacking and dense entangled fibres led to blockage of solvent passage in and out of the network. Strong peptide denaturing agents like concentrated hydrochloric acid or urea could do no good to gel dissolution. This unique gel was then used for specific enzyme storage purposes at ambient conditions.[61] Recently, Hauser's group has introduced a N-acyl-IVFK peptide which forms nanofibrous hydrogel with ECM -resembling network structure.[62] Another series of N-acyl and C-terminal lysine containing self-assembling peptides were designed where, the hexapeptide, Ac-ILVAGK-NH_2 formed a stable, nanofibrous 3D hydrogels with stiffness as high as 40 kPa. These hydrogels were capable of 3D cell-culture of human stem cells.[63] Naphthalene conjugated ultrashort cationic self-assembled peptides are emerging as a new class of innovative and cost-effective strategy to form antibacterial nanomaterials for their potent antimicrobial activities.[64,65] Chemical structures of some ultrashort peptide hydrogelators are enumerated in Figure 1.5.

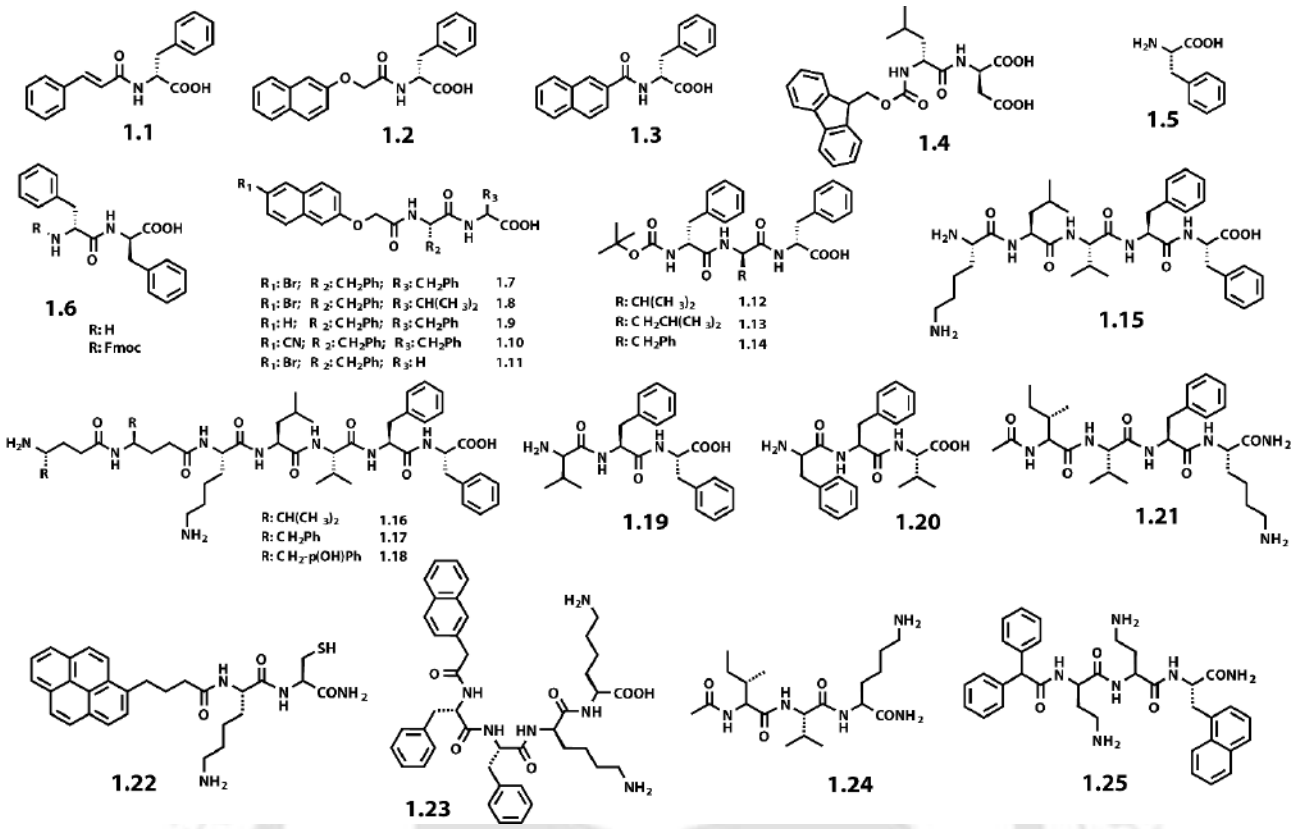

Figure 1.5 Chemical structures of some ultrashort peptide hydrogelators.

1.3.1.3 Coassembled peptide hydrogels

The concept of coassembly permit blending of different functional characteristics within a single system which makes them smarter soft materials. The idea of supramolecular coassembly is an extremely effective tool in the present scenario where mankind is in need of advanced solutions for complex problems, but in a simple process. Therefore, this added benefit is being extensively exploited in different routes to design advanced functional soft materials.[66] For example, multicomponent systems bypass the synthetic challenges for specific functionalisation. Composite systems are often preferred over single systems to increase the robustness and applicability of the soft material. In many instances, coassembly techniques have been used to incorporate the drug and cargo inside the gel network during the course of hydrogelation and hence the efficiency of the drug-delivery system is enhanced.[67, 68] Ulijn et al. have investigated the orthogonal coassembly of serine surfactants and diphenylalanine hydrogelators. Herein, the gelation behaviour of the singular systems is not affected, except for the additional emergent property in the coassembled system.[69] The same group have reported a library of charge-transfer induced coassembled hydrogel with combination of an electron acceptor containing amino acid hydrogelator with an electron donor molecule (Figure 1.6).[70]

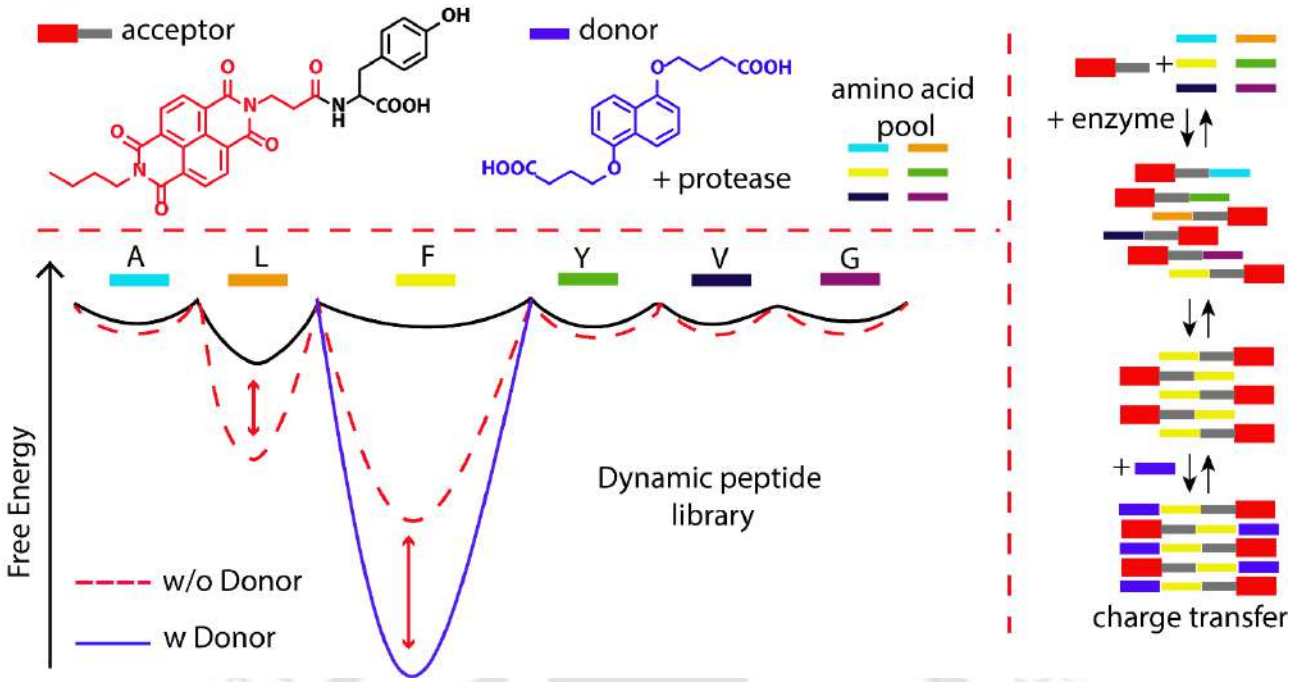

Figure 1.6 A combinatorial peptide library of charge-transfer induced coassembled hydrogel with combination of an electron acceptor containing amino acid hydrogelator with an electron donor molecule.

Zhang and co-workers have reported the electrostatic interaction triggered coassembled hydrogelation of a monocationic and dicationic peptide. The single peptides, Fmoc-VRGDV and Fmoc-KKRGDK formed hydrogels in acidic and basic pH respectively. A mixed hydrogel of the two peptides formed hydrogels at neutral pH.[71] An important side of peptide coassembly has been lit up by Lynn's group. Two oppositely charged amino acids were attached to the N-terminal of a β-sheet forming peptide sequence, LVFFAL to create two new peptides. The coassembly of these two peptides form stacks of antiparallel β-sheet layers with precisely patterned charged lattices stabilizing the bilayer leaflet interface. The resultant nanotubes behave like an asymmetric bilayer with oppositely charged surfaces on the inner and outer wall of the tubes.[72] Similarly, Nisbet *et al.* investigated the coassembly and hydrogelation two short Fmoc-derivatized peptides in which the assembly motif was modified with either RGD or IKVAV sequences. Both the peptide sequences are well-known components of mammalian extracellular matrix (ECM). The multicomponent hydrogel of Fmoc-FRGDF and Fmoc-DIKVAV was mechanically stronger than either of the single component gels. Apart from this, the multicomponent hydrogel synergistically improved efficacy of *in vitro* growth and viability of C212 myoblast cells, compared to singular self-assembled gels or the one with preassembled fibres of the single component systems.[73] Peptide surfactants C_4-Bhc-EE-NH_2 and C_{14}-FKK-NH_2 mixtures were found to form coassembled hydrogels with varied molecular assembly mechanisms and macroscopic properties.[74]

Abramovich and co-workers reported a collagen-inspired helical peptide coassembled hydrogel. It is known that a-helical conformation is attained with not less than 3-10 amino acid sequence. However, a single unit of collagen in its protected form, Fmoc-Gly-Pro-Hyp formed collagen-like helical patterns. When mixed with known hydrogelator, Fmoc-Phe-Phe, the composite system formed stronger hydrogels with polyproline-II conformation. Therefore, the composite hydrogel was found to have inherited properties of both the single systems (Figure 1.7).[75]

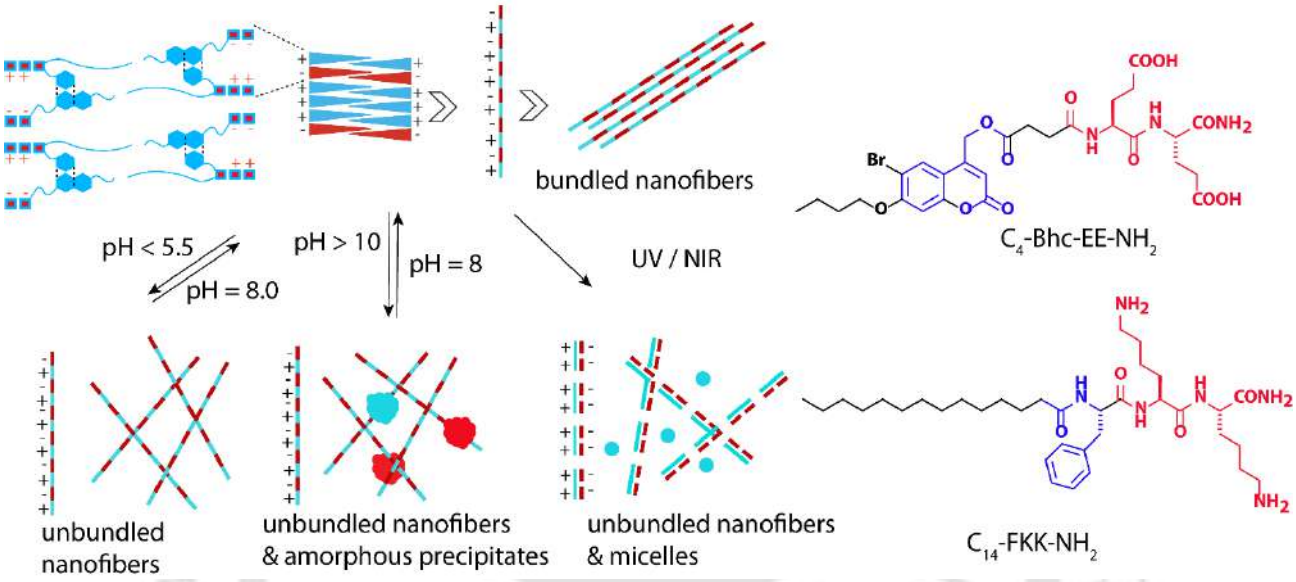

Figure 1.7 Various macroscopic properties depicted from coassembly of two peptides under various conditions.

1.3.2 Peptide-based supramolecular polymers

Supramolecular polymers are a resultant of polymeric arrays of monomeric units with the aid of directional non-covalent interactions to generate distinct structural entities performing specific functions. The characteristics of the polymers rely on the structural signature of the monomers and the nature of the interactions. Naturally occurring peptide based supramolecular polymers are collagen, amyloid fibrils, actin filaments, microtubules and viral protein polymers. The growth of polymers can occur either in unidirectional or multidirectional pathway. Linear polymers are obtained when the monomers arrange themselves in an axis perpendicular to the long axis of the monomer giving rise to fibrils or microtubules. Cross-linked polymers are obtained when the monomeric system contains more than nodes for one similar or dissimilar secondary interactions. Both types of peptide polymers have found profound applications in dedicated fields.

1.3.2.1 Linear polymers

Otto and his group have reported a series of self-synthesizing macrocycles based on dynamic covalent chemistry of disulphides. A dithiol-based β-sheet functionalized peptide, GLKLK, could

reversibly assemble and disassemble to form an equilibrating mixture of disulphide-linked macrocycles under oxidising conditions, known as the dynamic combinatorial library (DCL). The equilibrium could be shifted by using specific templates which increases the affinity of a definite sized macrocycle. Later, they proved that the library could be shifted even when thermodynamics prefer self-assembly of one macrocycle over the others. The resultant of this chemistry is formation of elongated microtubules containing repeating units of the 6mer macrocycle through peptide β-sheet secondary interactions.[76] Stupp and co-workers have designed peptide amphiphiles that form long fibres due to hydrophobic interactions of alkyl chains and hydrogen bonding interactions of the peptide segments. These molecules often yield in uncontrolled polymerization.[77] Hartgerink and his group have designed a family of triblock A-B-A oligopeptide, where A blocks were oligolysines and B blocks contained alternate glutamine-leucine stretches capable of β-sheet formation. Supramolecular polymerization in this case followed a competing mechanism between attractive interactions of the β-sheet segments and the electrostatic repulsions from the oligolysine stretches at a particular ionic strength and pH. Due to 'molecular frustration', peptides yielded finite sized nanofibers.[78] Tovar and his group have developed electronically active peptide coassembly. DFAA flanked 1,4-distyrylbenzene (OPV3), HODFAA-OPV3-AAFD-OH and quaterthiophene (4T), HODFAA-4T-AAFD-OH were soluble in basic pH. In acidic pH, the peptide segments formed b-sheets and hence led to coassembly to form long fibres. By CD Spectroscopy, UV-Vis Spectroscopy, and transient photoluminescence studies, coassembly and FRET phenomena was confirmed. These types of systems were utilized in developing supramolecular bioorganic optoelectronic materials (Figure 1.8).[79, 80]

Host-guest complexation chemistry is another interesting mode of secondary interaction which is recently been explored for developing stimuli-responsive and biologically active soft materials.[81, 82] Cyclodextrins and cucurbiturils are two important families of macrocyclic hosts that has been extensively exploited in articulation of biopolymers because of their water solubility and biocompatibility. has also been utilized in this regard to form linear supramolecular polymerization by end-to-end binding. Having known this, host-guest chemistry has been scarcely exploited in regard to supramolecular peptide polymers.

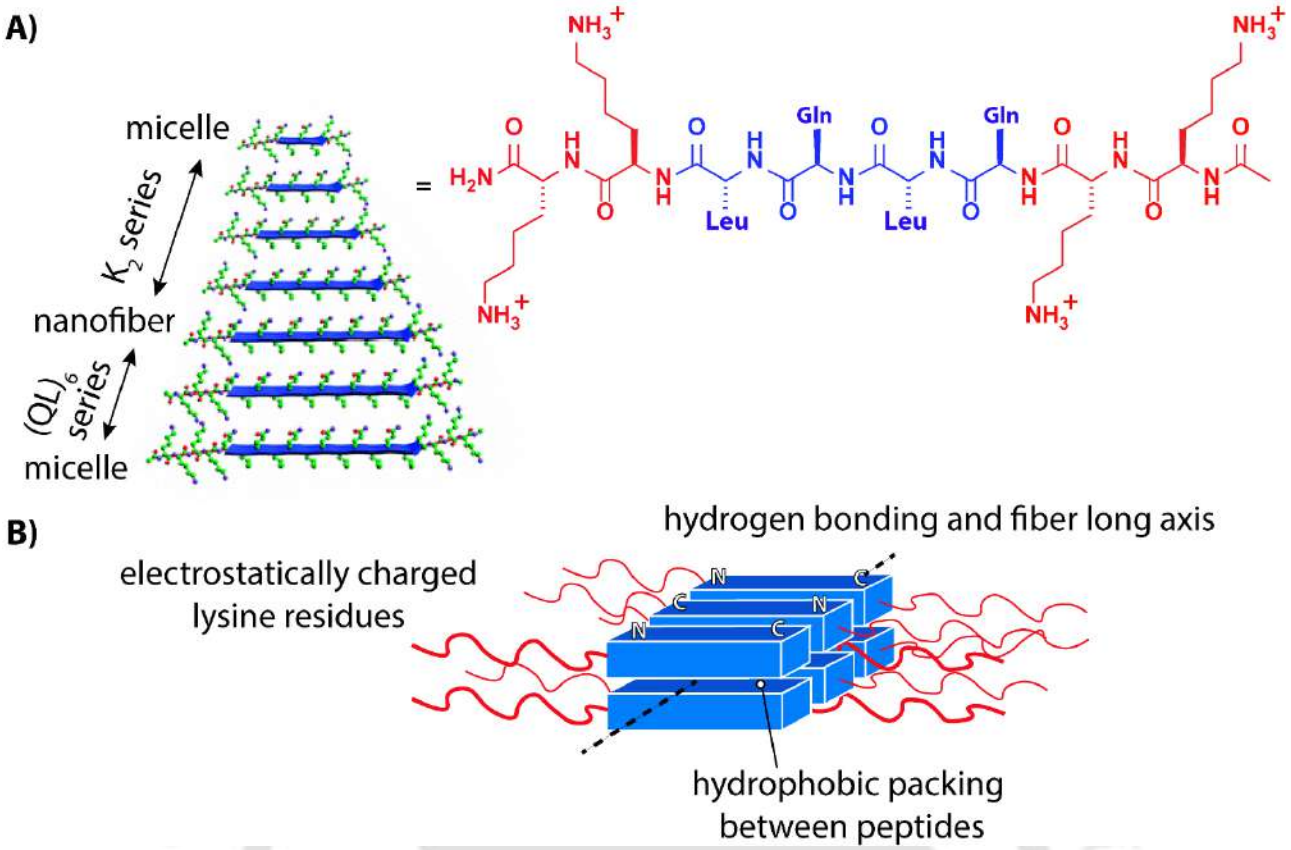

Figure 1.8 (A) Primary structures of the K_2 and $(QL)_6$ series of peptides showing the comparative domain size. (B) Proposed model of nanofiber self-assembly indicating hydrophobic packing region, axis of hydrogen bonding, and repulsive positive charges.

1.3.2.2 Cross-linked polymers

Peptide-based supramolecular cross-linked polymers have been relatively less cultivated as compared to the peptide-based linear supramolecular polymers. Reports of cross-linked peptide-based polymers depict their potential biological applications.[83, 84] In contrast to previous reports, development of cross-linked polymers is utilizing less number to supramolecular cross-linkers than covalent ones to curb the dynamicity and compromising robustness of purely supramolecular cross-linked polymers. A cross-linked gelatin based hydrogel was prepared using supramolecular host-guest chemistry of FGGC peptide and CB[8]. Norbornene-grafted gelatin polymer was treated with 2FGGC⊂CB[8] ternary complex followed by a photoinitiator. UV-light triggered covalent reaction of cysteines from peptides with norbornene units yields to an on-demand supramolecular injectable hydrogel (Figure 1.9).[85]

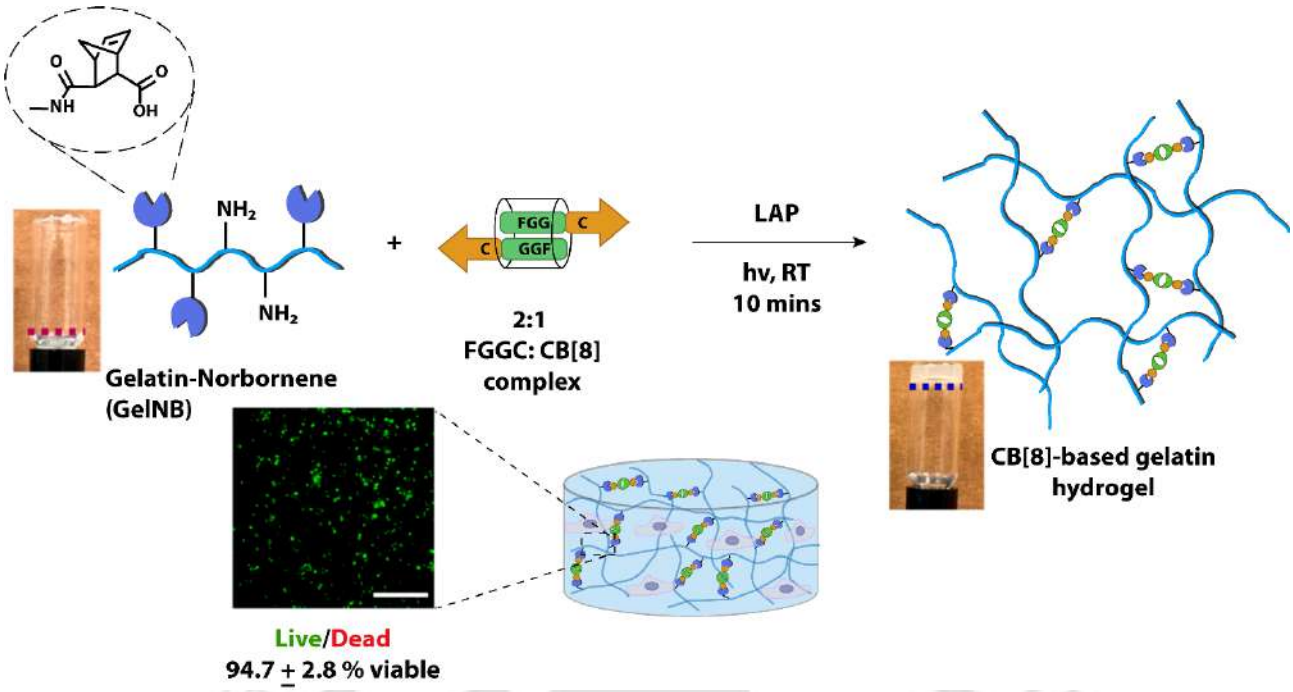

Figure 1.9 Schematic representation of user triggered cross-linking of norbornene-grafted gelatin and preassembled CB[8]·FGGC peptide ternary complexes, and the resultant CB[8]-based gelatin hydrogels under cell-compatible conditions.

A polyoxometalate based supramolecular underwater adhesive have been developed using short tripeptides as supramolecular cross-linkers. Tripeptide H_2N-GHK-COOH when mixed with polyoxometalate, forms complex coacervates in pH 6.5. Decreasing the pH to 4.5 yields to a hydrogel. A hydrogel was also obtained upon addition of Co^{2+} ions.[86] In a report from Tovar's group, a short peptide–chromophore–peptide triblock pregelator was designed. The peptide motif displayed reactive functional groups to form covalent cross-links with appropriately modified bifunctional polyethylene glycol (PEG)-based small guest molecules. These peptides undergo pH dependent supramolecular assembled linear π-conjugated structures. Covalent cross-linking was exploited to build a secondary network and trigger hydrogelation.[87] Human fibrinogen is the major protein constituent of blood clots and the provisional scaffold of wound healing. Exploiting this knowledge, a self-assembling biomaterial was constructed from a designed peptide inspired by the coiled coil domain of human fibrin, which was linked with PEG chain to produce a triblock peptide-PEG-peptide bioconjugate which self-assembled into viscoelastic hydrogel biomaterials via supramolecular coiled-coil secondary conformation.[88] An interesting system of redox-mediated reversible supramolecular assembly is demonstrated in a peptide-selenopolypeptide conjugate exhibiting interplay of peptide secondary structures. An α-helical peptide backbone is functionalized with β-sheet forming side-chain Nap-FFC short peptides. Initially, the backbone α-helical conformation screens the β-sheet propensity of the side

chain peptide. Once the oxidation of the selenium units is performed, the helical conformation of the backbone falls apart to give a random coil and unleashes the Nap-FFC to form β-sheet conformation.[89] In another report, as a proof-of-concept, it was depicted that when an adamantane-connected hydrogelator peptide was mixed with β-cyclodextrin vesicles, it formed hydrogels as a lower gelator concentration, as compared to the gelator without adamantyl groups. This was due to the additional supramolecular host-guest interactions between β-cyclodextrin and adamantane units imparts strength to the cross-linked hydrogel (Figure 1.10).[90]

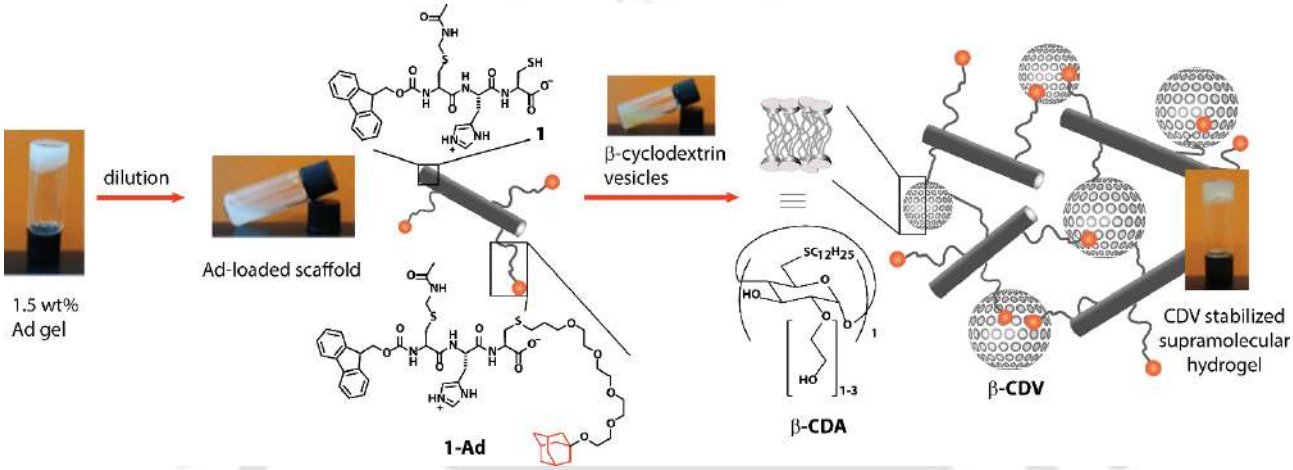

Figure 1.10 Formation of a CDV-stabilized supramolecular hydrogel of adamantane functionalized peptide scaffolds (9: 1 mixture of **1:1-Ad)** and cyclodextrin vesicles (CDV) of amphiphilic β-cyclodextrin host molecules (β-CDA) via multivalent host–guest inclusion complexes at pH 6 (final concentrations are 0.75 wt% of 1 and 2 mM (0.6 wt%) CDV).

1.3.3 Other types of peptide assemblies

Apart from hydrogels and polymers, there are a bulk of reports exhibiting various other types of versatile structural architectures demonstrate by peptides. Scrupulous engineering of peptide design has been effective in generating essential functional nanostructures for varied applications, nanotubes, nanotapes, nanobelts, nanoparticles, micelles and vesicles to name a few. Nanotubes have drawn interest of scientists because of its versatile uses in nanomedicine, biosensors, purifications, transport channels and catalysis.[91] Self-organization of molecules into tubular structures allows control of the external and internal diameters of such structures which is necessary for guest storage or membrane spanning nanotubes. Peptide based nanotubular structures can be attained in two pathways, coiling of linear peptides or linear stacking of cyclic peptides by β-sheet formation. De Santis *et al.* had first proposed peptide nanotube formation from cyclic peptides containing alternate D- and L- amino acids.[92] Ghadiri *et al.* had reported peptide nanotube formation by acidification of a pH responsive cyclic octapeptide.[93] Orientation of the amide bonds run perpendicular to the peptide ring axis which orients the amino acid side

chains towards the equatorial sites. This helps in further interactions and dimer formation. One of the drawbacks of this pathway is uncontrolled growth, solutions to this have been found in polymer conjugated cyclic peptides, 'layer-by-layer deposition' of alternate D- and L-cyclic peptides containing α-amino acids on gold surfaces, or through electrostatic interactions of opposite charges on successive peptides in assembly processes.[94] Diphenylalanine containing free amine and acid terminals is also reported to form structurally robust nanotubes.[95] Bola-amphiphilic peptides can also form nanotubes with a wide range of dimeters (20 nm to 1 micron) when kept in water for several days.[96] This methodology finds a great opportunity to be used as templates for nanowire fabrication for electronics and sensors. Tubular structures are also formed by peptide amphiphiles (Figure 1.11).[97]

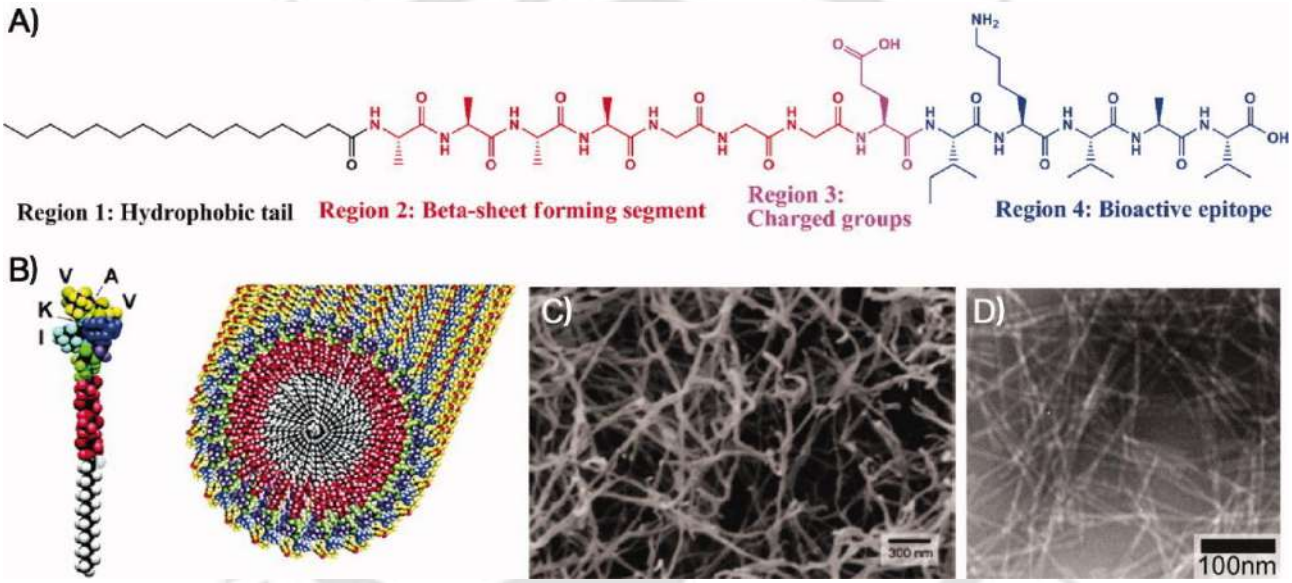

Figure 1.11 Molecular structure of a representative PA with four rationally designed chemical entities. (B) Diagrammatic illustration of an IKVAV-containing PA molecule and its self-assembly into nanofibers. (C) SEM images of the IKVAV nanofiber network formed by adding cell-culture media (DMEM) to the PA aqueous solution. (D) Transmission electron micrograph of the IKVAV nanofibers.

Vesicles are self-assembled compartmentalized structures with solvent-filled internal cavity to encapsulate substances and release them in a controlled fashion through diffusion processes. Vesicles have therefore been used as models for prebiotic cells.[2] Peptide vesicles are potent candidates for controlled drug delivery applications. Kimura *et al.* had first reported that PEG conjugated peptide, gramicidin-A formed vesicles in water. The antiparallel double-stranded helices packed side by side to formed the wall of the vesicle with PEG chains interacted with the solvent inside and outside the membrane.[98] A series of tryptophan-based linear and dendritic peptides was designed and synthesized that showed self-assembly to spherical vesicles.[99] The N-protected peptides formed spherical vesicles in 1:1 $CHCl_3$/MeOH, while N-deprotected derivatives

formed spherical vesicles in 1:1 MeOH/water. The spherical vesicles were found to encapsulate dye rhodamine B and showed cell internalization without effective peptide loss. In another design, Haridas *et al.* reported vesicle formation of a cysteine-based redox-active dipeptide dimer. Amine protected molecules formed vesicles in methanol whereas the one with free amines formed vesicles in water. The vesicles released entrapped drug, doxorubicin in a redox-responsive fashion in cervical cancer (HeLa) and breast cancer cells.[100] Banerjee et al. have attempted to design short water-soluble dipeptides based vesicular structures. An interesting architecture of vesicles-within-a-vesicle was obtained. The nano-assemblies were stable within a wide pH range (pH 2-12) but disassembled in presence of calcium ions. These nanovesicular structures were used as carriers of adenosine monophosphate keeping its biological activity intact and calcium ion induced release.[101] Amphiphilic peptides are also found to assemble into vesicular nanoassemblies.[39, 102-104] Cucurbit[8]uril, a macrocyclic host has been used in developing three-component supramolecular assemblies through host-guest association chemistry. Scherman and his group has reported a peptide-based vesicular system with a pyrene conjugated peptide and long alkyl chain containing viologen. Pyrene and viologen forms a donor-acceptor charge-transfer complex within the hydrophobic cavity of the host and this drives to the formation of vesicles in aqueous solution.[105] This work was extended by our group to form light-responsive vesicles where an azobenzene-conjugated peptide acted as the second guest for CB[8] after viologen moiety. Trans- form of azobenzene can allow another guest inside the CB[8] cavity, whereas the cis- form (obtained from UV irradiation) expels the other guest, thereby causing the vesicle disassembly. This system could be used as light-responsive soft materials.[106]

Among other nanostructures achieved by peptides, nanofibers are most commonly occurring ones since they are generally formed by β-sheet interactions which is the simplest form of secondary interaction attained by peptides. Some of the instances have been discussed here in an earlier segment. There has been reports of some pyrene end functionalized pentapeptides which proved to form α-helical to β-sheet structures and fibres. Aromatic-aromatic interactions and hydrogen bonding were found responsible for the self-assembly mechanisms.[107] Gazit and co-workers have reported a series of minimalist rigid peptides containing natural non-coded α-aminoisobutyric acid (Aib) which form cylindrical micelles to superhelical assemblies to nanofibrils and these are used as bioemulsifiers and thickeners.[108] An amphiphilic procollagen I derived peptide, C_{16}-KTTKS self-assembled into extended nanotapes in aqueous solution. Addition of anionic surfactant sodium dodecyl sulphate causes counterion condensation and transforms from

nanotapes to stripped fibrils.[109] Guler and his group has reported a series of four histidine-rich peptide amphiphiles along with their chiral counterparts. It was observed that upon increasing the pH, peptides transformed from nanosheets to closed nanotubes and in all the cases, the molecular chirality was transformed to supramolecular chiral nanostructures.[110] Tirrell and his group had designed a peptide amphiphile which contains a short α-helical peptide (W3K) sequence connected to a hexadecyl chain. The PA forms spherical micelles in aqueous solution which prevails for several days, after which spherical micelles get converted to extended wormlike micelles which is concurrent with the secondary structural transformation from α-helix to β-sheets. Therefore, cylindrical micelles were considered as ramification of thermodynamic pathway whereas spherical micelles are resultant of kinetic pathway of self-assembly.[111] A TPE conjugated multi-domain peptide amphiphile micelles were used for targeted drug delivery applications.

1.4 Applications of peptide-based soft materials

For quite a few decades now, since peptide self-assembly has become a comprehensive tool directing to various classes of nanomaterials, peptides have become akin to "clay in a potter's hand". The designing skill narrates the functional efficacy of soft materials to conquer multiple realms of applications like drug delivery, platform for tissue engineering, biosensors for disease diagnosis, biocatalysis. Peptide-based materials have always proved to be a step ahead of the other competent materials because of its inherent chemical diversity, propensity for self-assembly and facile derivatization techniques. Peptide nanomaterials assure biocompatibility and can be modulated to reduce drug toxicity and improve directed drug-delivery. A peptidic shell allows enhanced solubilization of the capsuled hydrophobic drugs.[112] Upon injection followed by application of suitable trigger helps in delivery of the drug at a desired site. Drug-delivery systems are designed by the modes of ex-situ construction, in-situ morphology transformation, and in-situ construction of peptide nanomaterials for drug delivery. Both physical and chemical modes of drug entrapment are used. Single peptide systems (without a true drug molecule) can also act as a drug system in suitable conditions which is an excellent exploring ground in modern nanomedicine.

1.4.1 Drug delivery

There are quite a number of reports where peptide-polymer conjugates have been shown to act as drug-delivery systems. The delivery vehicle was made to accumulate by passive tumor targeting effect around the tumor cells by EPR effect and thereby the drug is released in the tumor

cells.[113-115] The positive charge of nanoparticles accelerates the rate of its internalization within cells because of the negative charge of the cell membranes. However, the positive surfaces can reduce circulation half-time in blood. To counter this effect, blood circulation enduring nanoparticles were designed such that positively charged peptides are exposed in the tumor microenvironment, causing their effective internalization into tumor cells. Owing to the change of surface charge from negative to positive, the nanoparticles exhibit high efficiency of entering cells.[116, 117] Cell-penetrating peptides are a class of peptides rich in positively charged amino acids which facilitates efficient drug internalization for improved cellular delivery.[118-120] Some peptide sequences can transform their secondary conformations upon pH variations. Since pH of the tumor cells is acidic, the peptides transform to helical structures upon experiencing the acidic environment and perturbs the cell membrane and facilitates internalization through membrane binding.[77, 121, 122] A histidine containing peptide-guided prodrug was designed where a drug, doxorubicin was incorporated in a pH-sensitive hydrazone bridge. This peptide-drug conjugate was developed for targeted ablation of cancer cells with minimal side cytotoxicity.[123] A short peptide, Nap-GFFYGD derivative-based hydrogel was developed which contained a hydrogen peroxide (H_2O_2) responsive thiazolidinone at the C-terminal of the peptide. At the cellular level, where there is excess H_2O_2, the thiazolidinones are removed to trigger the gel–sol phase transition of hydrogels for releasing gemcitabine continuously and controllably.[124] A novel self-assembling peptide-based supramolecular hydrogel was developed by simultaneously conjugating small-molecule drug chlorambucil (CRB) and peptide drug tyroservatide (YSV) to the self-assembling peptide. The resulting nanofibers of the hydrogel showed enhanced stability against proteinase K degradation, improved cellular uptake and exhibited enhanced antitumor efficiency both in vitro and in vivo compared to the free molecules. Such systems can be used as a reference system in cancer combination therapy (Figure 1.12).[125]

There have been peptides designed which undergo in-situ transformation to construct the functional drug-delivery vehicles.[126, 127] A multi-functionalized nanometre sized albumin-based drug-delivery system was designed which was conjugated with tumor-targeting, cell-penetrating, and endolysosomal pH-responsive properties, cRGD-BSA/KALA/DOX. The nanoparticles were fabricated by self-assembly through electrostatic interaction between cell-penetrating peptide KALA and cRGD-BSA. Under acidic conditions of the lysosomal environment, the changes in the electric charges of cRGD-BSA and KALA led to the disassembly of the nanoparticles to accelerate intracellular drug release. The nanoparticles also exhibited enhanced inhibitory effect in the

growth of αvβ3-integrin-overexpressed tumor cells, indicating promising application in cancer treatments.[128] Enzyme responsive peptide-drugs can also be designed A review by Stenzel discusses various other peptides that play an important role in treating various diseases.[129]

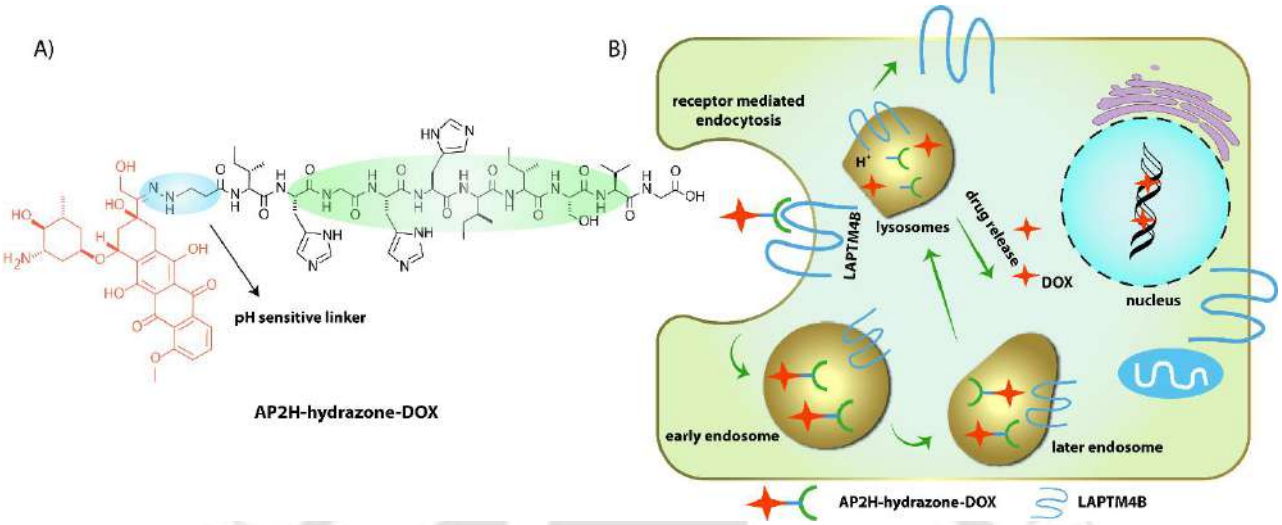

Figure 1.12 (A) Chemical structure of the tumor specific peptide prodrug **AP2H-hydrazone-DOX**. (B) LAPTM4B guided AP2H-hydrazone–DOX internalization and pH mediated drug release process.

1.4.2 Tissue-engineering scaffolds

Peptide-based supramolecular polymeric scaffolds are often biologically more relevant than covalent polymeric scaffold materials for tissue engineering applications. Inspite of hundreds-to-thousands fold greater mechanical strengths and robustness of covalent polymers compared to supramolecular polymers, the latter is often procured for developing biomimetic tissue scaffolds. Both, synthetic polymers and peptide-based materials are under the scanner to create such platform, where peptides are frequently recruited because of wide range of functionality and inherent biocompatibility.[18, 38, 130-135] However, linear peptides provide such surface for cell-adhesion through hierarchical supramolecular assembly. On the other hand, in a cross-linked polymer, the network is an integral part of the polymer and attachment of cell-adhesive units on the network surface provide the desired surface for cell attachment and growth. Moreover, the size of the cross-linked polymer is also of prime concern for their potential use as ECM or other biological applications. Some cross-linked peptide based polymeric systems are reported in literature.[136-139] However, controlling the size of the polymer is a difficult task. This is because supramolecular polymers can regain more than 90 percent of the mechanical strength failed due to applied strains. However, purely supramolecular polymers can face risk of disintegration in presence of the strenuous cellular environment as cells can generate significant amount of force to the surrounding milieu. Therefore, to toughen the scaffold material, covalent polymers are

conjugated to peptides to form flexible, yet robust biomimetic materials.[140-142] Another benefit appreciated by peptide hydrogels for scaffolds is their self-assembly in presence of ions present in physiological solutions (or added separately) which assists in-situ construction of tissue scaffolds. Several reports in this regard have established different polymer- peptide based tissue engineering scaffolds, where different secondary structural motifs of peptides have been exploited as the point supramolecular cross-links.[143-145] Stevens and his group has utilized a (γ-glutamic acid) polymer and grafted it with different amounts of β-sheet forming sequence, $D_2I_4D_2$. The quantity of β-sheets, strength of the cross-linked hydrogel and intensity of self-healing activity could be tailored by the percentage of polymer grafting.[146] In concern of tackling on spinal cord injuries, Gao and his group attempted a hyaluronic acid scaffold modified with a cell adhering peptide sequence, PPFLMLLKGSTR. The peptide-modified hydrogel scaffold facilitates 3D growth of mesenchymal stem cells in-situ. The implantation also effectively prevents post injury factors.[147] Recently, solely peptide-based supramolecular scaffolds have been proved as promising tissue engineering scaffolds without the aid of covalent polymeric backbones.[148, 149] A coassembled peptide hydrogel containing Fmoc-FF and Fmoc-Arg was constructed which projected the arginine on the surface of the hydrogels. Hydroxyapatite was allowed to interact with the coassembled hydrogel to mimic a biomimetic scaffold for bone regeneration.[150] Amoc-protected dipeptides that were capable of forming injectable and self-healable hydrogels have been explored for tissue culture. Amoc-dipeptide hydrogels show antibacterial activity, hemocompatibility and has been applied for effective cell proliferation on cultured bacterial and human white blood cells.[151] Lampe et al. established a unique class of short five-residue peptide hydrogels which was successfully used for neural tissue engineering. The designed peptides formed sequence-dependent and pH dependent nanofiber formation with KYFIL sequence forming twisted ribbon shaped amyloid-like structures. This sequence formed an injectable hydrogel which could encapsulate oligodendrocyte progenitor cells (OPCs) and prevent mechanical membrane disruption and acute loss of viability during syringe injections (Figure 1.13).[152]

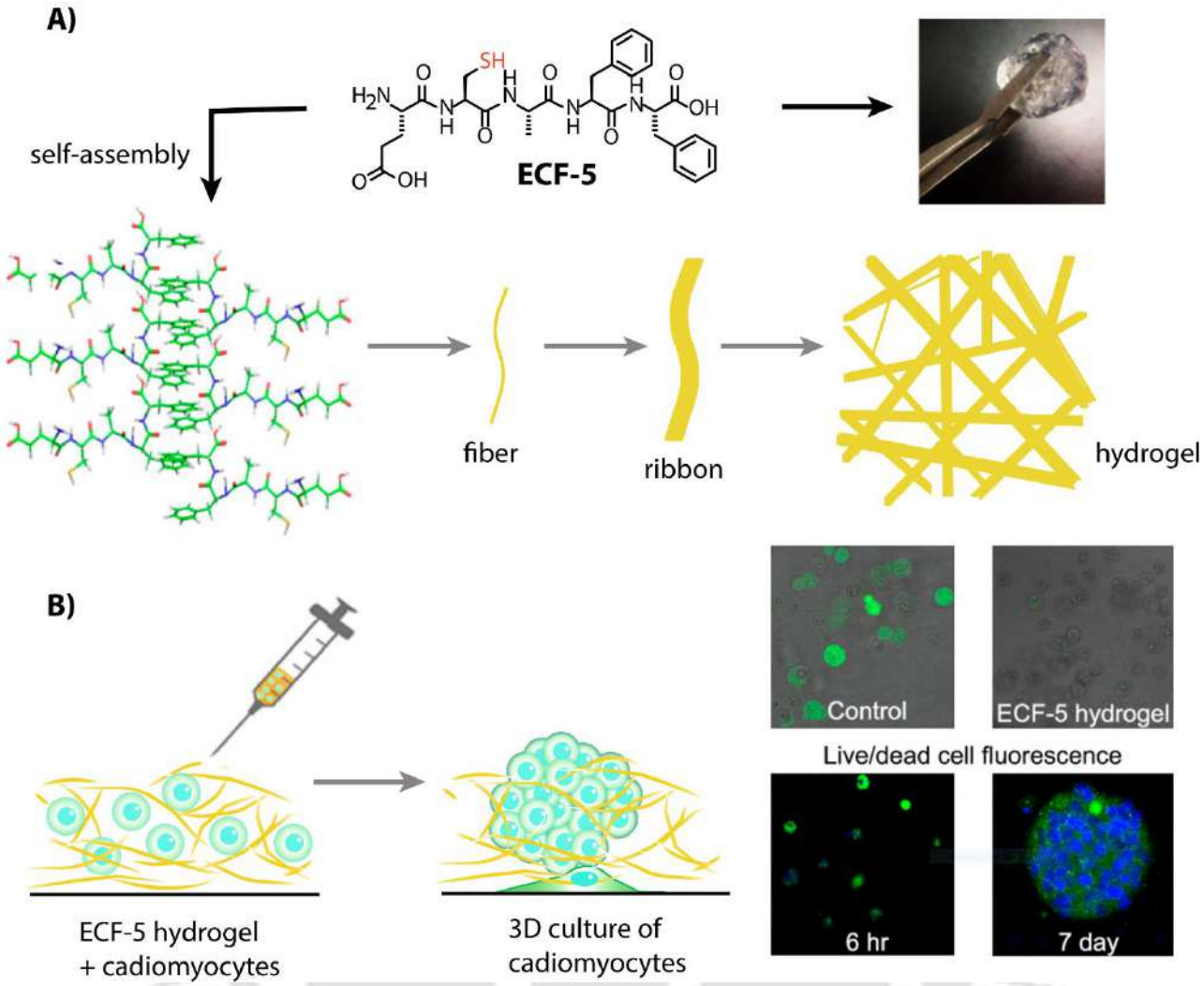

Figure 1.13 (A) Chemical structure of the peptide along with picture of a 1.5 wt. % hydrogel. Schematic representation of ECF-5 molecules that form nanofibers and hydrogels. (B) 3D culture of cardiomyocytes in the ECF-5 hydrogel. Schematic drawing of the cells that were buried in the ECF-5 hydrogel. Fluorescent images of the cardiomyocytes in the 3D culture medium containing only cells, only ECF-5 hydrogel and cells in ECF-5 hydrogel, revealing the cell viability and morphology after being in the culture for 6 h and 3 days.

1.4.3 Artificial biocatalysts

Enzymes are examples of very efficient biocatalysts that carry out biochemical functions under mild conditions to sustain the cellular functions and metabolic activities of living organisms. However, working with real enzymes is not an easy task owing to its propensity to denaturation under ambient conditions. Therefore, deciphering the mechanisms of catalytic action, structure-function relationships and developing robust artificial biocatalysts that can mimic the functions of an enzyme has become an immense necessity. Peptides are the most promising building blocks for designing artificial biocatalysts as they are also the constituents of enzymes.[153] The concept of supramolecular catalysis uses simpler building blocks which join up to form complex structures which concentrates the catalytic sites on the surfaces for comparable or enhanced activity than

natural enzymes.[154] Much like the non-covalent basis of structural construction in enzymes, smaller peptide fragments are capable of forming various structural constructions by supramolecular interactions. The self-assembly attained by peptides could provide hydrophobic surfaces for substrate interaction or hydrogen bonding motifs to drive selective substrate recognition. In this way, the actual catalytic site can be mimicked without the use of the non-catalytic bulk portion of the enzyme. Ester hydrolysis is a very common reaction carried out by enzymes within a biological system. Therefore, many groups have expanded the concept of supramolecular catalysis to mimic hydrolase/esterase activity (Figure 1.14).[155, 156]

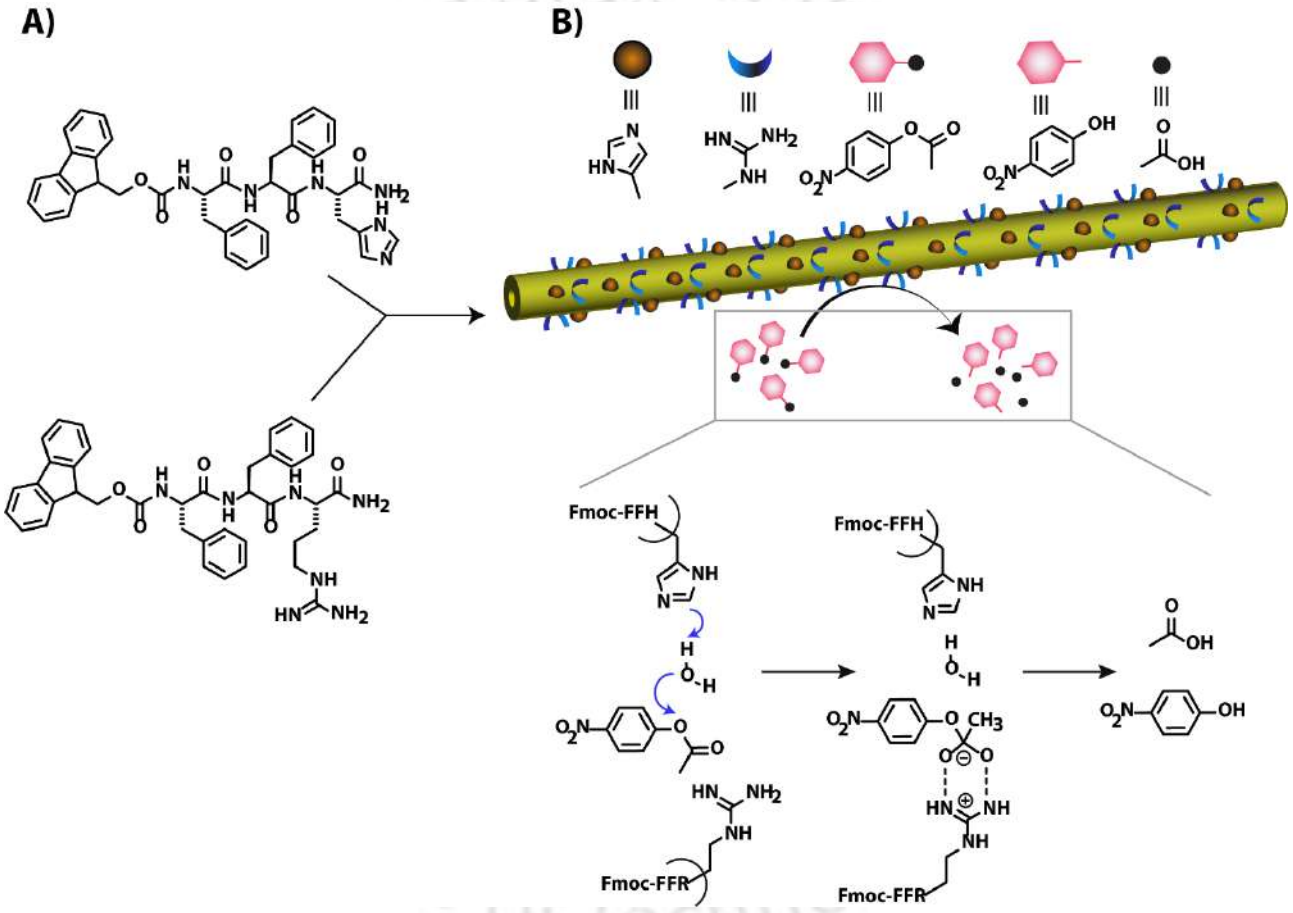

Figure 1.14 (A) Chemical structures of the peptide components of the nanotube. (B) Schematic representation of the possible mechanism for the cleavage of PNPA catalyzed by PepNTs-His-Arg_{max}.

A family of amyloid forming peptides were designed by modifying parent peptide sequence, Fmoc-LKLKLKL-$CONH_2$. Two hydrophilic lysine were replaced with histidine and the rest with other hydrophilic amino acids. The modified peptides behaved as efficient metallocatalysts in presence of Zn^{2+} ions, to catalyse the hydrolysis of *p*-NPA. Further rational structural modifications led to improved catalytic efficiency $(k_{cat}/K_M)_{max}$ of 19 200 M^{-1} min^{-1}. The amyloid-like fibrils were responsible for the catalytic activity, whereas the monomers were silent towards hydrolase

activity.[157] The same group has reported a series of heptapeptides, which are able to bind copper through self-assembly and activates oxygen for oxidation of 2,6-dimethoxyphenol. [158] Recently, Das and his group have analysed covalent catalysis by β-amyloid nanotubes. An interesting correlation between amino acid choice, sequence specificity and catalytic activity was brought out. Various experimental analyses proved that an adjacent lysine to a histidine synergistically assisted and enhanced esterase activity of inactivated keto-ester substrates through dynamic covalent imine bond formation.[159] Natural carbonic anhydrase enzyme functions with the combined redox and hydrogen-bonding interactions of histidine and Zn^{2+} ions. Some self-assembling peptide sequences are found to mimic similar enzymatic activity.[160] A unique single amino acid assembly based carbonic anhydrase mimic was discovered. In presence of Zn^{2+} ions, phenylalanine forms rapid coassembly to form coordination complex extending to form fibrillar structures by cross β-sheet layered organization. This metal induced phenylalanine organized structure shows carbonic anhydrase like activity.[161] Lysine and proline can catalyse aldol C–C coupling reaction by forming an enamine intermediate with ketone, where the prolyl-enamine participates in the nucleophilic addition to the aldehyde. Some groups have expanded the concept of peptide based supramolecular catalysis for mimicking aldolase and retro aldolase activities.[162, 163] The basicity of L-Proline at different states of molecular organization can direct the type of aldol product between nitroalkanes and aldehydes. L-Proline shows higher basicity in assembled gel state than in solution state.[164] Therefore, different types of condensation products could be produced at below/above the critical gel temperature.

1.5 Present thesis

Through the four chapters spanning the present thesis, different small peptide based soft materials were developed using the concepts of peptide self-assembly. All the peptides were essentially synthesized using solid phase peptide synthesis protocol, unless otherwise mentioned. Characterizations were done using NMR, HPLC and HRMS. Conformational studies were performed with the help of CD and IR spectroscopy. Various supramolecular interactions were determined from ITC, NMR, IR, UV-Vis, fluorescence spectroscopic techniques. Particle sizes of various assemblies were monitored by DLS whereas morphological analyses were performed using FESEM, FETEM and AFM microscopic techniques. Mechanical properties of hydrogels were determined from rheological experiments. Information regarding thermal stabilities and pore-size diameters of functionalized silica nanoparticles were procured from TGA and BET experiments.

The four chapters of the thesis are as follows:

I. A small peptide-based pH responsive hydrogel was developed which showed thixotropic properties. The gelator was a shorter version of the original MAX1 sequence, and modified with a C-terminal cysteine residue. A strong supramolecular hydrogel was obtained in basic condition due to formation of β-sheets. The hydrogel reverted to sol in acidic conditions. The hydrogel remained intact even after four repetitive cycles of shear-thinning experiments.

II. Another short peptide coassembled hydrogel was created which had cell receptor binding properties. A disease-causing protozoan cell-line is known to contain mannose binding sites on its surface. A coassembled hydrogel with surface decorated mannose units was utilized for cellular internalization of the hydrogel for potential therapeutic applications. For this, Nap-FFGE (gelator) sequence, was mixed with its C-terminal mannose conjugate, Nap-FF-Man (non-gelator) in desired ratios to obtain a temperature assisted hydrogel. Additionally, it was shown that different mixing ratios of the two components affected the time of gelation and mechanistic properties of the hydrogels.

III. A multiple cross-linked peptide supramolecular polymer was constituted for potential application in cell adhesion and proliferation. A novel peptide was designed which contained amino acid residues that were capable of forming orthogonal cross-links. FGG motif mediated CB[8] assisted host-guest chemistry, disulfide cross-linking of cysteine and enzymatic cross-linking of tyrosine were used as various modes of peptide polymerization. Simultaneous cross-linking of the monomer yielded to water insoluble polymer nanoparticles with surface decorated RGDS sequence for cell adhesion. This designed polymer could be used to construct multi stimuli-responsive soft material.

IV. A catalytic peptide was systematically designed inspired from natural hydrolases. This peptide catalyst was immobilized on silica surface to enhance catalyst robustness. This immobilized catalyst showed higher extents of hydrolysis as compared to the homogeneous catalysts at similar concentrations. The immobilization of catalysts also imparted greater stereoselectivity to the reactions and could be used as a reusable artificial hydrolase for enhanced rates of reactions.

Chapter-2: pH and Secondary Structure Instructed Aggregation to a Thixotropic Hydrogel by a Peptide Amphiphile

2.1 INTRODUCTION

In recent years, search for supramolecular hydrogels with thixotropic (or injectable) property has gained attention owing to their possible application in localized drug delivery.[165-169] In this regard, supramolecular hydrogels prepared from the peptides can be an effective way to create such kind of soft materials.[38, 170] Peptide-based hydrogels have been meticulously applied for various applications like, tissue engineering,[171, 172] drug delivery,[173, 174] protein protection,[61] nanofabrication,[175, 176] sensing[177, 178] and so on. The self-assembly in small-peptide hydrogels is based on secondary structures are often initiated by the appropriate stimuli like pH, ionic strength, light, etc. Among the possible secondary conformations, among which β-sheet is the most explored one towards constructing peptide-based hydrogels.[38, 179]

Amphiphilic peptides, prepared from alternate hydrophobic and hydrophilic residues is a common approach to construct b-sheet like assemblies which form hydrogel in a concentration-dependent manner.[180] In this regard, Schneider[181-186] introduced a β-hairpin forming peptide amphiphile series where Val and Lys residues are placed in an alternate fashion and the two strands are connected through a type II β-turn sequence of ^{D}Pro–^{L}Pro. We envisioned that a simple Val–Lys stretch can also adopt β-sheet like secondary structure and that may eventually result in the formation of hydrogel. Since, Lys is the only hydrophilic residue, the self-assembly can easily be controlled by changing the pH of the medium.

In this work, we report a small peptide (**PA-2.1**, Scheme 2.1) where a Cys residue is attached at the C-terminal to a $(VK)_5$ sequence using a spacer (γ-Aminobutyric acid, GABA). The presence of Lys residues can introduce the pH responsive aggregation property, while the alternate Valine- Lysine arrangement will result in β-sheet like secondary structure formation. Introduction of the C-terminal residue was made on purpose to find whether the disulfide linkage between two peptide molecules could affect the aggregation pattern imparted by the β-sheet forming $(VK)_5$ segment. Moreover, there might also be a possible competition between the aggregation of **PA-2.1** and the disulfide linkage processes. Cys forms disulfide bonds in basic pH or by oxidation of dissolved oxygen in solvents.[187, 188] This chemistry is widely observed in biological systems to stabilize secondary and tertiary structures of protein. The pH instructed hydrogel was found to be reversible and the pH induced sol–gel transitions can be achieved for several cycles. Moreover, under basic medium, the β-sheet aggregation was found to be spontaneous and extremely fast, which does not allow the disulfide bond formation between two Cys residues. As expected, the hydrogel also showed thixotropic behavior.

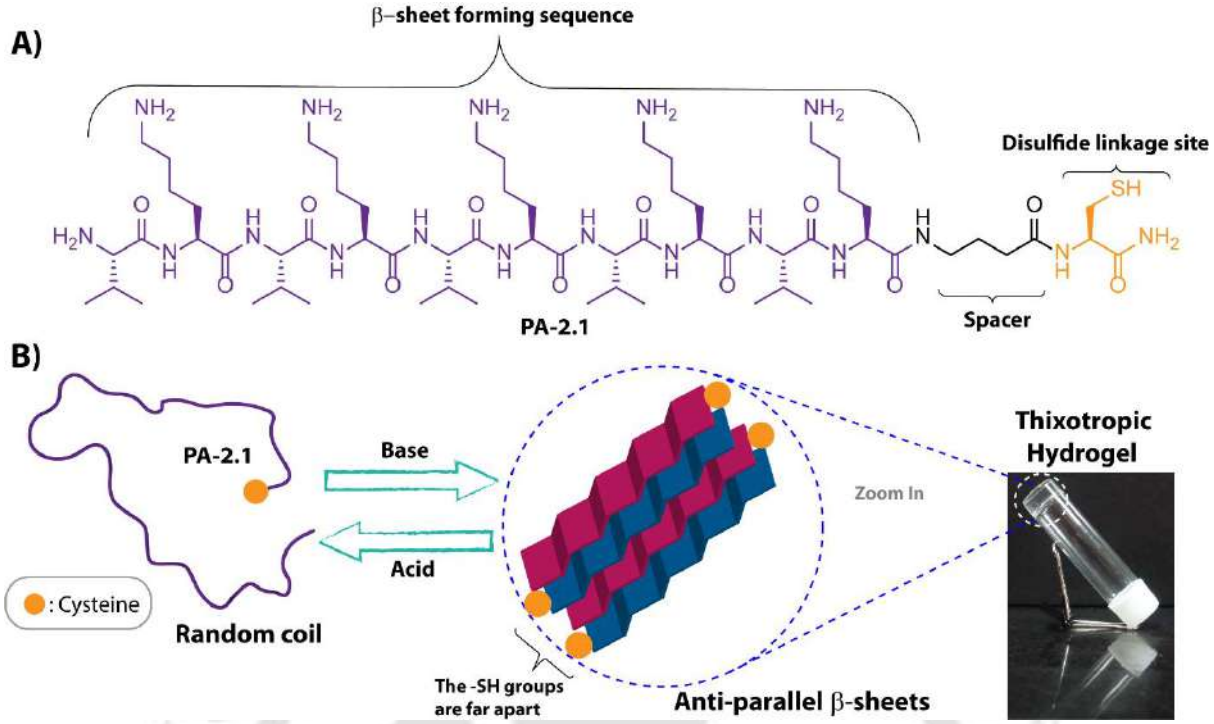

Scheme 2.1 Chemical structure of **PA-2.1** highlighting different segments of the same and (B) Graphical representation of the pH and secondary structure directed hydrogelation by **PA-2.1** and photograph of the hydrogel (1 wt. %, pH 9).

2.2 EXPERIMENTAL SECTION

2.2.1 General

Resin, Fmoc-protected amino acids, coupling agent and DIPEA were purchased from GL Biochem (China). All other chemicals and solvents were procured from Spectrochem (India) and Fisher Scientific (India), respectively. For sample preparations, Milli-Q water with a conductivity of less than 2 μS cm^{-1} was used. ESI-MS was performed with a Q-tof-micro quadrupole mass spectrometer (Micromass). CD experiments were performed on a Jasco J-1500 spectropolarimeter. HPLC purifications were carried out on a Dionex Ultimate 3000 HPLC using a Luna 5 μm (C18) column (Phenomenex). NMR spectra were recorded with a Bruker Ascend 600 MHz (Bruker, Coventry, UK) spectrometer. FTIR spectra were recorded on a Nicolet is10 spectrometer. FESEM was performed on Gemini SEM 300 (Sigma Zeiss). Rheology experiments were performed using a rheometer (Anton-Paar MCR 102).

2.2.2 Synthesis of PA-2.1

PA-2.1 was prepared using Rink amide MBHA resin. Standard Fmoc (9-fluorenylmethoxycarbonyl) solid phase peptide synthesis (SPPS) method was employed. For a standard coupling, DMF solutions of protected amino acid (3 equiv.) HBTU (3 equiv.) and DIPEA (6 equiv.) with respect to the loading of the resin were added to the resin. The resin was shaken for 1 hour before washing

with DMF several times. Fmoc-deprotection was carried out using 20% piperidine followed by thorough washing with DMF and DCM. Following the sequence, proper elongation of the peptide was done at the N-terminal by repeating this procedure. Finally, the peptide was cleaved from the resin using a mixture of TFA/TES/water (8.5:1:0.5 v/v). The cleaved peptide was then precipitated from cold dry ether, washed and lyophilized before purifying on HPLC. Purification was done using an eluent of acetonitrile and water 100% H_2O to 20% ACN/H_2O (in 20 minutes) to 40% ACN/H_2O (in 30 minutes) to 100 % ACN/H_2O (in 35 minutes). The pure peptide eluted at a retention time of 20 minutes. The pure lyophilized peptide was obtained in 70% yield. ^{1}H NMR (600 MHz, D_2O, 25 °C) δ (ppm): 4.34 (dd, 1H), 4.28 (dd, 1H), 4.20 – 4.17 (m, 3H), 4.04 (d, 1H), 3.96 – 3.90 (m, 5H), 3.65 (d, 1H), 3.09 (t, 3H), 2.86 – 2.79 (m, 13H), 2.76 – 2.73 (m, 1H), 2.22 (td, 2H), 2.07 – 2.02 (m, 1H), 1.93 – 1.83 (m, 5H), 1.60 (dp, 28H), 1.34 – 1.20 (m, 13H), 0.86 (t, 7H), 0.79 (td, 32H).

2.2.3 Hydrogel preparation

5 mg of **PA-2.1** was dissolved in 450 μL of water and completely solubilized by gentle shaking. To this freshly prepared solution, 40 μL of 2 M NaOH was added and tapped gently for mixing. The resultant solution formed a transparent hydrogel within few minutes. The pH of the system was noted as 9.0.

2.2.4 FTIR spectroscopy

FTIR experiments were performed in solid state and liquid state. For as synthesized **PA-2.1**, the solid was mixed with KBr to prepare a palette and the IR spectrum of the palette was recorded. For liquid state analyses, 2 μL solution or gel was casted in between CaF_2 windows and analyzed after subtracting the baseline. Experiments were carried out with 1 wt. % samples.

2.2.5 CD spectroscopy

For CD experiments, 100 μM peptide solutions was prepared in pure water or the desired buffer solutions. For the gel state, a 24 hours-matured gel was diluted in water to reach the appropriate concentration of 100 μM and the CD spectra were measured.

2.2.6 FESEM

10 μL of the respective sample solutions/gels were incubated at room temperature for 24 hours and casted on silicon wafers and air-dried for at least 1 day. Images were taken on a GEMINI SEM 300 (Sigma Zeiss) instrument.

2.2.7 Rheology experiments

The rheological measurements of the hydrogel were performed on a MCR 102 rheometer (AntonPaar) with a 20 mm parallel plate at 25 °C. The linear viscoelastic region (LVR) was identified first by a strain sweep test over a range from 0.01 to 100 % strain at a fixed oscillatory frequency of 1 rad/s. Next the oscillatory test (frequency sweep) was carried out under a strain (γ) = 0.1 %.

2.3 RESULTS AND DISCUSSION

PA-2.1 was synthesized following solid phase peptide synthesis protocol using Rink amide MBHA resin. The peptide was obtained in 70% yield after HPLC purification. To test the hydrogelation, 5 mg of the peptide was weighed and dissolved in 500 μL pure water by shaking. The solution was incubated at room temperature for 24 hours to allow disulfide formation. It remained as clear solution for a long time. At different time interval, the ESI-Mass of this solution was checked and the mass corresponding to the dimer appeared for the first time after 30 minutes. Within 24 hours, all **PA-2.1** was found to be dimerized as no signal corresponding to **PA-2.1** was obtained after this time. CD spectra of this 24 hours-matured solution of **PA-2.1** dimer showed no features for a particular secondary structure and thus it can be concluded that the system possessed random coil conformation (Figure 2.1 A).[189] Increasing the pH of this solution by addition of base up to pH 11 did not change the conformation as well as no hydrogel was formed (data not shown). Similarly, addition of acid to lower the pH also could not produce any change. However, when NaOH solution was added to a freshly prepared aqueous solution of **PA-2.1** (where no dimer is present), the solution turned into a self-supporting hydrogel within a minute (Figure 2.2 A). Careful measurements showed that the hydrogel could be formed at a pH as low as 9 with a minimum gelation concentration (MGC) of 0.85 wt. %.

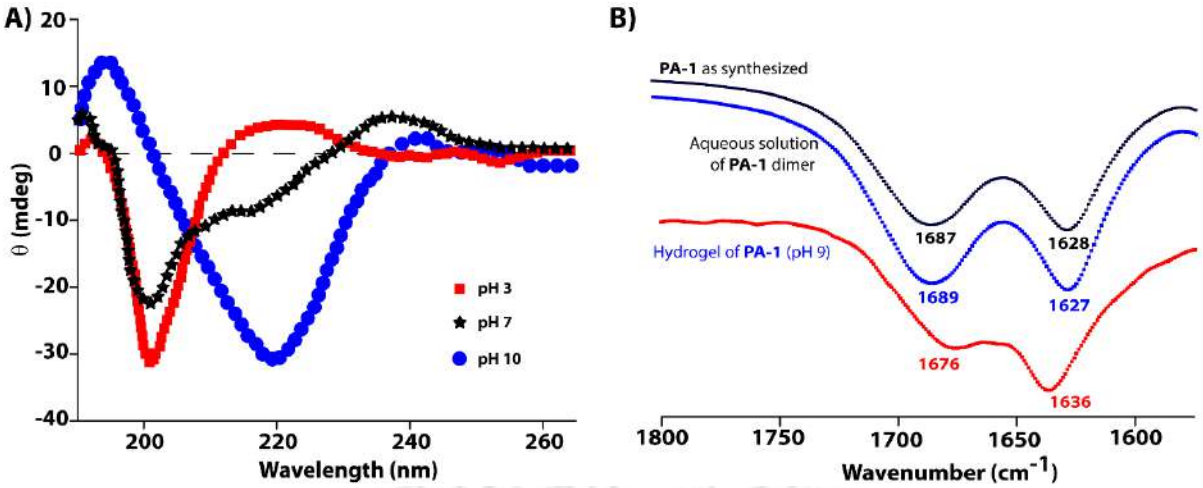

Figure 2.1 (A) CD spectra of PA-2.1 under various pH and (B) FTIR spectra of as-synthesized **PA-2.1**, solution of its dimer and hydrogel of **PA-2.1**.

CD spectroscopic analyses of the system in basic medium showed a positive cotton effect at 195 nm followed by a strong negative signal at 218 nm. These are characteristic signals of β-sheet formation.[189] Further, FTIR analyses of the hydrogel showed two characteristic signals at 1636 and 1676 cm^{-1} (Figure 2.1 B) which correspond to β-sheet.[190-192] The as-synthesized powdered peptide or the sample of **PA-1** dimer showed two signals at 1628/1627 and 1687/1689 cm^{-1} (Figure 2.1 B) which confirms the random coil arrangement as found from CD experiments (Figure 2.1 A). Repeated and extensive analyses of the hydrogel by ESI-MS and MALDI-MS could not produce any trace of the dimer. Interestingly, even a seven days-mature hydrogel sample also did not show the presence of the dimer. The extremely fast gelation upon increasing the pH and the fact that the dimer solution at above MGC that failed to form the hydrogel suggest that under basic medium, the conformational change and aggregation is a much faster process than the disulfide bond formation. Once the molecules adopt anti-parallel -sheet conformation and self-assemble, the dynamic nature of the system get restricted and the -SH groups of Cys residues could not come close to form the disulfide linkage.

After getting these observations, behavioral change of the hydrogel under pH variations was studied. It is worth mentioning here that **PA-2.1** failed to form any gel in the entire acidic pH range. When 5 μL of 12 N HCl solution was placed on top of a 2 wt. % gel (500 μL, pH 9), the gel started melting immediately and with little shaking, it became sol within 30 seconds. To the same solution, addition of 40 μL of 2 M NaOH solution and gentle shaking results into the reformation of the gel state within a minute. This gel-sol-gel transition can be repeated for several cycles as long as the concentration of **PA-2.1** remain above MGC. With higher concentration gel, the number of cycles can be increased.

In a separate set of experiment, the CD spectra of the samples were measured after each transition (Figure 2.2 B). For the acid treated sol state, the CD spectra showed a negative band at ~ 200 nm and were very similar to that obtained from aqueous solution of **PA-2.1**. It can be concluded that the solutions predominantly contained random coil structures. For NaOH treated gel states, a small portion of the gel was dissolved in deionized water (pH was maintained above 9) and the CD spectra were recorded. In each case, the characteristic peak for β-sheet at 218 nm were observed similar to that shown in Figure 2.1 A for pH 9. Though not shown, overall pattern remained unaltered after every cycle for both sol and gel states.

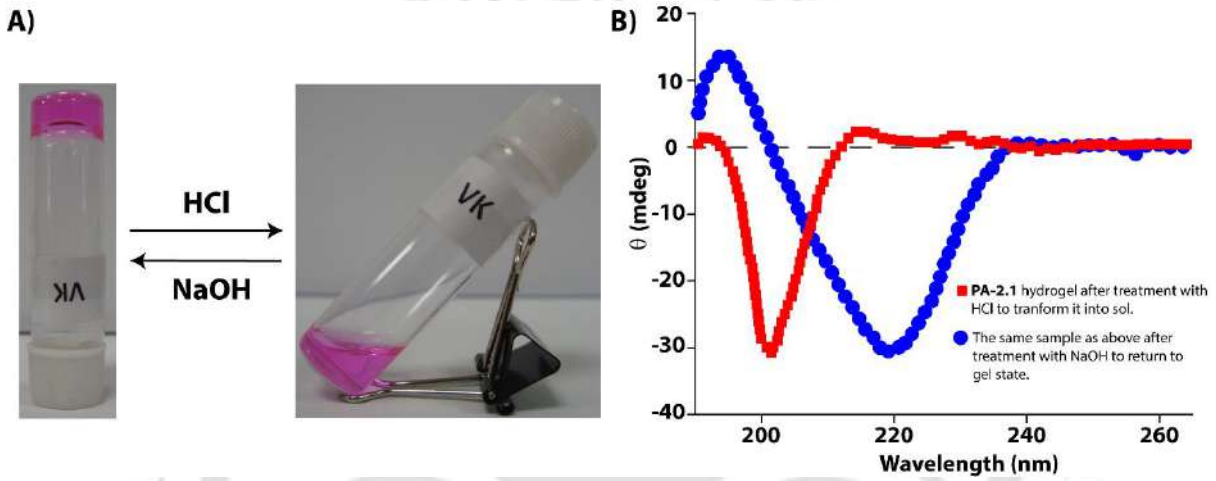

Figure 2.2 (A) Photographs of rhodamine B-loaded hydrogel and its gel–sol–gel transitions induced by the addition of acid or base (B) CD spectra of **PA-2.1** hydrogel through one cycle of gel-sol-gel transition through change in pH.

Further the morphology of a freshly prepared hydrogel of 1 wt. % **PA-2.1** was checked using field emission scanning electron microscope (FESEM). As can be seen from Figure 2.3 A, bunches of needle-like aggregates were obtained which are more than 1 μm long and average diameter of ~200 nm. In another test, the hydrogel (1 wt. %) was prepared by dissolving **PA-2.1** in 20 mM phosphate buffer (pH 9) to find any change in the aggregation pattern that may happen owing to the difference in preparation procedure. Importantly, as can be seen from Figure 2.3 B, similar bunches of needles were also found in this case as well. Next, samples of the gel-sol transitions were tested for morphology. As expected, no particular pattern or morphology could be seen in the acid treated sample (Figure 2.3 C). When the same sample was treated with NaOH to regenerate the gel state, the original needle like morphology was regenerated (Figure 2.3 D).

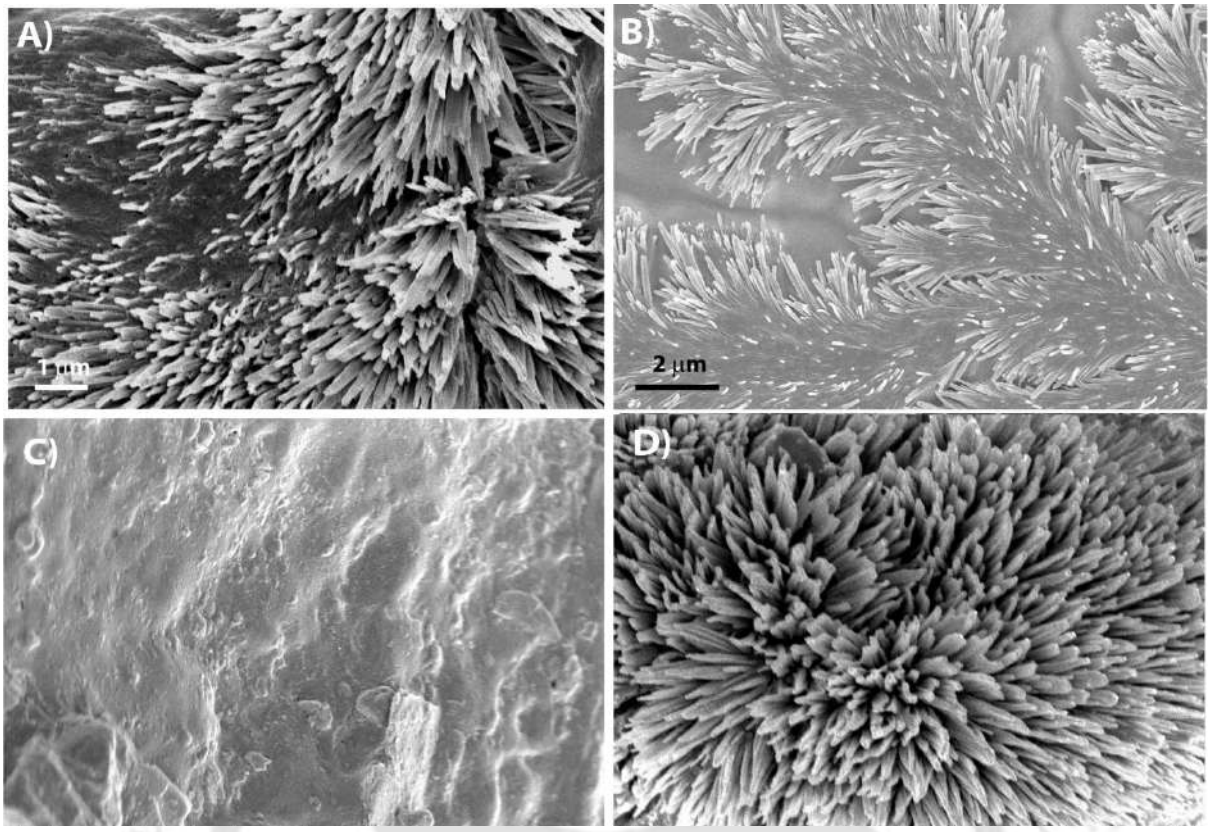

Figure 2.3 FESEM images of **PA-2.1** under various conditions. (A) 1 wt. % hydrogel of **PA-2.1** prepared by dissolving it in water and immediate addition of base, (B) 1 wt. % hydrogel of **PA-2.1** prepared by dissolving it in 20 mM phosphate buffer at pH 9, (C) Solution of **PA-2.1** at pH 3 and (D) sample from (A) after one cycle of gel–sol–gel transition. (A) Photographs of rhodamine B-loaded hydrogel and its gel–sol–gel transitions induced by the addition of acid or base (B) CD spectra of **PA-2.1** hydrogel through one cycle of gel-sol-gel transition through change in pH.

The gelation mechanism can be summarized from the obtained experimental results. Five Lys residues of the **PA-2.1** peptide makes it highly soluble under neutral or acidic condition. At this sol state, the peptide amphiphile adopts no particular secondary structure and remain in random coil conformation. This random coil structures thus prevent the molecule toward any kind of self-assembly. Upon addition of base, when pH of the system exceeds the pK_a value of Lys side chain amines, the amine groups get deprotonated and the solubility decreases drastically. Under this condition, **PA-2.1** molecules immediately arrange themselves in an anti-parallel -sheet conformation and these -sheets results into the formation of the hydrogel through higher order aggregation as shown in Scheme 2.1 B. Importantly, the self-aggregation into the -sheet and hydrogelation is found to be an extremely fast process in this particular case. Thus, though a favorable pH is obtained for disulfide bond formation, the Cys residues could not be connected to form the dimer of **PA-2.1**. The -sheet formation presumably restricted the –SH groups to come to close proximity and form the disulfide linkages. One interesting observation that needs to pointed out that the dimer of **PA-2.1** failed to show any particular secondary structure even at

elevated pH. A probable reason for this observation could be the presence of the GABA unit which restricted the hairpin formation which is a common phenomenon for ^{D}Pro-^{L}Pro peptides.[183, 185]

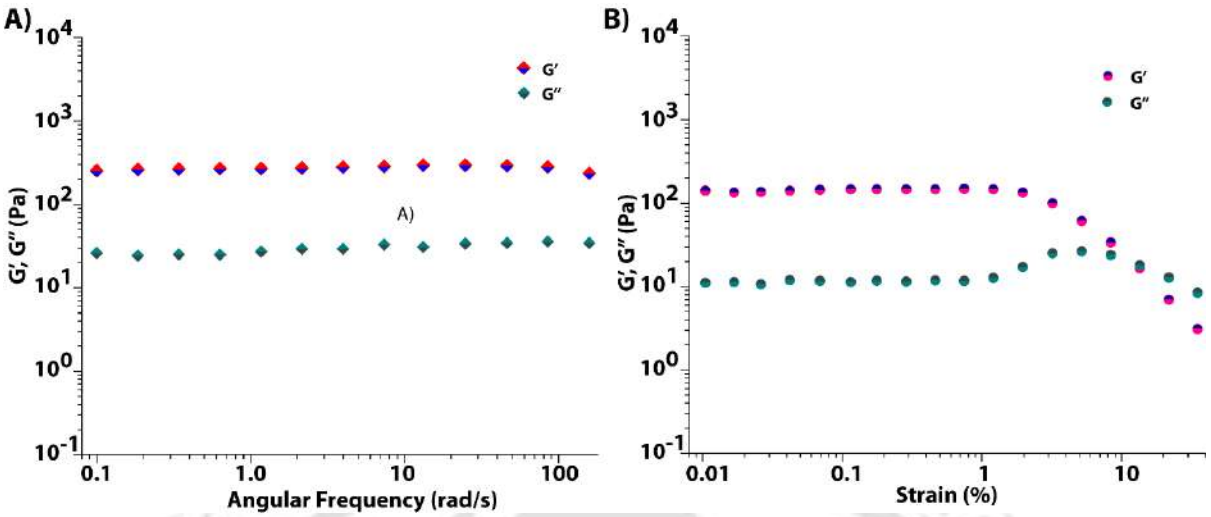

Figure 2.4 (A) Frequency sweep and (B) amplitude sweep data for 1 wt. % hydrogel of **PA-2.1** (pH 9) at room temperature.

As the hydrogelation process of **PA-2.1** is understood, its material property was explored. The gel-sol transition temperature (Tg) was measured using dropping ball method The hydrogel could be heated up to 85 °C, after which the water from the gel started evaporating out leaving behind the dry xerogel. No clear Tg was found. This is an interesting and rare property found among supramolecular hydrogels. detailed rheology study was performed. The rheological analyses of a 1 wt. % hydrogel (pH 9) at room temperature showed that the storage modulus (G') was considerably higher than the loss modulus (G") over a range of applied frequencies (Figure 2.4 A). The G' value obtained was in the range of 250 Pa and the ratio, G'/G" was ~ 10 which signifies strong gel character. When the % strain was varied at a particular frequency (1 rad/s), the G' remained higher than that of G" upto 5% and then they cross each other signifying melting of the hydrogel to sol (Figure 2.4 B). Based on these data, we assumed that the hydrogel might have the thixotropic character.[193, 194] Further, the thixotropic behavior was checked for a 1 wt. % hydrogel of **PA-2.1** (pH 9). Cyclic strain time sweep experiment was performed where strain was applied to break the hydrogel and when the applied strain was released, the hydrogel recovered its initial mechanical strength and the mechanical strength is sustained even after 4 cyclic strain cycles (Figure 2.5 A).

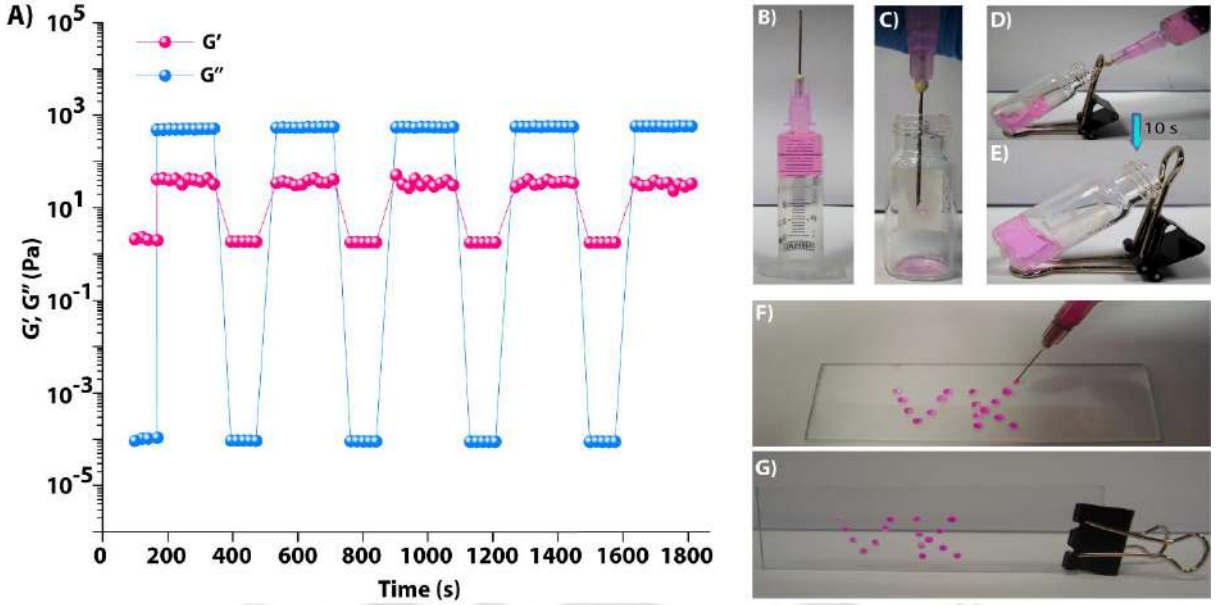

Figure 2.5 (A) Cyclic strain time sweep data for 1 wt. % hydrogel of **PA-2.1** (pH 9) at room temperature. (B-G) Visual presentation of injectability of the **PA-2.1** hydrogel. (B) The hydrogel in a syringe, (C) injecting the hydrogel from (B), (D) the injected sol in (C) and (E) the same sol within 10 s to form hydrogel. Dropping of hydrogel from syringe on a glass-plate. (F) Drop casting the hydrogel from (B) and (G) the drops turn into hydrogel within 10 s.

The clinical value of a peptide hydrogel is enhanced by its injectable property. The result obtained in Figure 2.5 A indicated injectable behavior. A Rhodamine B loaded hydrogel was prepared in a syringe (Figure 2.5 B) and when the plunger was pressed slowly, the hydrogel came out easily as a liquid (Figure 2.5 C-D). The sol turned into sol within 10 seconds as can be seen from Figure 2.5 E. In another experiment, small drops of the hydrogel were cast from the syringe on a glass plate and when held vertically, no downward movement could be seen from these drops (Figure 2.5 F-G). Thus, it can be concluded that the presented hydrogel is thixotropic in nature and has injectable property.

2.4 CONCLUSION

To summarize, a peptide amphiphile with alternate hydrophobic-hydrophilic amino acid residues is reported. Under neutral or acidic condition, the peptide remain in random coil conformation and self-assemble quickly to form anti-parallel β-sheet when the pH of the system is adjusted above 9. The β-sheet arrangement further leads to hydrogelation through hierarchical self-assembly process. The pH and secondary structure instructed hydrogelation is found to be a reversible process with no loss/change in aggregation pattern even after several cycles. The hydrogel showed strong rheological behavior and is found to have thixotropic nature. The hydrogel thus can be further explored as an injectable smart soft material for drug delivery purposes.

Chapter-3: Mannose-Decorated Composite Peptide Hydrogel with Thixotropic and Syneresis Properties and its Application in Treatment of Leishmaniasis

3.1 INTRODUCTION

Over the last couple of decades, supramolecular self-assembled soft materials such as hydrogels have gained tremendous attention due to their potential biomedical and therapeutic applications.[38, 195] In this regard, peptide-based hydrogels have come to the forefront due to the remarkable combination of properties such as biodegradability, biocompatibility, tunability of hydrophilic-lipophilic balance (HLB), the introduction of stimuli responsiveness, adjustable mechanical properties, etc.[18, 187, 196-202] Peptide hydrogels are often used in biomedical applications such as cell-proliferation, tissue-culture scaffolds, drug entrapment, localized drug delivery, and as antimicrobial agents, to name a few.[7, 203-206]

Targeted drug delivery is a demanding area of research, as it minimizes side effects and provides better results with a lesser dose of drugs. To this end, Leishmaniasis is a critical but relatively neglected vector-borne disease.[207] The disease, caused by the protozoan parasite *Leishmania donovani* (*L. d.*), if untreated becomes fatal. *Leishmania* invades the reticuloendothelial system of the mammalian host and replicates within the macrophages. The parasites usually enter macrophages through phagocytosis, and this process is facilitated by various ligand-receptor interactions between *L. donovani* and macrophages. [208, 209] One such receptor is mannose receptors present at the surface of macrophages. [210-213] Therefore, anti-Leishmanial drugs can be delivered to infected macrophages using mannose functionalized carriers. [214-217] Peptide-based hydrogels have recently entered the avenue for potential drug-delivery systems.[218, 219] However, to the best of our knowledge, no such effort has been made to create peptide-based drug delivery vehicles to tackle Leishmaniasis. Systems that can target and deliver the therapeutics to the macrophages need to fulfil the following criteria, a) the hydrogel must be decorated with mannose to target the mannose receptors; b) must possess injectability (shear thinning) as the drug loaded hydrogels should be administered locally. Fulfilling both the criteria in a single peptide-based hydrogel is a challenging task.

In this regard, single component hydrogels sometimes lack the required functionality or essential properties for a particular application. The solution lies in the coassembly of two or more components.[73, 220] Coassembled peptide hydrogels allow the incorporation of functional complexities without hampering the self-assembly behavior.[67, 74, 221] Composite hydrogels are generally prepared by combining one self-aggregating molecule with a non-aggregating molecule. In this process, the self-assembling unit leads to hydrogel formation, while the non-

assembling component brings the desired functionality required for a particular application. Therefore, with simple designs, systems with practical applications can be achieved with peptide coassembly.[68, 75, 222] Recently, the development of peptide hydrogels with the coassembly technique has proved to be an efficient breakthrough in medical sciences to design better therapeutic agents.[223, 224]

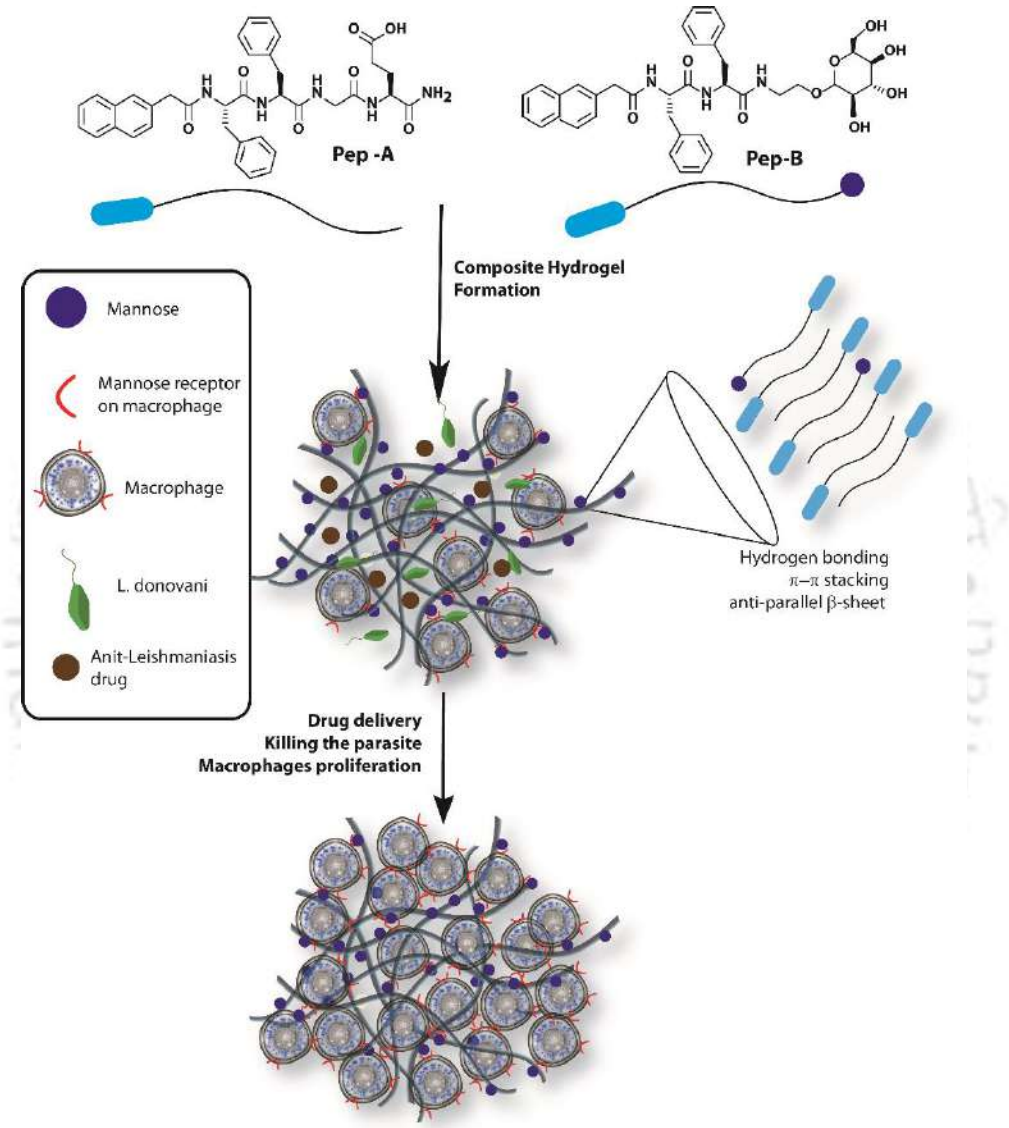

Scheme 3.1 (A) Chemical structures of the designed peptides, schematic representation of peptide coassembly. (B) Pictorial representation of hydrogel scaffold mediated intracellular drug delivery for Leishmania treatment.

In the present work, we have devised a mannose-decorated peptide coassembled hydrogel. Nap-FF is a known peptide hydrogelator forming nanofibrous structures.[225] Taking advantage of the self-assembling ability of Nap-FF, here, we prepared the hydrogelator, Nap-FFGE-NH_2 (**Pep-A**, Scheme 3.1). The introduction of Gly-Glu (GE) segment to the Nap-FF peptide was purposefully done to make the peptide anionic in nature and soluble in the basic buffer. **Pep-A** is coassembled

with a nongelator peptide, Nap-FF-mannosyl (**Pep-B**). As Nap-FF is common in both sequences, the gelator peptide helps sequestration of the mannosyl containing non-gelator peptide during the aggregation process, resulting in a mannosyl-decorated hydrogel scaffold. The composite hydrogel provides an excellent three-dimensional (3D) matrix for macrophage growth and survival. As anticipated, the composite hydrogel was found to deliver the anti-Leishmaniasis drug to the macrophages to kill the parasite effectively.

3.2 EXPERIMENTAL SECTION

3.2.1 General

Rink amide MBHA resin, Fmoc-protected amino acids, HBTU and HOBT were procured from GL Biochem, China. All other fine chemicals were procured from Sigma Aldrich, USA. To prepare samples, Milli-Q water with a conductivity of less than 2 $mScm^{-1}$ was used. Chromatographic purifications were performed on a Luna 5 µm (C18, 250x10 mm) column (Phenomenex) and analytical HPLC were performed on a Luna 5 µm (C18, 250 × 4.6 mm) column (Phenomenex) using a Dionex Ultimate 3000 HPLC. UV-Visible spectra were recorded on a PerkinElmer Lambda 750 spectrometer, while fluorescence measurements were performed on a Fluoromax 4 (Horiba) spectrophotometer. Standard 10 mm-path quartz cuvettes were used for all spectroscopic measurements. ^{1}H NMR, ^{13}C NMR were recorded with a Bruker Ascend 400 MHz (Bruker, Coventry, UK) spectrometer and referenced to deuterated solvents. ESI-MS were performed with a Q-Tof Micro Quadrupole mass spectrophotometer (Micromass). FESEM images were taken using Zeiss, Sigma microscope. Atomic Force Microscope images were taken on Nanosurf Flex-Axiom (Nanosurf, Switzerland). CD experiments were performed on a Jasco J-1500 spectropolarimeter.

3.2.2 Synthetic protocols

Synthesis of Nap-FFGE-NH_2 (Pep-A)

The peptide was synthesized using solid phase peptide synthesis technique employing Rink-amide MBHA resin as the solid support. Sequence elongation at the N-terminus was performed by coupling the appropriate Fmoc protected amino acids (3 equiv.) under standard conditions employing HBTU (3 equiv.) and DIPEA (6 equiv.) as coupling reagents in DMF. Fmoc deprotection was achieved by treating the resin bound peptide with 20% piperidine in DMF. The peptide was cleaved from the resin using a cocktail of TFA/TES in a ratio of 9.5:0.5. Precipitation from dry ether followed by purification using semi-prep HPLC (acetonitrile/water system as the eluent) and lyophilisation provided the pure peptides. ^{1}H NMR (600 MHz, DMSO-d_6) δ (ppm): 12.11 (s, 1H), 8.26

– 8.20 (m, 2H), 7.90 (d, *J* = 8.1 Hz, 1H), 7.85 (d, *J* = 7.8 Hz, 1H), 7.76 (dd, *J* = 22.5, 8.1 Hz, 2H), 7.58 (s, 1H), 7.49 – 7.43 (m, 2H), 7.34 (d, *J* = 2.1 Hz, 1H), 7.24 – 7.08 (m, 10H), 4.52 (ddd, *J* = 12.8, 6.6, 3.4 Hz, 2H), 4.24 – 4.19 (m, 1H), 3.81 – 3.68 (m, 2H), 3.58 – 3.46 (m, 2H), 3.01 (ddd, *J* = 35.1, 13.9, 4.5 Hz, 2H), 2.83 (dd, *J* = 14.0, 9.2 Hz, 1H), 2.75 – 2.68 (m, 1H), 2.23 (ddd, *J* = 9.3, 6.5, 2.9 Hz, 2H), 1.99 – 1.91 (m, 1H), 1.77 – 1.71 (m, 1H). ^{13}C NMR (151 MHz, DMSO-d_6) δ (ppm): 174.55, 173.66, 171.83, 170.48, 138.13, 138.00, 134.22, 133.34, 132.17, 129.67, 129.62, 128.57, 128.42, 128.01, 127.93, 127.89, 127.81, 127.69, 126.79, 126.66, 126.47, 125.96, 54.66, 54.23, 52.21, 42.62, 42.56, 37.75, 30.63, 27.68.

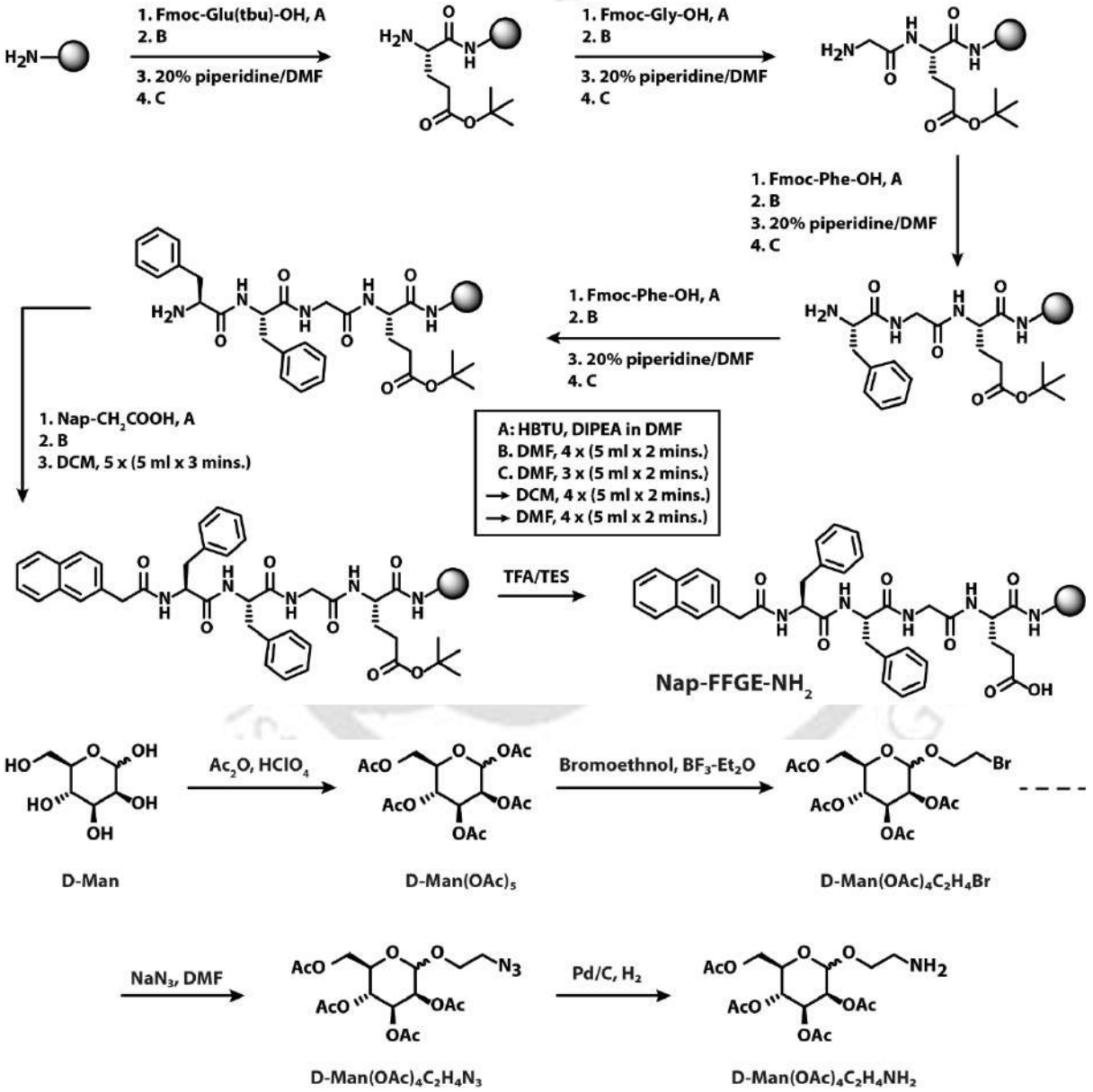

Synthesis of Man(OAc)$_5$

15 ml of acetic anhydride was taken in a round bottomed flask and stirred in ice bath for some time under argon atmosphere. Another separate mixture of 4.5 ml of acetic anhydride and 100 l perchloric acid ($HClO_4$) (665 moles) was prepared and maintained in ice bath. This mixture was dropwise added in cold condition to the previous acetic acid solution. Then, mannose (5 g, 0.02 moles) was added in small portions over a duration of 1 hour under cold and argon atmosphere for complete solubilization. Completion of reaction was confirmed with TLC in 4:6 ethyl acetate/hexane. The TLC was visualized by charring method. Solvent was reduced in a rotary evaporator and the obtained material was dissolved in ethyl acetate and washed twice with water and once with brine. The organic portions were collected, dried over anhydrous sodium sulphate and concentrated to obtain a pale-yellow oil. ^{1}H NMR (600 MHz, $CDCl_3$) δ (ppm): 6.07 (d, *J* = 2.0 Hz, 1H), 5.33 (d, *J* = 6.3 Hz, 2H), 5.24 (s, 1H), 4.27 (dd, *J* = 12.4, 4.8 Hz, 1H), 4.10 – 4.01 (m, 2H), 2.16 (d, *J* = 5.0 Hz, 6H), 2.08 (s, 3H), 2.04 (s, 3H), 1.99 (s, 3H). ^{13}C NMR (151 MHz, $CDCl_3$) δ (ppm): 170.70, 170.04, 169.79, 169.57, 168.11, 90.58, 70.58, 68.72, 68.31, 65.48, 62.08, 20.89, 20.66.

Synthesis of Man(OAc)$_4$C$_2$H$_4$Br

Man(OAc)$_5$(1 g, 2.56 mmol) was dissolved in dry DCM at stirred in ice bath. Then bromoethanol (5.12 mmol) was added under ice cold condition. Then to this solution, BF_3-Et_2O (12.8 mmol) was added under argon atmosphere in dark and ice-cold condition. Reaction mixture was stirred under cold condition for 1 h and then in room temperature for 12 hours. After completion, the reaction was dropped in cold water, aqueous portion was extracted with DCM. Organic portions were washed with saturated sodium bicarbonate, water and brine, then dried over anhydrous sodium sulphate and concentrated to obtain a white solid. ^{1}H NMR (600 MHz, $CDCl_3$) δ (ppm): 5.34 (dd, *J* = 10.1, 3.4 Hz, 1H), 5.31 – 5.25 (m, 2H), 4.87 (s, 1H), 4.27 (dd, *J* = 12.8, 6.0 Hz, 1H), 4.12 (d, *J* = 10.2 Hz, 2H), 3.97 (dt, *J* = 11.2, 6.3 Hz, 1H), 3.88 (dt, *J* = 11.2, 5.7 Hz, 1H), 3.51 (t, *J* = 6.0 Hz, 2H), 2.15 (s, 3H), 2.10 (s, 3H), 2.05 (s, 3H), 1.99 (s, 3H), 1.65 (s, 1H).^{13}C NMR (151 MHz, $CDCl_3$) δ (ppm): 170.68, 170.08, 169.91, 169.81, 97.75, 69.42, 69.01, 68.95, 68.49, 65.98, 62.41, 29.67, 20.92, 20.79, 20.75, 20.72.

Synthesis of Man(OAc)$_4$C$_2$H$_4$N$_3$

Man(OAc)$_4$C$_2$H$_4$Br (600 mg, 1.3 mmol) and sodium azide (10.5 mmol) was weighed in a round bottomed flask and sealed. The reaction set-up was purged with argon for 30 minutes and then dry DMF was added and stirred at 60 °C for 14 hours. Thereafter, the reaction was cooled to room

temperature and extracted with ethyl acetate and washed several times with cold water to remove DMF. The organic portion was concentrated to obtain a yellow oil. ^{1}H NMR (600 MHz, $CDCl_3$) δ (ppm): 5.36 (dd, *J* = 10.0, 3.4 Hz, 1H), 5.33 – 5.26 (m, 2H), 4.87 (s, 1H), 4.29 (dd, *J* = 12.3, 5.3 Hz, 1H), 4.12 (dd, *J* = 12.3, 2.4 Hz, 1H), 4.05 (ddd, *J* = 10.0, 5.3, 2.4 Hz, 1H), 3.87 (ddd, *J* = 10.6, 7.1, 3.6 Hz, 1H), 3.67 (ddd, *J* = 10.6, 6.0, 3.5 Hz, 1H), 3.47 (ddd, *J* = 20.1, 6.5, 3.5 Hz, 2H), 2.16 (s, 3H), 2.11 (s, 3H), 2.05 (s, 3H), 1.99 (s, 3H), 1.60 (s, 2H). ^{13}C NMR (151 MHz, $CDCl_3$) δ (ppm): 170.68, 170.07, 169.86, 169.80, 97.75, 69.39, 68.85, 67.08, 65.98, 62.46, 50.36, 20.92, 20.78, 20.75, 20.70.

Synthesis of $Man(OAc)_4C_2H_4NH_2$

$Man(OAc)_4C_2H_4N_3$ (0.5 g) was dissolved in dry THF. Then palladium/charcoal was added and the reaction was sealed. Hydrogen gas was constantly purged into the reaction until completion of reduction. The reaction was then filtered through sintered glass funnel and washed with THF. The collective organic portion was concentrated to obtain a yellow oil. ^{1}H NMR (600 MHz, $CDCl_3$) δ (ppm): 5.27 (d, *J* = 1.4 Hz, 2H), 4.85 (dd, *J* = 18.4, 1.8 Hz, 1H), 4.27 (d, *J* = 12.1 Hz, 1H), 4.14 (dd, *J* = 12.1, 2.8 Hz, 1H), 4.04 – 3.98 (m, 1H), 3.79 (dq, *J* = 9.8, 3.7, 3.0 Hz, 2H), 3.56 (d, *J* = 3.1 Hz, 1H), 3.43 (d, *J* = 5.0 Hz, 1H), 2.20 – 1.99 (m, 12H).^{13}C NMR (151 MHz, $CDCl_3$) δ (ppm): 170.71, 170.42, 170.19, 169.72, 97.67, 69.36, 69.02, 68.73, 67.51, 66.15, 62.53, 39.10, 23.21, 20.87, 20.71, 15.26.

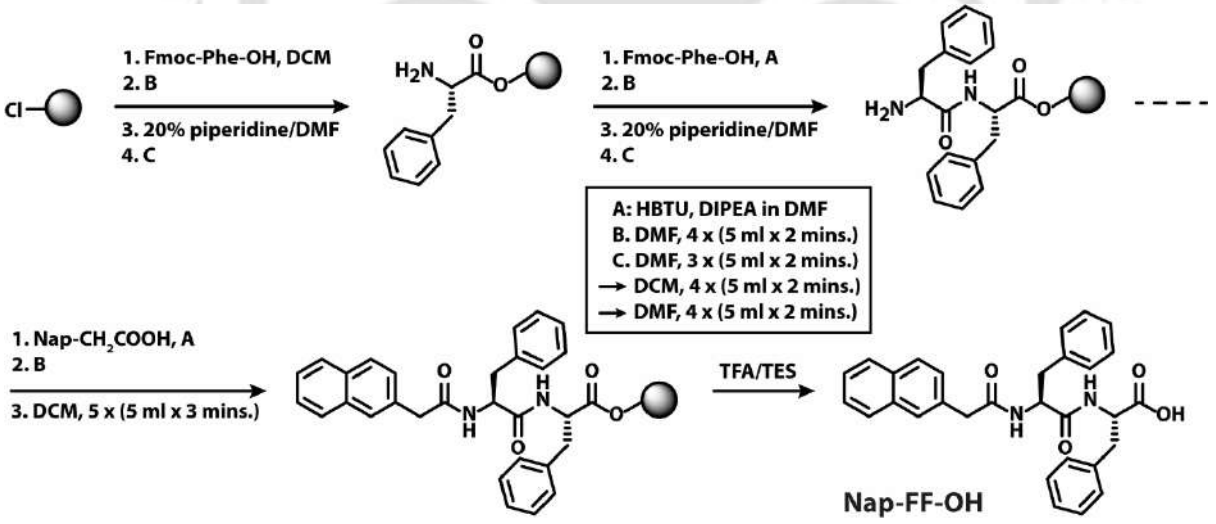

Synthesis of Nap-FF-OH

The peptide was synthesized using solid phase peptide synthesis technique employing trityl chloride resin as the solid support. To the dried resin, dry DCM was added for swelling. Then a DCM mixture of Fmoc-Phenylalanine (2 equivalents) and DIPEA (4 equivalents) was added and stirred overnight. Sequence elongation at the N-terminus was performed by coupling the appropriate Fmoc protected amino acids (3 equiv.) under standard conditions employing HBTU

(3 equiv.) and DIPEA (6 equiv.) as coupling reagents in DMF. Fmoc deprotection was achieved by treating the resin bound peptide with 20% piperidine in DMF. The peptide was cleaved from the resin using a cocktail of TFA/TES in a ratio of 9.5:0.5. Precipitation from dry ether followed by lyophilisation provided the crude peptide which was used for further coupling reaction with compound *4*. ^{1}H NMR (600 MHz, $CDCl_3$) δ (ppm): 7.85 (s, 1H), 7.77 (t, *J* = 9.3 Hz, 2H), 7.57 (s, 1H), 7.52 (s, 2H), 7.21 (d, *J* = 7.4 Hz, 4H), 7.10 (s, 1H), 7.01 (s, 2H), 6.91 (d, *J* = 17.9 Hz, 4H), 6.36 (s, 1H), 5.85 (s, 1H), 4.73 (s, 1H), 4.61 (s, 1H), 3.69 (s, 3H), 3.65 (d, *J* = 10.6 Hz, 1H), 3.04 (s, 1H), 2.97 (s, 2H), 2.91 (s, 1H). ^{13}C NMR (151 MHz, $CDCl_3$) δ (ppm): 173.40, 170.95, 135.89, 133.47, 132.53, 129.46, 129.39, 129.23, 129.17, 128.73, 128.52, 128.49, 128.36, 128.27, 127.75, 127.70, 127.09, 126.98, 126.50, 126.34, 126.05, 54.06, 53.22, 43.52, 43.42, 38.33, 37.58.

Synthesis of Nap-FF-Mannosyl (Peptide B)

Nap-FF-OH (0.8 g, 1.72 mmol) and HBTU (0.8 g, 2.1 mmol) were weighed in a round bottomed flask and purged sufficiently with argon. Dry DCM and DIPEA (0.8 ml, 5.2 mmol) was added under argon atmosphere and the mixture was stirred in ice bath for 30 minutes. Then a separately prepared solution of $Man(OAc)_4C_2H_4NH_2$ in dry DCM was added slowly with the help of a syringe to the previous solution. The reaction was stirred at room temperature under argon atmosphere for 12 hours. After that, DCM was reduced in a rotary evaporator and the crude mixture was purified with column chromatography using 1:4 ethyl acetate/hexane to obtain a white solid. This solid compound was redissolved in dry methanol and treated with NaOMe (4 equiv.) and stirred at room temperature for 12 hours. Then the solvent was removed and a white sticky solid was obtained which was washed several times with ether to obtain a white powder. The crude material was purified with semi-prep HPLC (acetonitrile/water system as the eluent) and lyophilized to obtain the pure product. ^{1}H NMR (600 MHz, DMSO-d_6) δ 8.27 (d, *J* = 22.6 Hz, 1H), 8.14 (d, *J* = 8.0 Hz, 1H), 7.84 (s, 1H), 7.75 (d, *J* = 8.4 Hz, 2H), 7.60 (s, 1H), 7.47 (d, *J* = 2.1 Hz, 2H), 7.29 – 7.08 (m, 10H), 6.98 (s, 1H), 6.76 – 6.48 (m, 2H), 4.86 – 4.42 (m, 7H), 3.05 – 2.90 (m, 2H), 2.87 – 2.67 (m, 2H), 2.57 – 2.48 (m, 3H), 1.91 (s, 1H), 1.37 – 1.19 (m, 4H). ^{13}C NMR (150 MHz, DMSO-d_6) δ 177.71, 171.93, 132.16, 129.53, 129.46, 128.68, 128.58, 128.15, 127.81, 127.66, 126.62, 126.20, 99.93, 73.59, 70.97, 70.46, 67.07, 65.66, 61.27, 53.90, 42.27, 24.67, 22.66, 17.64, 12.79.

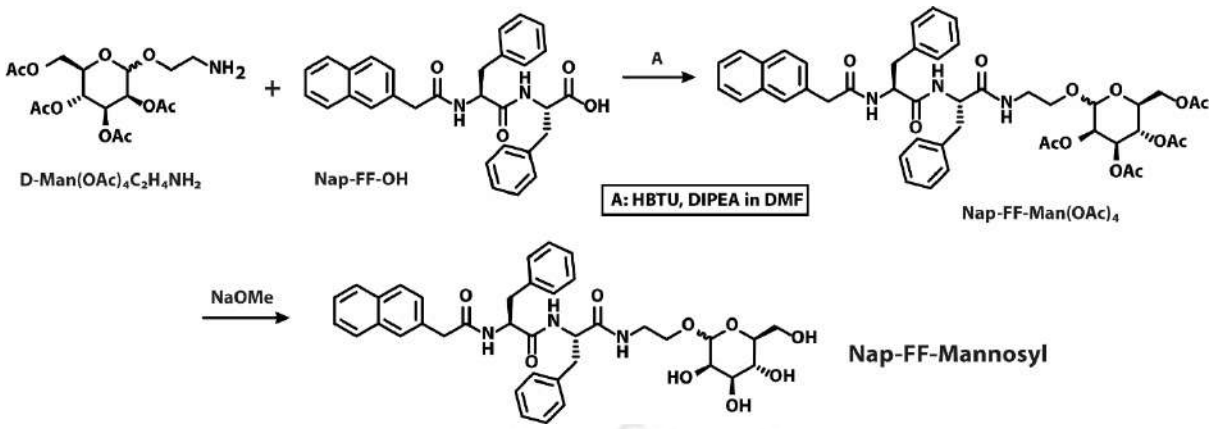

3.2.3 Preparation of Hydrogel

A) Gel A: 5 mg of Pep-A (HFIP treated) was added into 250 L of sodium phosphate buffer (pH 11, 20 mM) and dissolved by sonication for 1 min followed by heating and gentle shaking for 5 mins at 50 °C. The solution was allowed to cool down to room temperature. To this solution, solid GDL was added and tapped gently for homogenization followed by incubation at room temperature to get self-supporting hydrogel. Final concentration of Pep-A was 30 mM.

B) Gel B: 4 mg of Pep-A (HFIP treated) was mixed with 1 mg of Pep-B (from DMSO stock, 4 μL, i.e., 4 mL/mg). 250 μL sodium phosphate buffer (pH 11) was added to the peptide mixture and dissolved by sonication for 1 min followed by heating and gentle shaking for 5 mins at 50 °C. The solution was allowed to cool down to room temperature. To this solution, solid GDL was added and tapped gently for homogenization followed by incubation at room temperature to get self-supporting hydrogel. Final concentrations of Pep-A and Pep-B were 24 and 6 mM respectively.

3.2.4 NMR Studies

^{1}H NMR spectra of pure peptides were recorded in DMSO-d_6. For determination of hydrogen bonding interactions, 5 mM peptide solutions were prepared in DMSO-d_6 containing different amounts of water. For studying the pH and temperature dependent aggregation, 7.5 mM peptide solution was prepared in NaOD/D_2O. Then GDL was added and the solution immediately transferred to NMR tube. NMR spectra was recorded immediately and after every 5 minutes for 35 minutes. After 24 hours, spectra of the same samples were recorded at desired temperatures. 2D-NMR spectra of Gel-A and Gel-B (5 mM) were recorded in 30% D_2O/ DMSO-d_6.

3.2.5 UV-Vis Spectroscopy

A series of peptide solutions were prepared with increasing concentrations in 20 mM pH 7 buffer. All solutions were incubated in room temperature for 24 hours before recording the spectra. Absorbance values obtained at 270 nm were plotted against the corresponding concentrations to obtain the minimum aggregation concentration of the peptide.

3.2.6 Fluorescence Spectroscopy

Gelation kinetics of Gel-A and Gel-B was demonstrated by decrease in the fluorescence intensity at 337 nm. 1 wt.% hydrogels were prepared in 1 ml fluorescence cuvettes and fluorescence kinetics were performed at excitation wavelength: 275 nm. Gelation time of the hydrogels were determined from the tangents drawn to the two different slopes of the curve.

3.2.7 FT-IR Spectroscopy

For FT-IR analyses, small pinch of lyophilized gels was mixed with KBr to form a thin pellet. The pellets were mounted in the IR sample holder and scanned from 800-4000 cm^{-1}. The results were subtracted from the background spectra of dried KBr pellet.

3.2.8 X-Ray Diffraction

X-ray diffraction (PXRD) studies on samples were carried out using a high-resolution Rigaku Micromax-007HF diffractometer with a Cu-Ka monochromated beam (λ= 15406 Å) produced at 40 kV and 40 mA. Lyophilized gel samples were scanned from 2-theta angle range of 3-40° at a step size of 0.021 and a count time of 1.6 s per step.

3.2.9 Rheology

The viscoelastic properties of the hydrogel were characterized using rheometer (AntonPaar MCR 102) equipped with a 20 mm parallel plate (with 0.3 mm zero gap) measuring system at 25 °C. A strain sweep test was performed first to identify the linear viscoelastic region (LVR) over a range from 0.01 to 100 % strain at a fixed oscillatory frequency of 1 rad/s. The LVR can be defined as, where strain has no impact upon G' and G''. Further, the mechanical strength of the gel was determined from oscillatory test *i.e.*, frequency sweep, which was carried out under an appropriate strain (γ = 0.1 %) selected from the LVR with the frequency ranging from 0.1 to 1000 rad/s at 25 °C. For time dependent gelation studies, the experiment was set up at constant strain of 0.5% and constant frequency of 5 Hz. The whole experiment was done at 25 °C and measured for 2 hours. Solutions of 1 wt.% gelator concentration were prepared and samples were taken from

the hydrogel at different time interval. Each sample analysed for one hour. The plot was obtained by combining the G' and G" values with time.

3.2.10 FESEM and AFM

A minute amount of 1 wt.% hydrogel samples were extracted with a pointed spatula and spread uniformly on silicon wafers. Samples were air dried for several days before taking the FESEM images. For AFM analyses, 5 μL of 1 mM gelator solutions were cast on silicon wafers and thoroughly air dried for several days before analyses.

3.2.11 Enzymatic Degradation Study

0.4 mg of Pep-A and Pep-B were separately dissolved in pH 7.4 phosphate buffer containing Proteinase K at a concentration of 2 U/mL. Solutions were incubated at 37 °C for 24 hours. 10 microliters of the solutions were removed at different time intervals and the reduced volume was adjusted with pH 7 buffer. The removed samples were diluted with acetonitrile and analysed through HPLC.

3.2.12 Stability in Cell Culture Media

500 microliters of Gel-A and Gel-B were prepared in separate vials, and to each vial, 600 microlitres of culture media (DMEM supplemented with10% heat-inactivated fetal bovine serum,100 U/mL penicillin, and 100 μg/mL streptomycin) was added and incubated at 37 °C for 24 hours. The internalization of media and stability of hydrogels were monitored through visual photographs.

3.2.13 Cell Culture and Infection

The murine macrophage cell line RAW264.7 was cultured at 37 °C with 5% CO_2 in DMEM (Invitrogen, Carlsbad, CA, USA) supplemented with 10% heat-inactivated FBS, 100 μg/ml streptomycin and 100 U/ml penicillin. L. donovani (MHOM/IN/1983/AG83) parasites were cultured in medium M199 (Invitrogen) with Hanks salt containing HEPES (12 mM), L-glutamine (20 mM), 10% heat-inactivated fetal bovine serum (FBS), 50 U/ml penicillin and 50 μg/ml streptomycin (Invitrogen) as promastigotes. For in vitro infection, macrophages were infected with L. donovani promastigotes at a parasite: cell ratio of 10:1. For 2 D system of cell culture, gelation mixture was prepared and plated onto coverslips and allowed to get solidified. After 24 hours, macrophage cells were resuspended in DMEM medium and plated onto the solidified gel on coverslips. After 4 hours, when cells adhered then cells were infected and further analysis was conducted. For 3 D system of cell culture, macrophage cells were dissolved in gelation mixture and cell culture medium DMEM was added to it. The mixture was then overlayered on coverslips and left for 24

hours to solidify. Later, these were processed for microscopy experiments. For gel internalisation studies, Gel-A or Gel-B was allowed to solidify and then it was stripped with sterilised needle into small pieces and gel pieces were dissolved in DMEM medium and incubated with cells plated onto cell culture dishes, allowing them to get internalised.

3.2.14 MTT Assay

MTT assay for estimating cellular toxicities or cell viability or cell proliferation was conducted with MTT kit according to manufacturers' instructions following protocol guidelines from Sigma.

3.2.15 Fluorescence Microscopy

Macrophages were plated onto 18 mm^2 coverslips and cultured overnight. The cells were cultured in 2D or 3D system as mentioned before and infected with L. donovani promastigotes. Either Rhodamine dye or Drug Amphotericin conjugated to rhodamine was added in gelation mixture. Cells washed twice in PBS, and fixed with methanol for 10 min at room temperature. After washing, the cells were stained with DAPI (1 µg/ml) in PBS plus 10 µg/ml RNase A to label the nucleus, mounted on slides and visualized under fluorescence microscope. The images thus captured were analysed using Adobe Photoshop software.

3.3 RESULTS AND DISCUSSION

3.3.1 Formation and characterization of composite hydrogel

All studies were performed with HFIP treated peptides to ensure no pre-existing aggregation. The hydrogel of **Pep-A** (Gel-A) was prepared by dissolving it in phosphate buffer (pH 11, 20 mM) in the presence of gluconolactone (GDL). The basic pH allows the peptide to get dissolved as the side chain carboxylic acid of Glutamic acid gets deprotonated and thereby enhances the solubility. However, with this increased solubility, the peptides do not tend to aggregate at this pH. The slow hydrolysis of GDL to gluconic acid[226, 227] decreases the pH of the system to a point where the solubility of the peptide is optimum. Therefore, they self-assemble to form the hydrogel. In addition, as reported on many previous occasions, the slow pH control allows the formation of homogeneous assembly.[228] After 24 hours of incubation, the final pH of the hydrogel was measured as 6.8 with no further change in the value, suggesting complete consumption of GDL. The minimum gelation concentration of the hydrogel of **Pep-A** was recorded as 0.5 wt.% (7.5 mM). Below this concentration, though a highly viscous material was obtained, it could not have sustained the inverted vial test as an instant downward flow of the liquid was observed upon inversion.

In order to understand the self-assembly process, the presence of different supramolecular interactions was extensively investigated with the help of NMR analysis. DMSO was found to be a non-gelling solvent for **Pep-A**. No shift in the peak positions as well as peak patterns were observed in the ^{1}H NMR spectra with varying concentrations of **Pep-A** (data not shown). To evaluate the role of hydrogen bonding in the self-aggregation of **Pep-A**, ^{1}H NMR spectra were recorded for solutions of the peptide in different compositions of DMSO-d_6 and H_2O.[229, 230] As the peptide failed to self-assemble in DMSO, the peaks in DMSO-d_6 were considered as the reference for this study. With the increase in water content, the aromatic protons (from the Phe and Naphthalene units) show an apparent up-field shift (blue box in Figure 3.1 A). Along with peak shifting, the spectra also become disfigured due to self-assembly.[229] It is worth mentioning that it was difficult to get a clear spectrum beyond 40% water as the peak corresponding to H_2O masked most of the spectrum. However, the clear up-field shift of the aromatic protons suggests the presence of stacked aromatic groups as the molecules self-aggregate. On the other hand, amide protons undergo down-field shifts due to hydrogen bonding interactions (green lines). The C-terminal amide at 7.35 ppm undergoes a significant down-field shift.[231] This shift happened possibly because the amide is most exposed to the surrounding water and involved in maximum hydrogen-bonding interactions. The amide peaks at 8.3 ppm split upon increasing water content due to differential hydrogen-bonding interactions which are attributed to differential exposure of the amides to the added water. These peaks correspond to the diphenylalanine amides that lose exposure to external water and shift up-field upon increasing water content. This observation is attributed to $\pi - \pi$ interactions prevalent in phenylalanine groups in aqueous medium.

Next, the pH-dependent self-assembly behavior was also monitored by NMR analysis. A 5 mM **Pep-A** solution was prepared in D_2O containing 2 mM NaOD. After recording the spectrum, GDL was added, mixed quickly, and the spectra were recorded at different time intervals. To monitor the pH changes in the system during the NMR measurements, another sample with similar concentrations were prepared following a similar process, and the pH of this sample was recorded as a function of time. The pH changes of this sample were considered as the approximate pH of the sample under NMR experiment. From these two parallel experiments, it was observed that pH decreased from 11 (initial) to 7.2 (within 15 minutes) and down to 6.8 in 35 minutes. The recorded spectra and the corresponding pH values at different times are shown in Figure 3.1 B. As can be seen, apparent up-field shifts are visible for the aromatic protons for up to 40 minutes, and after that, no such changes were observed. However, due to the very broad nature of the spectra, it was

challenging to identify the amide protons. At pH 11, all the side chain residues of glutamic acid are deprotonated, and due to electrostatic repulsions, the peptide remains completely water-soluble. With GDL-assisted gradual decrease in pH, there is partial protonation of the carboxylates and the protons get trapped near the acid moieties and undergoes hydrogen-bonding. Due to partial neutralization of the negative charges, self-association takes place.

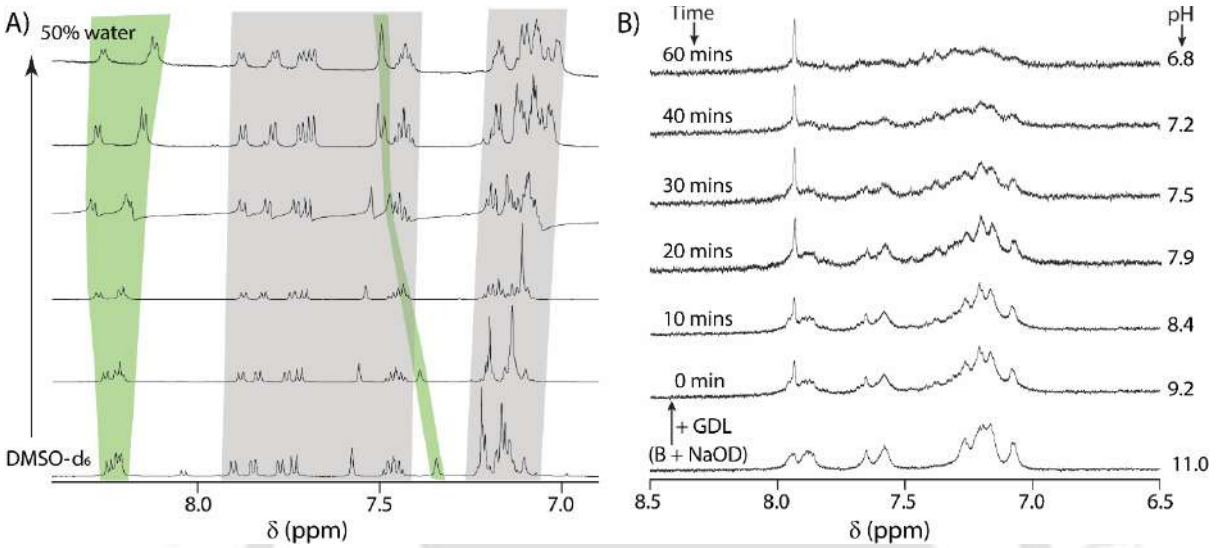

Figure 3.1 (A) Partial ^{1}H NMR spectra of Pep-A in DMSO-d_6 with varying water content. (B) Partial ^{1}H NMR spectra of **Pep-A** in NaOD/D_2O in presence of 2 mM GDL at different time interval along with the corresponding pH values. All experiments were carried out at RT.

As mentioned before, we aimed to create a mannose functionalized hydrogel. For that purpose, we designed another non-gelling peptide, **Pep-B** (Scheme 3.1). The peptide is designed by keeping the self-assembling unit, Nap-FF, and attaching a mannose unit at the C-terminal. The idea was to coassemble these two peptides where **Pep-A** will form the hydrogel network and **Pep-B**, due to the presence of Nap-FF unit will allow the smooth coassembly and thereby incorporate the mannose units within the hydrogel network. We anticipated that the coassembled hydrogel system would portray differential chemical and material properties. As expected, due to the presence of mannose unit, **Pep-B** showed higher and pH-independent solubility and was unable to form any hydrogel even at a very high concentration (30 mM). Next, the effect of **Pep-B** on the gelation process of **Pep-A** was investigated. Four different gelation sets (1 wt.%, pH 6.8) were prepared where mole percent of **Pep-B** was varied from 0% to 50%. All these solutions formed gels (Figure. 3.2 A). From rheology experiments, it was found that gel strengths decreased upon increasing the percentage of **Pep-B**. It was expected that the presence of **Pep-B** would weaken the hydrogels. Gel-A (made of only **Pep-A**) was found to be the strongest in the series. However, among the composite gels, Gel-B showed the highest strength (Figure 3.2 B and C). The strength

of the hydrogels weakened with a further increase in the **Pep-B** content. From the above observations, Gel-B was selected as the model system for our work.

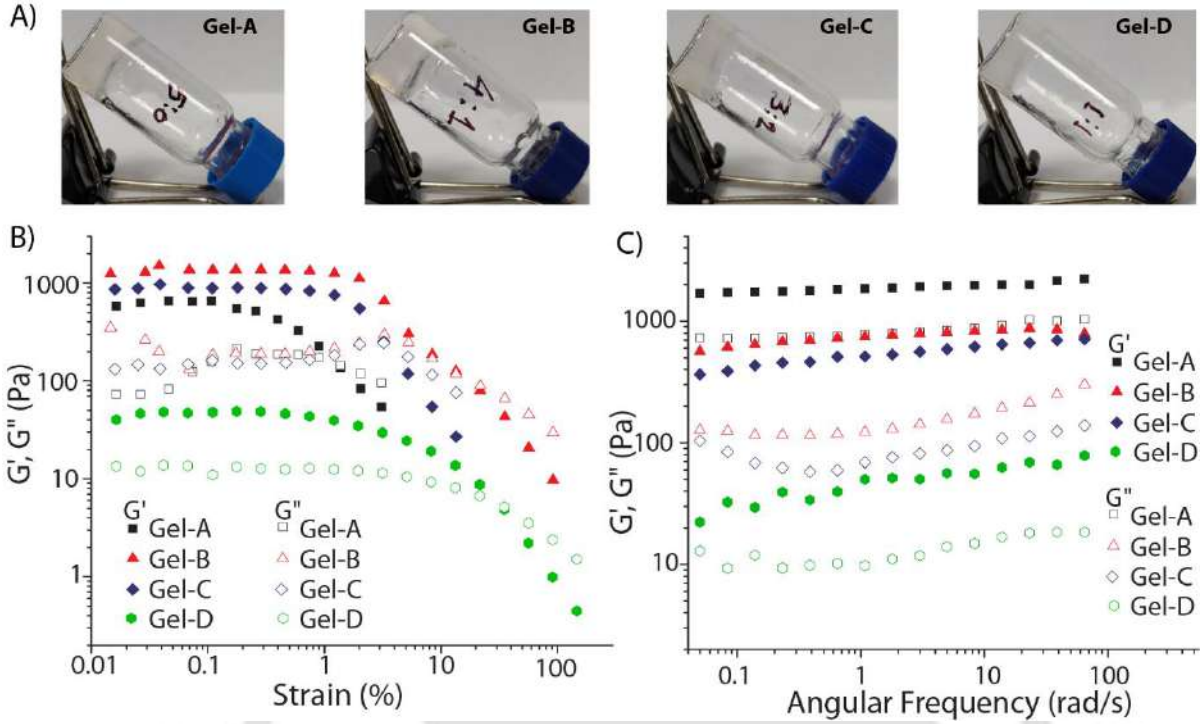

Figure 3.2 (A) Photographs of 1 wt.% hydrogels with varying Pep-A: Pep-B ratios. (B) Amplitude-sweep and (C) frequency sweep curves of hydrogels prepared in (A). All experiments were performed at RT.

In order to get some insight into the molecular interactions between **Pep-A** and **Pep-B** during self-assembly, we have performed NOESY NMR spectra of single and composite peptide solutions. Due to extensive aggregations in water, we could not detect any peak in D_2O system. Therefore, we attempted to carry out the experiment in 30% DMSO-d_6/H_2O which allows partial aggregation. In Gel-A, aromatic protons of naphthalene (7.70 ppm) interacted with aromatic protons of phenylalanine (7.12 ppm). The glycine protons (4.11 ppm) also interacted with the ethylene groups of glutamic acid residues (1.75, 1.95, 2.23 ppm). This is attributed to intermolecular hydrogen bonding of the glutamic acid residues (Figure 3.3 A). In the composite hydrogel (Gel-B) system, hydroxyl groups of mannose unit (4.59 ppm) interacted with the methylene linker of the naphthalene moiety (3.50, 3.62 ppm). Additionally, benzyl protons of phenylalanine (2.90 ppm) also interacted with the ethylene linker of the mannose group (3.29 ppm). These interactions suggest that **Pep-B** was incorporated within the assembled network of the **Pep-A** during self-assembly (Figure 3.3 B). Cross-peaks of mannosyl chiral protons (1.22, 1.49 ppm) and glutamate ethylene groups (1.75, 1.95, 2.23 ppm) could also be detected, which indicated possible intermolecular hydrogen bonding interactions of glutamic acid and mannose groups (Figure 3.3

C). Similarly, cross-peaks at (3.76, 3.25) and (3.73, 3.25) were also observed, which correspond to weak interactions between mannosyl moiety and glycine residues (Figure 3.3 D). These results indicate the proximity of two peptides which assisted the assembly of the non-gelator in forming the cooperative self-assembly.

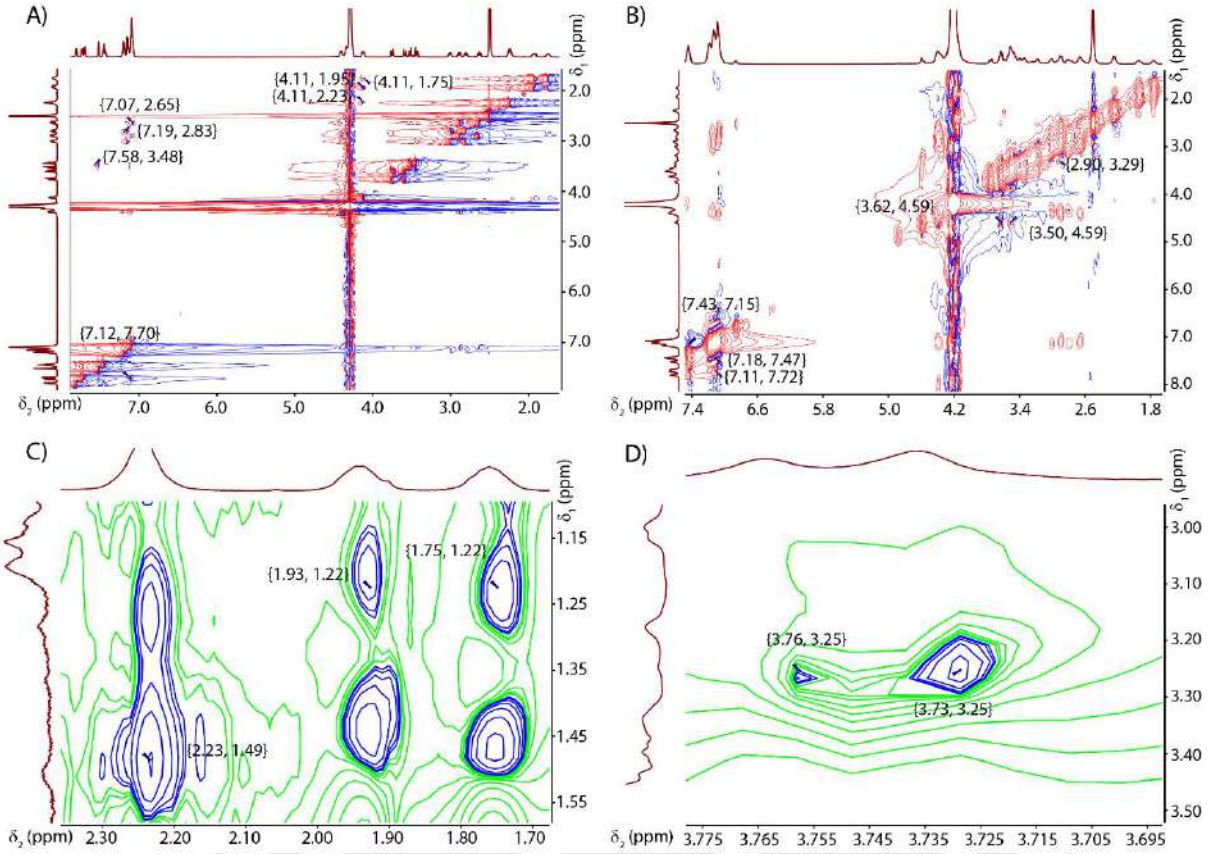

Figure 3.3 (A) NOESY NMR spectra of 'Solution A' in 30% DMSO-d_6/H_2O. (B) NOESY NMR spectra of 'Solution B' in 30% DMSO-d_6/H_2O. (C) and (D) magnified NOESY NMR spectra of 'Solution B' showing weak interactions of **Pep-A** and **Pep-B.**

Thereafter, we moved on to optimize the gelation kinetics of Gel-A and Gel-B. The gelation kinetics of 1 wt.% (15 mM) pre-gelation solutions of Gel-A (Sol-A) and Gel-B (Sol-B) was monitored through time-dependent quenching of naphthalene fluorescence detected at 337 nm.[232] From the obtained curve, it is deciphered that 'Sol-A' forms hydrogel within 5 minutes. 'Sol-B' followed a slower path and formed gel after 10 minutes (Figure 3.4 A). In the rheology experiment, G' and G" were scanned for 1 hour. For Sol-A, G' crossed G" within 3-5 minutes. For 'Sol-B', G' and G" remains essentially merged for 10 minutes. After 10 minutes, the separation between G' and G" gradually increases, which signifies the commencement of the gelation process (Figure 3.4 B). These observations corroborate with the fluorescence data.

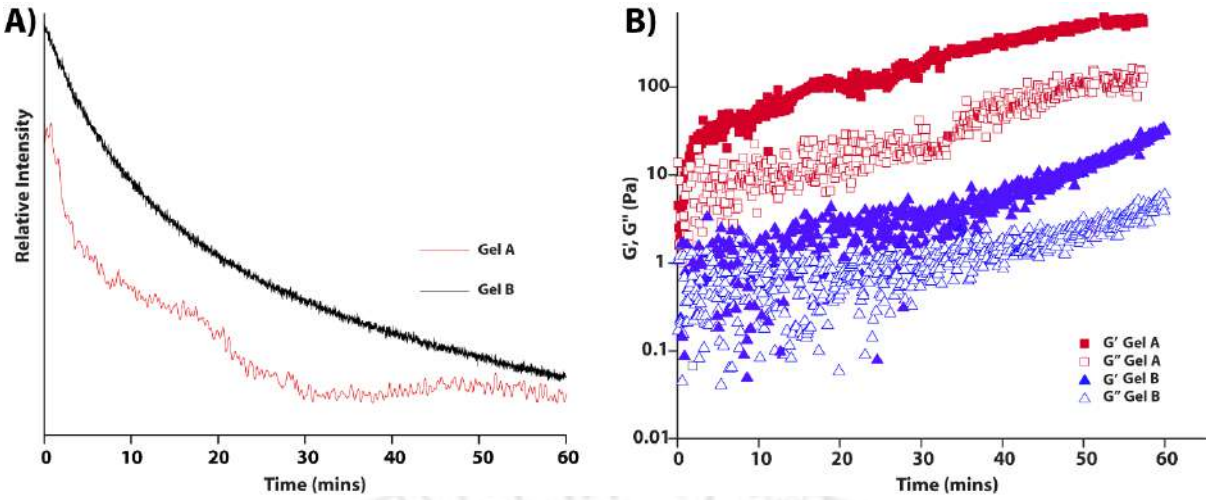

Figure 3.4 A) Fluorescence kinetics of 1 wt.% hydrogels monitored at 337 nm (λ_{ex}: 275 nm). B) Gelation kinetics of 1 wt.% hydrogels.

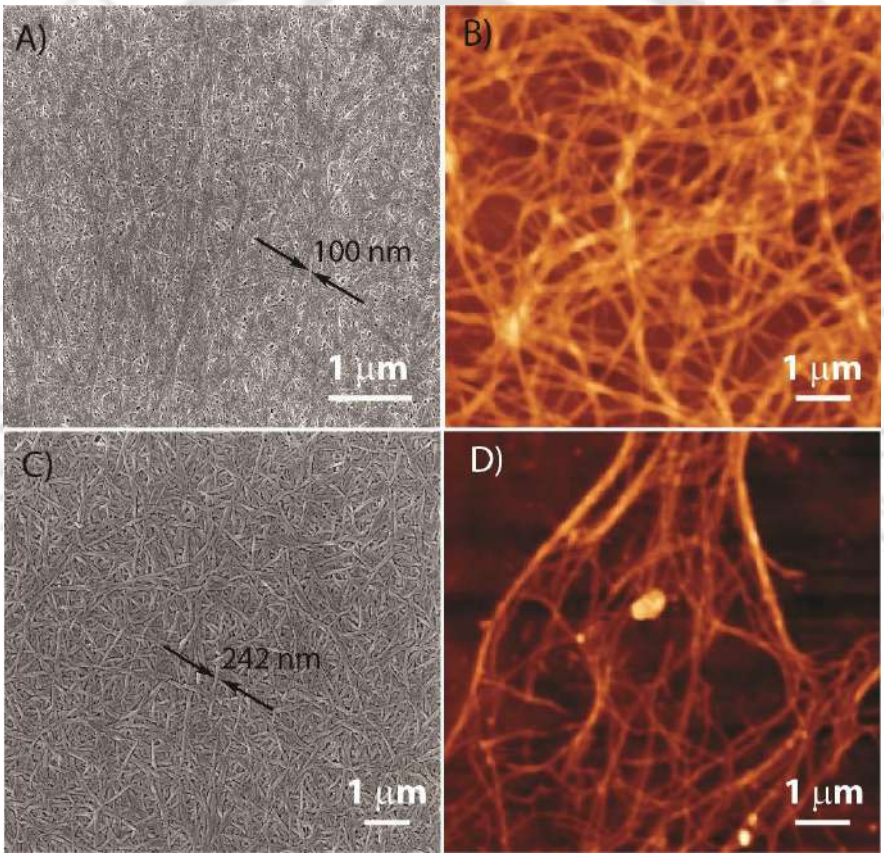

Figure 3.5 (A) FESEM and (B) AFM images of 1 wt.% Gel-A. (C) FESEM and (D) AFM images and photograph of 1 wt.% Gel-B.

Next, the morphologies of the hydrogels were analysed. As can be seen from the FESEM and AFM images (Figure 3.5), both hydrogels formed a tightly knitted network of fibres. The fibres are several micrometres long. However, for Gel-A, the fibres are thinner (~100nm) and less dense than Gel-B (~ 250 nm as obtained from FESEM images).

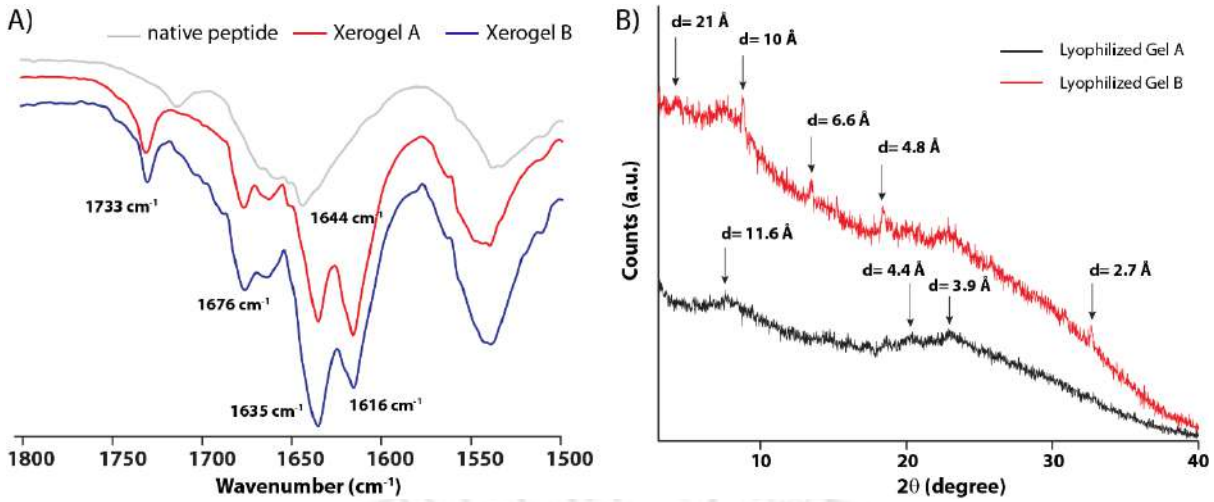

Figure 3.6 (A) IR spectra and (B) PXRD of lyophilized 1 wt.% Gel-A and Gel-B samples.

Both hydrogels acquired β-sheet-like aggregation, which was supported by the FTIR spectra of the xerogels (Figure 3.6 A). The HFIP treated peptides showed very similar FTIR spectra with a band at ~1644 cm^{-1}, while the hydrogel samples showed peaks at 1635 cm^{-1} (amide I) and 1616 cm^{-1} (amide II). The presence of these bands supports the formation of antiparallel β-sheet like arrangements in both hydrogels.[233, 234] Peaks at 1733 and 1676 cm^{-1} correspond to the C=O stretching bands for protonated carboxylic acids and residual carboxylate anions respectively.[235]

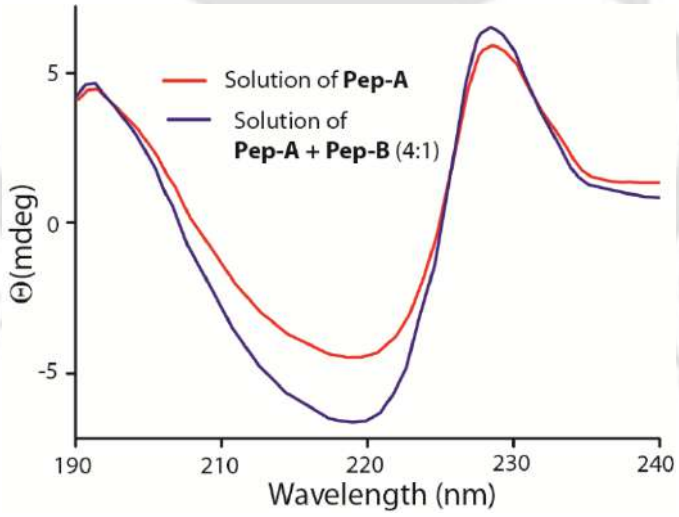

Figure 3.7 CD spectra of 0.05 wt.% solutions of **Pep-A** and mixture of **Pep-A** and **Pep-B** measured at room temperature.

The formation of β-sheet in both cases was confirmed by Circular Dichroism (CD) spectra (Figure 3.7). Both solutions (Pep-A and a 1:4 mixture of Pep-A and Pep-B in pH 6.5 buffer) showed a characteristic negative cotton effect at 220 nm. Powder XRD analyses (Figure 3.6 B) of the lyophilized hydrogels showed signals at 3.9 Å (2θ = 22.9°), a signature of phenylalanine

interactions.[236] 4.4 Å (2θ = 20.27°)and 4.8 Å (2θ = 18.43°) are the intra-strand distances, whereas 10 Å (2θ = 8.8°) and 11.6 Å (2θ = 7.6°) are due to inter-sheet distances.[237]

From all these analyses, it can be concluded that **Pep-A** self-assemble through an antiparallel orientation. The molecular arrangement is achieved by hydrogen bonding between the peptide molecules and water molecules. The aggregation is also strongly supported by the π-π interaction between the aromatic groups. The presence of **Pep-B** in Gel-B, though decreased the strength of the hydrogel, the overall assembly process of Pep-A presumably remained unaltered.

To check the melting temperature, both the hydrogels (400 microlitres, 1 wt. %) were gradually heated from 23 to 75 °C at 1°/min. Both the hydrogels were found to release some portions of the entrapped water instead of the usual melting phenomena. Such release of the trapped solvent by a gel is called syneresis.[238, 239] The amount of water released while heating the gel samples at 60 °C were then measured at different time intervals until a time was reached when no further water was released. It was interesting to find that Gel-A released 275 microlitres (68.75%) of entrapped water while 195 microlitres (48.75%) of the trapped water was released from Gel-B (Figure 3.8 A). Further, we investigated the temperature-dependent changes in the ^{1}H NMR spectra of both the hydrogels. As can be seen from Figure 3.8 B, the aromatic protons undergo down-field shifts with an increase in temperature. This can presumably be attributed to the disassembly process, which occurs at higher temperatures. With the temperature rise, as the weak supramolecular interactions break, sharp peaks generally appear at the higher temperature.[240] However, in the present cases, spectra do not regain the original pattern and remain disfigured. At temperatures above 60 °C, the gel shrinks and expels water to form a more compact gel (Figure 3.9). Amplitude sweep experiments were performed on the shrunken gels (obtained after removing the discharged water). As expected, there was an overall enhancement of the gel strength noticed for both cases (Figure 3.8 B).

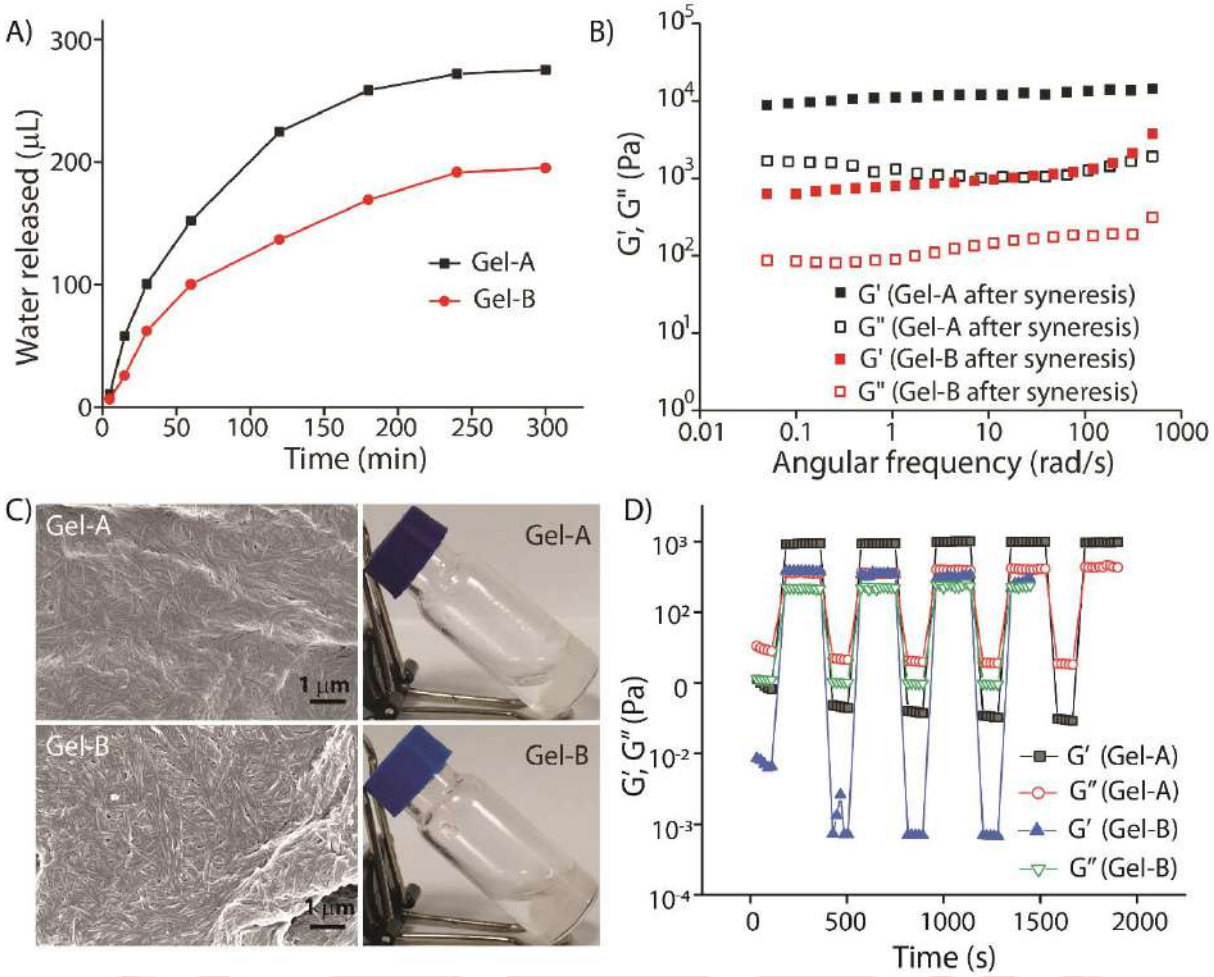

Figure 3.8 (A) Time-dependent water-release experiment of 1 wt.% Gel-A and Gel-B at 60 °C. (B) Amplitude sweep experiment of synerised 1 wt.% Gel-A and Gel-B. (C) FESEM images and photographs of synerised 1 wt.% Gel-A and Gel-B. (D) Cyclic strain time sweep data for 1 wt.% Gel-A and Gel-B (pH 6.8) at room temperature.

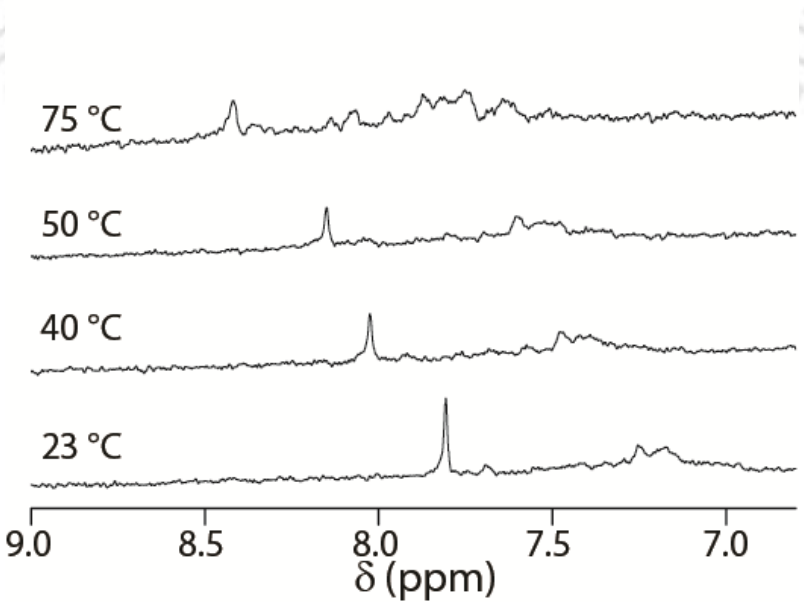

Figure 3.9 Temperature-dependent partial ^{1}H NMR spectra of 1 wt.% Gel-A and Gel-B.

When subjected to morphology analyses, though the pattern did not change, the shrunken gels showed much denser packing of the fibres compared to that of the original hydrogels (Figure 3.9).

3.3.2 Shear-thinning, biodegradability, stability and in-vitro drug release

As the composite hydrogel was prepared to use for the treatment of Leishmaniasis, it could be beneficial if it shows shear-thinning or thixotropic properties. A shear-thinning hydrogel shows a fall in viscosity and displays fluid-like properties once a shear of large amplitude is applied. On removing the shear, the fluid recovers back to the original hydrogel form in a time-dependent manner (Self-healing).[241] To check the shear-thinning property of the present hydrogels, detailed rheological analyses were performed. We noticed from the initial amplitude sweep experiments that when the % strain was varied at a particular frequency (1 rad/s), the G' remained higher than that of G" up to 2%, and then they crossed each other, signifying melting of the hydrogel to sol (Figure 3.2 B) in both hydrogels. We assumed that the hydrogels might have the shear-thinning character. Further, the thixotropic behaviour was checked for the 1 wt.% hydrogels (pH 6.8). Cyclic strain time sweep experiments were performed where strain was applied to break the hydrogels and when the applied strain was released, the hydrogels recovered their initial mechanical strength. This process was repeated four times without any noticeable change (Figure 3.8 D). These results confirm the shear-thinning and thixotropic behaviour of both gels which are important for drug delivery applications.[203]

Gaining knowledge about the material and thixotropic properties of the designed composite hydrogel (Gel-B), we wanted to move on to the biological applications. Before analysing the biological applications, it was essential to determine their biodegradability. For that purpose, we have performed the Proteinase K biodegradation assay of both the components. **Pep-A** or **Pep-B** were dissolved in pH 7.4 phosphate buffer containing Proteinase K at a concentration of 2 U/mL. Solutions were incubated at 37 °C for 24 hours, and the amount of peptide that remained unaltered was monitored through HPLC. From Figure 3.10 A, it can be seen that both peptides were almost completely biodegradable within 24 hours. Therefore, the hydrogel prepared by combining these two peptides can be used for biological applications without any accumulation of peptides inside the body. A similar study with Gel-B was then performed. In this case, the total amount of intact peptides (**Pep-A** and **Pep-B**) was calculated. Similar to individual peptides, Gel-B also showed complete degradation within 24 hours. The stability of the hydrogels was monitored for 24 hours in the presence of culture media (DMEM supplemented with10% heat-

inactivated fetal bovine serum,100 U/mL penicillin, and 100 µg/mL streptomycin). 500 µl of Gel-A and Gel-B were prepared in separate vials, and to each vial, 600 microlitres of culture media were added and incubated at room temperature for 24 hours. Both the gels remained intact without any dissolution in the desired culture media (Figure 3.10 B).

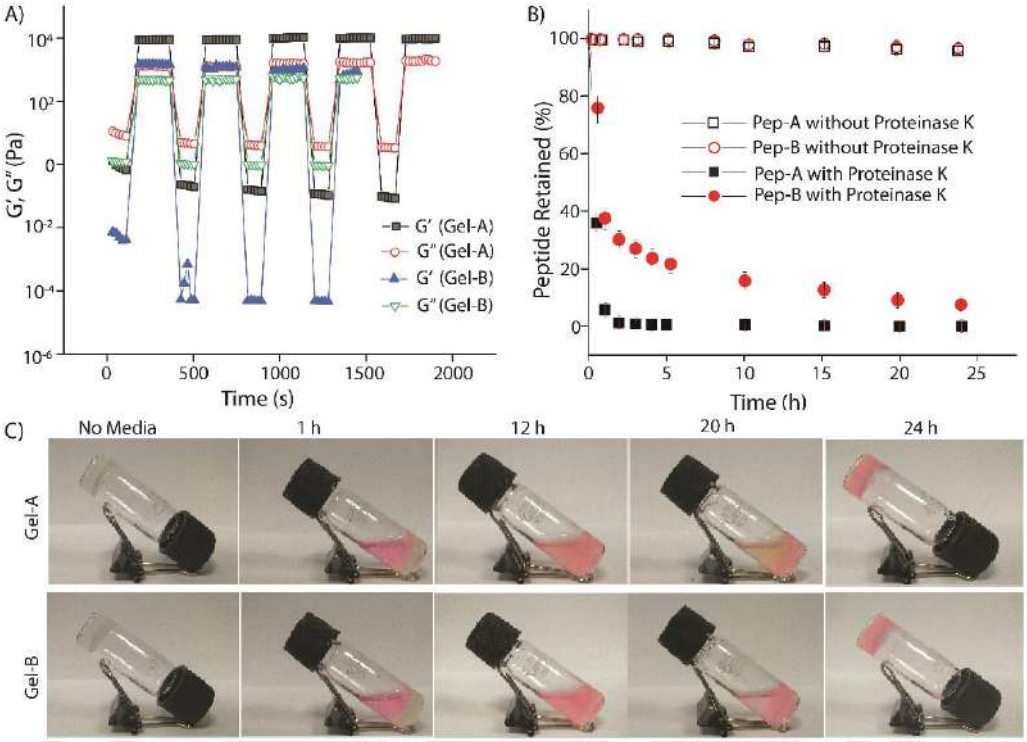

Figure 3.10 (A) % of peptide retained with time during Proteinase K assay as obtained from HPLC analyses. (B) Photographs of gel stabilities in presence of culture media (DMEM supplemented with10% heat-inactivated fetal bovine serum,100 U/mL penicillin, and 100 µg/mL streptomycin) at room temperature. (C) In-vitro drug release profile for Gel-B encapsulated AmpB-Rho studied in different buffers at room temperature.

3.3.3 Effect of composite hydrogel on cell viability and proliferation

The mannose content in the composite hydrogel (Gel-B) makes it a good target for mannose binding receptors on macrophages. It is imperative to determine whether the gel supports cell proliferation or not. For this purpose, control (healthy) and infected macrophages (with *Leishmania*) were either left alone or incubated with Gel-B. Cells were incubated for 3 days with serum-supplemented fresh cell culture medium (DMEM), and then MTT assays were performed to assess cell proliferation (Figure 3.11 A). No significant change in percentage of cell proliferation was noticed in cells incubated with Gel-B compared to control cells without the hydrogel. (Figure 3.11 A). These results suggest that mannosylated composite gel did not alter cell growth or proliferation, implying that Gel-B could be utilized as a drug-delivery vehicle without compromising cellular proliferation.

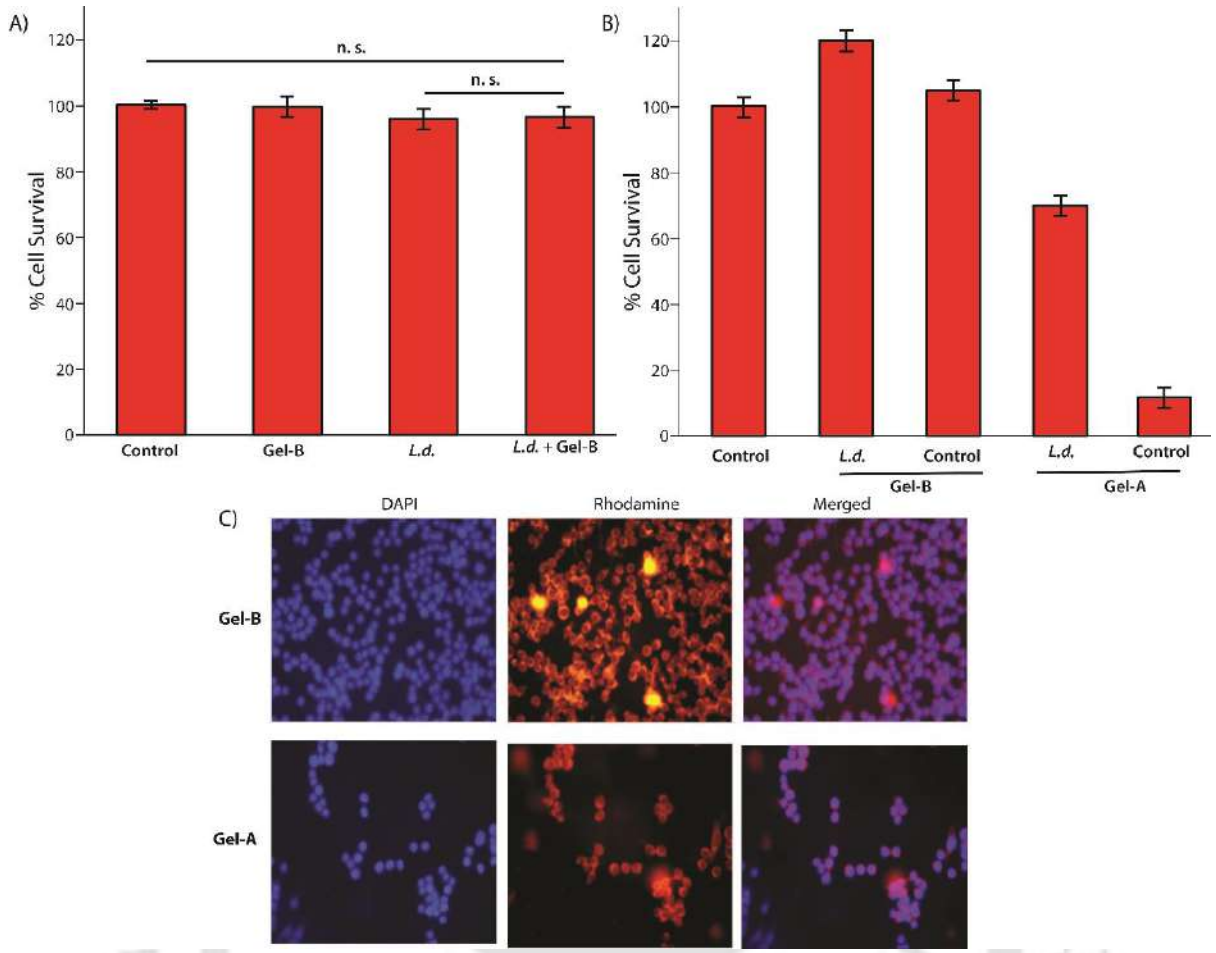

Figure 3.11 Impact of composite gel on cell growth and viability. (A) Macrophages (10^6 cells/mL) were seeded in tissue culture plates and were either infected with *L. donovani* parasites or left alone and incubated with Gel-B for internalization. Cells were further incubated for 3 days with a serum-supplemented medium at 37 °C. After that, cells were subjected to MTT assay to determine viability. (B-C) Cell growth analysis in 2D and 3D systems. (B) Gelation mixture of either Gel-A or Gel-B was plated onto coverslips, kept in tissue culture dishes, and allowed to solidify for 24 hours. Macrophages (10^6 cells/mL) were seeded onto the surfaces of these gels and were then either infected with *L. donovani* (10:1 parasite: cells) or left alone. Cells were washed, and 10 µl of MTT labelling reagent was added and incubated for 4 hours in a humidified atmosphere. The solubilizing agent was then added and kept overnight in a humidified atmosphere and absorbance of formed formazan was spectrophotometrically measured in ELISA reader at 595 nm with reference wavelength > 650 nm. (C) Macrophages were resuspended with the gelation mixture of either Gel-A or Gel-B, containing Rhodamine (Rho), and plated onto coverslips. Cells were allowed to grow, incubating at 37 °C. Cells were washed, fixed with methanol, and then further stained with DAPI (4′,6-diamidino-2-phenylindole,1 µg/mL) and analysed under a fluorescence microscope.

3.3.4 Gel-B as a 2D matrix for cell growth and proliferation

After finding out that gel B shows no apparent cytotoxicity, we next wanted to explore their potential as a matrix for cell growth. Both the gels (Gel-A and Gel-B) were allowed to form on the surface of coverslips and used as solid support. Macrophage cells were plated onto the surface of these gels. To check the effect of hydrogel attachment on cell growth, both control macrophages and infected macrophages were used for the study. Cells plated onto hydrogel bearing coverslips were further incubated for 3 days with serum-supplemented fresh cell culture medium (DMEM),

and then MTT assay was performed to assess cell growth or proliferation (Figure 3.11 B). Cells growing on surface of Gel-B showed increase in percentage of cell survival as compared to untreated cells that are growing on no-gel support. In contrast, cells growing on Gel-A showed a significant decrease in the percentage of cell survival compared to untreated cells without the hydrogel support (Figure 3.11 B). This might be because of the lack of cell adhesion in the case of Gel A. However, the infected cells on the surface of Gel-A showed a relatively higher percentage of cell growth than uninfected controls, suggesting that Leishmania perhaps is modulating the inhibitory potential of Gel-A to facilitate its survival. Collectively, these results indicate that cell growth is more feasible on Gel-B than on Gel-A.

3.3.5 Cell growth analysis in 3D system

Since, MTT assay demonstrated that cells growing on the surface of the composite hydrogel (Gel-B) had increased survival. In contrast, cells on Gel-A showed decreased survival, and we wanted to check the extent of cell growth in 3D systems. RAW cells were resuspended with the gelation mixture of either Gel-A or Gel-B, containing Rhodamine (Rho), and plated onto coverslips. Rhodamine was used as a model dye to find out the feasibility of drug delivery in 3D system. Cells were allowed to grow after incubating at 37 °C. Cells were then further stained with DAPI for visualization of cell nuclei and analysed under fluorescence microscope. The microscopic studies demonstrated that substantial cell growth occurred in Gel-B compared to Gel-A. As revealed from merged images (Figure 3.11 C), it is clear that Rho entered the cells and also the cell nuclei to some extent. The observations indicate that Gel-B can support better cell growth than Gel-A, and drugs can also be delivered by the system.

3.3.6 Drug delivery through 3D system

Having proved that Gel-B facilitates better cell growth in the 3D system, we next wanted to check the delivery of a drug into macrophage cells in the 3D system of cell culture. An anti-leishmanial drug, Amphotericin B (AmpB)[242, 243] conjugated with Rho (AmpB-Rho), was used for the study. RAW macrophages were resuspended with the gelation mixture of either Gel-A or Gel-B, containing AmpB-Rho and plated onto coverslips. Cells were allowed to grow incubating them at 37 °C. Additionally, another similar experiment was set up which were subjected to Leishmania donovani infection (at the multiplicity of infection 10:1). Cells of all sets were then further stained with DAPI for visualisation of cell nuclei and analysed under fluorescence microscope (Figure 3.12). The microscopic studies demonstrated that substantial cell-growth occurs in 3D Gel-B

compared to the cell-growth in Gel-A as shown in Figure 3.11 B. Notably, it was also observed that AmpB-Rho entered into most of the cells, as revealed from merged images as shown in Figure 3.11. On the contrary, only very few cells showed drug entry in case of Gel-A trapped cells. Infected Gel-A or Gel-B also mitigated similar findings, thus indicating that both control or infected macrophages grows substantially in Gel-B and drug delivery in either case is considerably higher than in the case of Gel-A (Figure 3.11). This probably indicates that mannose binding receptor on macrophages helps in better cell adhesion in case of the composite system (Gel-B) which possibly helps in better cell-growth and drug-delivery.

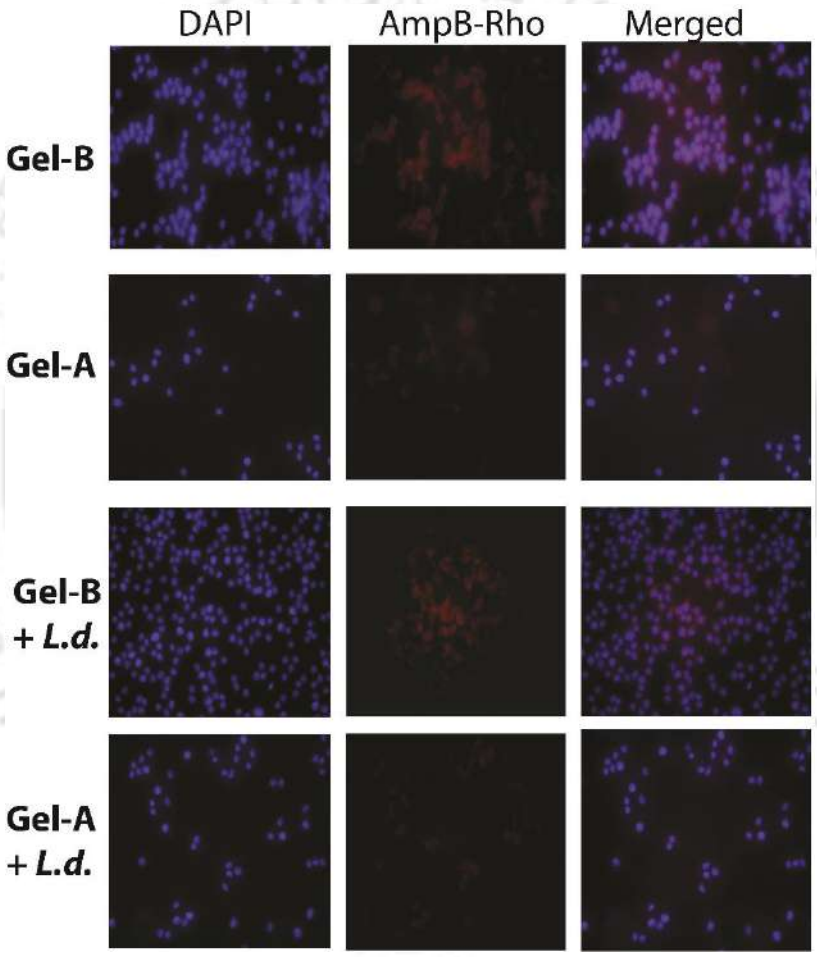

Figure 3.12 Drug delivery in 3D system. Macrophages were resuspended with the gelation mixture of either Gel-A or Gel-B, containing the drug amphotericin B conjugated to Rhodamine (AmpB-Rho) and plated onto coverslips. Cells were allowed to grow, incubating at 37 °C. Cells were washed, fixed with methanol, and then further stained with DAPI (1 µg/mL) and analysed under a fluorescence microscope.

3.3.7 Effect of Gel-B mediated drug delivery on parasite survival

Having demonstrated that Gel-B can support better cell growth or enhanced drug delivery in 3D system of cell culture, we next wanted to check its effect on parasite survival. To this end, infected macrophages were either allowed to grow in Gel-B (3D system) with AmpB-Rho or left alone

untreated with the drug, and intracellular parasite burden was estimated. Compared to infected untreated macrophages (264 ± 17 Amastigotes/100 macrophages), drug-treated infected cells showed a significant reduction in parasite burden (75 ± 10.8 Amastigotes/100 macrophages) (Figure 3.13). The reduced parasite burden in the case of AmpB-Rho-loaded Gel-B clearly shows effective targeted drug delivery. The results are promising and indeed indicate that Gel-B can be used for targeted drug delivery to treat Leishmaniasis.

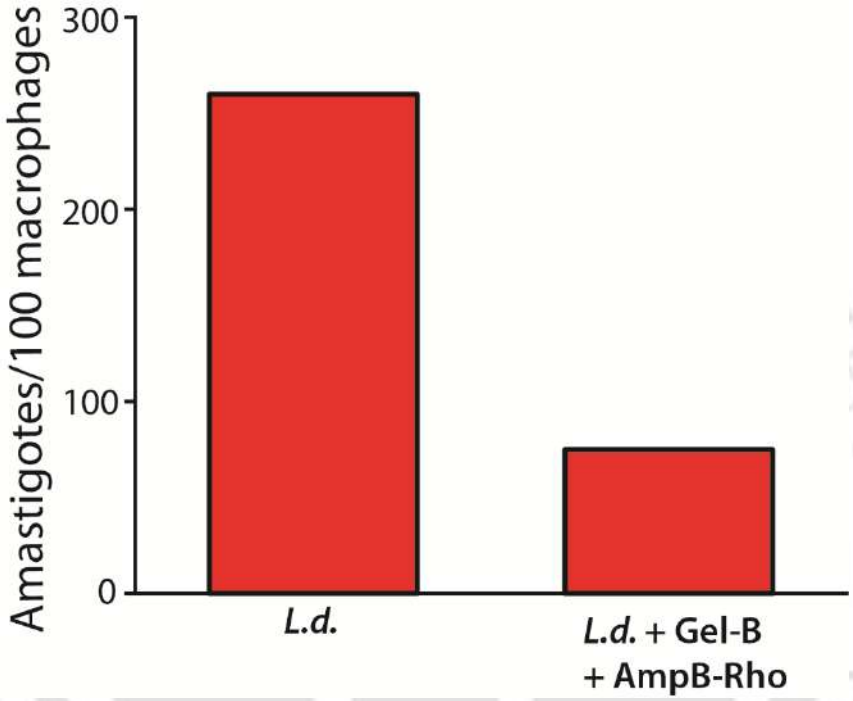

Figure 3.13 Effect of drug delivery upon parasite survival. The parasite burden after the treatment of AmpB-Rho-loaded Gel-B.

3.4 CONCLUSION

In summary, we have successfully prepared a mannose decorated composite hydrogel to combat Leishmaniasis. The combination of a hydrogel forming peptide and a mannose functionalized non-gelling peptide leads to the formation of an injectable hydrogel which also showed heat induced syneresis property. The peptides self-organize in an antiparallel b-sheet like arrangement through $\pi-\pi$ stacking and hydrogen bonding interactions. The composite hydrogel was found to be non-toxic to Raw 264.7 macrophage cells. Moreover, both, healthy and Leishmania infected macrophages can grow efficiently on the surface as well as inside the hydrogel scaffold (3D) showing no effect on their proliferation from the composite hydrogel. The internalization of the hydrogel into the macrophages were found to be an effective way to fight against Leishmaniasis. The mannose receptors of the macrophages allowed effective adhesion of the mannose

functionalized composite hydrogel which essentially leads to the delivery of anti-Leishmaniasis drug and reduce the parasite load significantly. The injectability and the syneresis property of the composite hydrogel along with this effective cellular delivery of the drug makes the hydrogel a potential candidate for combating Leishmaniasis.

Chapter-4: Preparation of a Short Peptide-Based Biopolymer with Efficient Cell Adhesion and Proliferation Property using Multiple Cross-Linking Strategy

4.1 INTRODUCTION

The progress of synthetic biomaterials with applications in tissue engineering and regenerative medicine is a major area of academic and commercial importance.[130, 244, 245] A new and promising approach is to produce artificial ECM that can be used as templates for cell-adhesion and proliferation to regenerate the tissue.[246, 247] Peptide-based polymers are frequently recruited because of wide range of functionality and inherent biocompatibility.[18, 38, 130-135] Some cross-linked peptide based polymeric systems are reported in literature.[136-139] However, controlling the size of the polymer is a difficult task. A cross-linking strategy to prepare peptide-based polymer particles with efficient cell adhesion and proliferation ability and where the size of the particles can be easily tuned is thus highly desirable.

The host-guest chemistry of macrocyclic host, Cucurbit[8]uril (CB[8]) has been utilized successfully to construct supramolecular soft-materials with biological applications.[248-253] This ternary complexation of CB[8] is used extensively to construct supramolecular amphiphiles,[105, 106] polymers,[254, 255] and various other conjugates.[256-259] Disulfide linkages are ubiquitous in nature and many proteins utilize this particular covalent linkage to attain the native tertiary or quaternary structure and hence the activity. Another covalent cross-linking strategy that can be applied to peptide/proteins is the bio-catalytic dimerization of Tyrosine residues. Construction of soft-materials using these two covalent cross-linking approaches are reported in literature.[260-262]

Based on these reports, we have come up with a novel strategy, with the aid of two covalent strategy in combination with the ternary complexation of CB[8], to develop a multiple cross-linked polymer with controllable size and shape. Herein, we present, a new strategy to create a peptide based cross-linked polymer. Three different cross-linking pathways were applied to a rationally designed small peptide (**4.1**, Scheme 4.1). Covalent linkage by S-S (disulfide) bonds, supramolecular conjugation using ternary complexation by CB[8] and enzymatic cross-linking via horseradish peroxidase (HRP) mediated dimerization of Tyr lead to the formation of highly cross-linked bio-polymers (**P1** and **P2**, Scheme 4.1). We have shown that by varying the cross-linking order, polymer particles with different sizes can be prepared easily. The surface of the cross-linked polymer is covered with the well-known cell-adhesive sequence, RGDS,[229, 263] which served as an efficient cell adhesion and proliferation platform.

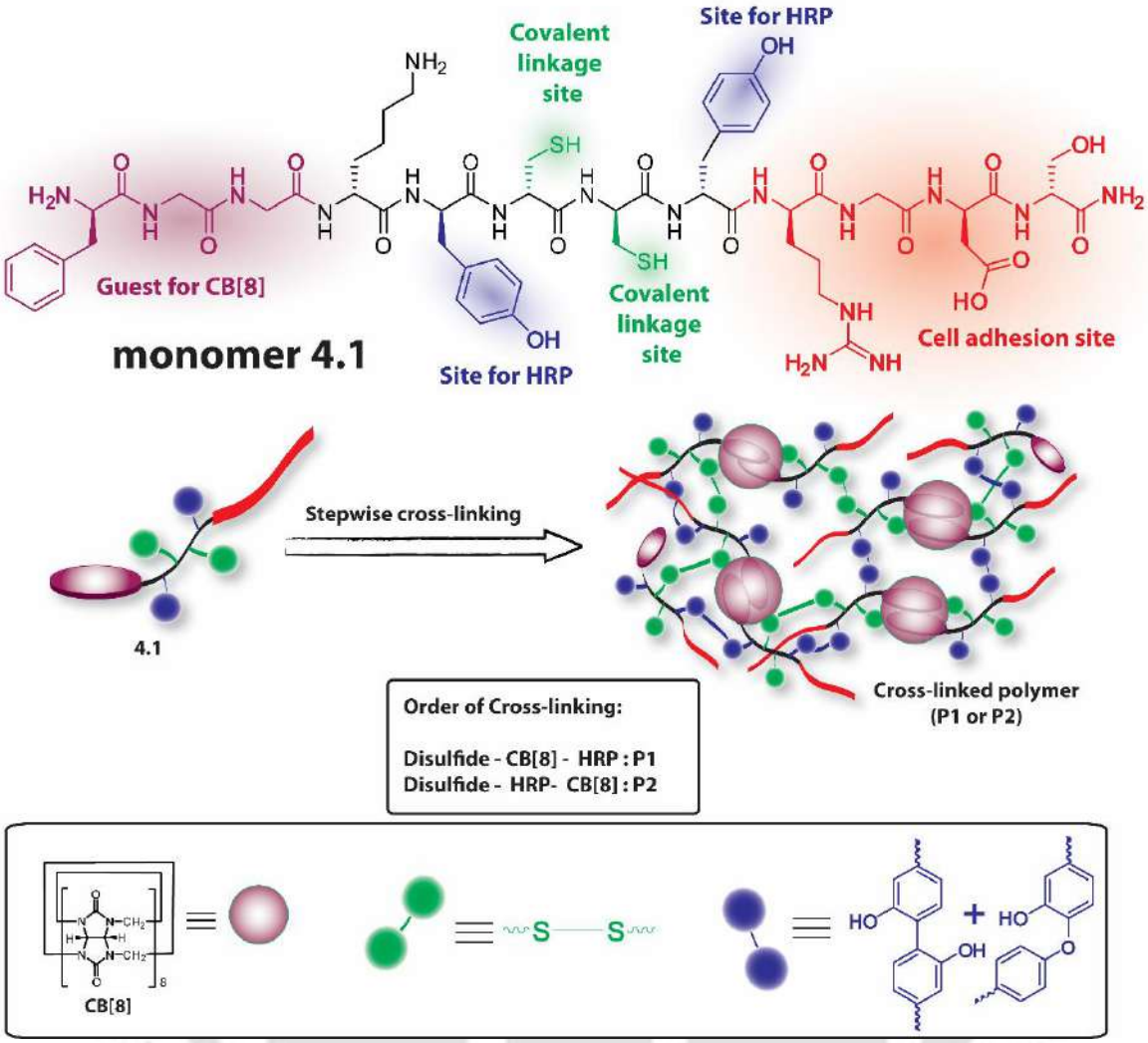

Scheme 4.1 Chemical structure of the peptide monomer **4.1** and CB[8] and schematic presentation of the cross-linking strategies.

4.2 EXPERIMENTAL SECTION

4.2.1 General

Fmoc-rink amide resin, protected amino acids, HBTU and DIPEA were purchased from GL Biochem (China). TFA and TES were purchased from Spectrochem (India). Horseradish Peroxidase (HRP) was procured from Sigma Aldrich (USA). HPLC-grade DMF and ACN were procured from Spectrochem (India) and Fisher Scientific (India), respectively. All sample preparations were done with Milli-Q water with a conductivity of less than 2 µS/cm. ESI-MS was performed with a Q-tof-micro quadrupole mass spectrophotometer (Micromass). MALDI-TOF measurements were performed on AUTOFLEX SPEED (Bruker) instrument using sinapic acid and DHB as the matrix. UV-Vis data was recorded with a PerkinElmer Lambda 35 spectrometer. Fluorescence measurements were performed with a Carry Eclipse spectrophotometer (Agilent). Circular dichroism (CD) experiments were performed on a Jasco J-1500 spectropolarimeter. Dynamic light scattering and zeta

potentials were measured using Zetasizer Nano-ZS90 (Malvern). Confocal laser scanning microscopic (CLSM) images were recorded on a TCS SP8 microscope from Leica, Germany.

4.2.2 Synthesis of monomer 4.1

Peptide **4.1** was synthesized on Rink amide MBHA resin using standard Fmoc (9-fluorenylmethoxycarbonyl) solid phase peptide synthesis (SPPS) method. In a standard coupling, 3 equiv. of protected amino acid (with respect to the loading of the resin), 3 equiv. of HBTU, and 6 equiv. of DIPEA were taken in 5 mL of DMF (for 0.1 mmol scale with respect to the resin loading) and stirred for 5 minutes prior to addition of the mixture to the resin. The reaction mixture was shaken for 1 hour and the resin was washed several times with DMF. The Fmoc-deprotection was achieved by treatment of the resin with 20% piperidine/DMF (5 mL, 5 minutes, three times) followed by thorough washing of the resin with DMF. The Fmoc-deprotection and coupling steps were repeated until the designed peptide sequence was obtained. After the final Fmoc-deprotection, the peptide loaded resin was washed several times with DMF followed by DCM and dried under reduced pressure. The dried resin was then treated with freshly prepared mixture of TFA/TES/p-cresol/water (75:15:5:5 v/v) and stirred for 1 hour. The resin was finally washed with DCM. The cleavage cocktail and the washings combined and concentrated to a minimum volume on a rotary evaporator. The cleaved peptide was then precipitated from cold dry ether, centrifuged and lyophilized to get the crude peptide. Purification was done in a semi-preparative HPLC using a Luna 5 μm (C18) column (Phenomenex) and an eluent of acetonitrile and water starting at 5% ACN/H_2O reaching at 100% ACN in 18 minutes to complete the chromatogram in 22 minutes. The pure lyophilized peptide was obtained in 70% yield. ^{1}H NMR (600 MHz, D_2O, 25 °C) δ (ppm): 7.26 (s, 3H), 7.15 (s, 2H), 6.98 (s, 4H), 6.73 – 6.57 (m, 4H), 4.68 – 4.60 (m, 6H), 4.57 (s, 2H), 4.43 (s, 2H), 4.25 (s, 2H), 4.18 – 4.06 (m, 3H), 3.78 (dd, 6H), 3.04 (d, 4H), 2.83 (d, 6H), 2.67 (d, 4H), 1.68 (s, 2H), 1.47 (s, 8H), 1.14 (s, 4H); ^{13}C NMR (125 MHz, D_2O, 25 °C) δ (ppm): 35.97, 36.74, 39.09, 42.16, 42.33, 42.45, 54.46, 54.78, 115.37, 115.42, 128.02, 128.51, 129.16, 129.39, 130.59, 133.71, 154.37, 169.81, 170.71, 171.42, 171.71, 171.95, 175.51; ESI-MS calcd. for $[M + H]^+$: 1354.52; found: 1354.56 $[M + H]^+$.

4.2.3 Synthesis of Cucurbit[8]uril (CB[8])

CB[8] was synthesized following previously published protocol.[264] ^{1}H NMR (600 MHz, $D_2O/CF_3CO_2D/D_2SO_4$ (1:1:0.15), 25 °C) δ (ppm): 4.25 (d, 16H), 5.55 (s, 16H), 5.86 (d, 16H) ppm; MS (ESI): *m/z* 1461.41 $(CB[8] + Cs)^+$.

4.2.4 Cross-linking of monomer 4.1

Order A. Monomer **4.1** was dissolved in water to achieve a concentration of 1 mM and to it 30% H_2O_2 solution was added (>1% v/v). The solution was shaken slowly under ambient condition for 24 hours. After 24 hours, CB[8] was added to maintain 1:2 ratio with **4.1**. The solution was sonicated for 30 minutes and then incubated at room temperature for 24 hours. To this solution, H_2O_2 (30 %) and HRP solutions were added to maintain their respective concentrations (9.7 mM and 2×10^{-4} mM respectively). The solution was gently mixed by micro tip mixing. Within 20 minutes, the solution became turbid and after 45 minutes, white precipitate appeared. After 1.5 hours, no further precipitation was observed and the solution was incubated at 4 °C for 24 hours and then the precipitate was collected by centrifugation and freeze dried.

Order B. Monomer **1** was dissolved in water to achieve a concentration of 1 mM and to it 30% H_2O_2 solution was added (>1% v/v). The solution was shaken slowly under ambient condition for 24 hours. H_2O_2 (30 %) and HRP solutions were added to maintain their respective concentrations (9.7 mM and 2×10^{-4} mM respectively). The solution was gently mixed by micro-tip mixing and incubated at 4 °C for 24 hours. After 24 hours, CB[8] was added to maintain 1:2 ratio with **1**. The solution was sonicated for 30 minutes and then incubated at room temperature for 24 hours. Finally, the precipitate was collected by centrifugation and freeze dried.

Cross-linked polymer sample preparation. Many of the experiments were performed during the cross-linking processes using the solutions directly. However, some experiments including the cytotoxicity and cell adhesion studies were carried out with the separated **P1** and **P2**. The polymer was found to be soluble in 10 mM PBS buffer pH 7.4 and the experiments were performed using a stock solution of **P1** in this buffer and diluting it according to the requirement. As both, the peptide (M.W. = 1353) and CB[8] (M.W. = 1329) are having similar molecular weights, the concentrations for P1 solutions were calculated using the molecular weight of **1** and denoted as [**1** in **P1**].

4.2.5 ITC experiments

Peptide **4.1** at 25 °C in 10 mM sodium phosphate (pH 7.0) was treated with 3 equiv. of DTT in order to prevent and disulphide bond formation and this solution was titrated at 1 mM into a 0.05 mM solution of CB[8]. The raw data for power versus time, and the integrated enthalpy values versus the molar ratio of peptide:CB[8] was generated from the instrument. These data were fit to the "sequential binding model" using Origin 7.0 software.

4.2.6 HPLC analysis

The chromatographic analysis of the polymer formation was performed on an analytical HPLC (Ultimate 3000, Dionex) and a C-18 Luna 5-micron analytical column from Phenomenex. The same solvent gradient was used as in the HPLC purification of the peptide. After 24 hours incubation of the aqueous solution of the peptide **4.1**, the solution was analyzed to see the appearance of the polymer peak.

4.2.7 NMR studies

^{1}H NMR spectra were recorded during the cross-linking process at every step. Peptide **4.1** (1 mM) was dissolved in D_2O and incubated for 72 hours at room temperature before recording the NMR spectra. To this solution, CB[8] was added, sonicated for 30 minutes and incubated at room temperature for 24 hours prior to recording the NMR spectrum of CB[8] cross-linked polymer. To this solution, HRP and H_2O_2 were added and after 15 minutes, the NMR spectrum was recorded in order to avoid any precipitation. All the measurements were water suppressed to get proper signals in the aromatic region.

4.2.8 CD spectroscopy

Circular dichroism measurements of the aqueous sample solutions were taken in a quartz cuvette of 0.5 mm path length and measured taking band width 1 nm and scanning wavelength 200 to 600 nm at a rate of 100 nm/min. Measurements were done using the same solution at different stages of the cross-linking process at 25 °C.

4.2.9 DLS studies

Similar to the NMR experiment, the cross-linking was monitored at different stages of a 1 mM solution of **4.1**. For **P1** and **P2**, solutions of the freeze-dried polymer were used.

4.2.10 Cytotoxicity

MTT assay was performed to see the effect of the polymer on cell viability. **P1 and P2** was initially dissolved in deionized water and then diluted to prepare working concentrations of 10 µM, 20 µM, 40 µM, 80µM, 160 µM, 320 µM, 640 µM, 1280 µM. A 96 well plate was U.V. cross-linked with different concentrations of **P1** and **P2** overnight. Then, 10^4 cells were grown in **P1 and P2** coated 96 well plate and incubated for 24 hours. Thereafter MTT (5mg/ml) was added to the plates and incubated at 37 °C for 4 hours. Finally, formazan crystals were solubilized in solubilization buffer and absorbance was measured at 570 nm. All assays were performed in triplicates. The extent of cell viability was measured as the percent decrease in viability with respect to untreated cells.

4.2.11 Cell adhesion assay

Cell adhesion property of **P1** and **P2** was assessed according to the method described in Yeo et al,[265] which is a slight modification of the cell count assay by crystal violet described by Kueng et al.[266] A 96 well ELISA plate was first UV cross-linked overnight with **P1** and **P2** of different working concentrations. Then the wells were blocked with 100 µl of 3% BSA in DMEM for 1 hour. Then the wells were washed twice with DMEM containing 0.1% BSA. Next RAW 264.7 macrophage cells were re-suspended in DMEM containing 0.1% BSA. 100 µl of the cell suspension containing 10^4 cells were added to each well and incubated at 37 °C for 1 hour in 5% CO_2. Finally, the cells were stained with 0.5% Crystal Violet aqueous solution in 20% methanol for 10 minutes. The unattached cells were washed 3 times with deionized waters and visualized under Nikon Ts2R-FL microscope equipped with 40X objective. The images thus captured were processed by Image J program downloaded from National Institute of Health (//rsb.info.nih.gov) and mounted using Adobe Photoshop Software. To measure quantitatively, 200 µl of 0.1% SDS were added to each well to solubilize the stain and absorbance was measured at 570 nm. All assays were performed in triplicates. The cell adhesion was measured as the fold change in cell number (which is proportional to measured O.D.) with respect to control untreated cells.

4.2.12 Cell proliferation assay

Raw 264.7 macrophage cells were plated at a density of 10^4 cells/well in a 96 well **P1** and **P2** (10-1280 µM) coated microplates (Tarsons). After 24-, 48-, and 72-hours incubation in medium, cell proliferation was determined by using CyQUANT Direct Cell Proliferation Assay Kit (Thermo Fisher Scientific). Briefly, after incubation of cells, medium was removed and cells were incubated with CyQUANT reagent for 1 hour at 37 °C according to manufacturer's instructions. Plates were analyzed by using a microplate reader (Excitation 508 nm, Emission 527 nm).

4.3 RESULTS AND DISCUSSION

4.3.1 Design of the peptide monomer

In order to create the planned cross-linked peptide polymer, a twelve amino acid long peptide was designed (monomer **4.1**, Scheme 4.1). The peptide monomer **4.1** contains four different regions, two Cysteines for cross-linking through disulfide bridges, two Tyr units for enzyme catalyzed cross-linking, N-terminal FGG unit for complexation with CB[8], and C-terminal RGDS sequence as cell adhesive unit. The formation of ternary complex by FGG (Phe-Gly-Gly) motif inside CB[8] cavity is well established in literature.[259, 267] The binding constant for this ternary-

complexes fall in the range of 10^{10}-10^{12} M^{-2} which is substantially high to construct stable supramolecular conjugates. The incorporation of one Lys unit is to provide sufficient solubility in water.

4.3.2 Cross-linking of peptide monomer 4.1

Three different cross-linking strategies were used to create the planned cross-linked polymer. The Cys residues were used for the disulfide linkage while Tyr moieties were conjugated using HRP. For supramolecular cross-linking, the FGG units at the N-terminus was utilized for ternary complexation by CB[8]. However, the order of these cross-linking processes was a matter of concern as there are two possible orders (*Order A* and *B*) to construct the polymer as shown in Scheme 4.1. Since, disulfide linkage cannot be controlled in aqueous medium, it remains as the first step in both cases. The order of cross-linking by CB[8] and Tyr conjugation thus can be altered. To see any difference, the order of cross-linking may cause, we have performed the cross-linking following both orders.

4.3.3 Disulfide linkage

The covalent cross-linking via disulfide bridges was established by slow shaking of a 1 mM solution of **4.1** in water in presence of H_2O_2 for 24 hours under ambient condition. In absence of H_2O_2, the reaction was found to be slow and takes more than 48 hours to reach saturation. MALDI-MS analysis showed a polymeric mass ~16,200 suggesting cross-linking of the monomers. A time dependent MALDI experiment showed no further change in the MS pattern after 4 hours indicating the completion of the reaction. HPLC analysis confirmed the appearance of a new peak and disappearance of the monomer peak in the chromatogram (Figure 4.1 A). The dynamic light scattering (DLS) experiment showed a distribution of particles centered at ~230 nm (Figure 4.1 B). To further confirm the formation of cross-links, a well-known disulfide bond breaker, DTT was added to a portion of the solution and analyzed using chromatography, MALDI-MS as well as DLS. Interestingly, the DTT treated solution showed complete disappearance of the new chromatographic peak and reappearance of the monomer peak in the chromatogram. Moreover, no measurable distribution in the DLS measurement was obtained for this solution. Additionally, the polymeric mass disappeared from the MALDI-MS spectrum. All these observations unequivocally confirm the cross-linking of the peptide via disulfide linkages and analysis of the mass of the polymer suggested that average number of monomers present in the cross-linked polymer was 13.

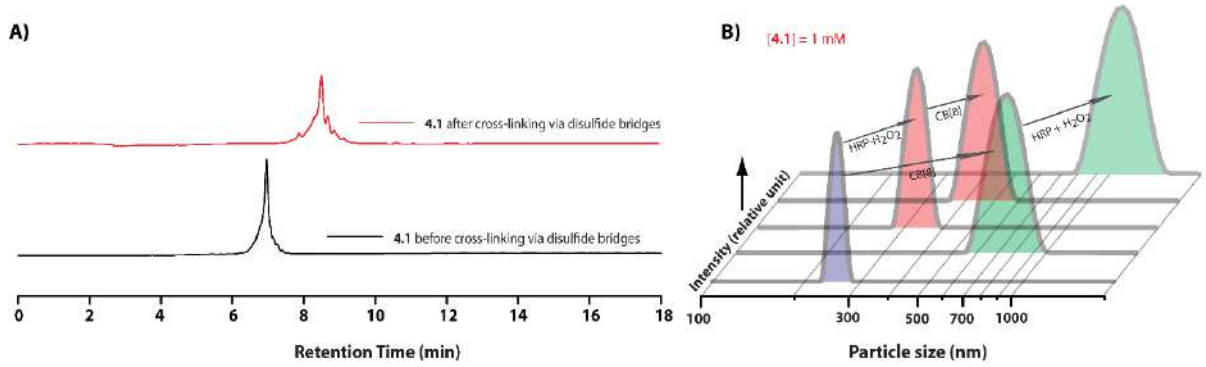

Figure 4.1 (A) Chromatograms of **4.1** before and after disulfide cross-linking. (B) Intensity weighed DLS profiles of solutions at different stages of cross-linking processes of **4.1**.

4.3.4 Cross-linking *Order A*

Before conducting the supramolecular cross-linking, the ternary complexation efficiency was measured for peptide **1** and CB[8]. The calorimetric changes of a DTT treated (in order to avoid any disulfide linkage induced contribution) solution of **4.1** upon titration with CB[8]. A 2:1 association between **4.1** and CB[8] was recorded (Figure 4.2 A) with a binding constant of 10^{11} M^{-2} which is within the range of previously reported ternary complexation between FGG units and CB[8].[259, 267] The ITC experiment thus confirmed the possibility of conjugating the peptide N-terminals via ternary complexation.

MALDI-MS was employed to detect the mass of the cross-linked polymer. However, it was unsuccessful after repeated attempts to find any enhancement in the mass owing to the ternary complexation. It is worth mentioning that our previous experiences of detecting ternary complexes using MALDI-MS also never provided any satisfactory result probably because of the ionization technique utilized in MALDI-MS. To further confirm the formation of the inclusion complex, the solution was treated with DTT to break all disulfide linkages and the ESI-MS was recorded. 2:1 complex formation is confirmed by the appearance of the respective mass to charge ratio signals of the complex (Figure 4.2 B). A sharp increase in the particle size was observed which enhanced to ~ 720 nm from 230 nm which suggests probable cross-linking between 2-3 particles of the disulfide linked polymer (Figure 4.1 B).

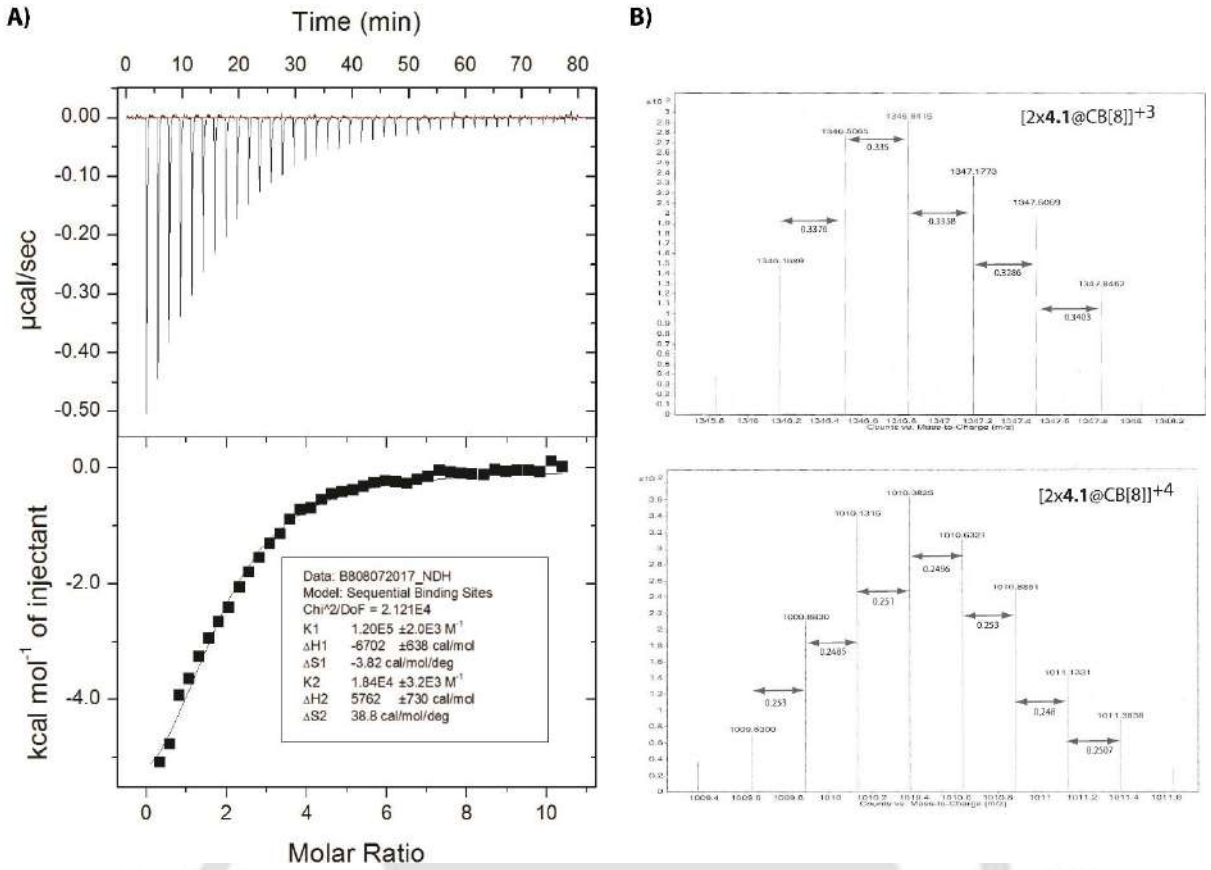

Figure 4.2 (A) Binding constant determination for supramolecular cross-linking of DTT treated monomer **4.1** and CB[8]. (B) ESI-MS of CB[8] cross-linked **4.1** after DTT treatment to show the formation of 2:1 complex between **4.1** and CB[8].

Next, the supramolecular cross-linking was established. CB[8] was added to the disulfide cross-linked polymer solution to maintain a concentration of 0.5 mM (0.5 equivalent with respect to the monomer). The initial suspension became clear after 30 minutes of sonication indicating the complexation. The solution was incubated at room temperature for 24 hours before carrying out further experiments. As UV-visible or fluorescence spectroscopy did not provide much information about the ternary complexation apart from prominent decrease in the absorption as well as emission intensity (Figures 4.3). The complexation was confirmed by monitoring the ^{1}H NMR signals arising from phenylalanine (Phe). As can be seen in Figure 4.4 A, addition of CB[8] results in a significant up-field shift of the "Phe" protons whereas the signals from Tyr remained at their original positions. As expected, only a small portion of the un-complexed Phe units could be seen. As the monomers are already cross-linked via disulfide linkages, it is comprehensible that all the FGG groups are not accessible for cross-linking through CB[8]. The ^{1}H NMR were recorded at different time interval to find the saturation time and after 6 hours, no further change in the proton signals were observed which can be considered as the time of completion for the complexation process.

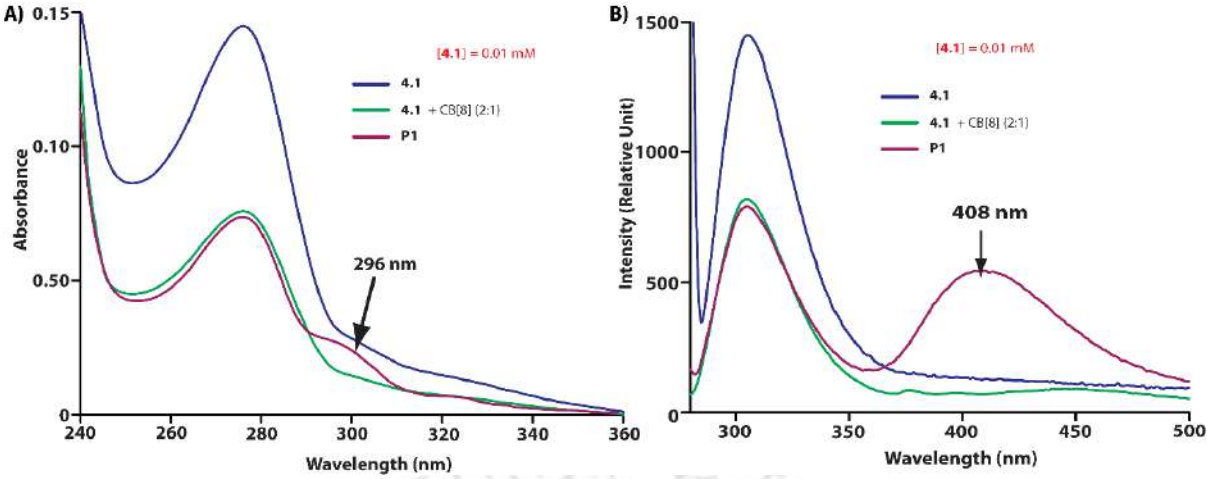

Figure 4.3 (A) UV–visible absorption and (B) emission spectra at different stages of the cross-linking process of **4.1** (*Order A*). For B, λ_{ex} = 275 nm. All experiments were carried out under ambient condition. [**4.1**] = 0.01 mM. All experiments were carried out at 25 °C during the cross-linking processes in water.

The enzymatic cross-linking was achieved by addition of H_2O_2 and HRP to the above solution. HRP is a well-studied enzyme which dimerizes Tyr moieties catalytically via C-O or C-C bond formation as shown in Scheme 4.1.[268, 269] Addition of HRP (2×10^{-4} mM) and H_2O_2 (9.7 mM) to above solution quickly produced the third cross-linking. The reaction was extremely fast and within 20 minutes, the solution became turbid (Scheme 4.1).[255] This solution was incubated at 4 °C for 24 hours, centrifuged and the obtained solid was freeze-dried to get the cross-linked polymer (**P1**). The polymer was found to be soluble in 10 mM PBS buffer pH 7.4 and all the experiments were performed using a stock solution of **P1** in this buffer and diluting it as required.

^{1}H NMR spectra (Figure 4.4 A) of the HRP treated solution confirmed the bio-catalytic formation of cross-links at the Tyr sites. The signals corresponding to Tyr protons showed a downfield shift and appeared as a broad peak which is characteristic of Tyr dimerization (Figure. 4.4 A). Further proofs of enzymatic cross-linking were obtained from UV-visible and emission spectroscopy (Figure 4.3). Though no further change in the absorbance was noted at λ_{max}, a broad new band centered at ~296 nm generated in the enzyme treated sample which indicates the dimerization of Tyr units.[268, 269] When excited at 275 nm, the sample showed a new broad emission band at 408 nm (Figure 4.3 B). This new band was arising from the dimerized Tyr units as reported previously.[270] The appearance of the emission peak at 408 nm was used to monitor the reaction rate but due to the precipitation of the polymer, the study resulted in irreproducible data. Particle size analysis showed an increment from ~ 720 nm in the average diameter to 1020 nm (Figure 4.1 B). It is worth mentioning here that the stepwise cross-linking of the monomer **4.1** was also monitored through

Circular Dichroism (CD). Though no proper secondary structure was observed at any stage, every cross-linking step resulted in significant change in the CD profile (Figure 4.4 B).

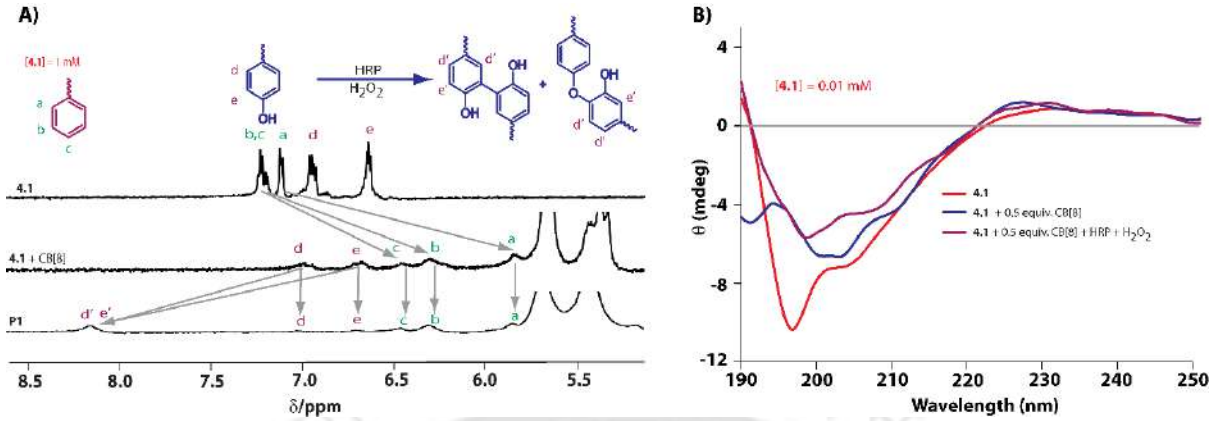

Figure 4.4 (A) Partial ^{1}H NMR spectra at different stages of the cross-linking process of **4.1** (*Order A*). (B) CD spectra at different stages of the cross-linking of monomer **4.1** (initial concentration of **4.1** for this experiment = 0.01 mM) during the preparation of **P1** following *Order A*. All experiments were performed using the same solution at different stages of the cross-linking in water at 25 °C.

4.3.5 Cross-linking *Order B*

In this case, supramolecular cross-linking by CB[8] was performed after the enzymatic cross-linking by HRP. Interestingly, this process led to a much smaller particle size for **P2** than in the previous case of **P1**. The average particle size as obtained from DLS measurement was ~ 500 nm for **P2** compared to ~1 μm of **P1**. A stepwise particle size analysis showed that the disulfide cross linked polymer after treatment with HRP and H_2O_2 resulted in a particle size of ~350 nm (Figure 4.1 B). The particle size further enhanced to ~ 500 nm after CB[8] assisted cross-linking. Similar changes in the NMR, absorbance and emission behavior were observed as in case of "*Order A*" confirming the tyrosine cross-linking as well as ternary complexation in this case.

4.3.6 Morphology and stability of P1 and P2

Further confirmation about sizes of the particles were obtained from FESEM, FETEM, AFM and CLSM images of the polymers. Interestingly, after disulfide linkage, crystalline particles were obtained while the second cross-liking in both cases lead to spherical particles as can be seen from Figure 4.5. The final products of cross-linking processes *i.e.*, **P1** and **P2** were both spherical as well. The particle sizes obtained from FESEM images at any stage of the cross-linking processes match closely with that obtained from DLS measurements. Notably, the particle size of the cross-linked polymer can be controlled through the order of cross-linking and a varied range of polymer particles (200-1000 nm) can thus be prepared.

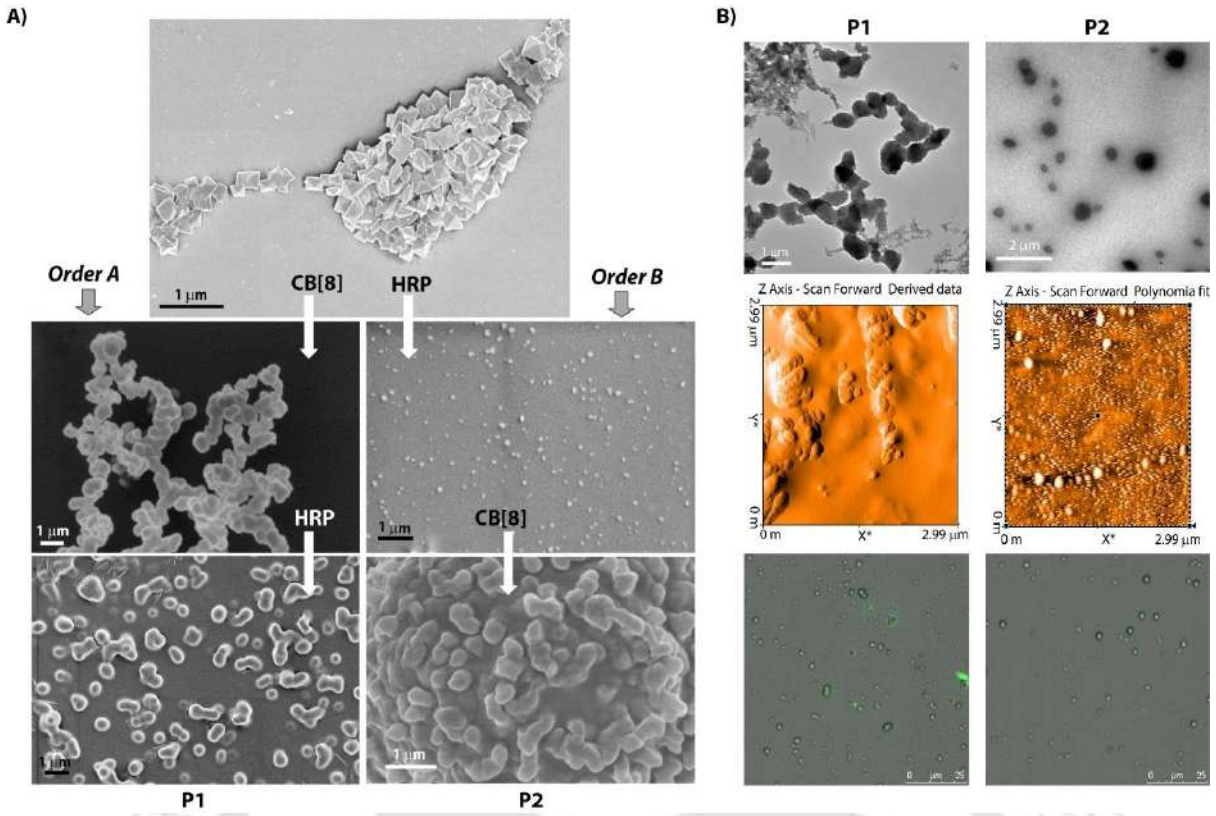

Figure 4.5 (A) FESEM images of solutions at different stages of cross-linking processes of **4.1.** (B) FETEM (top), AFM (middle), CLSM (bottom) images of **P1** and **P2** respectively.

Interesting results obtained from zeta potential (ζ) measurements at different stages of polymerization. The ζ value obtained for disulfide linked polymer was 17 ± 0.2 mV. In case of *Order A*, the introduction of CB[8] to the solution enhanced the ζ value to 38.5 ± 0.2 mV and it remained the similar (38 ± 0.1 mV) even after Tyr cross-linking. On the other hand, for *Order B*, Tyr cross-linking leads to a decrease in the ζ value from 17 ± 0.2 mV to 10.2 ± 0.5mV. Further cross-linking by CB[8] leads to an enhancement to 37 ± 0.5mV which is very similar to that of **P1**. Notably, the positive ζ value in all cases is a result of the surface charges of the polymer and the main contributors to that are the Lys and Arg residues. The presence of CB[8] is certainly stabilizing the polymer particles as well as presumably exposing the RGDS residues at the surfaces of both the polymers.

The stability of **P1** was investigated by varying the temperature (up to 75 °C) of the polymer solution. Over this temperature range, the particle size remained constant (data not shown) confirming that the cross-linked polymer is stable within this temperature range and no change in the absorption and emission behavior was monitored. The stability was also monitored at different pH. Solution of the cross-linked polymer (10% v/v) was mixed with buffers of different pH (1-11) and incubated for 24 hours at room temperature before measuring the particle size as

well as the absorption and emission. The absorption and emission behavior remained almost unaffected throughout the pH range. In case of the particle size, apart from a little (~50 nm) enhancement of size in the acidic pH, no other changes were monitored in the entire pH range. Notably, the results from these studies clearly demonstrate the stability of the **P1** at elevated temperature and wide range of pH.

4.3.7 Cytotoxicity

The cross-linked polymers have surfaces decorated with RGDS sequence which is well-known for its cell-binding properties. Cytotoxicity assay was done with both the polymers, **P1** and **P2**. Different concentrations of **P1** and **P2** (10-1280 µM) were tested for cytotoxicity against RAW264.7 murine macrophage cell line (Figure 4.6 A and B). No significant changes were observed in cell viability when cells were incubated with up to 1280 µM of **P1** and **P2** ($p>0.03$) as ascertained by MTT assay. These results suggest that both the polymers **P1** and **P2** had no significant toxic effect on RAW264.7 macrophage cells up to 1280 µM concentration. The result is representative of means ± SD of three independent experiments.

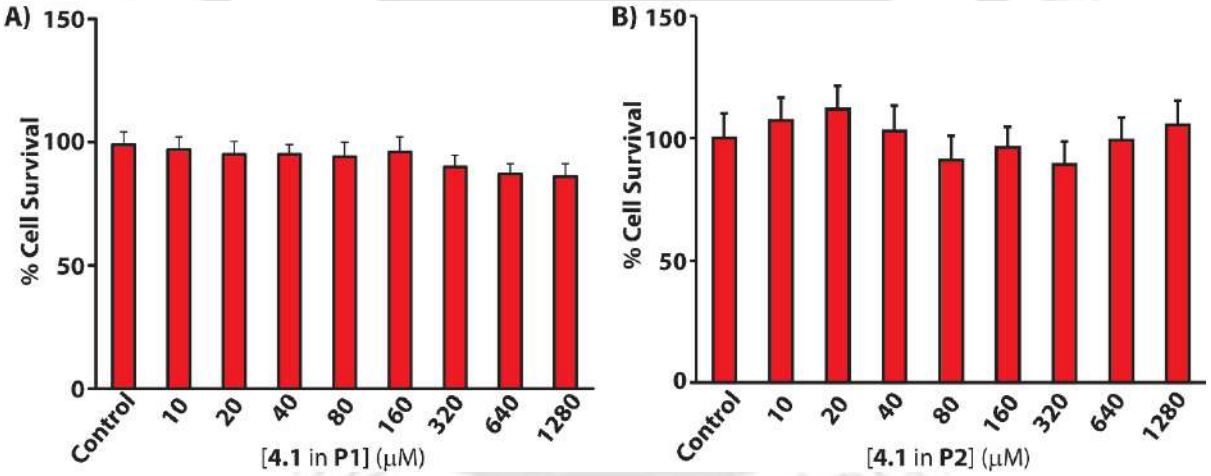

Figure 4.6 Cytotoxic activity of (A) **P1** and (B) **P2** against RAW264.7 macrophage cells.

4.3.8 Cell adhesion

Eight working concentrations of **P1**and **P2** were prepared with deionized water such as 10 µM, 20µM, 40 µM, 80 µM, 160 µM, 320 µM, 640 µM and 1280 µM and cell adhesion assay was performed (Figure 4.7 A, B). The fold changes were calculated with respect to the control cells. Up to 160 µM concentration of **P1**, a little hike in cell adhesion property of the polymer was observed. At 320 and 640 µM, 3-fold changes were recorded (with respect to the control). Dose dependent gradual increase in cell adhesion property was also observed when RAW cells were incubated with **P2**. However, at 1280 µM concentration, Polymer **P1** showed greater cell adhesion property (9.38-fold

as compared to control, p<0.0001) than polymer **P2** (6.4-fold over control, p<0.0001). The result is representative of means ± SD of three independent experiments. These results suggest that both **P1** and **P2** at this concentration range, can bind cells significantly. Microscopic images of the growth of RAW264.7 macrophage cells with different concentrations of **P1** and **P2** are shown in Figure 4.7 C, D.

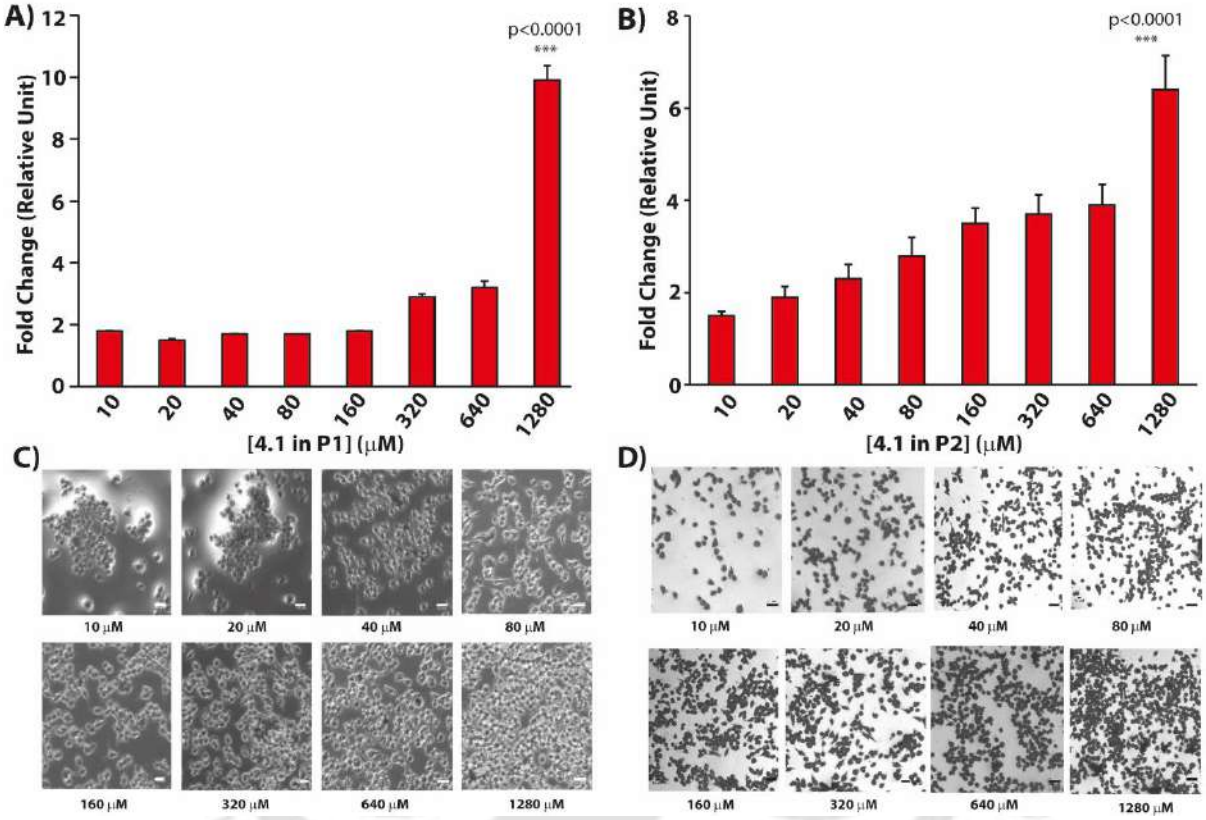

Figure 4.7 (A, B) RAW 264.7 macrophage cells seeded on culture plates for 24 hours-pretreated with different concentrations of (A) **P1** and (B) **P2** for overnight. The result is representative of means ± SD of three independent experiments. (C, D) Microscopic images of RAW 264.7 macrophage cells adhering to (C) **P1** and (D) **P2** of different concentration. Bar = 10 μm.

4.3.9 Effect of P1 and P2 on cell proliferation

Cells were incubated with different concentrations of **P1** and **P2** and cell proliferation was measured after 24, 48 and 72 hours using CyQUANT cell proliferation assay kit and measuring fluorescence intensity on a microplate reader (Figure 4.8 A, B). Values were calculated as the percentage of proliferating cells. After 24 hours of incubation, no significant change in cell proliferation was observed when cells were incubated with up to 1280 μM peptide (p>0.02). After 48 hours, cellular proliferation increased by 36.81 ± 6% (for **P1**) and 40.15±5% (for **P2**) on an average with respect to 24 hours incubated cells, whereas 72 hours incubation increased cellular proliferation by 52.4 ± 5% (for **P1**) and 33.5±4% (for **P2**) on an average compared with 48 hours

incubated cells. The result is representative of means ± SD of three independent experiments. Different dosage of peptide was unable to make any significant changes in cell proliferation at a specific incubation time point. This result suggests that cells can proliferate in these polymers coated microplates. However, **P1** was found to be marginally better than **P2** in this respect.

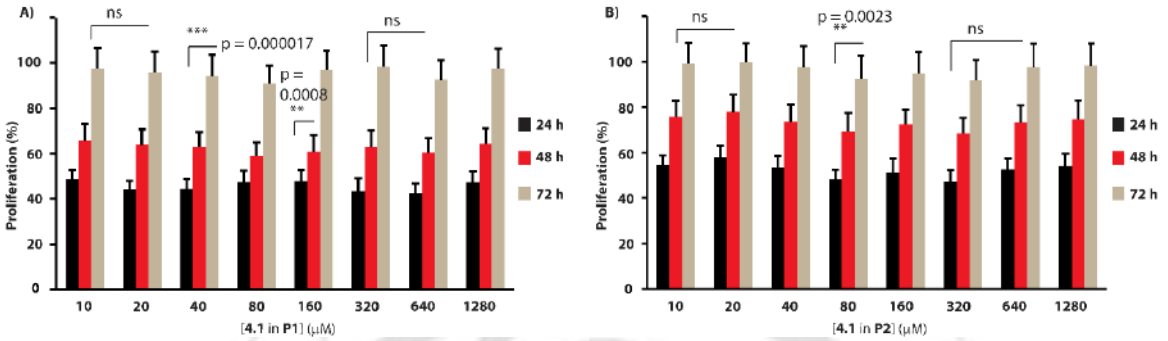

Figure 4.8 Microscopic images of RAW264.7 macrophage cells adhering to (A) **P1** and (B) **P2** of different concentration. Bar = 10 μm.

4.4 CONCLUSION

In summary, a new and simple approach is developed to create peptide based cross-linked polymer. The cross-linking of a small peptide is achieved through covalent disulfide bonds, supramolecular ternary complexes of CB[8] and HRP catalyzed Tyr dimerization. The size of the polymer can be tuned by changing the sequence of cross-linking. A pendent RGDS sequence at the surfaces of these polymers allowed to utilize the non-cytotoxic cross-linked polymers for efficient adhesion and proliferation of RAW264.7 murine macrophages. The effective cell adhesion and proliferation at these polymer surfaces promises further application of this strategy to prepare artificial ECM. Animal model-based therapeutics do not always reflect similar scenario in humans. Therefore, synthesizing ECM from cell adhesive sequence containing artificial scaffolds is a crying need. Similar approach can also be taken for use in other applications by modifying the sequence.

Chapter-5: Development of a Hydrolase Mimicking Peptide Amphiphile and its Immobilization on Silica Surface for Enhanced and Stereoselective Catalysis

5.1 INTRODUCTION

Enzymes are a class of proteins that act as efficient biocatalysts and attract numerous research efforts for endless industrial applications.[271-273]. Biocatalysts for industrial applications are generated by immobilization of enzymes on solid surfaces for enhancement of catalytic sites.[274, 275] In recent years, several efforts have been put-in for production of solid surface-supported biocatalysts to make a breakthrough in developing cost-effective and enhanced chemical reactions. [276-283] However, some major challenges toward using enzymes in industrial processes are, a) lack of availability in bulk quantity; b) possible denaturation due to subtle changes in the environment like rise in temperature or pH; c) problems associated with the development of heterogeneous catalysts using enzymes.[284]

To this end, artificial enzymes or enzyme mimicking molecules appeared to be an attractive alternative.[285-291] The three-dimensional arrangement of the catalytic pocket is extremely challenging to mimic precisely. However, incorporating the amino acids present in the catalytic pocket in a synthetic molecule/system can lead to artificial enzyme that can be used for specific and stereoselective organic transformations.[157, 292-301] A plethora of effort have so far been made to construct artificial enzymes with similar or superior activity than the enzymes.[295, 302, 303]

In this regard, peptide-based systems come to forefront as suitable design of peptides can provide the required amino acid functionalities to create the catalytic activity. Peptide self-assembled superstructures have proven to be efficient artificial biocatalysts in aqueous media,[294, 296-298] peroxidases,[299] and histidine-based esterases,[155, 157, 300, 301] to name a few. Hydrolytic enzymes like, lipase, a-chymotrypsin etc. have received significant interest owing to their abundance in living organisms and ever-increasing industrial importance.[161, 304-306] Various research groups have developed artificial esterases with properly oriented catalytic groups by recreating a hydrophobic core for substrate-binding, as observed in natural enzymes.[307, 306]

In this work, a short-branched peptide amphiphile (PA) based artificial esterase has been developed through systematic screening of a library of PAs. The design of the PAs was inspired from well-documented catalytic triad His-Ser-Asp, where cooperative assistance of histidine, serine and aspartic acid stabilizes the transition state of the resultant hydrolysis product from a particular substrate.[308-311] The identified PA has been immobilized on silica nanoparticle surface using simple covalent functionalization to create a heterogeneous catalyst. The catalyst not only showed much superior activity compared to a natural esterase but also demonstrated high

stereoselectivity. Moreover, the catalyst was found to be highly robust and recyclable without losing activity for several cycles.

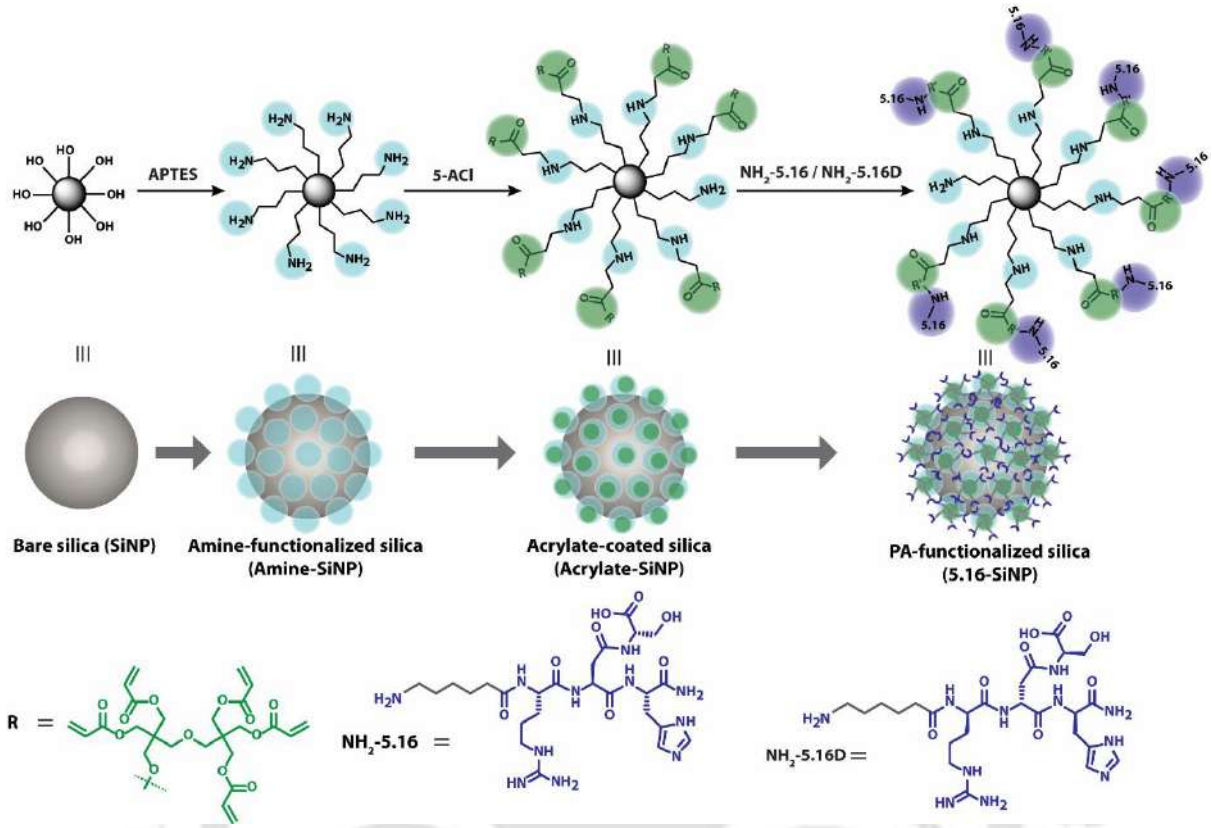

Scheme 5.1 Schematic presentation of the synthesis of **5.16**-functionalized silica nanoparticles.

5.2 EXPRIMENTAL SECTION

5.2.1 General

Rink amide MBHA resin, Fmoc-Arg(Pbf)OH, Fmoc-Asp(Otbu)-OH, Fmoc-Ser(tbu)-OH, Fmoc-His(Trt)-OH, Fmoc-L-Asp(OAll)-OH, Boc-L/D-Phe-OH, HBTU and were procured from GL Biochem, China. TEOS, APTES, 5Acl, phenylsilane, $Pd(PPh_3)_4$ catalyst, caproic acid, butyric acid, caprylic acid, acetyl chloride, allyl alcohol, CV Lipase and TES were purchased from Sigma Aldrich. 6-Aminocaproic acid, p-Nitrophenol, Fmoc-Cl, DCC, Ac_2O and $(Boc)_2O$ was purchased from Spectrochem. Dioxane, TFA, phenol, HPLC-grade solvents, like DMF, ACN, hexane and IPA were procured from Merck. To prepare samples, Milli-Q water with a conductivity of less than 2 $mScm^{-1}$ was used. Chromatographic purifications were performed on a Luna 5 µm (C18, 250 × 10 mm) column (Phenomenex) whereas, analytical HPLC were performed on a Luna 5 µm (C18, 250 × 4.6 mm) column (Phenomenex) using a Dionex Ultimate 3000 HPLC. Identification of L/D Boc-Phe-OH, L/D Boc-Phe-PNP were performed on a Diacel (CHIRALPAK-AD-H) 5 mm, 150 x 4.6 mm analytical column. UV-Visible spectra were recorded on a PerkinElmer Lambda 750 spectrometer.

Standard 10 mm-path quartz cuvettes were used for all spectroscopic measurements. ^{1}H NMR, ^{13}C NMR were recorded with a Bruker Ascend 600 MHz (Bruker, Coventry, UK) spectrometer and referenced to deuterated solvents. ESI-MS were performed with a Q-Tof Micro Quadrupole mass spectrophotometer (Micromass). FETEM images were taken using JEOL JEM-2100F microscope. TGA analysis were performed on a Netzsch instrument, whereas BET experiments were performed on a Quantachrome Autosorb-IQ MP instrument.

5.2.2 Synthetic protocols

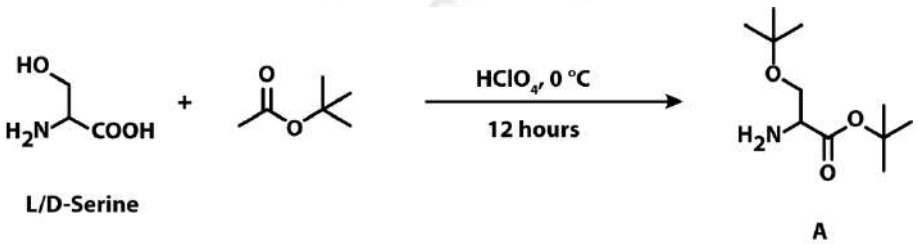

Synthesis of Compound A

Compound A was synthesized according to a previously reported procedure.[312] Briefly, perchloric acid (20.8 mmol) was added slowly to a suspension of L/D-serine (1 g, 9.6 mmol) and tert-butyl acetate (26 mL, 190.3 mmol) maintained at 0 °C. The reaction mixture was allowed to come to room temperature and stirred for 12 hours. After that, 60 ml water was added followed by 1 M HCl to attain pH 3. The pH of the mixture was further raised to 9 with 10% K_2CO_3 solution, and the reaction mixture was extracted with DCM three times. The organic portions were dried over anhydrous Na_2SO_4 and concentrated to obtain a yellow oil. The crude material was purified with column chromatography using 2% Methanol/DCM. Yield: 95%. ^{1}H NMR (600 MHz, $CDCL_3$) δ (ppm): 3.69 (m, 1H), 3.66 (m, 1H), 3.45 (m, 1H), 1.42 (s, 9H), 1.11 (s, 9H). ESI-MS, calculated for $C_{11}H_{23}NO_3$: 218.17 $[M+H]^+$, obtained, 218.19.

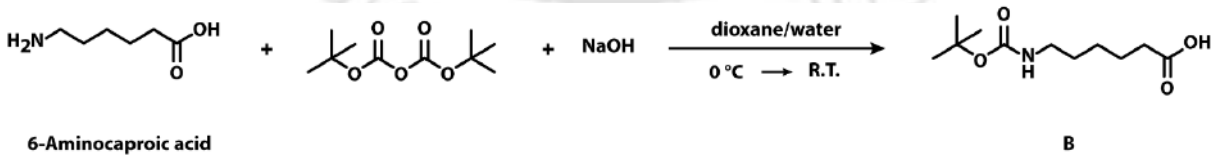

Synthesis of Compound B

Compound B was synthesized according to a previously reported procedure.[313] 6-aminocaproic acid (1 g, 6.8 mmol) and sodium hydroxide (0.27 g, 6.8 mmol) were dissolved in dioxane/water (2:1, 21 mL) and the reaction flask was flushed with argon. The temperature was adjusted to 0 °C. Then $(Boc)_2O$ (2.4 g, 10.8 mmol) solution in dioxane/water was added dropwise under ice-cold condition and the reaction was stirred at room temperature overnight. Dioxane was removed

under reduced pressure and 20 mL water was added and washed three times with equal volumes of ethyl acetate. The aqueous portion was neutralized with 1 M HCl to attain complete precipitation. The reaction mixture was then extracted with ethyl acetate three times, organic portion was dried over anhydrous Na_2SO_4 and concentrated to obtain a colourless oil which was dried under high vacuum to obtain a white solid. Yield: 90%. ^{1}H NMR (600 MHz, $CDCL_3$) δ (ppm): 3.18 (t, 2H), 2.23 (t, 2H), 1.58 (m, 4H), 1.42 (s, 9H),1.35 (m, 2H). ESI-MS, calculated for $C_{11}H_{21}NO_4$: 232.15 [M+ H]$^+$, obtained, 232.11.

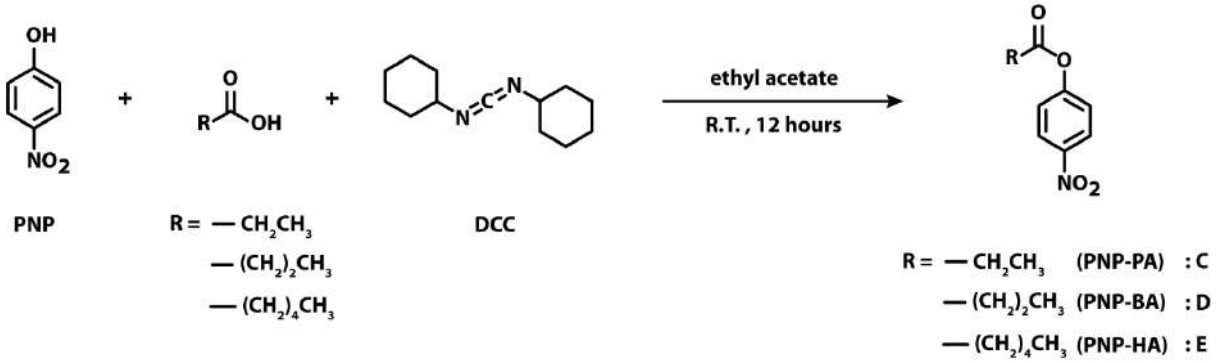

Synthesis of Compounds C, D, E

The PNP-esters were synthesized according to a reported procedure.[314] Alkanoic acids (3.25 mmol) and DCC (1.38 g, 6.53 mmol) were mixed together and dissolved in distilled ethyl acetate. Then 0.5 g PNP (0.5 g, 3.59 mmol) was added and stirred at room temperature for 12 hours. After that, ethyl acetate was removed under reduced pressure and the crude material was purified with column chromatography using 5% ethyl acetate/hexane. PNP-propanoate ester was obtained as a white solid. PNP-butanoate and PNP-hexanoate esters were obtained as yellow liquids.

Compound C: Yield: 72%. ^{1}H NMR (600 MHz, $CDCL_3$) δ (ppm): 8.27 (d, *J* = 9.2 Hz, 2H), 7.28 (d, *J* = 9.1 Hz, 2H), 2.64 (q, *J* = 7.5 Hz, 2H), 1.28 (t, *J* = 7.6 Hz, 3H). ESI-MS, calculated for $C_9H_9NO_4$: 196.05 [M+ H]$^+$, obtained, 196.08.

Compound D: Yield: 68%. ^{1}H NMR (600 MHz, $CDCL_3$) δ (ppm): 8.29 (d, *J* = 9.1 Hz, 2H), 7.30 (d, *J* = 9.2 Hz, 2H), 2.61 (t, *J* = 7.4 Hz, 2H), 1.82 (q, *J* = 7.4 Hz, 2H), 1.08 (t, *J* = 7.4 Hz, 3H). ESI-MS, calculated for $C_{10}H_{11}NO_4$: 210.07 [M+ H]$^+$, obtained, 210.08.

Compound D: Yield: 65%. ^{1}H NMR (600 MHz, $CDCL_3$) δ (ppm): 8.32 (d, *J* = 9.1 Hz, 2H), 7.53 (d, *J* = 9.2 Hz, 2H), 2.59 (t, *J* = 7.4 Hz, 2H), 1.71 (m, 6H), 1.08 (t, *J* = 7.4 Hz, 3H). ESI-MS, calculated for $C_{12}H_{15}NO_4$: 238.26 [M+ H]$^+$, obtained, 238.29.

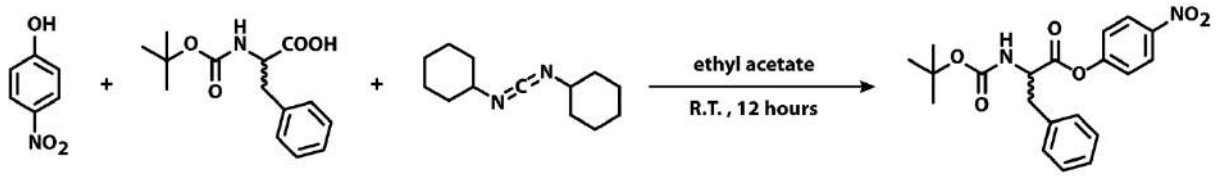

PNP Boc-L/D-Phe-OH DCC Boc-L-Phe-PNP : F Boc-D-Phe-PNP : G

Synthesis of Compounds F and G

Boc-L/D-Phe-OH (0.85 g, 3.23 mmol) and DCC (1.12g, 5.4 mmol) were dissolved in distilled ethyl acetate and to it PNP (0.5 g, 3.6 mmol) was added and the reaction was stirred at room temperature for 12 hours. After this, the reaction mixture was kept in cold condition to get precipitate of DCU which was filtered and the organic portion was washed twice with saturated $NaHCO_3$ solution, dried over anhydrous Na_2SO_4 and concentrated to obtain a yellow liquid. This yellow liquid was recrystallized from hot ethanol to obtain the white compound.

Compound F: Yield: 58%. ^{1}H NMR (600 MHz, $CDCL_3$) δ (ppm): 8.27 – 8.22 (m, 2H), 7.37 – 7.30 (m, 3H), 7.25 – 7.21 (m, 2H), 7.14 (d, *J* = 9.1 Hz, 2H), 5.04 (s, 1H), 4.80 (d, *J* = 7.2 Hz, 1H), 3.22 (dd, *J* = 10.2, 6.7 Hz, 2H), 1.45 (s, 9H). ESI-MS, calculated for $C_{20}H_{22}N_2O_6$: 387.15 $[M+H]^+$, obtained, 387.18.

Compound G: 60%. ^{1}H NMR (600 MHz, $CDCL_3$) δ (ppm): 8.25 (d, *J* = 8.9 Hz, 2H), 7.38 – 7.30 (m, 3H), 7.25 – 7.22 (m, 2H), 7.14 (d, *J* = 9.1 Hz, 2H), 5.04 (d, *J* = 7.9 Hz, 1H), 4.80 (d, *J* = 7.6 Hz, 1H), 3.22 (dd, *J* = 10.5, 6.7 Hz, 2H), 1.57 (s, 9H). ESI-MS, calculated for $C_{20}H_{22}N_2O_6$: 387.15 $[M+H]^+$, obtained, 387.16.

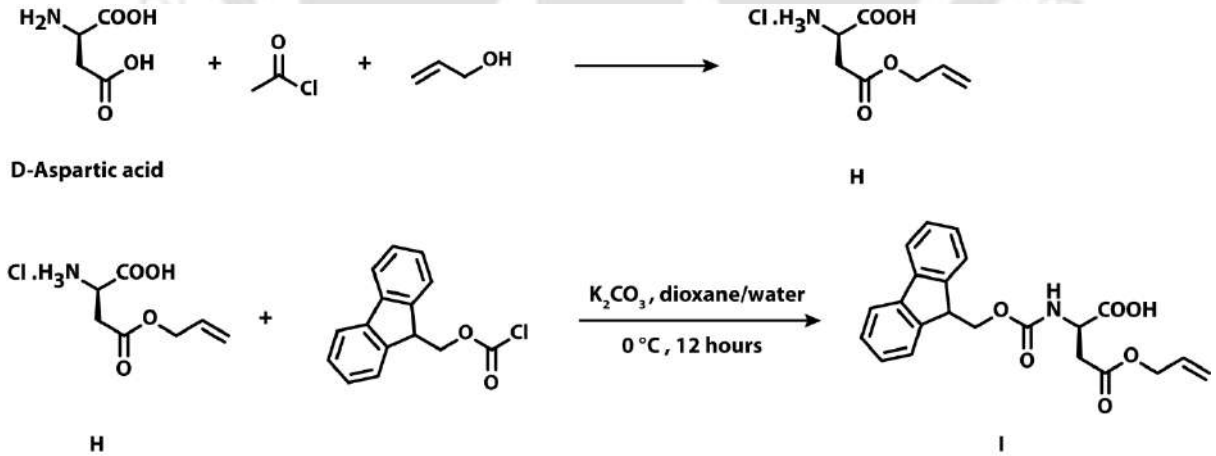

D-Aspartic acid H H I

Synthesis of Fmoc-D-Asp(OAll)-OH

Compound H and I were synthesized by a pre-established procedure.[315] Acetyl chloride (1.06 mL, 15 mmol) was added dropwise to 8.42 mL of allyl alcohol under ice-cold condition and argon atmosphere. The resulting solution was stirred at 0 °C for 15 minutes and then at room temperature for 1 hour. D-Aspartic acid (0.5 g, 3.76 mmol) was added in a single portion and the

suspension stirred for 18 hours and then poured into ice-cold diethyl ether (50 mL). After stirring at 0 °C for 1 hour the precipitate was collected by filtration and was washed on the pad with diethyl ether to give the hydrochloride as a white powder. To an ice-cold stirred aqueous suspension (20 mL) of g-allyl-D-aspartate hydrochloride (0.35 g, 2 mmol), K_2CO_3 (0.45 g, 3.2 mmol) was added. A pre-stirred solution of Fmoc-Cl (0.57 g, 2.2 mmol) in 15 mL dioxane was added. The reaction mixture was allowed to stir for 12 hours. The aqueous solution was washed with diethyl ether and acidified to pH 2 at 0 °C with 6 M HCl. The aqueous portion was extracted three times with diethyl ether. The organic portions were combined, dried over anhydrous Na_2SO_4 and concentrated to obtain a white solid. under cold condition After this, dioxane was removed under reduced pressure to obtain a white solid. Yield: 54% after two steps. ^{1}H NMR (600 MHz, $CDCL_3$) δ (ppm) 8.02 (t, *J* = 7.0 Hz, 3H), 7.91 – 7.81 (m, 3H), 7.65 (d, *J* = 7.5 Hz, 2H), 7.59 – 7.55 (m, 2H), 6.15 (td, *J* = 10.7, 5.2 Hz, 1H), 5.54 (dd, *J* = 44.9, 13.8 Hz, 2H), 5.09 – 5.01 (m, 2H), 4.95 (s, 1H), 4.73 – 4.58 (m, 2H), 4.52 – 4.28 (m, 2H), 3.35 (dd, *J* = 17.4, 4.8 Hz, 1H), 3.19 (dd, *J* = 17.3, 4.7 Hz, 1H). ^{13}C NMR (151 MHz, $CDCL_3$) δ (ppm)173.97, 170.90, 144.34, 143.68, 141.53, 141.32, 131.56, 127.62, 127.13, 127.10, 125.18, 124.79, 120.07, 120.03, 118.86, 65.91, 64.97, 50.22, 47.09, 36.45. ESI-MS, calculated for $C_{21}H_{19}NO_6$: 382.12 $[M+H]^+$, obtained, 382.16.

Synthesis of PAs

PAs 5.1-5.15 were synthesized on Rink amide MBHA resin using standard Fmoc (9-fluorenylmethoxycarbonyl) solid phase peptide synthesis (SPPS) method. In a standard coupling, 3 equiv. of protected amino acid (with respect to the loading of the resin), 3 equiv. of HBTU, and 6 equiv. of DIPEA were taken in 5 mL of DMF (for 0.1 mmol scale with respect to the resin loading) and stirred for 5 min prior to addition of the mixture to the resin. The reaction mixture was shaken for 60 min and the resin was washed several times with DMF. The Fmoc-deprotection was achieved by treatment of the resin with 20% piperidine (5 mL, 5 min, three times) followed by thorough washing of the resin with DMF. The Fmoc-deprotection and coupling steps were repeated until the designed peptide sequence was obtained. The peptide loaded resin was washed several times with DMF followed by DCM and dried under reduced pressure. The dried resin was then treated with freshly prepared mixture of TFA/TES/phenol/water (85: 5:5:5 v/v) and stirred for 4 hours. The resin was finally washed with DCM. The cleavage cocktail and the washings combined and concentrated to a minimum volume on a rotary evaporator. The cleaved peptide was then precipitated from cold dry ether, centrifuged and lyophilized to get the crude peptide. Purification was done in a semipreparative HPLC using a Luna 5 µm C18(2) column (Phenomenex)

and an eluent of acetonitrile and water starting at 10% ACN/H_2O reaching to 30 % ACN/H_2O in 15 minutes and finally to 100% ACN in 18 minutes to complete the chromatogram in 22 minutes. The pure lyophilized peptides were obtained in 65-70% yield.

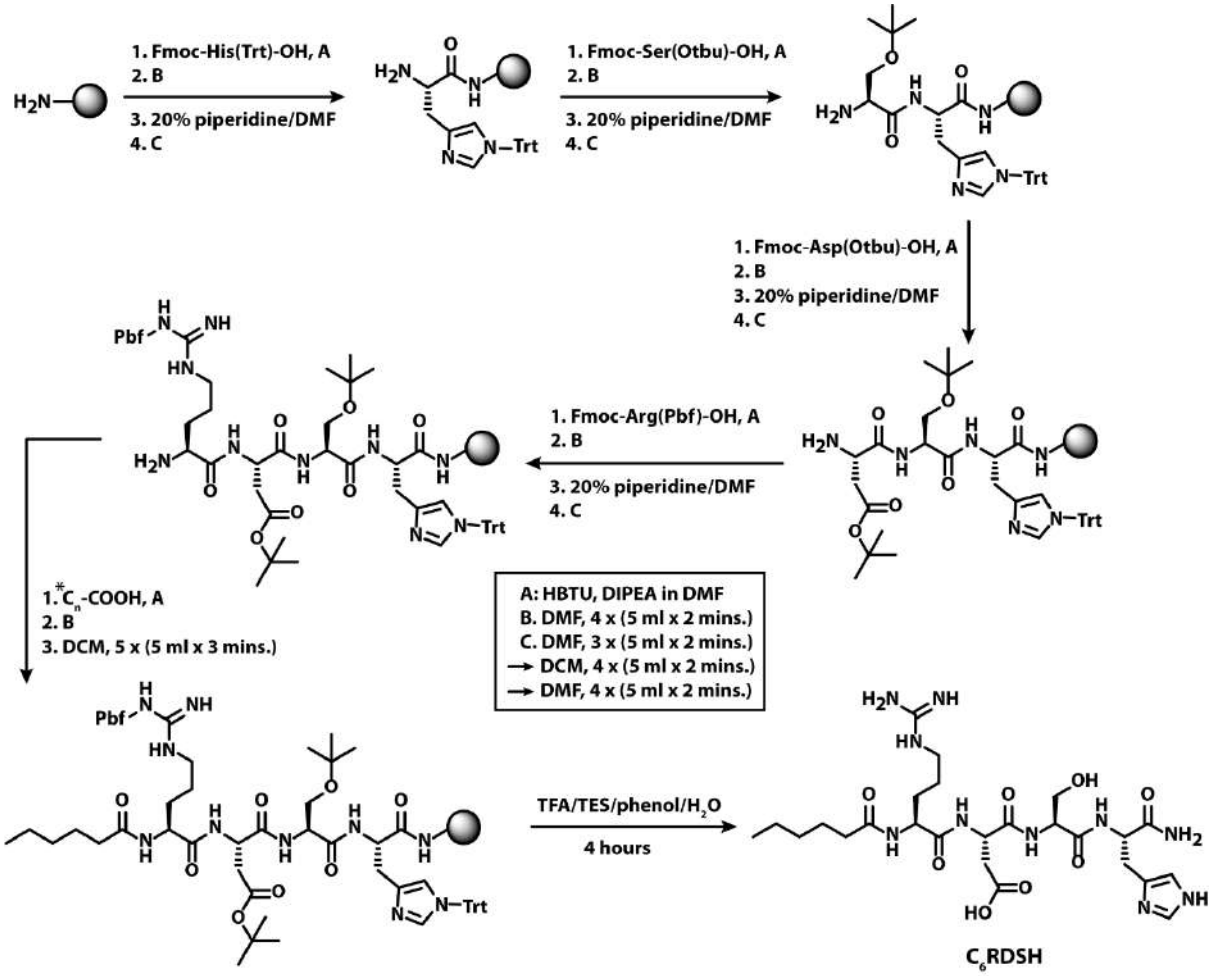

Amino acids were changed according to the synthesized sequences:

5.7 : C_6RDHS	5.12 : C_6RDSG
5.8 : C_6RHDS	5.13 : C_6RDGH
5.9 : C_6RHSD	5.14 : C_6RGSH
5.10 : C_6RSDH	5.15 : C_6GDSH
5.11 : C_6RSHD	

* n = 1 : C_2RDSH : 5.2
3 : C_4RDSH : 5.3
5 : C_6RDSH : 5.4
7 : C_8RDSH : 5.5
9 : C_{10}RDSH : 5.6

PA **5.1**. Yield: 86%. ^{1}H NMR (600 MHz, D_2O) δ (ppm): 8.63 (d, *J* = 1.5 Hz, 1H), 7.35 – 7.31 (m, 1H), 4.74 – 4.62 (m, 2H), 4.41 (d, *J* = 5.2 Hz, 1H), 4.06 (d, *J* = 6.5 Hz, 1H), 3.84 (dd, *J* = 21.4, 5.2 Hz, 2H), 3.34 (dd, *J* = 15.5, 5.5 Hz, 1H), 3.23 (t, *J* = 7.0 Hz, 3H), 2.99 – 2.94 (m, 1H), 2.88 – 2.82 (m, 1H), 1.99 – 1.91 (m, 2H), 1.69 – 1.60 (m, 2H). ^{13}C NMR (151 MHz, D_2O) δ (ppm): 173.96, 171.50, 169.34, 156.74, 133.42, 128.48, 117.22, 60.82, 55.73, 52.56, 52.35, 50.23, 40.30, 27.93, 26.12, 23.44. ESI-MS, calculated for $C_{19}H_{33}N_{10}O_7$: 513.25 $[M+H]^+$, obtained, 513.30.

PA **5.2**. Yield: 84%. ^{1}H NMR (600 MHz, D_2O) δ (ppm): 8.62 (s, 1H), 7.33 (s, 1H), 4.74 (d, *J* = 9.9 Hz, 2H), 4.38 (t, *J* = 5.2 Hz, 1H), 4.27 – 4.20 (m, 1H), 3.83 (dd, *J* = 22.0, 5.2 Hz, 2H), 3.21 (t, *J* = 7.3 Hz, 3H), 2.99

(dd, *J* = 17.0, 6.4 Hz, 1H), 2.88 – 2.82 (m, 1H), 2.04 (s, 3H), 1.86 – 1.73 (m, 2H), 1.64 (dt, *J* = 18.2, 7.2 Hz, 2H). ^{13}C NMR (151 MHz, D_2O) δ (ppm): 174.60, 174.24, 174.03, 173.99, 172.39, 171.62, 156.72, 133.41, 128.51, 117.24, 60.81, 55.77, 53.83, 52.26, 49.99, 40.44, 27.85, 26.06, 24.28, 21.59. ESI-MS, calculated for $C_{21}H_{35}N_{10}O_8$: 555.26 $[M+H]^+$, obtained, 555.30.

PA **5.3**. Yield: 81%. ^{1}H NMR (600 MHz, D_2O) δ (ppm): 8.62 (d, *J* = 1.4 Hz, 1H), 7.34 – 7.31 (m, 1H), 4.74 (d, *J* = 7.4 Hz, 2H), 4.38 (d, *J* = 5.3 Hz, 1H), 4.28 (d, *J* = 2.6 Hz, 1H), 3.83 (dd, *J* = 24.2, 5.2 Hz, 2H), 3.21 (d, *J* = 6.7 Hz, 3H), 2.99 – 2.91 (m, 1H), 2.87 – 2.78 (m, 1H), 2.28 (t, *J* = 7.3 Hz, 2H), 1.86 – 1.72 (m, 2H), 1.61 (q, *J* = 7.4 Hz, 4H), 0.90 (t, *J* = 7.4 Hz, 3H). ^{13}C NMR (151 MHz, D_2O) δ (ppm): 177.55, 174.37, 173.99, 172.43, 171.63, 156.71, 133.39, 128.52, 117.23, 60.82, 55.77, 53.59, 52.27, 50.02, 40.42, 37.19, 35.33, 27.87, 26.06, 24.37, 18.84, 12.74. ESI-MS, calculated for $C_{23}H_{39}N_{10}O_8$: 583.29 $[M+H]^+$, obtained, 583.33.

PA **5.4**. Yield: 85%. ^{1}H NMR (600 MHz, D_2O) δ (ppm): 8.62 (d, *J* = 1.5 Hz, 1H), 7.33 (s, 1H), 4.77 – 4.71 (m, 2H), 4.38 (t, *J* = 5.2 Hz, 1H), 4.29 – 4.25 (m, 1H), 3.83 (dd, *J* = 24.5, 5.3 Hz, 2H), 3.24 – 3.16 (m, 3H), 2.98 (dd, *J* = 16.8, 6.5 Hz, 1H), 2.85 (dd, *J* = 17.0, 7.1 Hz, 1H), 2.30 (td, *J* = 7.3, 3.5 Hz, 2H), 1.79 (ddd, *J* = 43.5, 7.5, 4.3 Hz, 2H), 1.59 (t, *J* = 7.4 Hz, 4H), 1.34 – 1.23 (m, 4H), 0.86 (t, *J* = 7.0 Hz, 3H). ^{13}C NMR (151 MHz, D_2O) δ (ppm): 177.76, 173.97, 173.94, 172.36, 171.62, 156.69, 133.40, 128.51, 117.23, 60.83, 55.78, 53.56, 52.26, 49.95, 40.41, 35.29, 30.46, 27.83, 26.07, 24.91, 24.41, 21.64, 13.15. ESI-MS, calculated for $C_{25}H_{43}N_{10}O_8$: 611.32 $[M+H]^+$, obtained, 611.33.

PA **5.5**. Yield: 72%. ^{1}H NMR (600 MHz, D_2O) δ (ppm): 8.62 (d, *J* = 1.5 Hz, 1H), 7.33 – 7.31 (m, 1H), 4.76 – 4.73 (m, 2H), 4.40 – 4.22 (m, 3H), 3.88 – 3.77 (m, 2H), 3.21 (t, *J* = 7.3 Hz, 3H), 2.90 (ddd, *J* = 78.5, 16.9, 6.9 Hz, 2H), 2.30 (dd, *J* = 7.4, 3.4 Hz, 2H), 1.88 – 1.55 (m, 7H), 1.32 – 1.20 (m, 8H), 0.88 – 0.82 (m, 3H). ^{13}C NMR (151 MHz, D_2O) δ (ppm): 177.77, 174.36, 173.97, 173.91, 172.41, 171.62, 156.68, 133.39, 128.52, 117.23, 60.82, 55.79, 53.54, 52.27, 50.01, 40.42, 35.32, 30.94, 28.12, 28.04, 27.83, 26.06, 25.20, 24.44, 21.91, 13.33. ESI-MS, calculated for $C_{27}H_{47}N_{10}O_8$: 639.35 $[M+H]^+$, obtained, 639.31.

PA **5.6**. Yield: 70%. ^{1}H NMR (600 MHz, D_2O) δ (ppm): 8.66 – 8.61 (m, 1H), 7.33 (s, 1H), 4.72 (d, *J* = 2.3 Hz, 2H), 4.42 (t, *J* = 5.2 Hz, 1H), 4.26 (dd, *J* = 8.9, 5.5 Hz, 1H), 3.95 – 3.88 (m, 2H), 3.23 (t, *J* = 7.1 Hz, 3H), 2.86 (dd, *J* = 23.4, 6.6 Hz, 2H), 2.30 (q, *J* = 7.4 Hz, 2H), 1.87 – 1.79 (m, 1H), 1.77 – 1.70 (m, 1H), 1.67 – 1.55 (m, 6H), 1.35 – 1.22 (m, 6H), 0.87 (t, *J* = 6.9 Hz, 3H). ^{13}C NMR (151 MHz, D_2O) δ (ppm): 177.76, 174.30, 173.91, 172.29, 171.46, 156.70, 133.45, 128.35, 117.29, 61.03, 55.42, 53.40, 52.61, 50.29, 40.40, 35.45, 35.32, 30.47, 29.82, 29.75, 28.75, 27.98, 27.83, 26.06, 24.94, 24.41, 21.64, 13.13. ESI-MS, calculated for $C_{29}H_{51}N_{10}O_8$: 667.38 $[M+H]^+$, obtained, 667.32.

PA **5.7**. Yield: 84%. ^{1}H NMR (600 MHz, D_2O) δ (ppm): 8.65 – 8.62 (m, 1H), 7.32 (s, 1H), 4.74 (d, *J* = 2.3 Hz, 2H), 4.43 (t, *J* = 5.2 Hz, 1H), 4.29 (dd, *J* = 8.9, 5.5 Hz, 1H), 3.91 – 3.83 (m, 2H), 3.21 (t, *J* = 7.1 Hz, 3H), 2.87 (dd, *J* = 23.4, 6.6 Hz, 2H), 2.30 (q, *J* = 7.4 Hz, 2H), 1.87 – 1.79 (m, 1H), 1.77 – 1.70 (m, 1H), 1.67 – 1.55 (m, 4H), 1.33 – 1.22 (m, 4H), 0.86 (t, *J* = 6.9 Hz, 3H). ^{13}C NMR (151 MHz, D_2O) δ (ppm): 177.72, 174.30, 173.91, 172.29, 171.46, 156.70, 133.45, 128.35, 117.29, 61.03, 55.42, 53.40, 52.61, 50.29, 40.40, 35.45, 35.32, 30.47, 27.83, 26.06, 24.94, 24.41, 21.64, 13.13. ESI-MS, calculated for ESI-MS, calculated for $C_{25}H_{43}N_{10}O_8$: 611.32 $[M+H]^+$, obtained, 611.35.

PA **5.8**. Yield: 82%. ^{1}H NMR (600 MHz, D_2O) δ (ppm): 8.64 (d, *J* = 1.4 Hz, 1H), 7.31 (s, 1H), 4.77 – 4.70 (m, 2H), 4.42 (t, *J* = 5.0 Hz, 1H), 4.26 (dd, *J* = 8.9, 5.6 Hz, 1H), 3.94 – 3.84 (m, 2H), 3.20 (dd, *J* = 8.1, 5.4 Hz, 3H), 2.99 – 2.93 (m, 1H), 2.87 (d, *J* = 7.5 Hz, 1H), 2.27 (td, *J* = 7.4, 3.3 Hz, 2H), 1.82 – 1.54 (m, 6H), 1.33 – 1.20 (m, 4H), 0.86 (t, *J* = 7.2 Hz, 3H). ^{13}C NMR (151 MHz, D_2O) δ (ppm): 177.50, 174.05, 174.00, 173.91, 172.13, 171.38, 156.69, 133.49, 128.30, 117.26, 61.02, 55.48, 53.21, 52.30, 50.20, 40.39, 35.40, 35.26, 30.42, 27.95, 26.07, 24.98, 24.47, 21.62, 13.16. ESI-MS, calculated for $C_{25}H_{43}N_{10}O_8$: 611.32 $[M+H]^+$, obtained, 611.39.

PA **5.9**. Yield: 70%. ^{1}H NMR (600 MHz, D_2O) δ (ppm): 8.65 – 8.61 (m, 1H), 7.32 (s, 1H), 4.75 (s, 2H), 4.45 (t, *J* = 5.7 Hz, 1H), 4.26 (dd, *J* = 8.9, 5.7 Hz, 1H), 3.86 (dd, *J* = 19.0, 5.7 Hz, 2H), 3.19 (t, *J* = 6.9 Hz, 3H), 3.00 – 2.85 (m, 2H), 2.28 (dd, *J* = 7.4, 3.4 Hz, 2H), 1.81 – 1.52 (m, 6H), 1.33 – 1.20 (m, 4H), 0.85 (t, *J* = 7.2 Hz, 3H). ^{13}C NMR (151 MHz, D_2O) δ (ppm): 177.52, 174.78, 174.10, 173.94, 171.45, 156.69, 133.50, 128.27, 117.32, 60.94, 55.42, 53.26, 52.32, 49.87, 40.38, 35.32, 35.26, 30.41, 27.92, 26.25, 24.97, 24.45, 21.62, 13.16. ESI-MS, calculated for $C_{25}H_{43}N_{10}O_8$: 611.32 $[M+H]^+$, obtained, 611.28.

PA **5.10**. Yield: 77%. ^{1}H NMR (600 MHz, D_2O) δ (ppm): 8.64 (d, *J* = 1.4 Hz, 1H), 7.34 – 7.30 (m, 1H), 4.74 – 4.65 (m, 2H), 4.44 (t, *J* = 5.6 Hz, 1H), 4.33 (dd, *J* = 8.8, 5.5 Hz, 1H), 3.85 (dd, *J* = 22.6, 5.6 Hz, 2H), 3.24 – 3.14 (m, 3H), 2.94 – 2.82 (m, 2H), 2.31 (td, *J* = 7.2, 2.0 Hz, 2H), 1.91 – 1.55 (m, 7H), 1.34 – 1.22 (m, 4H), 0.86 (t, *J* = 7.0 Hz, 3H). ^{13}C NMR (151 MHz, D_2O) δ (ppm): 177.78, 174.14, 174.01, 173.88, 172.10, 171.65, 133.46, 128.49, 117.19, 60.87, 55.25, 53.42, 52.27, 50.13, 40.44, 35.33, 35.17, 30.46, 28.00, 26.11, 24.95, 24.42, 21.65, 13.14. ESI-MS, calculated for $C_{25}H_{43}N_{10}O_8$: 611.32 $[M+H]^+$, obtained, 611.34.

PA **5.11**. Yield: 78%. ^{1}H NMR (600 MHz, D_2O) δ (ppm): 8.65 – 8.61 (m, 1H), 7.34 – 7.30 (m, 1H), 4.75 – 4.67 (m, 2H), 4.42 – 4.29 (m, 2H), 3.90 – 3.77 (m, 2H), 3.25 – 3.16 (m, 3H), 2.98 – 2.90 (m, 1H), 2.83 (dd, *J* = 17.0, 8.1 Hz, 1H), 2.31 (td, *J* = 7.3, 4.2 Hz, 2H), 1.90 – 1.54 (m, 6H), 1.33 – 1.21 (m, 4H), 0.85 (t, *J* = 6.9 Hz, 3H). ^{13}C NMR (151 MHz, D_2O) δ (ppm): 177.75, 174.54, 173.89, 171.26, 156.70, 133.45,

128.31, 117.26, 60.87, 55.51, 53.33, 52.59, 49.91, 40.42, 35.34, 30.46, 27.97, 25.93, 24.95, 24.41, 21.65, 13.14. ESI-MS, calculated for $C_{25}H_{43}N_{10}O_8$: 611.32 $[M+H]^+$, obtained, 611.39.

PA **5.12**. Yield: 81%. ESI-MS, calculated for $C_{21}H_{39}N_8O_8$: 531.28 $[M+H]^+$, obtained, 531.31.

PA **5.13**. Yield: 88%. ESI-MS, calculated for $C_{24}H_{41}N_{10}O_7$: 581.30 $[M+H]^+$, obtained, 582.36.

PA **5.14**. Yield: 90%. ESI-MS, calculated for $C_{23}H_{41}N_{10}O_6$: 553.31 $[M+H]^+$, obtained, 553.38.

PA **5.15**. Yield: 82%. ESI-MS, calculated for $C_{21}H_{34}N_7O_8$: 512.24 $[M+H]^+$, obtained, 511.29.

Synthesis of 5.16 and H_2N-5.16

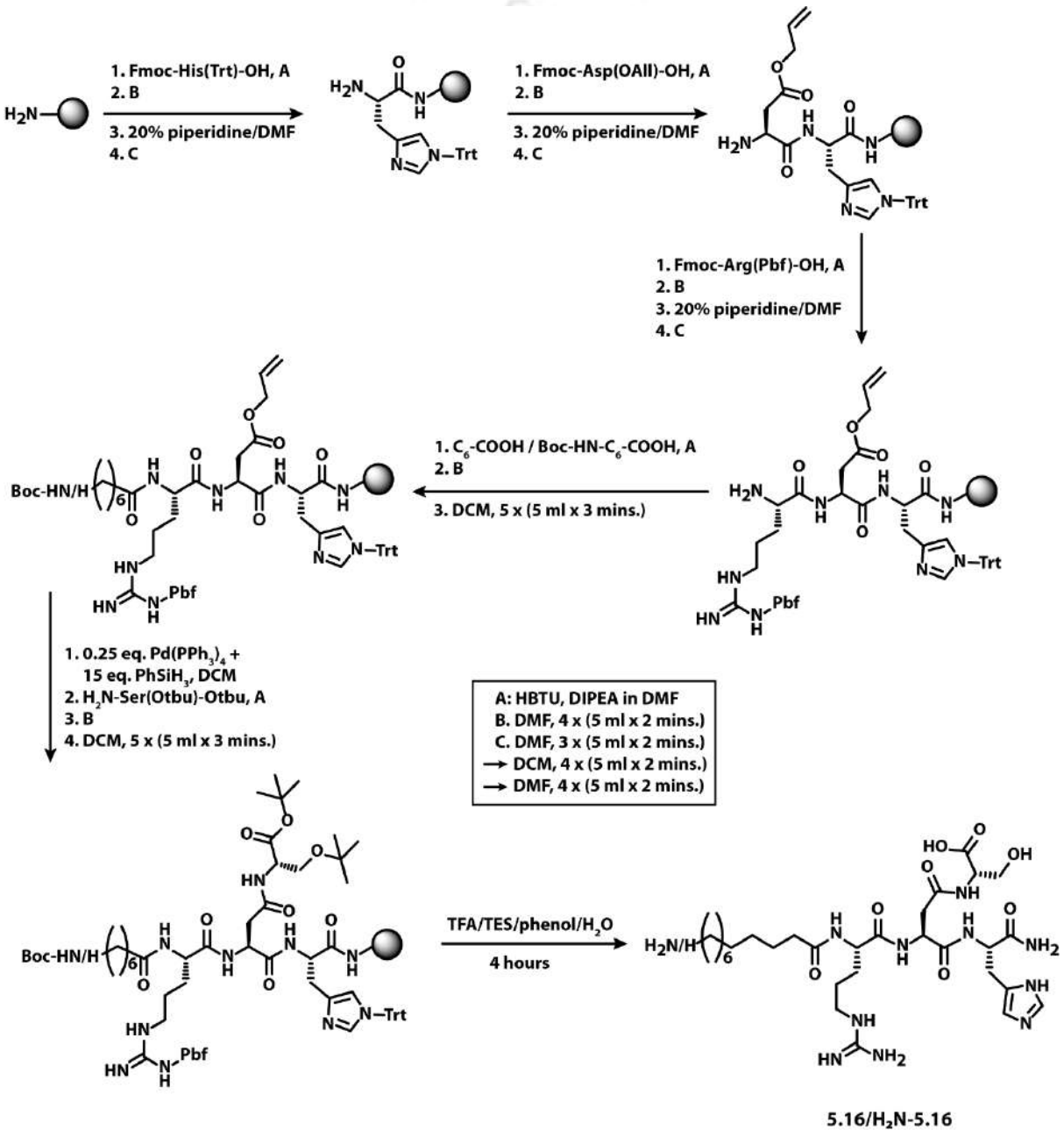

5.16 and H_2N-5.16 were synthesized by similar procedures on Rink amide MBHA resin using standard Fmoc (9-fluorenylmethoxycarbonyl) solid phase peptide synthesis (SPPS) method. In a

standard coupling, 3 equiv. of protected amino acids (with respect to the loading of the resin), 3 equiv. of HBTU, and 6 equiv. of DIPEA were taken in 5 mL of DMF (for 0.1 mmol scale with respect to the resin loading) and stirred for 5 min prior to addition of the mixture to the resin. The reaction mixture was shaken for 60 min and the resin was washed several times with DMF. The Fmoc-deprotection was achieved by treatment of the resin with 20% piperidine (5 mL, 5 min, three times) followed by thorough washing of the resin with DMF. The Fmoc-deprotection and coupling steps were repeated until the designed peptide sequence was obtained. After completing the coupling for the linear sequence, the resin was washed several times with DMF and finally with DCM and dried under argon. The flask washed then flushed with argon for 30 minutes. In another dry round-bottomed flask, 0.25 equiv. $Pd(PPh_3)_4$ and dry DCM was taken and degassed with argon for 30 minutes. This solution was transferred to the peptide flask containing the dried resin, using a syringe, under argon atmosphere. 15 equiv. $PhSiH_3$ was added with a syringe to the reacting flask. This step was followed two times, each for 1 hour. After the allyl-ester deprotection of the aspartic acid residue, the resin was washed with DCM thoroughly. Then, 3 equiv. of HBTU in 5 ml DMF was added to the resin, followed by addition of 6 equiv. DIPEA and stirred for 5 minutes. A solution containing 3 equiv. of Compound **A** in DMF was added to the resin and stirred for an hour. After the final coupling, the resin was washed with DMF and DCM several times and dried under reduced pressure. The dried resin was then treated with freshly prepared mixture of TFA/TES/phenol/water (85: 5:5:5 v/v) and stirred for 4 hours. The resin was finally washed with DCM. The cleavage cocktail and the washings combined and concentrated to a minimum volume on a rotary evaporator. The cleaved peptide was then precipitated from cold dry ether, centrifuged and lyophilized to get the crude peptide. Purification was done in a semipreparative HPLC using a Luna 5 µm C18(2) column (Phenomenex) and an eluent of acetonitrile and water starting at 10% ACN/H_2O reaching to 30 % ACN/H_2O in 15 minutes and finally to 100% ACN in 18 minutes to complete the chromatogram in 22 minutes. The pure lyophilized peptide was obtained in 70% yield.

PA **5.16**: Yield: 70%. ^{1}H NMR (600 MHz, D_2O) δ (ppm): 8.54 (dd, *J* = 8.9, 1.4 Hz, 1H), 7.27 – 7.21 (m, 1H), 4.66 – 4.53 (m, 2H), 4.47 – 4.36 (m, 1H), 4.20 (dd, *J* = 9.1, 5.4 Hz, 1H), 3.89 – 3.75 (m, 2H), 3.29 – 3.21 (m, 1H), 3.16 – 3.07 (m, 3H), 2.79 (d, *J* = 6.6 Hz, 1H), 2.21 (d, *J* = 7.1 Hz, 2H), 1.80 – 1.45 (m, 7H), 1.24 – 1.13 (m, 4H), 0.77 (t, *J* = 7.0 Hz, 3H). ^{13}C NMR (151 MHz, D_2O) δ (ppm): 177.72, 173.91, 172.14, 156.70, 133.39, 128.54, 117.39, 117.17, 61.07, 53.38, 53.10, 52.41, 52.30, 50.46, 49.02, 40.39, 36.23,

35.34, 35.31, 34.25, 30.48, 30.42, 27.92, 27.84, 26.13, 24.95, 24.93, 24.41, 23.08, 21.65, 13.15. ESI-MS, calculated for $C_{25}H_{43}N_{10}O_8$: 611.32 $[M+H]^+$, obtained, 611.29.

PA **H_2N-5.16**: Yield: 69%. ^1H NMR (600 MHz, D_2O) δ (ppm): 8.52 (dd, *J* = 8.9, 1.4 Hz, 1H), 7.37 – 7.25 (m, 1H), 4.68 – 4.53 (m, 2H), 4.44 – 4.36 (m, 1H), 4.22 (dd, *J* = 9.1, 5.4 Hz, 1H), 3.89 – 3.75 (m, 2H), 3.29 – 3.21 (m, 1H), 3.16 – 3.07 (m, 3H), 2.79 (d, *J* = 6.6 Hz, 1H), 2.21 (d, *J* = 7.1 Hz, 2H), 1.80 – 1.45 (m, 7H), 1.24 – 1.13 (m, 6H). ^{13}C NMR (151 MHz, D_2O) δ (ppm): 177.72, 173.91, 172.14, 156.70, 133.39, 128.54, 117.39, 117.17, 61.07, 53.38, 53.10, 52.41, 52.30, 50.46, 49.02, 40.39, 36.23, 35.34, 35.31, 34.25, 30.48, 30.42, 27.92, 27.84, 27.24, 26.13, 24.95, 24.93, 24.41, 23.08, 21.65, 13.15, ESI-MS, calculated for $C_{25}H_{43}N_{11}O_8$: 625.33 $[M+H]^+$, obtained, 625.29.

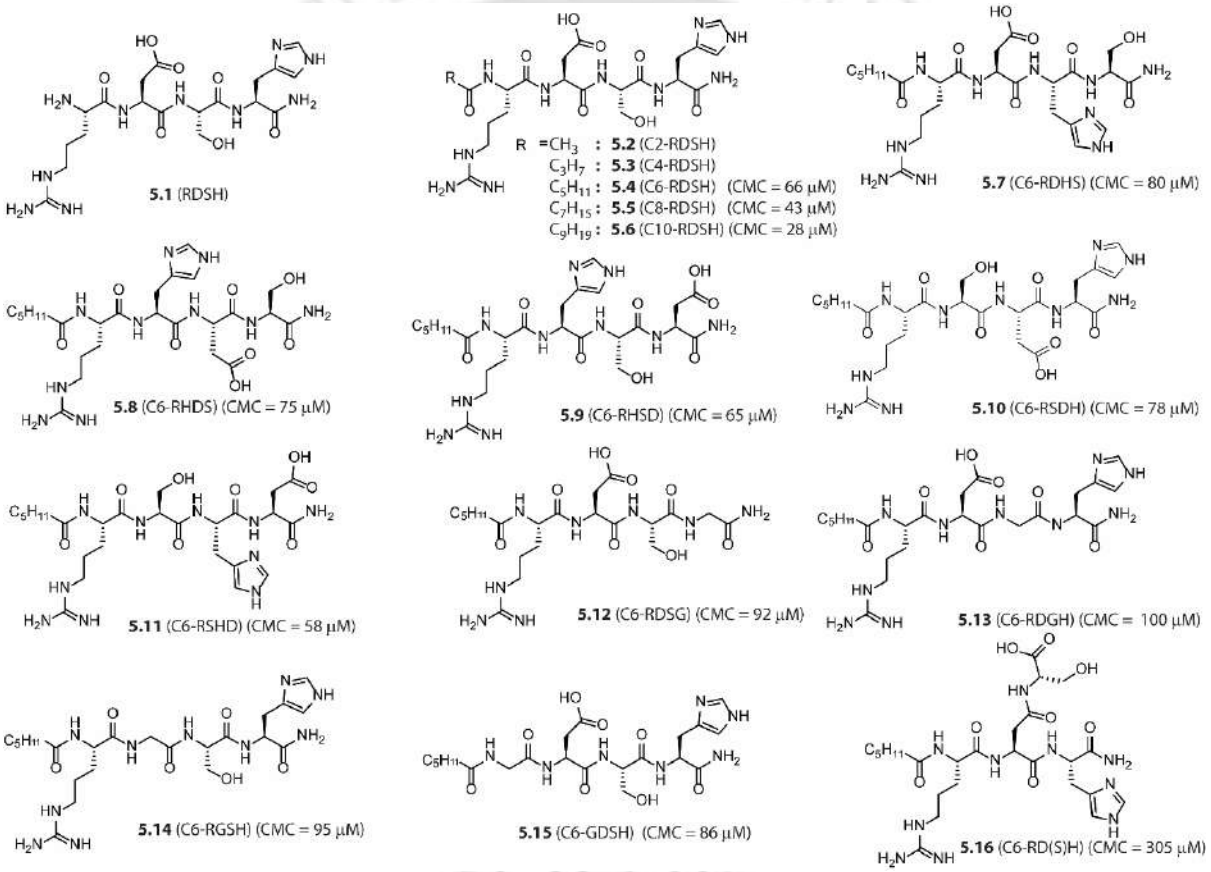

Chart 5.1 Chemical structures and the CMC values of all the peptides/PAs used for the study.

5.2.3 Synthesis of functionalized silica nanoparticles

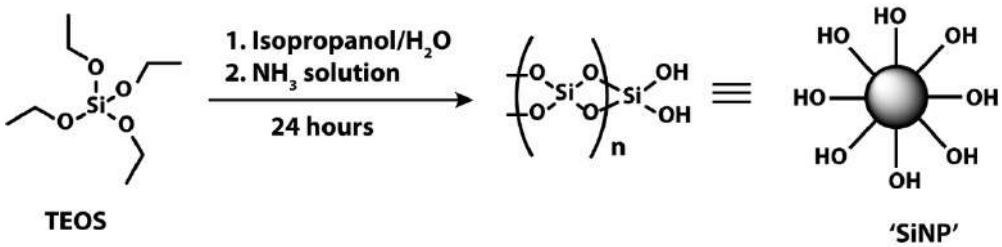

Bare silica (SiNP)

Silica nanoparticles were synthesized by Stöber method.[316] 2.7 ml of Isopropyl alcohol (IPA) was mixed with 0.54 ml (30 mmol) of water in a round bottom flask and cooled to 5 °C. This mixture was blended for 10 minutes at 5 °C after adding 0.375 ml (5 mmol) of ammonia solution to it. To this mixture, 1.38 ml (6.2 mmol) of TEOS was added and stirred for 2 minutes. The mixture was then kept undisturbed for 5 hours at 5°C. After 5 hours of reaction, the suspension was transferred into a centrifuge tube and centrifuged at 6000 rpm for 20 minutes. The supernatant was removed and the solid was washed several times with ethanol before drying it overnight at 150°C in hot air oven.

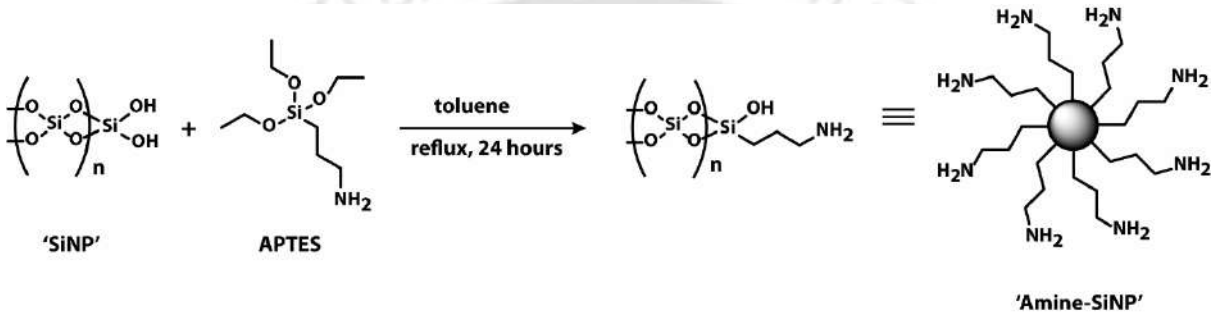

Synthesis of silica nanoparticles (Amine-SiNP)

360 mg of prepared SiNP was dispersed in 38.3 ml of toluene in a round bottom flask. To this, 11.7 ml (50 mmol) of APTES was added and refluxed for 24 hours. The solid product was separated by centrifugation at 6000 rpm and washed several times with ethanol. The product was dried at 70°C for 24 hours.

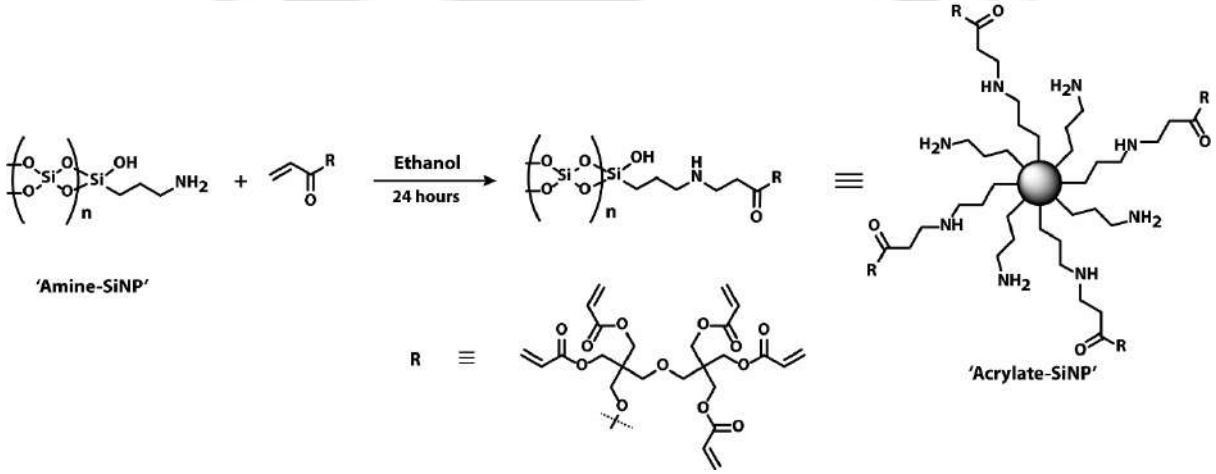

Synthesis of silica nanoparticles (Acrylate-SiNP)

10.6 mg of Amine-SiNP was dispersed in 2 ml of dry ethanol. A solution of 7 g of 5-ACl (1.4 gmL^{-1}) in 5 ml dry ethanol was added to the mixture. The reaction mixture was then shaken gently on a

mechanical shaker for 24 hours at room temperature. The mixture was centrifuged to separate out the silica nanoparticles. The product was washed for several times with ethanol and dried overnight at 70 °C.

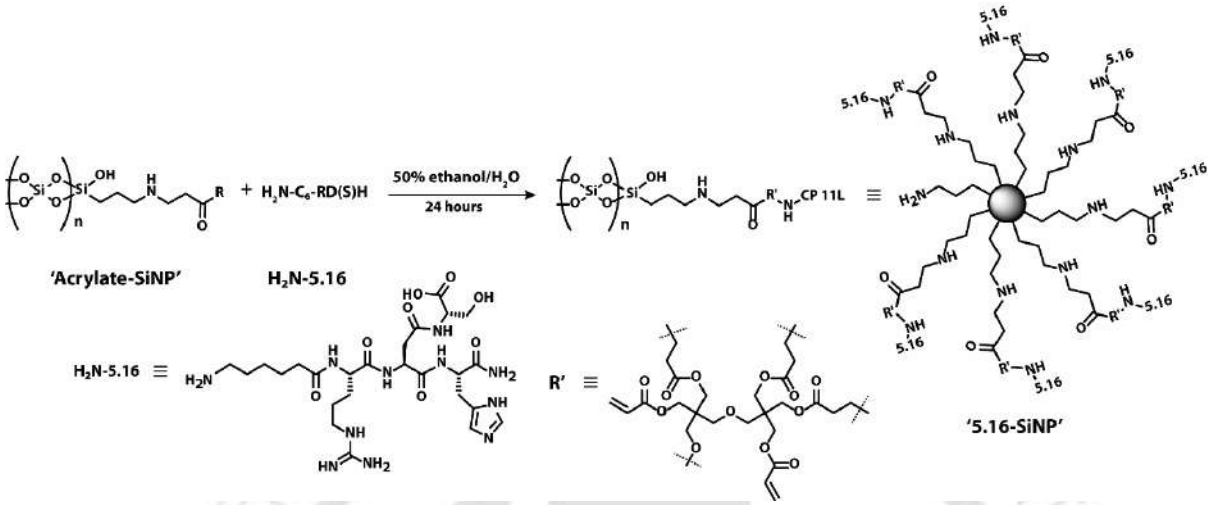

Synthesis of silica nanoparticles (5.16-SiNP)

20 mg of Acrylate-SiNP were dispersed in 4 mL of a solution containing 100 mg of NH_2-**5.16** (prepared in 50% ethanol/H_2O) and sonicated for 10 minutes at 18 °C to distribute the silica nanoparticles uniformly. The mixture was shaken gently at room temperature for 24 hours. The peptide-functionalized silica nanoparticles were then centrifuged at 6000 rpm, washed thoroughly with 50% ethanol/H_2O followed by ethanol and finally dried overnight at 70 °C.

5.2.4 Determination of CMCs

20 mM stock solutions of all the peptides were prepared in 20 mM phosphate buffer pH 7. A solution of pyrene was prepared by adding a pinch of pyrene in 100 mL of 20 mM sodium phosphate buffer pH 7 and sonicating it for 6 h followed by filtration. The concentration of Pyrene was estimated as 0.1 mM from the absorbance spectra of the solution. The emission spectra of the solution were recorded and then the solution was titrated with the peptide stock solutions and after each addition of the stock, the solution was stirred for 2 mins followed by resting for 3 mins. The emission spectra were recoded after each addition. The value of CMC was determined from the point of difference of the two slopes obtained, when I_1/I_3 was plotted against concentration of peptide. I_{ex} for pyrene: 337 nm. Emission spectra was collected from 340 to 600 nm. I_1 for pyrene: 375 nm, I_3: 415 nm.

5.2.5 TGA analysis

Thermogravimetric analyses (TGA/DTG) of various silica nanoparticles were performed under argon flow (100 ml min^{-1}) with a SETSYS Evolution TGA-DTA/DSC thermobalance, heating from 40 to 800 °C at 5 °C min^{-1}. The degree of functionalization (*DoF*) at different stages were calculated using the data from the DTG profiles following equations 5.1 and 2 as shown below.[317]

$$m(FG) = \Delta m_{sam} - \Delta m_{ref} \qquad (5.1)$$

where Δm(FG) is the mass loss of the sample in the main mass loss region and Δm_{Ref}, is the mass loss of the reference sample (previous step of functionalization) in that temperature range. Δm_{sam} represents the mass loss of the concerned sample in the main mass loss region. Subsequently, DoF can be calculated utilizing equation (5.2)

$$DoF = \frac{\Delta \mathrm{m\ (FG)} * M}{\mathrm{m} * M(FG)} \qquad (5.2)$$

Where 'M' is the molar mass of TEOS (208.33 g/mol), 'm' the mass of remaining sample at 800 °C and M(FG) are the molar masses of the functional groups respectively.

5.2.6 BET experiments

N_2 physisorption measurements were carried out at 77 K in the relative pressure range from 1 x 10^{-6} to 1 P/P_0 using a Quantachrome Autosorb1MP/TCD instrument. Prior to the analysis, the samples were degassed at 393 K for 3 hours (residual pressure lower than 10^{-6} Torr). Specific surface areas were determined using the BET equation, in the relative pressure range from 0.01 to 0.1 P/P_0. Pore size distributions were obtained by applying the DFT method and using the desorption branch of the N_2 physisorption isotherm.

5.2.7 Determination of hydrodynamic radii of particles

The silica particles were dispersed in buffer as mentioned earlier and the measurements were performed using these suspensions. The scattering angle of light was fixed at 90°. All the measurements were taken five times, and each reading was in turn a weighted average of 10 scans.

5.2.8 Morphology

For the silica nanoparticles, a pinch of the solid was dispersed in ethanol to make a very dilute solution and sonicated for 10 minutes. These dispersions were cast on silicon wafers air-dried and analyzed by FESEM.

5.2.9 Catalysis experiments with PAs

Unless otherwise mentioned, all the catalytic experiments involving PAs were performed in 20 mM sodium phosphate buffer pH 7 at 25 °C. The catalytic cycles were monitored by UV-Vis spectroscopy for 3 minutes at the isosbestic point for *p*-Nitrophenol (348 nm) as obtained from the absorption spectra of PNP. In every case, the catalysts were added in desired volume of buffer solution and incubated for 5 minutes and then substrate (desired volume was added from 12.5 mM stock in ACN, and total measurement solution was 3 mL) solutions were added, mixed and immediately placed for measurement. In all the cases, the background hydrolyses of the substrates (without adding catalyst) were separately measured in the desired experimental conditions and subsequently subtracted from the original catalysis data (with catalyst). The resultant plot was used as the activity of the catalysts on the substrates. Extinction coefficient of PNP was determined from the calibration plot, measured in 20 mM sodium phosphate buffer pH 7 at 25 °C; ε: 5910 $M^{-1}cm^{-1}$.

5.2.10 Measurement of catalytic activity of 5.16-SiNP

Unless otherwise mentioned, for all heterogeneous catalysis, the concentration of **5.16**-SiNP was maintained as 1 mg/ml in 20 mM phosphate buffer pH 7. The solid catalyst was dispersed in buffer, and vortexed for 1 minute followed by sonicated for 10 minutes at a constant temperature bath maintained at 25 °C. This cycle of vortexing and sonication was performed three times to get a homogeneous suspension. 100 mL of this catalyst suspension was placed in two wells of a 96-well-plate. The initial readings (absorbance at 348 nm) were collected using 96-well plate reader. PNPP (6 μL of 12.5 mM solution in ACN to reach final concentration of 0.75 mM) was then added to the sample well and absorbance at 348 nm was recorded every 30 seconds for 5 minutes. Simultaneously, the absorbance from the reference well (containing only the catalyst) were recorded and the corresponding values were subtracted from the sample data to avoid any contribution that may arise from the catalyst only. To eliminate any product formation by self-hydrolysis of the substrate, in another well, only the substrate was added maintaining all other parameters (except the presence of the catalyst) and the absorbance at 348 nm was recorded every 30 seconds for 5 minutes. These values were further subtracted from the sample values to get the absorbance arising from the catalysis by the catalyst only. From these subtracted values, using the calibration plot of PNP, the amount of PNP formation and subsequently the rate of hydrolysis was determined. CV Lipase was used as a reference to compare the activity of our catalyst. For this purpose, 100 μL of CV lipase (20 mM phosphate buffer pH 7) containing 70 units

was used in place of **5.16**-SiNP and similar procedure was used for the determination of the rate of hydrolysis by CV Lipase.

5.2.11 Catalyst reusability test

For the reusability test, as the 96 well plate reader was not suitable, we adopted a different technique. In this case, the catalysts were dispersed (1 mg/mL) in 940 µL of 20 mM phosphate buffer pH 7 following similar protocol mentioned earlier. To this suspension, substrate (60 µL of 12.5 mM solution in ACN to reach final concentration of 0.75 mM) was added and the sample was shaken on a mechanical shaker for 3 minutes. Immediately after that the sample was centrifuged for 30 seconds and the supernatant was transferred to the cuvette and the absorbance of the solution at 348 nm was recorded. To eliminate any absorbance that might come from the catalyst or substrate, the absorbances of only catalyst (exact concentrations used for the samples after similar treatment without adding substrate) or the substrate (exact concentrations used for the samples) were recorded at 348 nm and subtracted from the data obtained for the samples. All steps were performed in triplicate. Using calibration curve of PNP, the amount of PNP formed in each case were calculated. After every cycle, the catalysts were washed with water (5 times) followed by ACN (5 times) and dried under vacuum at 90 °C for 12 hours. The dried catalyst was further used for subsequent cycles using exactly the same process.

5.2.12 Determination of catalyst stereoselectivity

1 mg of **5.16**-SiNP or **5.16**D-SiNP were dispersed (following the protocol mentioned earlier) in 940 µL of 20 mM phosphate buffer pH 7. 60 µL of pre-mixed solution of Boc-D/L-Phe-PNP (1:1; 12.5 mM in ACN) was then added to the catalyst suspension and shaken on a mechanical shaker for 3 minutes. The sample was immediately centrifuged for 30 seconds and the supernatant was lyophilized. The lyophilized solid was re-dissolved in 1 mL of 8% Isopropanol/Hexane and analyzed through chiral HPLC. The % enantioexcess were calculated using the following equation (5.3),

$$\%\ enatioexcess = \frac{\text{Area of excess isomer} \times 100}{\text{Total Peak area of both isomers}} \qquad (5.3)$$

5.3 RESULTS AND DISCUSSION

5.3.1 Rational and systematic design of the hydrolase mimicking PA

The esterase catalytic triad consists of Ser, Asp or Glu, and His. Also, it was shown recently shown that presence of Arg in the system enhances the catalytic performance significantly. Based on this

knowledge, initially, a short peptide sequence was designed as, RDSH (**5.1**, Chart 5.1). The catalytic activity was studied at 1 mM concentration of **5.1** in 20 mM pH 7 buffer using (PNPA) as the substrate. The initial velocity (v_i) was observed to be 0.008 ± 0.0001 $\mu M^{-1}s^{-1}$ (Figure 5.1 A). We anticipated that the activity of the peptide could be enhanced in its self-assembled form owing to the cooperative effect of the participating amino acids as well as effective higher local concentration of the substrate at the surface of the aggregates.[318, 319] To verify the hypothesis, the peptide was modified by attaching hydrophobic tail (C6) at the N-terminal of the sequence and converted it to the peptide amphiphile **5.4**. The critical micellar concentration of the PA was measured using pyrene emission technique and observed to be 66 μM (Figure 5.2 B).[320] As the CMC was observed to be much lower than the concentration (1mM) of the PA used for catalysis, we continued using 1 mM solution of **5.4** to assess the catalytic efficiency. ~ 4.5-fold (v_i = 0.036 ± 0.0002 $\mu M^{-1}s^{-1}$) increase in the activity was observed compared to **5.1**.

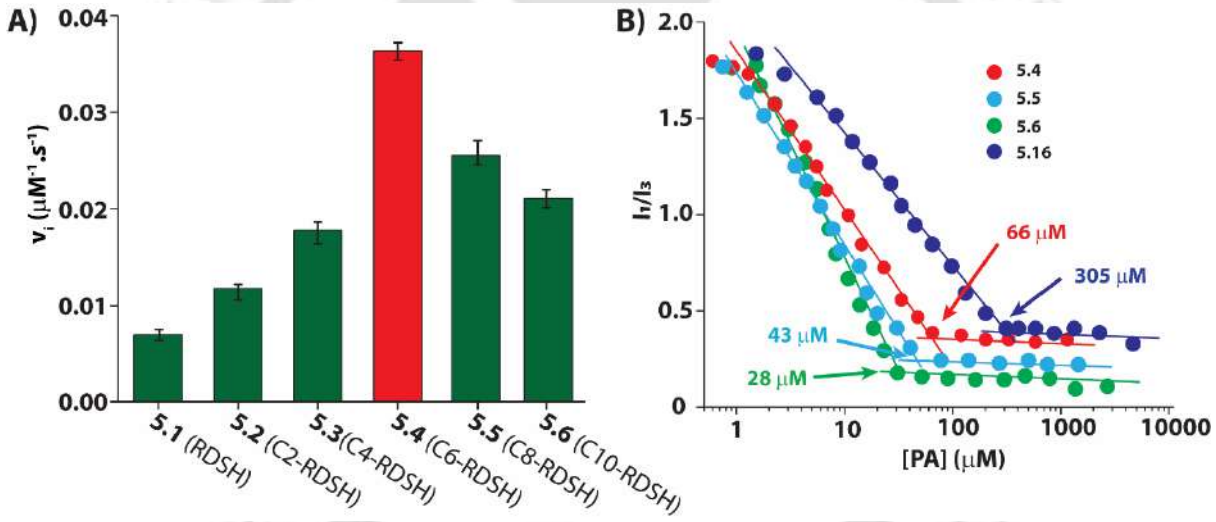

Figure 5.1 (A) Initial velocities observed for different peptides as catalyst for PNP. [PA] = 1mM, [PNPA] = 0.75 mM in 20 mM Phosphate buffer pH 7at room temperature. (B) Representative examples of CMC measurements for some of the PAs measured at room temperature.

The significant enhancement in the rate of hydrolysis prompted us to find the role of chain length of the tail. The chain length was then varied from C2 to C10 (**5.2** to **5.6**, Chart 5.1). The CMC for all these PAs were measured. However, understandably, for **5.2** and **5.3**, no clear values were found as they do not possess the proper hydrophilic-lipophilic balance to form micelles. The CMC of **5.5** and **5.6** were observed to be 43 and 28 μM respectively and as they are sufficiently lower than 1 mM, we did all further studies at this concentration. Interestingly, the hydrolysis activity showed a bell-shaped relation with the tail length. PA **5.4**, with C6 chain, showed significantly higher activity compared to all other PAs tested. The results indicate that the packing of the micellar

aggregates in case of **5.4** is the optimum in the present case that allowed better catalytic activity on its surface.

Next, the role of the positions of the respective amino acids have been tested. For this purpose, five new sequences (**5.7** to **5.11,** Chart 5.1) were prepared where the positions of the amino acids are altered. Interestingly, the rates of the catalytic processes were found to be similar to that of PA **5.4** as can be seen from Figure 5.2. The results clearly indicate that the position of the amino acid sequence does not impart much effect on the catalytic efficiency. The next question that arises at this point was the effect of each of the amino acids in the sequence. In order to find that out, another series of five new PAs (**5.12** to **5.16**) were prepared following the sequence of **5.4** and replacing one of the amino acids with Gly in each of the new sequences. When subjected to test the catalytic efficiency of these peptides, all of them showed much lowered activity compared to that of **5.4**. The lowest activity found was in case of **5.12** ($v_i = 0.001 \pm 0.0005$ $\mu M^{-1}s^{-1}$) which is very much understandable as the peptide does not have any His unit which is essential for the esterase like activity. In cases of **5.13** ($v_i = 0.01 \pm 0.001$ $\mu M^{-1}s^{-1}$), and 5.**14** ($v_i = 0.011 \pm 0.001$ $\mu M^{-1}s^{-1}$) the rate of hydrolysis were found to be considerably higher than that of **5.12**. Moreover, even higher rate of conversion was achieved in case of **5.15** ($v_i = 0.025 \pm 0.001$ $\mu M^{-1}s^{-1}$). These results indicate the essential role of all the amino acids present in the peptide sequence of **5.4**. As reported before, both, Ser and Asp helps in enhancing the catalytic efficiency by cooperatively binding with the substrate along with His. As mentioned in previous reports, though the role of Arg is not very clear, it is certain that the presence of guanidinium unit certainly affect the overall esterase activity.

5.3.2 Branching in the sequence to enhance activity

It has previously been shown that for such small peptide-based sequence, branched peptides work more efficiently than the linear ones as branching provides a three-dimensional binding possibility for the functional groups present in the catalytic site (Imidazole, -OH and -COOH in this case). To evaluate the possibility of enhancing the catalytic activity through branching in the sequence, we introduced PA **5.16** (C6-RD(S)H). The derivative had been designed such that the main functional units, namely imidazolium, hydroxyl and carboxylate groups were aligned in close proximities to form a pre-organized pocket for improved substrate binding. The Michaelis-Menten constants (K_m)s were derived from Michaelis-Menten plots (Figure 5.3 A) as 12104.33 μM and 6344.75 μM respectively for **5.4** and **5.16** respectively. The K_{cat}/K_m values for these two systems (0.53×10^{-7} and 1.79×10^{-7} $\mu M^{-1}s^{-1}$ respectively) are shown in Figure 5.3 B. The three-dimensional

arrangement of the catalytic triad in case of **5.16** presumably helped in the stronger binding of the substrate and resulted in higher catalytic efficiency.

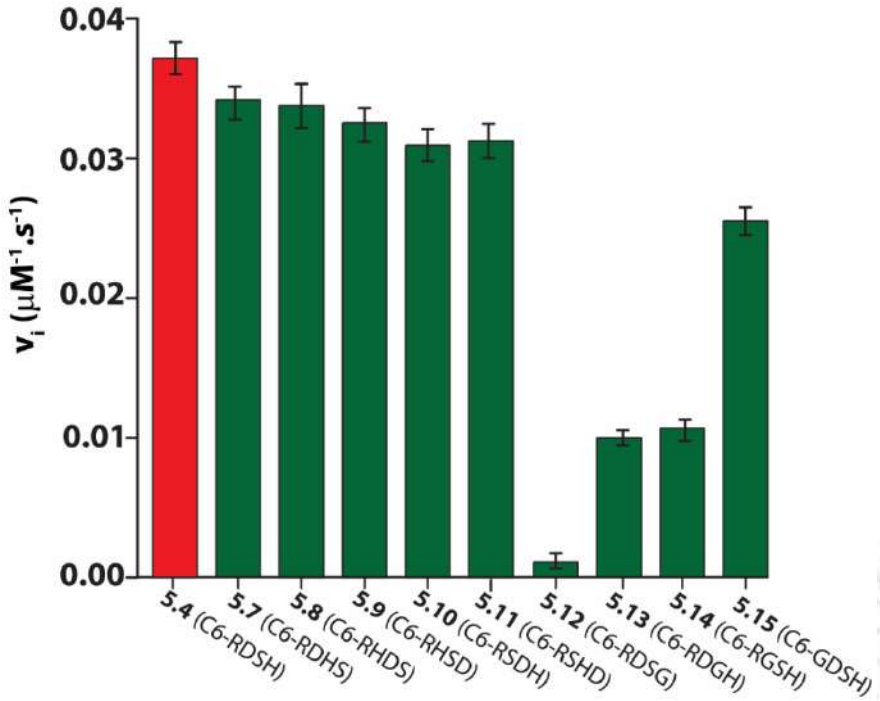

Figure 5.2 Initial velocities observed for different peptides as catalyst for PNP. [PA] = 1mM, [PNPA] = 0.75 mM in 20 mM phosphate buffer pH 7at room temperature.

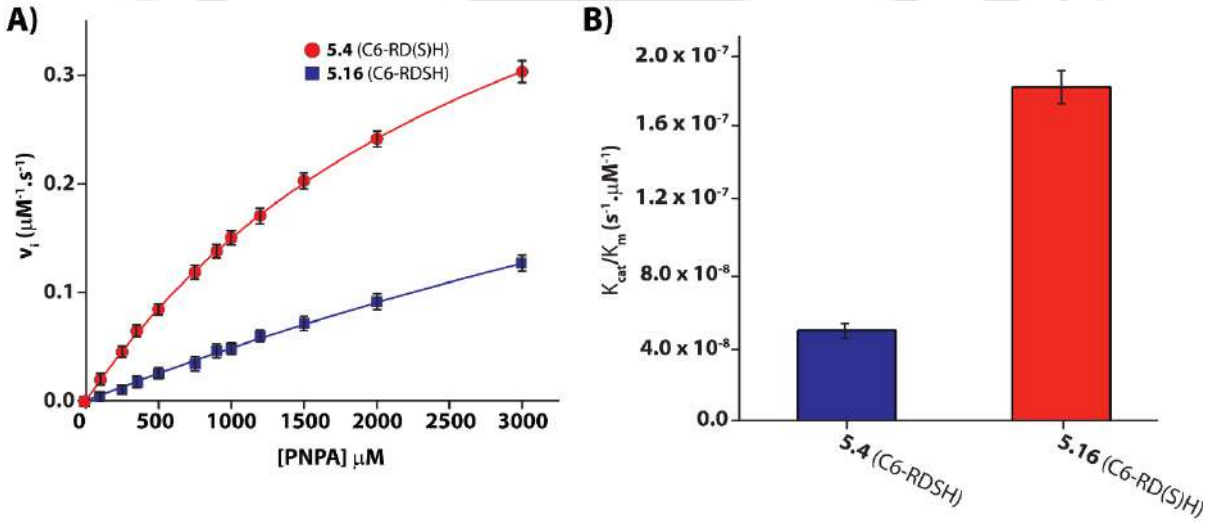

Figure 5.3 (A) Michaelis-Menten plot for **5.4** and **5.16** as catalyst for PNP. [PA] = 1mM, in 20 mM phosphate buffer pH 7at room temperature. (B) Comparison of catalytic efficiencies of **5.4** and **5.16** as catalyst for PNP. [PA] = 1mM, in 20 mM phosphate buffer pH 7at room temperature.

5.3.3 Effect of pH, temperature, additives and substrates on the catalytic activity

It is clear from all the above-mentioned studies that the branched peptide, **5.16** has the highest ability to hydrolyze esters. Based on this fact, peptide **5.16** was chosen for all further experiments. The effect of pH, temperature, salt and other additives on the activity of **5.16** were then analyzed.

As can be seen from Figure 5.4 A, when the pH of the reaction medium was varied from 1 – 11, a significant difference in the catalytic activity was observed with the highest activity shown at pH 7. The catalytic activity of **5.16** was found to be negligible under acidic conditions. This was due to the fact that under acidic conditions, imidazole units exist in protonated form and therefore unable to conduct the proton shuttle which is essential for the hydrolysis reaction. When pH crosses the pK_a of His, there is a sudden increase in the rate of hydrolysis (Figure 5.4 A). However, the activity decreases as the pH moves to higher value. It is to be noted that in all cases, the self-hydrolyses (without the catalytic peptide) were taken care of by subtracting the values obtained from the same. At higher pH, PNPA undergoes hydrolysis by direct attack of OH^- ions which is fast and irreversible process, and takes place without the assistance of any catalyst. The pH profile closely matches with the reported results for hydrolases like Lipase and the optimum pH for the catalyst was considered as ~7.

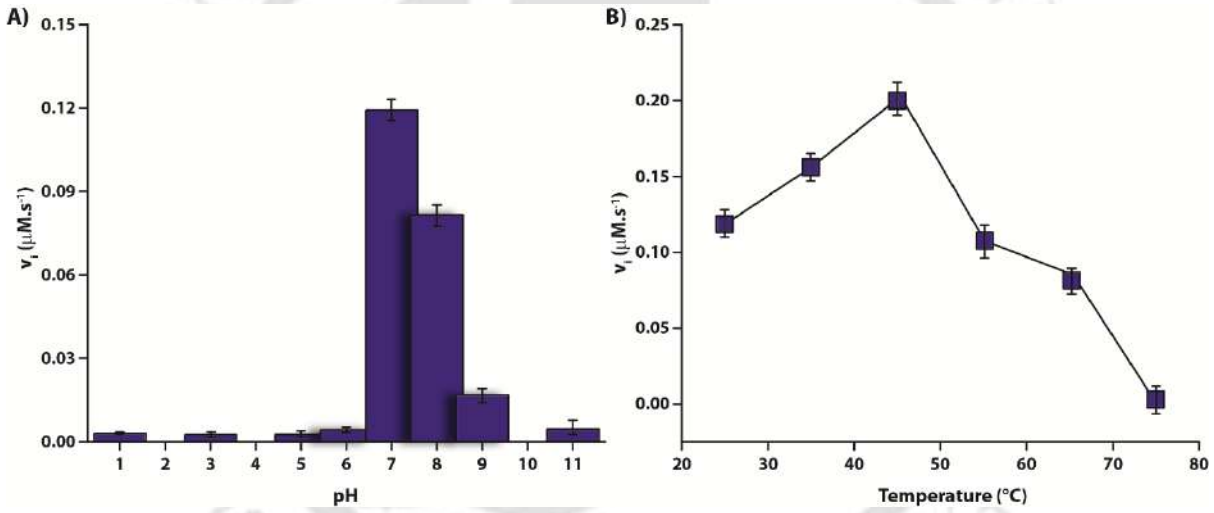

Figure 5.4 Effect of (A) pH and (B) Temperature on the rate of catalysis of **5.16**. [PNPA] = 0.75 mM, [**5.16**] = 1 mM.

Temperature of the system has been found to impart profound effect on the sensitivity of a catalyst. Similar to pH, the temperature profile also shows a bell-shaped curve with highest activity found at 45 °C (Figure 5.4 B). Lower temperature decreases the kinetic energy of the molecules which leads to slower rate of collisions of substrates with catalyst and therefore diminished rate of reactions. Increasing the temperature facilitates the rate of reaction through increased number of collisions within a short time. On the other hand, further higher temperatures cause adverse effect on the catalyst activity by destabilizing the non-bonding interactions within a catalyst. Higher temperatures might also destabilize the transitory catalyst-substrate complex.[321, 322] Moreover, as the temperature increases, there is a high possibility that the micellar aggregates of the PA break down and consequently, the cooperative effect gained by the self-aggregation also

diminishes. A temperature dependent CMC measurement (Figure 5.5) for **5.16** confirms that the PA has higher CMCs above 45 °C than the concentration used for the catalysis experiments (1 mM). These results clearly explain the decrease in activity above 45 °C.

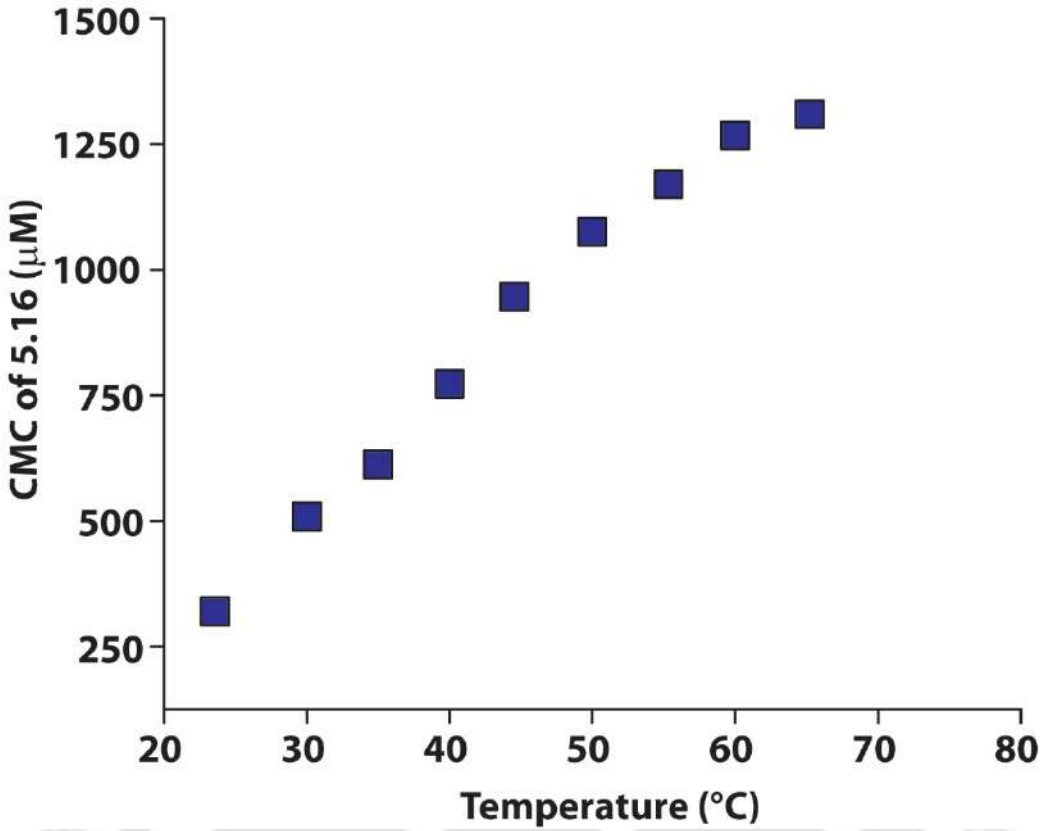

Figure 5.5 Variation of CMC of **5.16** with temperature.

Interestingly, addition of salts, like 150 mM NaCl did not improve the activity (Figure 5.6 A). Common inhibitors for hydrolases like methanol, ethanol and urea caused distinct decrease in the catalytic activity but failed to inhibit the catalytic activity completely. These inhibitors are usually known to break protein and peptide aggregations through disrupting the non-covalent interactions responsible for the protein folding and thereby inhibits the catalytic process. In the present case, the self-assembly is mainly driven by the hydrophilic-lipophilic balance (HLB)[323] of the PA and the contribution from the interactions like hydrogen bonding at the peptide segment is understandably lower.[324, 325] Though these hydrogen bonding interactions are weakened in the presence of these inhibitors, the PAs remain in micellar form and thus complete inhibition could not be observed.

To find out the effect of substrates on the rate of catalysis, five different esters (*p*-Nitrophenyl acetate (PNPA), p-Nitrophenyl propionate (PNPP), *p*-Nitrophenyl butanoate (PNPB), *p*-Nitrophenyl hexanoate (PNPH) and *p*-Nitrophenyl-ester of Boc-Phe-OH (Boc-Phe-PNP)) were employed. As can

be seen from Figure 5.6 B, PNPP underwent maximum hydrolysis, whereas Boc-Phe-PNP underwent minimum hydrolysis. The propyl chain of PNPP plausibly helped the substrate to bind to the micellar surface with optimum effect.

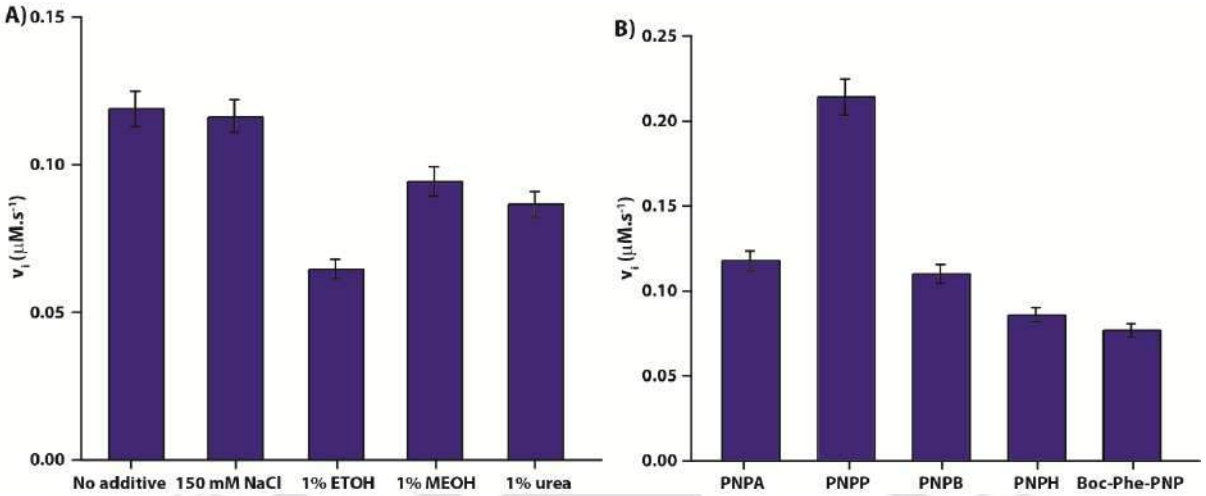

Figure 5.6 Effect of (A) different additives and (B) different substrates on the rate of catalysis by **5.16**. [**5.16**] = 1 mM, [Substrate] = 0.75 mM in 20 mM Phosphate buffer pH 7 at room temperature.

5.3.4 Immobilization on silica surface

From all the above-mentioned results, it was clear that PA **5.16** shows the highest hydrolase like activity. As discussed in the introduction, our goal was to create a heterogeneous catalyst using hydrolase mimicking PA and immobilizing it on silica surface. Immobilization on any solid surface is expected to enhance the catalytic efficiency further as the dynamic nature of the micellar aggregates gets restricted. Moreover, congregation of catalytic peptides on a solid-surface leads to integrated increment of robustness and reusability factors of the designed peptide catalyst without losing its catalytic efficiency.[326-330] With this aim, **5.16** was loaded onto silica nanoparticles following the strategy shown in Scheme 5.1. In brief, uniform sized (~600 nm) spherical SiNPs were prepared using well-established Stöber method. The surface was of the SiNPs were further amine functionalized using APTES. The amine functionalized SiNPs were then treated with 5Acl to get acrylate functionalized surface. On this surface, terminal amine functionalized **5.16** (**NH_2-5.16**, Scheme 5.1) were grafted via 1,4 Michael addition reaction to result the desired **5.16**-functionalized SiNPs.

The degree of functionalization at each step of SiNP formulation were determined from the percentage mass loss observed from thermogravimetric analysis (TGA) experiments, where Derivative Thermogravimetry (DTG) curves signify the rate of material weight changes upon heating (Figure 4A). The minima at 100 °C is referred to the loss of adsorbed water molecules. The

second minima in the DTG curve from 200 – 450 °C is referred to the organic functionalization of APTES, 5-ACl, or the peptide.[317, 331] Therefore this region was utilized to determine the percentages of successive functionalization with APTES/5-ACl/**16**. The obtained *DoF* were 8.97, 5.82, and 4.07 respectively for Amine-SiNP, Acrylate-SiNP and **16**-SiNPs. From this, the concentration of peptide **16** present in 1 mg/ml of **16**-SiNP was found to be 0.45 mM (M.W. of **16**: 625.67 g/mol).

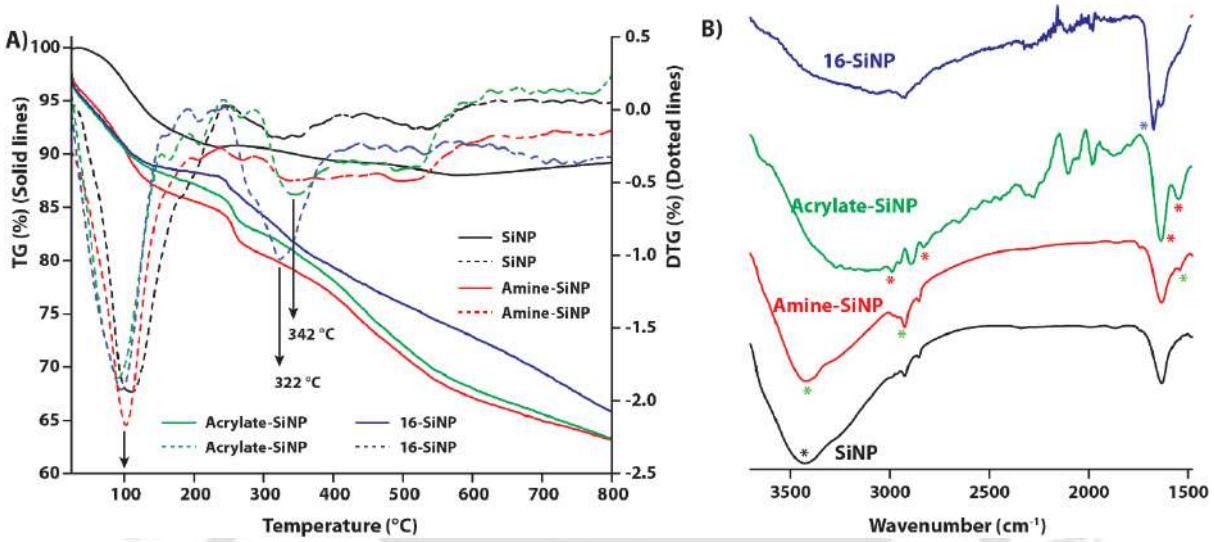

Figure 5.7 Characterization of silica nanoparticles. (A) TG and DTG curves, (B) FTIR spectra.

In the FTIR spectra (Figure 5.7 B), the peak at 3650 cm^{-1} was observed which was for the free silanol groups, whereas 2921, 2850 and 1484 cm^{-1} were assigned to C–H stretching and bending vibrations from the aminopropyl groups. The characteristic N-H bond stretching vibration at 3300 cm^{-1} broadened along with the broad peak of O – H stretch of that water molecules, captured inside the pores of the SiNPs. Acrylate-SiNP yielded two new peaks at 2990 and 2829 cm^{-1}, which were the indication of C – H stretching of – CH_3 and – CH_2 groups respectively.[326] The peak at 1632 cm^{-1} was due to the C = C stretch of acrylate groups. A distinct peak at 1673 cm^{-1} was observed in the **5.16**-SiNP due to the amide bonds of the peptide loaded silica (Figure 5.7 B).

The silica particles obtained at different stages were also analyzed for surface area and pore size measurements using BET method. The obtained BET specific surface areas and pore size parameters are tabulated in Figure 5.8. The adsorption/desorption isotherms of all samples displayed type IV behavior with H3 type hysteresis in the relative pressure range $0.1 < P/P_0 < 1$, which indicates the characteristic mesoporous structures.[332] The BET surface area of SiNP was found to be 42.74 m^2/g, which decreases sharply to 5.47 m^2/g in case of Amine-SiNP. This significant decrease in the surface area suggests clogging of the pores by the surface functionalities. However, the surface areas remained almost unchanged in the successive steps.

indicating clogging of pores by the incoming surface functionalities. The pore sizes increased with functionalization (5.32 for **5.16**-SiNP) when compared to SiNP (1.09 nm).

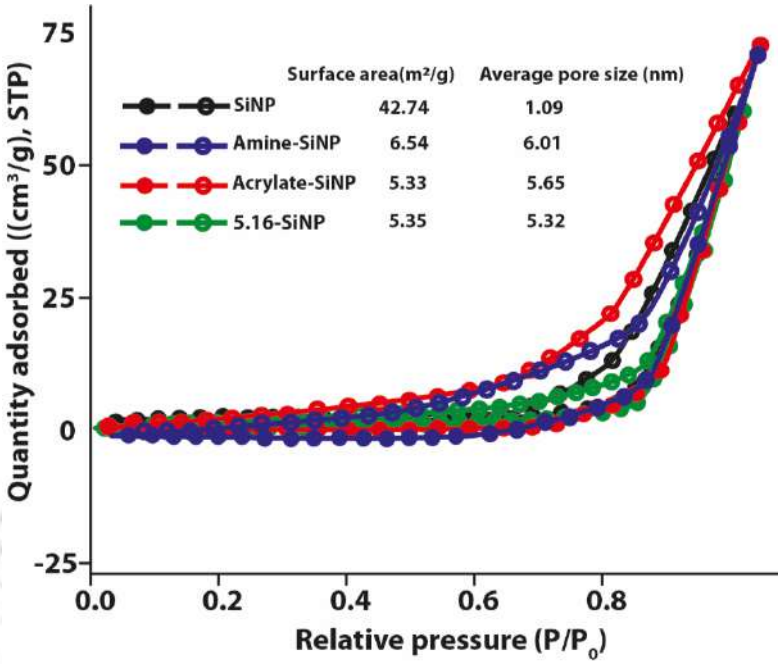

Figure 5.8 N_2 Adsorption/desorption isotherms of silica nanoparticles obtained from BET.

Stepwise functionalization of silica nanoparticles was also supported by DLS and FESEM analyses. In both cases, a clear increment in the average diameter of particles was observed. The particle size increases from 100 nm in case of SiNP to 600 nm for peptide functionalized silica, **5.16**-SiNP (Figure 5.9 A, B).

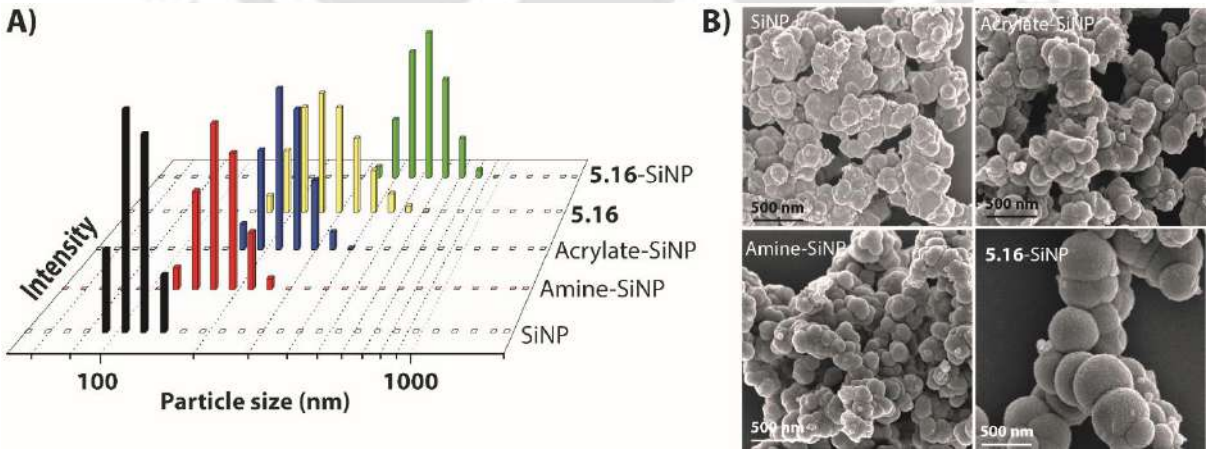

Figure 5.9 Characterization of silica nanoparticles. (A) Variation of particle sizes of silica nanoparticles at different stages of preparation of **5.16**-SiNP as obtained from DLS measurements and (B) FESEM images of the silica nanoparticles at different stages of the preparation of **5.16**-SiNP.

5.3.5 Heterogeneous catalysis on 5.16-SiNP surface

Spherical silica nanoparticles can have multiple catalytic peptides uniformly arranged on its surface without catalyst crowding which increases the relative surface area of the effective catalyst without the loss of cooperative effect of aggregated peptide catalysts. This facilitates the substrate binding process and thereby enhances the extent of product formation. To verify whether surface immobilization of the catalytic peptide actually helped in enhancing the efficiency of the catalytic process, hydrolysis of PNPP using **5.16**-SiNP was monitored. The concentration (1 mM) of the catalytic site (**5.16** in **5.16**-SiNP) was taken similar to that of the solution-based hydrolysis using **5.16**. As can be seen from Figure 5.10 A, there is a two-fold jump in the activity in case of **5.16**-SiNP.

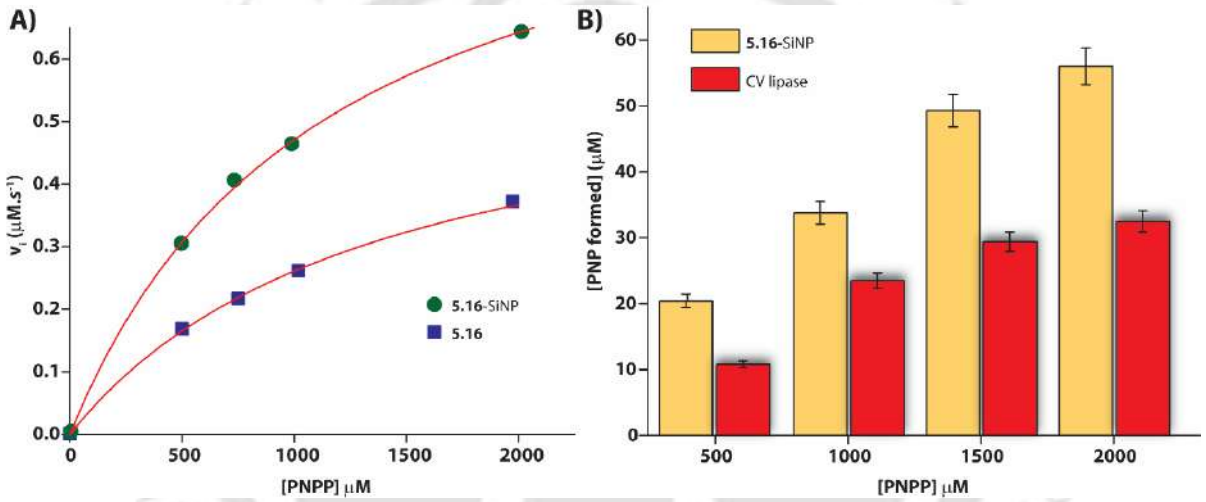

Figure 5.10 Heterogeneous catalysis using **5.16**-SiNP. (A) Rate of hydrolysis of PNPP (0.75 mM) in presence of 1 mg/mL **5.16**-SiNP and 70 units of CV lipase in 20 mM phosphate buffer (pH 7). (B) Amount of PNP formed within 5 minutes from different concentrations of PNPP using 1mg/mL **5.16**-SiNP and 70 units of CV lipase in 20 mM phosphate buffer (pH 7).

Next, **5.16**-SiNP was compared with *Chromobacterium viscosum* lipase (CV lipase) for hydrolase activity. The amount of formation of PNP from PNPP was found to be twice in case of **5.16**-SiNP (1 mg/mL) than that of 70 units of CV lipase in 1 mL buffer of pH 7 at room temperature (Figure 5.10 B). Further, the hydrolysis was monitored for varying concentration of PNPP using a fixed amount of **5.16**-SiNP (1 mg/mL) and compared with the same using 70 units of CV lipase. Interestingly, it is clear from Figure 5.11 that catalyst concentration as less as 1 mg/ml can act on higher range of substrate concentrations and in every case, the amount of PNP formed was observed to be much higher (~ twice) than CV lipase (Figure 5.10 B). Finally, the concentration of **5.16**-SiNP was varied for a fixed concentration of PNPP (0.75 mM). As the amount of the catalyst increased from 0.5

mg/mL to 1 mg/mL, an enhanced activity was noticed (Figure 5.11). However, with further increase in catalyst, no change was observed.

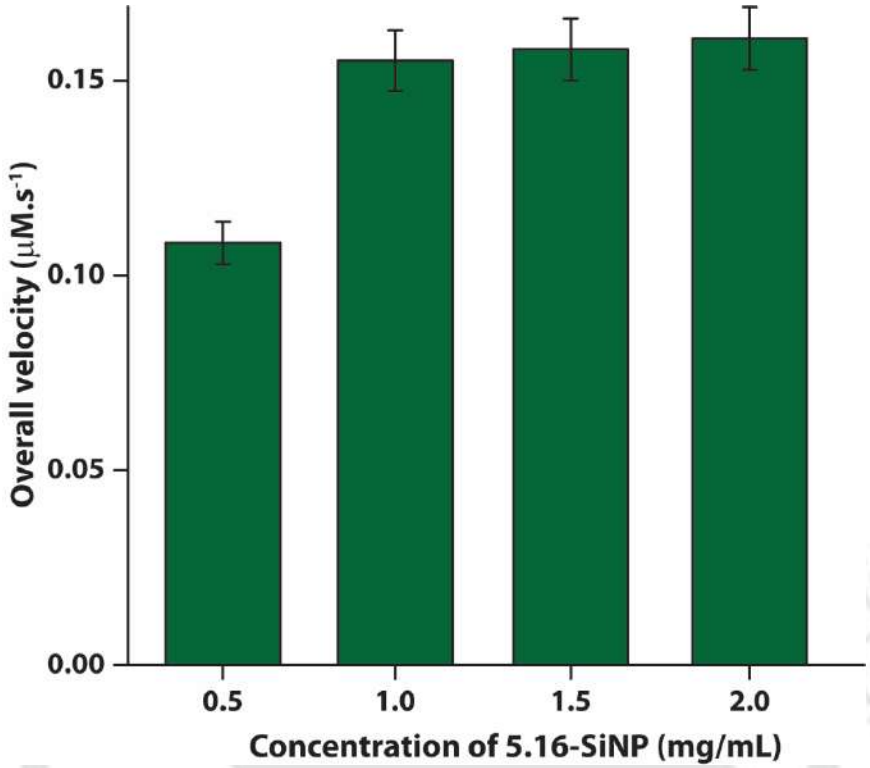

Figure 5.11 Rate of hydrolysis of 0.75 mM PNPP using varying amounts of **5.16**-SiNP.

Further, the stability, pH profile and effect of additives on the catalyst were evaluated. A temperature dependent study on the rate of catalysis showed continuous increase in the activity as we move from room temperature to 75 °C (Figure 5.12 A). However, after 50 °C, the slope of increase in activity diminished significantly. Unlike **16**, as the catalytic peptide is covalently attached on the surface of the SiNP, the dissociation of the aggregate is not possible in case of **5.16**-SiNP and thus, the activity enhances with increase in temperature. However, at higher temperature, the supramolecular forces get weakened and thus the system loses the cooperative effect from the neighboring peptides. This presumably leads to the decrease in the slope of activity increment. The pH profile of **5.16**-SiNP shows very similar activity profile to that of **5.16** (Figure 5.12 B). Additionally, the effect of different common denaturing agents was tested on **5.16**-SiNP. As can be seen from Figure 5.13, very similar trends were obtained to that of **5.16**. Moreover, to check the stability of **5.16**-SiNP, the catalyst was heated at 90 °C for 12 hours and brought back to room temperature before testing for the activity and no detectable loss in activity was observed. Similarly, the catalyst was kept open under ambient condition for three months

and showed similar activity to that of the freshly prepared catalyst. These results indicate that the catalyst is extremely robust and stable.

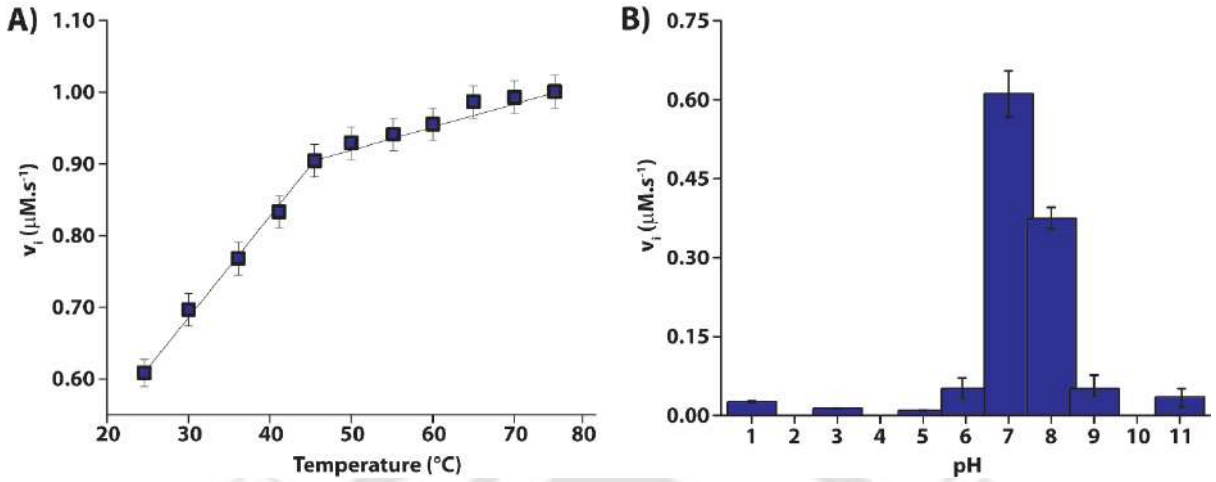

Figure 5.12 Stability of the heterogeneous catalyst. Effect of (A) temperature (B) pH on the rate of catalysis by **5.16**-SiNP. [**5.16**-SiNP] = 1 mg/mL; [PNPP] = 0.75 mM.

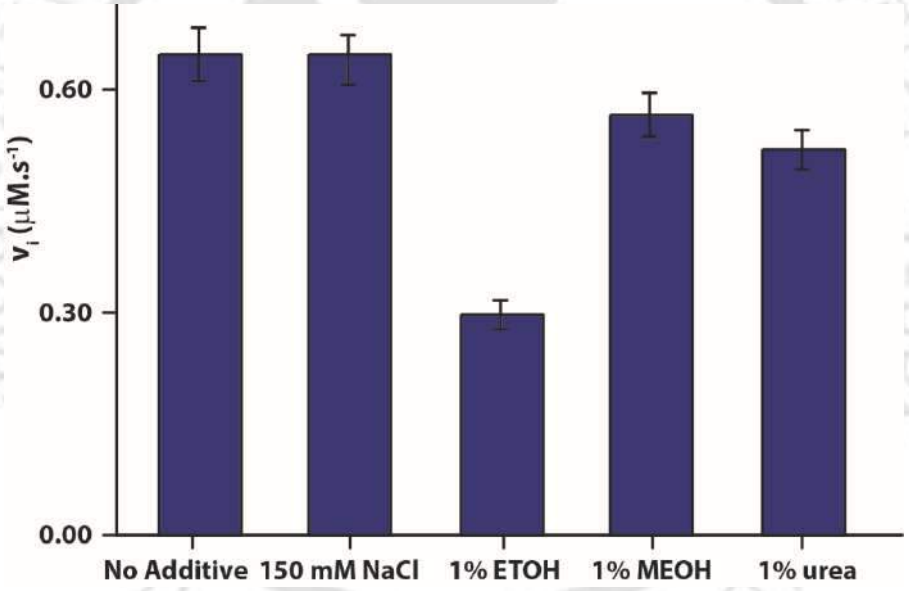

Figure 5.13 Initial activity of **5.16**-SiNP against PNPP (0.75 mM) in absence or presence of different additives. The experiments were performed in 20 mM phosphate buffer pH 7 at room temperature and in triplicate.

For any industrial application, one of the major concerns for a catalyst is its recyclability. To verify whether **5.16**-SiNP can be recycled after every use, we did one batch of catalysis reaction followed by removal of the catalyst by filtration, washing and drying. Once dried, the catalyst was used again for the next batch. The same process was repeated for five times. As can be seen from Figure 5.14 A, no significant loss in the activity was observed even during the fifth cycle. This confirms the recyclability of the developed catalyst. Moreover, as depicted in the experimental section, the recycling process is extremely easy and cost-effective.

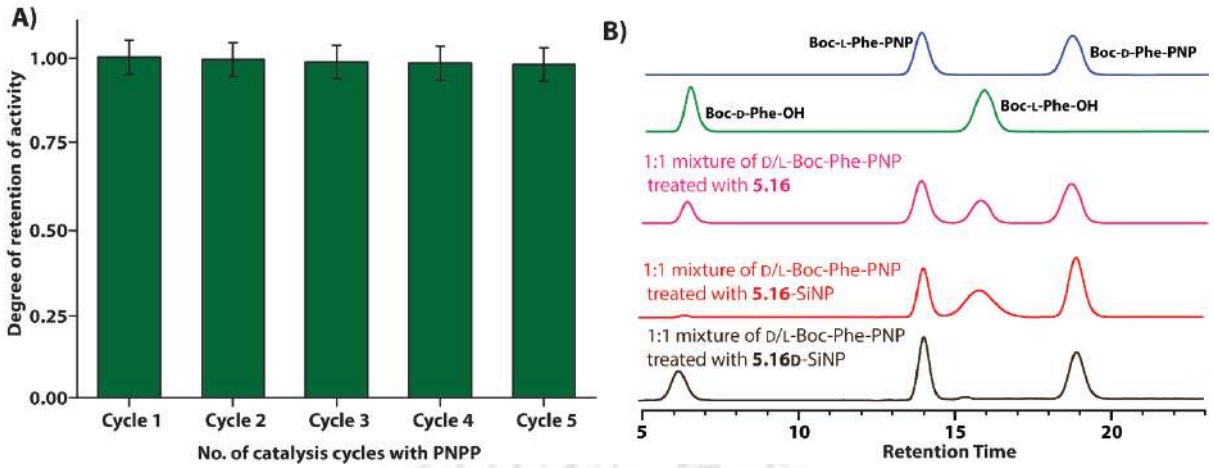

Figure 5.14 (A) Recyclability of **5.16**-SiNP while using it for hydrolysis of PNPP for several cycles. (B) Chromatograms of 1:1 mixture of Boc-D/L-Phe-PNP and Boc-D/L-Phe-OH before and after the hydrolysis using **5.16**, **5.16**-SiNP or **5.16**D-SiNP.

5.3.6 Stereoselective Catalysis by 5.16-SiNP

One of the most important features of enzymes is the stereoselective catalysis. Synthesis of enantiopure molecules is of high importance and extremely challenging for industrial processes. To verify the stereoselective catalysis of the newly designed catalyst, first, a 1:1 mixture of PNP ester of Boc-D/L-Phenylalanine (Boc-D/L-Phe) was subjected to hydrolysis using **5.16**-SiNP. Analytical HPLC analyses shows the formation of Boc-L-Phe with 95% excess (Figure 5.14 B). Further, we have prepared the D-version of the catalyst, **5.16**D-SiNP (Scheme 5.1) where the peptide is made with D-analogs of the corresponding amino acids. When similar experiment was performed with **5.16D**-SiNP, Boc-D-Phe with 95% excess was obtained. Interestingly, while using the PA (D or L **5.16**) for stereoselective catalysis, only ~ 10% excess of one isomer was obtained on both occasions. It was previously shown on many occasions that micellar/vesicular surfaces decorated with amino acids or peptides of one particular enantiomer lead to selective binding of substrates with specific stereochemistry.[333, 334] However, the stereoselective binding could not be translated to enantioselective product formation to a major extent due to dynamic nature of these aggregates.[333] However, in the present case, though the surface is decorated with the peptide of one particular enantiomer, the dynamicity is frozen due to the immobilization of the catalytic peptide on the solid surface. As the silica surface is functionalized with L-**5.16**, Boc- L-Phe-PNP preferentially bound to the surface and resulted into the formation of Boc-L-Phe-OH in excess. Similarly, **5.16D**-SiNP resulted into the excess formation of Boc-D-Phe-OH. These results clearly show the applicability of the reported catalyst could be an excellent candidate for stereoselective hydrolysis of esters.

5.4 CONCLUSION

In summary, we have systematically developed a peptide amphiphile that can efficiently catalyse ester hydrolysis. For this purpose, a library was methodically screened and the best PA (**5.16**) for this purpose was identified. The PA having a branched peptide sequence consisting of His, Ser and Arg residues could effectively bind to the surface in its micellar form. The aggregation of the PA provided the cooperative effect from neighbouring amphiphiles and thus enhances the rate of hydrolysis. The identified PA was further immobilized on silica nanoparticle surface to prepare a heterogenous catalyst. The catalyst showed much better activity than lipase and was found to be extremely robust against various denaturing effects. Additionally, the catalyst allowed stereoselective hydrolysis of chiral esters with high efficiency and could be reused for several cycles without any loss of activity. The developed catalyst with all these properties could be of high interest for future industrial applications.

6. REFERENCES

1. Zhang, S.; Holmes, T.; Lockshin, C.; Rich, A., Spontaneous assembly of a self-complementary oligopeptide to form a stable macroscopic membrane. *Proc. Natl. Acad. Sci.* **1993,** *90*, 3334-3338.
2. Frenkel-Pinter, M.; Samanta, M.; Ashkenasy, G.; Leman, L. J., Prebiotic Peptides: Molecular Hubs in the Origin of Life. *Chem. Rev.* **2020,** *120*, 4707-4765.
3. Zhao, X.; Zhang, S., Designer Self-Assembling Peptide Materials. *Macromol. Biosci.* **2007,** *7*, 13-22.
4. Stupp, S. I., Self-Assembly and Biomaterials. *Nano Lett.* **2010,** *10*, 4783-4786.
5. Gelain, F.; Luo, Z.; Zhang, S., Self-Assembling Peptide EAK16 and RADA16 Nanofiber Scaffold Hydrogel. *Chem. Rev.* **2020,** *120*, 13434-13460.
6. Kumar, M.; Son, J.; Huang, R. H.; Sementa, D.; Lee, M.; O'Brien, S.; Ulijn, R. V., In Situ, Noncovalent Labeling and Stimulated Emission Depletion-Based Super-Resolution Imaging of Supramolecular Peptide Nanostructures. *ACS Nano* **2020,** *14*, 15056-15063.
7. Dasgupta, A.; Das, D., Designer Peptide Amphiphiles: Self-Assembly to Applications. *Langmuir* **2019,** *35*, 10704-10724.
8. Rodrigues de Almeida, N.; Han, Y.; Perez, J.; Kirkpatrick, S.; Wang, Y.; Sheridan, M. C., Design, Synthesis, and Nanostructure-Dependent Antibacterial Activity of Cationic Peptide Amphiphiles. *ACS Appl. Mater. Interfaces* **2019,** *11*, 2790-2801.
9. Yan, X.; Zhu, P.; Li, J., Self-assembly and application of diphenylalanine-based nanostructures. *Chem. Soc. Rev.* **2010,** *39*, 1877-1890.
10. Li, J.; Du, X.; Hashim, S.; Shy, A.; Xu, B., Aromatic–Aromatic Interactions Enable α-Helix to β-Sheet Transition of Peptides to Form Supramolecular Hydrogels. *J. Am. Chem. Soc.* **2017,** *139*, 71-74.
11. Liang, R.; Wang, L.; Yu, H.; Khan, A.; Ul Amin, B.; Khan, R. U., Molecular design, synthesis and biomedical applications of stimuli-responsive shape memory hydrogels. *European Polymer Journal* **2019,** *114*, 380-396.
12. Paramonov, S. E.; Jun, H.-W.; Hartgerink, J. D., Self-Assembly of Peptide–Amphiphile Nanofibers: The Roles of Hydrogen Bonding and Amphiphilic Packing. *J. Am. Chem. Soc.* **2006,** *128*, 7291-7298.
13. Clark, T. D.; Buriak, J. M.; Kobayashi, K.; Isler, M. P.; McRee, D. E.; Ghadiri, M. R., Cylindrical β-Sheet Peptide Assemblies. *J. Am. Chem. Soc.* **1998,** *120*, 8949-8962.
14. Lopez-Silva, T. L.; Leach, D. G.; Li, I. C.; Wang, X.; Hartgerink, J. D., Self-Assembling Multidomain Peptides: Design and Characterization of Neutral Peptide-Based Materials with pH and Ionic Strength Independent Self-Assembly. *ACS Biomater. Sci. Eng.* **2019,** *5*, 977-985.
15. Webber, M. J.; Langer, R., Drug delivery by supramolecular design. *Chem. Soc. Rev.* **2017,** *46*, 6600-6620.
16. Chen, L.; Yang, D.; Feng, J.; Zhang, M.; Qian, Q.; Zhou, Y., Switchable modulation of bacterial growth and biofilm formation based on supramolecular tripeptide amphiphiles. *J. Mater. Chem. B* **2019,** *7*, 6420-6427.
17. Liu, Z.; Zhou, W.; Li, J.; Zhang, H.; Dai, X.; Liu, Y.; Liu, Y., High-efficiency dynamic sensing of biothiols in cancer cells with a fluorescent β-cyclodextrin supramolecular assembly. *Chem. Sci.* **2020,** *11*, 4791-4800.
18. Du, X.; Zhou, J.; Shi, J.; Xu, B., Supramolecular Hydrogelators and Hydrogels: From Soft Matter to Molecular Biomaterials. *Chem. Rev.* **2015,** *115*, 13165-13307.
19. Panda, S. S.; Katz, H. E.; Tovar, J. D., Solid-state electrical applications of protein and peptide based nanomaterials. *Chem. Soc. Rev.* **2018,** *47*, 3640-3658.

20. Kumar, M.; Ing, N. L.; Narang, V.; Wijerathne, N. K.; Hochbaum, A. I.; Ulijn, R. V., Amino-acid-encoded biocatalytic self-assembly enables the formation of transient conducting nanostructures. *Nat. Chem.* **2018,** *10*, 696-703.
21. Dimatteo, R.; Darling, N. J.; Segura, T., In situ forming injectable hydrogels for drug delivery and wound repair. *Adv. Drug. Deliv. Rev.* **2018,** *127*, 167-184.
22. Sun, J. E.; Stewart, B.; Litan, A.; Lee, S. J.; Schneider, J. P.; Langhans, S. A.; Pochan, D. J., Sustained release of active chemotherapeutics from injectable-solid β-hairpin peptide hydrogel. *Biomater. Sci.* **2016,** *4*, 839-48.
23. Chakraborty, P.; Guterman, T.; Adadi, N.; Yadid, M.; Brosh, T.; Adler-Abramovich, L.; Dvir, T.; Gazit, E., A Self-Healing, All-Organic, Conducting, Composite Peptide Hydrogel as Pressure Sensor and Electrogenic Cell Soft Substrate. *ACS Nano* **2019,** *13*, 163-175.
24. González-Rodríguez, D.; Schenning, A. P. H. J., Hydrogen-bonded Supramolecular π-Functional Materials. *Chem. Mater.* **2011,** *23*, 310-325.
25. ten Cate, A. T.; Kooijman, H.; Spek, A. L.; Sijbesma, R. P.; Meijer, E. W., Conformational Control in the Cyclization of Hydrogen-Bonded Supramolecular Polymers. *J. Am. Chem. Soc.* **2004,** *126*, 3801-3808.
26. Mabesoone, M. F. J.; ter Huurne, G. M.; Palmans, A. R. A.; Meijer, E. W., How Water in Aliphatic Solvents Directs the Interference of Chemical Reactivity in a Supramolecular System. *J. Am. Chem. Soc.* **2020,** *142*, 12400-12408.
27. Bai, Y.; Fan, X.-d.; Yao, H.; Yang, Z.; Liu, T.-t.; Zhang, H.-t.; Zhang, W.-b.; Tian, W., Probing into the Supramolecular Driving Force of an Amphiphilic β-Cyclodextrin Dimer in Various Solvents: Host–Guest Recognition or Hydrophilic–Hydrophobic Interaction? *J. Phys. Chem. B* **2015,** *119*, 11893-11899.
28. Stupp, S. I.; Palmer, L. C., Supramolecular Chemistry and Self-Assembly in Organic Materials Design. *Chem. Mater.* **2014,** *26*, 507-518.
29. Würthner, F.; Saha-Möller, C. R.; Fimmel, B.; Ogi, S.; Leowanawat, P.; Schmidt, D., Perylene Bisimide Dye Assemblies as Archetype Functional Supramolecular Materials. *Chem. Rev.* **2016,** *116*, 962-1052.
30. Tao, K.; Makam, P.; Aizen, R.; Gazit, E., Self-assembling peptide semiconductors. *Science (New York, N.Y.)* **2017,** *358*, 885-891.
31. Altunbas, A.; Pochan, D. J., Peptide-Based and Polypeptide-Based Hydrogels for Drug Delivery and Tissue Engineering. In *Peptide-Based Materials*, Deming, T., Ed. Springer Berlin Heidelberg: Berlin, Heidelberg, 2012; pp 135-167.
32. Aggeli, A.; Nyrkova, I. A.; Bell, M.; Harding, R.; Carrick, L.; McLeish, T. C. B.; Semenov, A. N.; Boden, N., Hierarchical self-assembly of chiral rod-like molecules as a model for peptide β-sheet tapes, ribbons, fibrils, and fibers. *Proc. Natl. Acad. Sci.* **2001,** *98*, 11857-11862.
33. Katyal, P.; Meleties, M.; Montclare, J. K., Self-Assembled Protein- and Peptide-Based Nanomaterials. *ACS Biomater. Sci. Eng.* **2019,** *5*, 4132-4147.
34. Fichman, G.; Gazit, E., Self-assembly of short peptides to form hydrogels: Design of building blocks, physical properties and technological applications. *Acta Biomater.* **2014,** *10*, 1671-1682.
35. Rubio, J.; Alfonso, I.; Burguete, M. I.; Luis, S. V., Interplay between hydrophilic and hydrophobic interactions in the self-assembly of a gemini amphiphilic pseudopeptide: from nano-spheres to hydrogels. *Chem. Commun.* **2012,** *48*, 2210-2212.
36. Lee, S.; Trinh, T. H. T.; Yoo, M.; Shin, J.; Lee, H.; Kim, J.; Hwang, E.; Lim, Y.-B.; Ryou, C., Self-Assembling Peptides and Their Application in the Treatment of Diseases. *Int J Mol Sci* **2019,** *20*, 5850-5871.

37. Schneider, J. P.; Pochan, D. J.; Ozbas, B.; Rajagopal, K.; Pakstis, L.; Kretsinger, J., Responsive Hydrogels from the Intramolecular Folding and Self-Assembly of a Designed Peptide. *J. Am. Chem. Soc.* **2002,** *124*, 15030-15037.
38. Dasgupta, A.; Mondal, J.; Das, D., Peptide hydrogels. *RSC Adv.* **2013,** *3*, 9117-9149.
39. Holowka, E. P.; Pochan, D. J.; Deming, T. J., Charged Polypeptide Vesicles with Controllable Diameter. *J. Am. Chem. Soc.* **2005,** *127*, 12423-12428.
40. Katchalski, E.; Sela, M., Synthesis and chemical properties of poly-alpha-amino acids. *Advances in protein chemistry* **1958,** *13*, 243-492.
41. Pochan, D. J.; Pakstis, L.; Ozbas, B.; Nowak, A. P.; Deming, T. J., SANS and Cryo-TEM Study of Self-Assembled Diblock Copolypeptide Hydrogels with Rich Nano- through Microscale Morphology. *Macromolecules* **2002,** *35*, 5358-5360.
42. Yokoi, H.; Kinoshita, T.; Zhang, S., Dynamic reassembly of peptide RADA16 nanofiber scaffold. *Proc. Natl. Acad. Sci.* **2005,** *102*, 8414-8419.
43. Hinterding, K.; Alonso-Díaz, D.; Waldmann, H., Organic Synthesis and Biological Signal Transduction. *Angew. Chem. Int. Ed.* **1998,** *37*, 688-749.
44. Hartgerink, J. D.; Beniash, E.; Stupp, S. I., Self-Assembly and Mineralization of Peptide-Amphiphile Nanofibers. *Science (New York, N.Y.)* **2001,** *294*, 1684-1688.
45. Fry, H. C.; Peters, B. L.; Ferguson, A. L., Pushing and Pulling: A Dual pH Trigger Controlled by Varying the Alkyl Tail Length in Heme Coordinating Peptide Amphiphiles. *J. Phys. Chem. B* **2021,** *125*, 1317-1330.
46. Cui, H.; Cheetham, A. G.; Pashuck, E. T.; Stupp, S. I., Amino Acid Sequence in Constitutionally Isomeric Tetrapeptide Amphiphiles Dictates Architecture of One-Dimensional Nanostructures. *J. Am. Chem. Soc.* **2014,** *136*, 12461-12468.
47. Castelletto, V.; Edwards-Gayle, C. J. C.; Greco, F.; Hamley, I. W.; Seitsonen, J.; Ruokolainen, J., Self-Assembly, Tunable Hydrogel Properties, and Selective Anti-Cancer Activity of a Carnosine-Derived Lipidated Peptide. *ACS Appl. Mater. Interfaces* **2019,** *11*, 33573-33580.
48. Shi, J.; Gao, Y.; Yang, Z.; Xu, B., Exceptionally small supramolecular hydrogelators based on aromatic-aromatic interactions. *Beilstein J. Org. Chem.* **2011,** *7*, 167-172.
49. Vegners, R.; Shestakova, I.; Kalvinsh, I.; Ezzell, R. M.; Janmey, P. A., Use of a gel-forming dipeptide derivative as a carrier for antigen presentation. *J. Pept. Sci.* **1995,** *1*, 371-378.
50. Reches, M.; Gazit, E., Casting Metal Nanowires Within Discrete Self-Assembled Peptide Nanotubes. *Science (New York, N.Y.)* **2003,** *300*, 625-627.
51. Mahler, A.; Reches, M.; Rechter, M.; Cohen, S.; Gazit, E., Rigid, Self-Assembled Hydrogel Composed of a Modified Aromatic Dipeptide. *Adv. Mater.* **2006,** *18*, 1365-1370.
52. Marchesan, S.; Easton, C. D.; Styan, K. E.; Waddington, L. J.; Kushkaki, F.; Goodall, L.; McLean, K. M.; Forsythe, J. S.; Hartley, P. G., Chirality effects at each amino acid position on tripeptide self-assembly into hydrogel biomaterials. *Nanoscale* **2014,** *6*, 5172-5180.
53. Chen, L.; Revel, S.; Morris, K.; C. Serpell, L.; Adams, D. J., Effect of Molecular Structure on the Properties of Naphthalene–Dipeptide Hydrogelators. *Langmuir* **2010,** *26*, 13466-13471.
54. Palui, G.; Nanda, J.; Ray, S.; Banerjee, A., Fabrication of Luminescent CdS Nanoparticles on Short-Peptide-Based Hydrogel Nanofibers: Tuning of Optoelectronic Properties. *Chem. Eur. J.* **2009,** *15*, 6902-6909.
55. Castelletto, V.; Cheng, G.; Hamley, I. W., Amyloid peptides incorporating a core sequence from the amyloid beta peptide and gamma amino acids: relating bioactivity to self-assembly. *Chem. Commun.* **2011,** *47*, 12470-12472.
56. Krysmann, M. J.; Castelletto, V.; Kelarakis, A.; Hamley, I. W.; Hule, R. A.; Pochan, D. J., Self-Assembly and Hydrogelation of an Amyloid Peptide Fragment. *Biochemistry* **2008,** *47*, 4597-4605.

57. Marchesan, S.; Easton, C. D.; Kushkaki, F.; Waddington, L.; Hartley, P. G., Tripeptide self-assembled hydrogels: unexpected twists of chirality. *Chem. Commun.* **2012,** *48*, 2195-2197.
58. Shaham-Niv, S.; Adler-Abramovich, L.; Schnaider, L.; Gazit, E., Extension of the generic amyloid hypothesis to nonproteinaceous metabolite assemblies. *Sci. Adv.* **2015,** *1*, e1500137-e1500143.
59. Zaguri, D.; Shaham-Niv, S.; Chakraborty, P.; Arnon, Z.; Makam, P.; Bera, S.; Rencus-Lazar, S.; Stoddart, P. R.; Gazit, E.; Reynolds, N. P., Nanomechanical Properties and Phase Behavior of Phenylalanine Amyloid Ribbon Assemblies and Amorphous Self-Healing Hydrogels. *ACS Appl. Mater. Interfaces* **2020,** *12*, 21992-22001.
60. Adler-Abramovich, L.; Vaks, L.; Carny, O.; Trudler, D.; Magno, A.; Caflisch, A.; Frenkel, D.; Gazit, E., Phenylalanine assembly into toxic fibrils suggests amyloid etiology in phenylketonuria. *Nat. Chem. Biol.* **2012,** *8*, 701-706.
61. Singha, N.; Srivastava, A.; Pramanik, B.; Ahmed, S.; Dowari, P.; Chowdhuri, S.; Das, B. K.; Debnath, A.; Das, D., Unusual confinement properties of a water insoluble small peptide hydrogel. *Chem. Sci.* **2019,** *10*, 5920-5928.
62. Alshehri, S.; Susapto, H. H.; Hauser, C. A. E., Scaffolds from Self-Assembling Tetrapeptides Support 3D Spreading, Osteogenic Differentiation, and Angiogenesis of Mesenchymal Stem Cells. *Biomacromolecules* **2021,** *22*, 2094-2106.
63. Loo, Y.; Lakshmanan, A.; Ni, M.; Toh, L. L.; Wang, S.; Hauser, C. A. E., Peptide Bioink: Self-Assembling Nanofibrous Scaffolds for Three-Dimensional Organotypic Cultures. *Nano Lett.* **2015,** *15*, 6919-6925.
64. Laverty, G.; McCloskey, A. P.; Gilmore, B. F.; Jones, D. S.; Zhou, J.; Xu, B., Ultrashort Cationic Naphthalene-Derived Self-Assembled Peptides as Antimicrobial Nanomaterials. *Biomacromolecules* **2014,** *15*, 3429-3439.
65. Glossop, H. D.; De Zoysa, G. H.; Hemar, Y.; Cardoso, P.; Wang, K.; Lu, J.; Valéry, C.; Sarojini, V., Battacin-Inspired Ultrashort Peptides: Nanostructure Analysis and Antimicrobial Activity. *Biomacromolecules* **2019,** *20*, 2515-2529.
66. Huang, L.; Wu, C.; Zhang, L.; Ma, Z.; Jia, X., A Mechanochromic and Photochromic Dual-Responsive Co-assembly with Multicolored Switch: A Peptide-Based Dendron Strategy. *ACS Appl. Mater. Interfaces* **2018,** *10*, 34475-34484.
67. Thota, C. K.; Berger, A. A.; Elomaa, L.; Nie, C.; Böttcher, C.; Koksch, B., Coassembly Generates Peptide Hydrogel with Wound Dressing Material Properties. *ACS Omega* **2020,** *5*, 8557-8563.
68. Jain, R.; Pal, V. K.; Roy, S., Triggering Supramolecular Hydrogelation Using a Protein–Peptide Coassembly Approach. *Biomacromolecules* **2020,** *21*, 4180-4193.
69. Fleming, S.; Debnath, S.; Frederix, P. W. J. M.; Hunt, N. T.; Ulijn, R. V., Insights into the Coassembly of Hydrogelators and Surfactants Based on Aromatic Peptide Amphiphiles. *Biomacromolecules* **2014,** *15*, 1171-1184.
70. Berdugo, C.; Nalluri, S. K. M.; Javid, N.; Escuder, B.; Miravet, J. F.; Ulijn, R. V., Dynamic Peptide Library for the Discovery of Charge Transfer Hydrogels. *ACS Appl. Mater. Interfaces* **2015,** *7*, 25946-25954.
71. Xu, X.-D.; Chen, C.-S.; Lu, B.; Cheng, S.-X.; Zhang, X.-Z.; Zhuo, R.-X., Coassembly of Oppositely Charged Short Peptides into Well-Defined Supramolecular Hydrogels. *J. Phys. Chem. B* **2010,** *114*, 2365-2372.
72. Li, S.; Mehta, A. K.; Sidorov, A. N.; Orlando, T. M.; Jiang, Z.; Anthony, N. R.; Lynn, D. G., Design of Asymmetric Peptide Bilayer Membranes. *J. Am. Chem. Soc.* **2016,** *138*, 3579-3586.
73. Horgan, C. C.; Rodriguez, A. L.; Li, R.; Bruggeman, K. F.; Stupka, N.; Raynes, J. K.; Day, L.; White, J. W.; Williams, R. J.; Nisbet, D. R., Characterisation of minimalist co-assembled

fluorenylmethyloxycarbonyl self-assembling peptide systems for presentation of multiple bioactive peptides. *Acta Biomater.* **2016,** *38*, 11-22.
74. Wang, D.; Hou, X.; Zhang, X.; Zhao, Y.; Ma, B.; Sun, Y.; Wang, J., Light- and pH-Controlled Hierarchical Coassembly of Peptide Amphiphiles. *Langmuir* **2019,** *35*, 9841-9847.
75. Ghosh, M.; Bera, S.; Schiffmann, S.; Shimon, L. J. W.; Adler-Abramovich, L., Collagen-Inspired Helical Peptide Coassembly Forms a Rigid Hydrogel with Twisted Polyproline II Architecture. *ACS Nano* **2020,** *14*, 9990-10000.
76. Carnall, J. M.; Waudby, C. A.; Belenguer, A. M.; Stuart, M. C.; Peyralans, J. J.; Otto, S., Mechanosensitive self-replication driven by self-organization. *Science (New York, N.Y.)* **2010,** *327*, 1502-1506.
77. Moyer, T. J.; Finbloom, J. A.; Chen, F.; Toft, D. J.; Cryns, V. L.; Stupp, S. I., pH and Amphiphilic Structure Direct Supramolecular Behavior in Biofunctional Assemblies. *J. Am. Chem. Soc.* **2014,** *136*, 14746-14752.
78. Dong, H.; Paramonov, S. E.; Aulisa, L.; Bakota, E. L.; Hartgerink, J. D., Self-assembly of multidomain peptides: balancing molecular frustration controls conformation and nanostructure. *J. Am. Chem. Soc.* **2007,** *129*, 12468-12472.
79. Ardoña, H. A. M.; Tovar, J. D., Energy transfer within responsive pi-conjugated coassembled peptide-based nanostructures in aqueous environments. *Chem. Sci.* **2015,** *6*, 1474-1484.
80. Ardoña, H. A. M.; Tovar, J. D., Peptide π-Electron Conjugates: Organic Electronics for Biology? *Bioconjugate Chem.* **2015,** *26*, 2290-2302.
81. Schneider, H.-J.; Agrawal, P.; Yatsimirsky, A. K., Supramolecular complexations of natural products. *Chem. Soc. Rev.* **2013,** *42*, 6777-6800.
82. Yu, G.; Jie, K.; Huang, F., Supramolecular Amphiphiles Based on Host–Guest Molecular Recognition Motifs. *Chem. Rev.* **2015,** *115*, 7240-7303.
83. Kumar, V. A.; Shi, S.; Wang, B. K.; Li, I. C.; Jalan, A. A.; Sarkar, B.; Wickremasinghe, N. C.; Hartgerink, J. D., Drug-Triggered and Cross-Linked Self-Assembling Nanofibrous Hydrogels. *J. Am. Chem. Soc.* **2015,** *137*, 4823-4830.
84. Yu, G.; Zhao, X.; Zhou, J.; Mao, Z.; Huang, X.; Wang, Z.; Hua, B.; Liu, Y.; Zhang, F.; He, Z.; Jacobson, O.; Gao, C.; Wang, W.; Yu, C.; Zhu, X.; Huang, F.; Chen, X., Supramolecular Polymer-Based Nanomedicine: High Therapeutic Performance and Negligible Long-Term Immunotoxicity. *J. Am. Chem. Soc.* **2018,** *140*, 8005-8019.
85. Madl, A. C.; Madl, C. M.; Myung, D., Injectable Cucurbit[8]uril-Based Supramolecular Gelatin Hydrogels for Cell Encapsulation. *ACS Macro Lett.* **2020,** *9*, 619-626.
86. Li, X.; Zheng, T.; Liu, X.; Du, Z.; Xie, X.; Li, B.; Wu, L.; Li, W., Coassembly of Short Peptide and Polyoxometalate into Complex Coacervate Adapted for pH and Metal Ion-Triggered Underwater Adhesion. *Langmuir* **2019,** *35*, 4995-5003.
87. Liyanage, W.; Ardoña, H. A. M.; Mao, H.-Q.; Tovar, J. D., Cross-Linking Approaches to Tuning the Mechanical Properties of Peptide π-Electron Hydrogels. *Bioconjug. Chem.* **2017,** *28*, 751-759.
88. Jing, P.; Rudra, J. S.; Herr, A. B.; Collier, J. H., Self-Assembling Peptide-Polymer Hydrogels Designed From the Coiled Coil Region of Fibrin. *Biomacromolecules* **2008,** *9*, 2438-2446.
89. Yao, Q.; Wu, G.; Hao, H.; Lu, H.; Gao, Y., Redox-Mediated Reversible Supramolecular Assemblies Driven by Switch and Interplay of Peptide Secondary Structures. *Biomacromolecules* **2021**, 2563-2572.
90. Lange, S.; Unsleber, J.; Drücker, P.; Galla, H.-J.; Waller, M.; Ravoo, B., PH response and molecular recognition in a low molecular weight peptide hydrogel. *Org. Biomol. Chem.* **2014,** *13*, 561-569.
91. Shimizu, T.; Ding, W.; Kameta, N., Soft-Matter Nanotubes: A Platform for Diverse Functions and Applications. *Chem. Rev.* **2020,** *120*, 2347-2407.

92. De Santis, P.; Morosetti, S.; Rizzo, R., Conformational Analysis of Regular Enantiomeric Sequences. *Macromolecules* **1974,** *7*, 52-58.
93. Ghadiri, M. R.; Granja, J. R.; Milligan, R. A.; McRee, D. E.; Khazanovich, N., Self-assembling organic nanotubes based on a cyclic peptide architecture. *Nature* **1993,** *366*, 324-327.
94. Chapman, R.; Danial, M.; Koh, M. L.; Jolliffe, K. A.; Perrier, S., Design and properties of functional nanotubes from the self-assembly of cyclic peptide templates. *Chem. Soc. Rev.* **2012,** *41*, 6023-6041.
95. Reches, M.; Gazit, E., Designed aromatic homo-dipeptides: formation of ordered nanostructures and potential nanotechnological applications. *Phys. Biol.* **2006,** *3*, S10-S19.
96. Matsui, H.; Gologan, B., Crystalline Glycylglycine Bolaamphiphile Tubules and Their pH-Sensitive Structural Transformation. *J. Phys. Chem. B* **2000,** *104*, 3383-3386.
97. Cui, H.; Webber, M. J.; Stupp, S. I., Self-assembly of peptide amphiphiles: from molecules to nanostructures to biomaterials. *Biopolymers* **2010,** *94*, 1-18.
98. Kimura, S.; Kim, D.-H.; Sugiyama, J.; Imanishi, Y., Vesicular Self-Assembly of a Helical Peptide in Water. *Langmuir* **1999,** *15*, 4461-4463.
99. Bhardwaj, I.; Jha, D.; Admane, P.; Panda, A. K.; Haridas, V., Self-assembling tryptophan-based designer peptides as intracellular delivery vehicles. *Bioorganic Med. Chem. Lett.* **2016,** *26*, 672-676.
100. Dhawan, S.; Ghosh, S.; Ravinder, R.; Bais, S. S.; Basak, S.; Krishnan, N. M. A.; Agarwal, M.; Banerjee, M.; Haridas, V., Redox Sensitive Self-Assembling Dipeptide for Sustained Intracellular Drug Delivery. *Bioconjugate Chem.* **2019,** *30*, 2458-2468.
101. Naskar, J.; Roy, S.; Joardar, A.; Das, S.; Banerjee, A., Self-assembling dipeptide-based nontoxic vesicles as carriers for drugs and other biologically important molecules. *Org. Biomol. Chem.* **2011,** *9*, 6610-6615.
102. van Hell, A. J.; Costa, C. I. C. A.; Flesch, F. M.; Sutter, M.; Jiskoot, W.; Crommelin, D. J. A.; Hennink, W. E.; Mastrobattista, E., Self-Assembly of Recombinant Amphiphilic Oligopeptides into Vesicles. *Biomacromolecules* **2007,** *8*, 2753-2761.
103. Rodríguez-Hernández, J.; Lecommandoux, S., Reversible Inside−Out Micellization of pH-responsive and Water-Soluble Vesicles Based on Polypeptide Diblock Copolymers. *J. Am. Chem. Soc.* **2005,** *127*, 2026-2027.
104. Yoon, Y.-R.; Lim, Y.-b.; Lee, E.; Lee, M., Self-assembly of a peptide rod–coil: a polyproline rod and a cell-penetrating peptide Tat coil. *Chem. Commun.* **2008**, 1892-1894.
105. Jiao, D.; Geng, J.; Loh, X. J.; Das, D.; Lee, T.-C.; Scherman, O. A., Supramolecular Peptide Amphiphile Vesicles through Host–Guest Complexation. *Angew. Chem. Int. Ed.* **2012,** *51*, 9633-9637.
106. Mondal, J. H.; Ahmed, S.; Ghosh, T.; Das, D., Reversible deformation–formation of a multistimuli responsive vesicle by a supramolecular peptide amphiphile. *Soft Matter* **2015,** *11*, 4912-4920.
107. Ma, M.; Kuang, Y.; Gao, Y.; Zhang, Y.; Gao, P.; Xu, B., Aromatic−Aromatic Interactions Induce the Self-Assembly of Pentapeptidic Derivatives in Water To Form Nanofibers and Supramolecular Hydrogels. *J. Am. Chem. Soc.* **2010,** *132*, 2719-2728.
108. Mondal, S.; Varenik, M.; Bloch, D. N.; Atsmon-Raz, Y.; Jacoby, G.; Adler-Abramovich, L.; Shimon, L. J. W.; Beck, R.; Miller, Y.; Regev, O.; Gazit, E., A minimal length rigid helical peptide motif allows rational design of modular surfactants. *Nat. Commun.* **2017,** *8*, 14018-14027.
109. Castelletto, V.; Hamley, I. W.; Adamcik, J.; Mezzenga, R.; Gummel, J. J. S. M., Modulating self-assembly of a nanotape-forming peptide amphiphile with an oppositely charged surfactant. *Soft Matter* **2012,** *8*, 217-226.

110. Hatip Koc, M.; Cinar Ciftci, G.; Baday, S.; Castelletto, V.; Hamley, I. W.; Guler, M. O., Hierarchical Self-Assembly of Histidine-Functionalized Peptide Amphiphiles into Supramolecular Chiral Nanostructures. *Langmuir* **2017,** *33*, 7947-7956.
111. Shimada, T.; Lee, S.; Bates, F. S.; Hotta, A.; Tirrell, M., Wormlike Micelle Formation in Peptide-Lipid Conjugates Driven by Secondary Structure Transformation of the Headgroups. *J. Phys. Chem. B* **2009,** *113*, 13711-13714.
112. Soukasene, S.; Toft, D. J.; Moyer, T. J.; Lu, H.; Lee, H.-K.; Standley, S. M.; Cryns, V. L.; Stupp, S. I., Antitumor Activity of Peptide Amphiphile Nanofiber-Encapsulated Camptothecin. *ACS Nano* **2011,** *5*, 9113-9121.
113. Qiao, Z.-Y.; Zhao, W.-J.; Cong, Y.; Zhang, D.; Hu, Z.; Duan, Z.-Y.; Wang, H., Self-Assembled ROS-Sensitive Polymer–Peptide Therapeutics Incorporating Built-in Reporters for Evaluation of Treatment Efficacy. *Biomacromolecules* **2016,** *17*, 1643-1652.
114. Qiao, Z. Y.; Hou, C. Y.; Zhang, D.; Liu, Y.; Lin, Y. X.; An, H. W.; Li, X. J.; Wang, H., Self-assembly of cytotoxic peptide conjugated poly(β-amino ester)s for synergistic cancer chemotherapy. *J. Mater. Chem. B* **2015,** *3*, 2943-2953.
115. Bian, Z.; Yan, J.; Wang, S.; Li, Y.; Guo, Y.; Ma, B.; Guo, H.; Lei, Z.; Yin, C.; Zhou, Y.; Liu, M.; Tao, K.; Hou, P.; He, W. J. T., Awakening p53 in vivo by D-peptides-functionalized ultra-small nanoparticles: Overcoming biological barriers to D-peptide drug delivery. *Theranostics* **2018,** *8*, 5320 - 5335.
116. Qiao, Z.-Y.; Zhao, W.-J.; Gao, Y.-J.; Cong, Y.; Zhao, L.; Hu, Z.; Wang, H., Reconfigurable Peptide Nanotherapeutics at Tumor Microenvironmental pH. *ACS Appl. Mater. Interfaces* **2017,** *9*, 30426-30436.
117. Cheng, H.; Zhu, J.-Y.; Xu, X.-D.; Qiu, W.-X.; Lei, Q.; Han, K.; Cheng, Y.-J.; Zhang, X.-Z., Activable Cell-Penetrating Peptide Conjugated Prodrug for Tumor Targeted Drug Delivery. *ACS Appl. Mater. Interfaces* **2015,** *7*, 16061-16069.
118. Park, S. E.; Sajid, M. I.; Parang, K.; Tiwari, R. K., Cyclic Cell-Penetrating Peptides as Efficient Intracellular Drug Delivery Tools. *Mol. Pharm.* **2019,** *16*, 3727-3743.
119. Habault, J.; Poyet, J.-L., Recent Advances in Cell Penetrating Peptide-Based Anticancer Therapies. *Molecules* **2019,** *24*, 927-943.
120. Gui, L.; Zhang, X.-H.; Qiao, Z.-Y.; Wang, H., Cell-Penetrating Peptides and Polymers for Improved Drug Delivery. *ChemNanoMat* **2020,** *6*, 1138-1148.
121. Choi, H.; Jeena, M. T.; Palanikumar, L.; Jeong, Y.; Park, S.; Lee, E.; Ryu, J.-H., The HA-incorporated nanostructure of a peptide–drug amphiphile for targeted anticancer drug delivery. *Chem. Commun.* **2016,** *52*, 5637-5640.
122. Wang, J.; Fang, T.; Li, M.; Zhang, W.; Zhang, Z.-P.; Zhang, X.-E.; Li, F., Intracellular delivery of peptide drugs using viral nanoparticles of bacteriophage P22: covalent loading and cleavable release. *J. Mater. Chem. B* **2018,** *6*, 3716-3726.
123. Jin, Y.; Huang, Y.; Yang, H.; Liu, G.; Zhao, R., A peptide-based pH-sensitive drug delivery system for targeted ablation of cancer cells. *Chem. Commun.* **2015,** *51*, 14454-14457.
124. Han, C.; Zhou, J.; Liang, C.; Liu, B.; Pan, X.; Zhang, Y.; Wang, Y.; Yan, B.; Xie, W.; Liu, F.; Yu, X. Y.; Li, Y., Human umbilical cord mesenchymal stem cell derived exosomes encapsulated in functional peptide hydrogels promote cardiac repair. *Biomater. Sci.* **2019,** *7*, 2920-2933.
125. Yang, L.; Zhang, C.; Ren, C.; Liu, J.; Zhang, Y.; Wang, J.; Huang, F.; Zhang, L.; Liu, J., Supramolecular Hydrogel Based on Chlorambucil and Peptide Drug for Cancer Combination Therapy. *ACS Appl. Mater. Interfaces* **2019,** *11*, 331-339.
126. Cheng, D.-B.; Wang, D.; Gao, Y.-J.; Wang, L.; Qiao, Z.-Y.; Wang, H., Autocatalytic Morphology Transformation Platform for Targeted Drug Accumulation. *J. Am. Chem. Soc.* **2019,** *141*, 4406-4411.

127. Du, W.; Hu, X.; Wei, W.; Liang, G., Intracellular Peptide Self-Assembly: A Biomimetic Approach for in Situ Nanodrug Preparation. *Bioconjugate Chemistry* **2018,** *29*, 826-837.
128. Chen, B.; He, X.-Y.; Yi, X.-Q.; Zhuo, R.-X.; Cheng, S.-X., Dual-Peptide-Functionalized Albumin-Based Nanoparticles with pH-Dependent Self-Assembly Behavior for Drug Delivery. *ACS Appl. Mater. Interfaces* **2015,** *7*, 15148-15153.
129. Du, A. W.; Stenzel, M. H., Drug Carriers for the Delivery of Therapeutic Peptides. *Biomacromolecules* **2014,** *15*, 1097-1114.
130. Goor, O. J. G. M.; Hendrikse, S. I. S.; Dankers, P. Y. W.; Meijer, E. W., From supramolecular polymers to multi-component biomaterials. *Chem. Soc. Rev.* **2017,** *46*, 6621-6637.
131. Kohane, D. S.; Langer, R., Polymeric Biomaterials in Tissue Engineering. *Pediatric Res.* **2008,** *63*, 487-491.
132. Freed, L. E.; Vunjak-Novakovic, G.; Biron, R. J.; Eagles, D. B.; Lesnoy, D. C.; Barlow, S. K.; Langer, R., Biodegradable Polymer Scaffolds for Tissue Engineering. *Nat. Biotechnol.* **1994,** *12*, 689-693.
133. Ulijn, R. V., Molecular self-assembly: Best of both worlds. *Nat. Nanotechnol.* **2015,** *10*, 295-296.
134. Wan, S.; Borland, S.; Richardson, S. M.; Merry, C. L. R.; Saiani, A.; Gough, J. E., Self-assembling peptide hydrogel for intervertebral disc tissue engineering. *Acta Biomater.* **2016,** *46*, 29-40.
135. Li, L.-L.; Qi, G.-B.; Yu, F.; Liu, S.-J.; Wang, H., An Adaptive Biointerface from Self-Assembled Functional Peptides for Tissue Engineering. *Adv. Mater.* **2015,** *27*, 3181-3188.
136. Ahmed, S.; Singha, N.; Pramanik, B.; Mondal, J. H.; Das, D., Redox controlled reversible transformation of a supramolecular alternating copolymer to a radical cation containing homo-polymer. *Polym. Chem.* **2016,** *7*, 4393-4401.
137. Zhao, T.; Sellers, D. L.; Cheng, Y.; Horner, P. J.; Pun, S. H., Tunable, Injectable Hydrogels Based on Peptide-Cross-Linked, Cyclized Polymer Nanoparticles for Neural Progenitor Cell Delivery. *Biomacromolecules* **2017,** *18*, 2723-2731.
138. Seow, W. Y.; Salgado, G.; Lane, E. B.; Hauser, C. A., Transparent crosslinked ultrashort peptide hydrogel dressing with high shape-fidelity accelerates healing of full-thickness excision wounds. *Sci. Rep.* **2016,** *6*, 32670-32681.
139. Ding, L.; Jiang, Y.; Zhang, J.; Klok, H.-A.; Zhong, Z., pH-Sensitive Coiled-Coil Peptide-Cross-Linked Hyaluronic Acid Nanogels: Synthesis and Targeted Intracellular Protein Delivery to CD44 Positive Cancer Cells. *Biomacromolecules* **2018,** *19*, 555-562.
140. Deng, Y.; Yang, Y.; Wei, S., Peptide-Decorated Nanofibrous Niche Augments In Vitro Directed Osteogenic Conversion of Human Pluripotent Stem Cells. *Biomacromolecules* **2017,** *18*, 587-598.
141. Mahou, R.; Vlahos, A. E.; Shulman, A.; Sefton, M. V., Interpenetrating Alginate-Collagen Polymer Network Microspheres for Modular Tissue Engineering. *ACS Biomater. Sci. Eng.* **2018,** *4*, 3704-3712.
142. Liao, S. W.; Yu, T.-B.; Guan, Z., De Novo Design of Saccharide–Peptide Hydrogels as Synthetic Scaffolds for Tailored Cell Responses. *J. Am. Chem. Soc.* **2009,** *131*, 17638-17646.
143. Wang, C.; Stewart, R. J.; KopeČek, J., Hybrid hydrogels assembled from synthetic polymers and coiled-coil protein domains. *Nature* **1999,** *397*, 417-420.
144. Elder, A. N.; Dangelo, N. M.; Kim, S. C.; Washburn, N. R., Conjugation of β-Sheet Peptides to Modify the Rheological Properties of Hyaluronic Acid. *Biomacromolecules* **2011,** *12*, 2610-2616.
145. Maslovskis, A.; Guilbaud, J. B.; Grillo, I.; Hodson, N.; Miller, A. F.; Saiani, A., Self-Assembling Peptide/Thermoresponsive Polymer Composite Hydrogels: Effect of Peptide–Polymer Interactions on Hydrogel Properties. *Langmuir* **2014,** *30*, 10471-10480.

146. Clarke, D. E.; Pashuck, E. T.; Bertazzo, S.; Weaver, J. V. M.; Stevens, M. M., Self-Healing, Self-Assembled β-Sheet Peptide–Poly(γ-glutamic acid) Hybrid Hydrogels. *J. Am. Chem. Soc.* **2017,** *139*, 7250-7255.
147. Li, L.-M.; Han, M.; Jiang, X.-C.; Yin, X.-Z.; Chen, F.; Zhang, T.-Y.; Ren, H.; Zhang, J.-W.; Hou, T.-J.; Chen, Z.; Ou-Yang, H.-W.; Tabata, Y.; Shen, Y.-Q.; Gao, J.-Q., Peptide-Tethered Hydrogel Scaffold Promotes Recovery from Spinal Cord Transection via Synergism with Mesenchymal Stem Cells. *ACS Appl. Mater. Interfaces* **2017,** *9*, 3330-3342.
148. Shen, Z.; Guo, Z.; Tan, T.; Hu, J.; Zhang, Y., Reactive Oxygen Species Scavenging and Biodegradable Peptide Hydrogel as 3D Culture Scaffold for Cardiomyocytes. *ACS Biomater. Sci. Eng.* **2020,** *6*, 3957-3966.
149. Mukherjee, K.; Ruan, Q.; Nutt, S.; Tao, J.; De Yoreo, J. J.; Moradian-Oldak, J., Peptide-Based Bioinspired Approach to Regrowing Multilayered Aprismatic Enamel. *ACS Omega* **2018,** *3*, 2546-2557.
150. Ghosh, M.; Halperin-Sternfeld, M.; Grigoriants, I.; Lee, J.; Nam, K. T.; Adler-Abramovich, L., Arginine-Presenting Peptide Hydrogels Decorated with Hydroxyapatite as Biomimetic Scaffolds for Bone Regeneration. *Biomacromolecules* **2017,** *18*, 3541-3550.
151. Gavel, P. K.; Dev, D.; Parmar, H. S.; Bhasin, S.; Das, A. K., Investigations of Peptide-Based Biocompatible Injectable Shape-Memory Hydrogels: Differential Biological Effects on Bacterial and Human Blood Cells. *ACS Appl. Mater. Interfaces* **2018,** *10*, 10729-10740.
152. Tang, J. D.; Mura, C.; Lampe, K. J., Stimuli-Responsive, Pentapeptide, Nanofiber Hydrogel for Tissue Engineering. *J. Am. Chem. Soc.* **2019,** *141*, 4886-4899.
153. Gao, Y.; Zhao, F.; Wang, Q.; Zhang, Y.; Xu, B., Small peptide nanofibers as the matrices of molecular hydrogels for mimicking enzymes and enhancing the activity of enzymes. *Chem. Soc. Rev.* **2010,** *39*, 3425-3433.
154. Dong, Z.; Luo, Q.; Liu, J., Artificial enzymes based on supramolecular scaffolds. *Chem. Soc. Rev.* **2012,** *41*, 7890-7908.
155. Huang, Z.; Guan, S.; Wang, Y.; Shi, G.; Cao, L.; Gao, Y.; Dong, Z.; Xu, J.; Luo, Q.; Liu, J., Self-assembly of amphiphilic peptides into bio-functionalized nanotubes: a novel hydrolase model. *J. Mater. Chem. B* **2013,** *1*, 2297-2304.
156. Gulseren, G.; Khalily, M. A.; Tekinay, A. B.; Guler, M. O., Catalytic supramolecular self-assembled peptide nanostructures for ester hydrolysis. *J. Mater. Chem. B* **2016,** *4*, 4605-4611.
157. Rufo, C. M.; Moroz, Y. S.; Moroz, O. V.; Stöhr, J.; Smith, T. A.; Hu, X.; DeGrado, W. F.; Korendovych, I. V., Short peptides self-assemble to produce catalytic amyloids. *Nat. Chem.* **2014,** *6*, 303-309.
158. Makhlynets, O. V.; Gosavi, P. M.; Korendovych, I. V., Short Self-Assembling Peptides Are Able to Bind to Copper and Activate Oxygen. *Angew. Chem. Int. Ed.* **2016,** *55*, 9017-9020.
159. Sarkhel, B.; Chatterjee, A.; Das, D., Covalent Catalysis by Cross β Amyloid Nanotubes. *J. Am. Chem. Soc.* **2020,** *142*, 4098-4103.
160. Al-Garawi, Z. S.; McIntosh, B. A.; Neill-Hall, D.; Hatimy, A. A.; Sweet, S. M.; Bagley, M. C.; Serpell, L. C., The amyloid architecture provides a scaffold for enzyme-like catalysts. *Nanoscale* **2017,** *9*, 10773-10783.
161. Makam, P.; Yamijala, S.; Tao, K.; Shimon, L. J. W.; Eisenberg, D. S.; Sawaya, M. R.; Wong, B. M.; Gazit, E., Non-proteinaceous hydrolase comprised of a phenylalanine metallo-supramolecular amyloid-like structure. *Nat. Catal.* **2019,** *2*, 977-985.
162. Rodríguez-Llansola, F.; Escuder, B.; Miravet, J. F., Switchable Perfomance of an l-Proline-Derived Basic Catalyst Controlled by Supramolecular Gelation. *J. Am. Chem. Soc.* **2009,** *131*, 11478-11484.

163. Duschmalé, J.; Kohrt, S.; Wennemers, H., Peptide catalysis in aqueous emulsions. *Chem. Commun.* **2014,** *50*, 8109-8112.
164. Singh, N.; Zhang, K.; Angulo-Pachón, C. A.; Mendes, E.; van Esch, J. H.; Escuder, B., Tandem reactions in self-sorted catalytic molecular hydrogels. *Chem. Sci.* **2016,** *7*, 5568-5572.
165. Gong, Z.; Yang, Y.; Ren, Q.; Chen, X.; Shao, Z., Injectable thixotropic hydrogel comprising regenerated silk fibroin and hydroxypropylcellulose. *Soft Matter* **2012,** *8*, 2875-2883.
166. Pramanik, B.; Ahmed, S.; Singha, N.; Das, B.; Dowari, P.; Das, D., Unorthodox Combination of Cation-π and Charge-Transfer Interactions within a Donor Acceptor Pair. *Langmuir* **2018,** *35*, 478–488.
167. Hamilton, T. D.; Bučar, D. K.; Baltrusaitis, J.; Flanagan, D. R.; Li, Y.; Ghorai, S., Thixotropic Hydrogel Derived from a Product of an Organic Solid-State Synthesis: Properties and Densities of Metal−Organic Nanoparticles. *J. Am. Chem. Soc.* **2011,** *133*, 3365–3371.
168. Lee, J. H., Injectable hydrogels delivering therapeutic agents for disease treatment and tissue engineering. *Biomater. Res.* **2018,** *22*, 235-248.
169. Mathew, A. P.; Uthaman, S.; Cho, K. H.; Cho, C. S.; Park, I. K., Injectable hydrogels for delivering biotherapeutic molecules. *Int. J. Biol. Macromol.* **2018,** *110*, 17-29.
170. Xing, R.; Li, S.; Zhang, N.; Shen, G.; Möhwald, H.; Yan, X., Self-Assembled Injectable Peptide Hydrogels Capable of Triggering Antitumor Immune Response. *Biomacromolecules* **2017,** *18*, 3514–3523.
171. Kumar, D.; Workman, V. L.; O'Brien, M.; McLaren, J.; White, L.; Ragunath, K., Peptide Hydrogels—A Tissue Engineering Strategy for the Prevention of Oesophageal Strictures. *Adv. Funct. Mater.* **2017,** *27*, 1702424-1702436.
172. Collier, J. H.; Rudra, J. S.; Gasiorowski, J. Z.; Jung, J. P., Multi-component extracellular matrices based on peptideself-assembly. *Chem. Soc. Rev.* **2010,** *39*, 3413-3424.
173. Altunbas A and Pochan D J 2012 in Peptide-based materials T Deming (ed) (Heidelberg, Berlin: Springer) p 135.
174. Nagai, Y.; Unsworth, L. D.; Koutsopoulos, S.; Zhang, S., Slow release of molecules in self-assembling peptide nanofiber scaffold. *J. Controlled Release* **2006,** *115*, 18-25.
175. Ahmed, S.; Mondal, J. H.; Behera, N.; Das, D., Self-Assembly of Peptide-Amphiphile Forming Helical Nanofibers and in Situ Template Synthesis of Uniform Mesoporous Single Wall Silica Nanotubes. *Langmuir* **2013,** *29*, 14274–14283.
176. Mitra, R. N.; Das, P. K., In situ Preparation of Gold Nanoparticles of Varying Shape in Molecular Hydrogel of Peptide Amphiphiles. *J. Phys. Chem. C* **2008,** *112*, 8159–8166.
177. Pramanik, B.; Singha, N.; Das, D., Sol-, Gel-, and Paper-Based Detection of Picric Acid at Femtogram Level by a Short Peptide Gelator. *ACS Appl. Polym. Mater.* **2019,** *1*, 833–843.
178. Singha, N.; Neogi, S.; Pramanik, B.; Das, S.; Dasgupta, A.; Ghosh, R., Ultrafast, Highly Sensitive, and Selective Detection of p-Xylene at Room Temperature by Peptide-Hydrogel-Based Composite Material. *ACS Appl. Polym. Mater.* **2019,** *1*, 2267–2272.
179. Li, J.; Xing, R.; Bai, S.; Yan, X., Recent advances of self-assembling peptide-based hydrogels for biomedical applications. *Soft Matter* **2019,** *15*, 1704-1715.
180. Cui, H.; Webber, M. J.; Stupp, S. I., Self-assembly of peptide amphiphiles: From molecules to nanostructures to biomaterials. *Peptide Sci.* **2010,** *94*, 1-18.
181. Pochan, D. J.; Schneider, J. P.; Kretsinger, J.; Ozbas, B.; Rajagopal, K.; Haines, L., Thermally Reversible Hydrogels via Intramolecular Folding and Consequent Self-Assembly of a de Novo Designed Peptide. *J. Am. Chem. Soc.* **2003,** *125*, 11802–11803.
182. Haines, L. A.; Rajagopal, K.; Ozbas, B.; Salick, D. A.; Pochan, D. J.; Schneider, J. P., Light-Activated Hydrogel Formation via the Triggered Folding and Self-Assembly of a Designed Peptide. *J. Am. Chem. Soc.* **2005,** *127*, 17025–17029.

183. Kretsinger, J. K.; Haines, L. A.; Ozbas, B.; Pochan, D. J.; Schneider, J. P., Cytocompatibility of self-assembled β-hairpin peptide hydrogel surfaces. *Biomaterials* **2005,** *26*, 5177-5186.
184. Haines-Butterick, L.; Rajagopal, K.; Branco, M.; Salick, D.; Rughani, R.; Pilarz, M., Controlling hydrogelation kinetics by peptide design for three-dimensional encapsulation and injectable delivery of cells. *Proc. Natl. Acad. Sci.* **2007,** *104*, 7791-7796.
185. Rughani, R. V.; Salick, D. A.; Lamm, M. S.; Yucel, T.; Pochan, D. J.; Schneider, J. P., Folding, Self-Assembly, and Bulk Material Properties of a De Novo Designed Three-Stranded β-Sheet Hydrogel. *Biomacromolecules* **2009,** *10*, 1295–1304.
186. Nagarkar, R. P.; Hule, R. A.; Pochan, D. J.; Schneider, J. P., De Novo Design of Strand-Swapped β-Hairpin Hydrogels. *J. Am. Chem. Soc.* **2008,** *130*, 4466–4474.
187. Singha, N.; Das, B. K.; Pramanik, B.; Das, S.; Das, D., Freeze the dynamicity: charge transfer complexation assisted control over the reaction pathway. *Chem. Sci.* **2019,** *10*, 10035-10039.
188. Black, S. P.; Sanders, J. K. M.; Stefankiewicz, A. R., Disulfide exchange: exposing supramolecular reactivity through dynamic covalent chemistry. *Chem. Soc. Rev.* **2014,** *43*, 1861-1872.
189. Wei, Y.; Thyparambil, A. A.; Latour, R. A., Biochim. *Biophys. Acta: Proteins and Proteomics* **2014,** *1844*, 2331-2337.
190. Niu, L.; Liu, L.; Xi, W.; Han, Q.; Li, Q.; Yu, Y., Synergistic Inhibitory Effect of Peptide–Organic Coassemblies on Amyloid Aggregation. *ACS Nano* **2016,** *10*, 4143–4153.
191. Smith, A. M.; Williams, R. J.; Tang, C.; Coppo, P.; Collins, R. F.; Turner, M. L., Fmoc-Diphenylalanine Self Assembles to a Hydrogel via a Novel Architecture Based on π–π Interlocked β-Sheets. *Adv. Mater.* **2008,** *20*, 37-41.
192. Madhu, C.; Roy, B.; Makam, P.; Govindaraju, T., Bicomponent β-sheet assembly of dipeptide fluorophores of opposite polarity and sensitive detection of nitro-explosives. *Chem. Commun.* **2018,** *54*, 2280-2283.
193. Ohrdorf K-H and Flachberger H 2015 in Polymer nanoclay composites S Laske (ed) (Oxford: William Andrew Publishing) p 1.
194. Tanner R I and Walters K 1998 in Rheology series (Amsterdam: Elsevier) Vol 7, p 159.
195. Seow, W. Y.; Hauser, C. A. E., Short to ultrashort peptide hydrogels for biomedical uses. *Mater. Today* **2014,** *17*, 381-388.
196. Adler-Abramovich, L.; Gazit, E., The physical properties of supramolecular peptide assemblies: from building block association to technological applications. *Chem. Soc. Rev.* **2014,** *43*, 6881-6893.
197. Lampel, A.; Ulijn, R. V.; Tuttle, T., Guiding principles for peptide nanotechnology through directed discovery. *Chem. Soc. Rev.* **2018,** *47*, 3737-3758.
198. Panja, S.; Adams, D. J., Stimuli responsive dynamic transformations in supramolecular gels. *Chem. Soc. Rev.* **2021,** *50*, 5165-5200.
199. Zhou, J.; Du, X.; Xu, B., Regulating the Rate of Molecular Self-Assembly for Targeting Cancer Cells. *Angew. Chem. Int. Ed.* **2016,** *55*, 5770-5775.
200. Hedegaard, C. L.; Collin, E. C.; Redondo-Gómez, C.; Nguyen, L. T. H.; Ng, K. W.; Castrejón-Pita, A. A.; Castrejón-Pita, J. R.; Mata, A., Hydrodynamically Guided Hierarchical Self-Assembly of Peptide–Protein Bioinks. *Adv. Funct. Mater.* **2018,** *28*, 1703716.
201. Singha, N.; Neogi, S.; Pramanik, B.; Das, S.; Dasgupta, A.; Ghosh, R.; Das, D., Ultrafast, Highly Sensitive, and Selective Detection of p-Xylene at Room Temperature by Peptide-Hydrogel-Based Composite Material. *ACS Appl. Polym. Mater.* **2019,** *1*, 2267-2272.
202. Pramanik, B.; Singha, N.; Das, D., Sol-, Gel-, and Paper-Based Detection of Picric Acid at Femtogram Level by a Short Peptide Gelator. *ACS Appl. Polym. Mater.* **2019,** *1*, 833-843.

203. Das, S.; Das, D., Rational Design of Peptide-based Smart Hydrogels for Therapeutic Applications. *Front. Chem.* **2021,** *9*, 770102.
204. Li, Y.; Wang, F.; Cui, H., Peptide-Based Supramolecular Hydrogels for Delivery of Biologics. *Bioeng. Transl. Med.* **2016,** *1*, 306-322.
205. Zhang, Z.; Ai, S.; Yang, Z.; Li, X., Peptide-based supramolecular hydrogels for local drug delivery. *Adv. Drug Delivery Rev.* **2021,** *174*, 482-503.
206. Cross, E. R.; Coulter, S. M.; Pentlavalli, S.; Laverty, G., Unravelling the antimicrobial activity of peptide hydrogel systems: current and future perspectives. *Soft matter* **2021,** *17*, 8001-8021.
207. Tomiotto-Pellissier, F.; Bortoleti, B. T. d. S.; Assolini, J. P.; Gonçalves, M. D.; Carloto, A. C. M.; Miranda-Sapla, M. M.; Conchon-Costa, I.; Bordignon, J.; Pavanelli, W. R., Macrophage Polarization in Leishmaniasis: Broadening Horizons. *Front. Immunol.* **2018,** *9*, 2529-2540.
208. Taylor, M. E.; Drickamer, K., Structural requirements for high affinity binding of complex ligands by the macrophage mannose receptor. *J. Biol. Chem.* **1993,** *268*, 399-404.
209. Ueno, N.; Wilson, M. E., Receptor-mediated phagocytosis of Leishmania: implications for intracellular survival. *Trends Parasitol.* **2012,** *28*, 335-344.
210. Mukhopadhyay, A.; Chaudhuri, G.; Arora, S. K.; Sehgal, S.; Basu, S. K., Receptor-Mediated Drug Delivery to Macrophages in Chemotherapy of Leishmaniasis. *Science (New York, N.Y.)* **1989,** *244*, 705-707.
211. Basu, M.; Lala, S., Macrophage Specific Drug Delivery in Experimental Leishmaniasis. *Curr. Mol. Med.* **2004,** *4*, 681-689.
212. Ghosh, S.; Das, S.; De, A. K.; Kar, N.; Bera, T., Amphotericin B-loaded mannose modified poly(d,l-lactide-co-glycolide) polymeric nanoparticles for the treatment of visceral leishmaniasis: in vitro and in vivo approaches. *RSC Adv.* **2017,** *7*, 29575-29590.
213. Ruan, G.-X.; Chen, Y.-Z.; Yao, X.-L.; Du, A.; Tang, G.-P.; Shen, Y.-Q.; Tabata, Y.; Gao, J.-Q., Macrophage mannose receptor-specific gene delivery vehicle for macrophage engineering. *Acta Biomater.* **2014,** *10*, 1847-1855.
214. Mukhopadhyay, A.; Basu, S. K., Intracellular delivery of drugs to macrophages. *Adv. Biochem. Eng. Biotechnol.* **2003,** *84*, 183-209.
215. Mondal, S.; Roy, P.; Das, S.; Halder, A.; Mukherjee, A.; Bera, T., In vitro susceptibilities of wild and drug resistant leishmania donovani amastigote stages to andrographolide nanoparticle: role of vitamin E derivative TPGS for nanoparticle efficacy. *PloS one* **2013,** *8*, e81492.
216. Asthana, S.; Gupta, P.; Jaiswal, A.; Dube, A.; Chourasia, M. K. J. P. R., Overexpressed Macrophage Mannose Receptor Targeted Nanocapsules- Mediated Cargo Delivery Approach for Eradication of Resident Parasite: In Vitro and In Vivo Studies. *Pharm. Res.* **2015,** *32*, 2663-2677.
217. Vossen, L. I.; Domínguez-Asenjo, B.; Gutiérrez-Corbo, C.; Pérez-Pertejo, M. Y.; Balaña-Fouce, R.; Reguera, R. M.; Calderón, M., Mannose-Decorated Dendritic Polyglycerol Nanocarriers Drive Antiparasitic Drugs To Leishmania infantum-Infected Macrophages. *Pharmaceutics* **2020,** *12*, 915-934.
218. Liberato, M. S.; Mancini, R. S. N.; Factori, I. M.; Ferreira, F. F.; de Oliveira, V. L.; Carnielli, J. B. T.; Guha, S.; Peroni, L. A.; Oliveira, M. A. L.; Alves, W. A., Peptide-Based Assemblies on Electrospun Polyamide-6/Chitosan Nanofibers for Detecting Visceral Leishmaniasis Antibodies. *ACS Appl. Electron. Mater* **2019,** *1*, 2086-2095.
219. Kumar, V.; Chugh, A., Peptide-mediated leishmaniasis management strategy: Tachyplesin emerges as an effective anti-leishmanial peptide against Leishmania donovani. *Biochim. Biophys. Acta - Biomembr.* **2021,** *1863*, 183629-1833636.
220. Chowdhuri, S.; Ghosh, M.; Adler-Abramovich, L.; Das, D., The Effects of a Short Self-Assembling Peptide on the Physical and Biological Properties of Biopolymer Hydrogels. *Pharmaceutics* **2021,** *13*, 1602.

221. Halperin-Sternfeld, M.; Ghosh, M.; Sevostianov, R.; Grigoriants, I.; Adler-Abramovich, L., Molecular co-assembly as a strategy for synergistic improvement of the mechanical properties of hydrogels. *Chem. Commun.* **2017,** *53*, 9586-9589.
222. Zhai, Z.; Xu, K.; Mei, L.; Wu, C.; Liu, J.; Liu, Z.; Wan, L.; Zhong, W., Co-assembled supramolecular hydrogels of cell adhesive peptide and alginate for rapid hemostasis and efficacious wound healing. *Soft Matter* **2019,** *15*, 8603-8610.
223. Hu, B.; Owh, C.; Chee, P. L.; Leow, W. R.; Liu, X.; Wu, Y.-L.; Guo, P.; Loh, X. J.; Chen, X., Supramolecular hydrogels for antimicrobial therapy. *Chem. Soc. Rev.* **2018,** *47*, 6917-6929.
224. Jain, R.; Roy, S., Designing a bioactive scaffold from coassembled collagen–laminin short peptide hydrogels for controlling cell behaviour. *RSC Adv.* **2019,** *9*, 38745-38759.
225. Zhang, Y.; Kuang, Y.; Gao, Y.; Xu, B., Versatile small-molecule motifs for self-assembly in water and the formation of biofunctional supramolecular hydrogels. *Langmuir* **2011,** *27*, 529-537.
226. Das, S.; Das, P.; Dowari, P.; Kanti Das, B.; Das, D., Bi-Directional Feedback Controlled Transience in Cucurbituril Based Tandem Nanozyme. *J. Colloid Interface Sci.* **2022,** *614*, 172-180.
227. Dowari, P.; Das, S.; Pramanik, B.; Das, D., pH clock instructed transient supramolecular peptide amphiphile and its vesicular assembly. *Chem. Commun.* **2019,** *55*, 14119-14122.
228. Adams, D. J.; Butler, M. F.; Frith, W. J.; Kirkland, M.; Mullen, L.; Sanderson, P., A new method for maintaining homogeneity during liquid–hydrogel transitions using low molecular weight hydrogelators. *Soft matter* **2009,** *5*, 1856-1862.
229. Singha, N.; Gupta, P.; Pramanik, B.; Ahmed, S.; Dasgupta, A.; Ukil, A.; Das, D., Hydrogelation of a Naphthalene Diimide Appended Peptide Amphiphile and Its Application in Cell Imaging and Intracellular pH Sensing. *Biomacromolecules* **2017,** *18*, 3630-3641.
230. Das, D.; Dasgupta, A.; Roy, S.; Mitra, R. N.; Debnath, S.; Das, P. K., Water Gelation of an Amino Acid-Based Amphiphile. *Che. Eur. J.* **2006,** *12*, 5068-5074.
231. Maity, S.; Das, P.; Reches, M., Inversion of Supramolecular Chirality by Sonication-Induced Organogelation. *Sci. Rep.* **2015,** *5*, 16365-16375.
232. McDougall, M.; Francisco, O.; Harder-Viddal, C.; Roshko, R.; Heide, F.; Sidhu, S.; Khajehpour, M.; Leslie, J.; Palace, V.; Tomy, G. T.; Stetefeld, J., Proteinaceous Nano container Encapsulate Polycyclic Aromatic Hydrocarbons. *Sci. Rep.* **2019,** *9*, 1058-1067.
233. Zou, Y.; Li, Y.; Hao, W.; Hu, X.; Ma, G., Parallel β-Sheet Fibril and Antiparallel β-Sheet Oligomer: New Insights into Amyloid Formation of Hen Egg White Lysozyme under Heat and Acidic Condition from FTIR Spectroscopy. *J. Phys. Chem. B* **2013,** *117*, 4003-4013.
234. Dowari, P.; Pramanik, B.; Das, D., pH and secondary structure instructed aggregation to a thixotropic hydrogel by a peptide amphiphile. *Bull. Mater. Sci.* **2020,** *43*, 70.
235. Comí, M.; Fernandez, M.; Santamaría, A.; Lligadas, G.; Ronda, J.; Galià, M.; Cadiz, V., Carboxylic Acid Ionic Modification of Castor-Oil-Based Polyurethanes Bearing Amine Groups: Chemically Tunable Physical Properties and Recyclability. *Macromol. Chem. Phys.* **2017,** *218*, 1700379-1700386.
236. Marchesan, S.; Styan, K. E.; Easton, C. D.; Waddington, L.; Vargiu, A. V., Higher and lower supramolecular orders for the design of self-assembled heterochiral tripeptide hydrogel biomaterials. *J. Mater. Chem. B* **2015,** *3*, 8123-8132.
237. Singh, V.; Snigdha, K.; Singh, C.; Sinha, N.; Thakur, A., Understanding the self-assembly of Fmoc-phenylalanine to hydrogel formation. *Soft Matter* **2015,** *11*, 5353-5364.
238. Conte, M. P.; Singh, N.; Sasselli, I. R.; Escuder, B.; Ulijn, R. V., Metastable hydrogels from aromatic dipeptides. *Chem. Commun.* **2016,** *52*, 13889-13892.
239. Das, B. K.; Pramanik, B.; Chowdhuri, S.; Scherman, O. A.; Das, D., Light-triggered syneresis of a water insoluble peptide-hydrogel effectively removes small molecule waste contaminants. *Chem. Commun.* **2020,** *56*, 3393-3396.

240. Ahmed, S.; Mondal, J. H.; Behera, N.; Das, D., Self-Assembly of Peptide-Amphiphile Forming Helical Nanofibers and in Situ Template Synthesis of Uniform Mesoporous Single Wall Silica Nanotubes. *Langmuir* **2013,** *29*, 14274-14283.
241. Pramanik, B.; Ahmed, S.; Singha, N.; Das, B. K.; Dowari, P.; Das, D., Unorthodox Combination of Cation−π and Charge-Transfer Interactions within a Donor–Acceptor Pair. *Langmuir* **2019,** *35*, 478-488.
242. Sundar, S.; Chakravarty, J.; Rai, V. K.; Agrawal, N.; Singh, S. P.; Chauhan, V.; Murray, H. W., Amphotericin B Treatment for Indian Visceral Leishmaniasis: Response to 15 Daily versus Alternate-Day Infusions. *Clin. Infect. Dis.* **2007,** *45*, 556-561.
243. Das, S.; Sardar, A. H.; Abhishek, K.; Kumar, A.; Rabidas, V. N.; Das, P., Cathelicidin augments VDR-dependent anti-leishmanial immune response in Indian Post-Kala-Azar Dermal Leishmaniasis. *Int. Immunopharmacol.* **2017,** *50*, 130-138.
244. Hinderer, S.; Layland, S. L.; Schenke-Layland, K., ECM and ECM-like materials — Biomaterials for applications in regenerative medicine and cancer therapy. *Adv. Drug Delivery Rev.* **2016,** *97*, 260-269.
245. Laurent, J.; Blin, G.; Chatelain, F.; Vanneaux, V.; Fuchs, A.; Larghero, J.; Théry, M., Convergence of microengineering and cellular self-organization towards functional tissue manufacturing. *Nat. Biomed. Engineering* **2017,** *1*, 939-956.
246. Huang, G.; Li, F.; Zhao, X.; Ma, Y.; Li, Y.; Lin, M.; Jin, G.; Lu, T. J.; Genin, G. M.; Xu, F., Functional and Biomimetic Materials for Engineering of the Three-Dimensional Cell Microenvironment. *Chem. Rev.* **2017,** *117*, 12764-12850.
247. Hamley, I. W., Small Bioactive Peptides for Biomaterials Design and Therapeutics. *Chem. Rev.* **2017**, 14015–14041.
248. Li, C., Pillararene-based supramolecular polymers: from molecular recognition to polymeric aggregates. *Chem. Commun.* **2014,** *50*, 12420-12433.
249. Li, Z.-Y.; Zhang, Y.; Zhang, C.-W.; Chen, L.-J.; Wang, C.; Tan, H.; Yu, Y.; Li, X.; Yang, H.-B., Cross-Linked Supramolecular Polymer Gels Constructed from Discrete Multi-pillar[5]arene Metallacycles and Their Multiple Stimuli-Responsive Behavior. *J. Am. Chem. Soc.* **2014,** *136*, 8577-8589.
250. Kaufmann, L.; Kennedy, S. R.; Jones, C. D.; Steed, J. W., Cavity-containing supramolecular gels as a crystallization tool for hydrophobic pharmaceuticals. *Chem. Commun.* **2016,** *52*, 10113-10116.
251. Li, H.; Meng, B.; Chai, S.-H.; Liu, H.; Dai, S., Hyper-crosslinked [small beta]-cyclodextrin porous polymer: an adsorption-facilitated molecular catalyst support for transformation of water-soluble aromatic molecules. *Chem. Sci.* **2016,** *7*, 905-909.
252. Barrow, S. J.; Kasera, S.; Rowland, M. J.; del Barrio, J.; Scherman, O. A., Cucurbituril-Based Molecular Recognition. *Chem. Rev.* **2015,** *115*, 12320-12406.
253. Das, D.; Scherman, O. A., Cucurbituril: At the Interface of Small Molecule Host–Guest Chemistry and Dynamic Aggregates. *Isr. J. Chem.* **2011,** *51*, 537-550.
254. Rauwald, U.; Scherman, O. A., Supramolecular Block Copolymers with Cucurbit[8]uril in Water. *Angew. Chem. Int. Ed.* **2008,** *47*, 3950-3953.
255. Huang, Z.; Fang, Y.; Luo, Q.; Liu, S.; An, G.; Hou, C.; Lang, C.; Xu, J.; Dong, Z.; Liu, J., Construction of supramolecular polymer by enzyme-triggered covalent condensation of CB[8]-FGG-based supramonomer. *Chem. Commun.* **2016,** *52*, 2083-2086.
256. Neirynck, P.; Brinkmann, J.; An, Q.; van der Schaft, D. W.; Milroy, L. G.; Jonkheijm, P.; Brunsveld, L., Supramolecular control of cell adhesion via ferrocene-cucurbit[7]uril host-guest binding on gold surfaces. *Chem. Commun.* **2013,** *49*, 3679-3681.

257. An, Q.; Brinkmann, J.; Huskens, J.; Krabbenborg, S.; de Boer, J.; Jonkheijm, P., A Supramolecular System for the Electrochemically Controlled Release of Cells. *Angew. Chem. Int. Ed.* **2012,** *51*, 12233-12237.
258. Huang, Z.; Qin, K.; Deng, G.; Wu, G.; Bai, Y.; Xu, J.-F.; Wang, Z.; Yu, Z.; Scherman, O. A.; Zhang, X., Supramolecular Chemistry of Cucurbiturils: Tuning Cooperativity with Multiple Noncovalent Interactions from Positive to Negative. *Langmuir* **2016,** *32*, 12352-12360.
259. Nguyen, H. D.; Dang, D. T.; van Dongen, J. L. J.; Brunsveld, L., Protein Dimerization Induced by Supramolecular Interactions with Cucurbit[8]uril. *Angew. Chem. Int. Ed.* **2010,** *49*, 895-898.
260. Elter, J. K.; Sentis, G.; Bellstedt, P.; Biehl, P.; Gottschaldt, M.; Schacher, F. H., Core-crosslinked diblock terpolymer micelles – taking a closer look on crosslinking efficiency. *Polym. Chem.* **2018,** *9*, 2247-2257.
261. Jang, H. S.; Lee, J. H.; Park, Y. S.; Kim, Y. O.; Park, J.; Yang, T. Y.; Jin, K.; Lee, J.; Park, S.; You, J. M.; Jeong, K. W.; Shin, A.; Oh, I. S.; Kwon, M. K.; Kim, Y. I.; Cho, H. H.; Han, H. N.; Kim, Y.; Chang, Y. H.; Paik, S. R.; Nam, K. T.; Lee, Y. S., Tyrosine-mediated two-dimensional peptide assembly and its role as a bio-inspired catalytic scaffold. *Nat. Commun.* **2014,** *5*, 3665-3675.
262. Ding, Y.; Li, Y.; Qin, M.; Cao, Y.; Wang, W., Photo-Cross-Linking Approach to Engineering Small Tyrosine-Containing Peptide Hydrogels with Enhanced Mechanical Stability. *Langmuir* **2013,** *29*, 13299-13306.
263. Ruoslahti, E.; Pierschbacher, M. D., New perspectives in cell adhesion: RGD and integrins. *Science (New York, N.Y.)* **1987,** *238*, 491-497.
264. Kim, J.; Jung, I.-S.; Kim, S.-Y.; Lee, E.; Kang, J.-K.; Sakamoto, S.; Yamaguchi, K.; Kim, K., New Cucurbituril Homologues: Syntheses, Isolation, Characterization, and X-ray Crystal Structures of Cucurbit[n]uril (n = 5, 7, and 8). *J. Am. Chem. Soc.* **2000,** *122*, 540-541.
265. Yeo, I.-S.; Min, S.-K.; Ki Kang, H.; Kwon, T.-K.; Youn Jung, S.; Min, B.-M., Adhesion and spreading of osteoblast-like cells on surfaces coated with laminin-derived bioactive core peptides. *Data Brief* **2015,** *5*, 411-415.
266. Kueng, W.; Silber, E.; Eppenberger, U., Quantification of cells cultured on 96-well plates. *Anal. Biochem.* **1989,** *182*, 16-19.
267. Heitmann, L. M.; Taylor, A. B.; Hart, P. J.; Urbach, A. R., Sequence-Specific Recognition and Cooperative Dimerization of N-Terminal Aromatic Peptides in Aqueous Solution by a Synthetic Host. *J. Am. Chem. Soc.* **2006,** *128*, 12574-12581.
268. Michon, T.; Chenu, M.; Kellershon, N.; Desmadril, M.; Guéguen, J., Horseradish Peroxidase Oxidation of Tyrosine-Containing Peptides and Their Subsequent Polymerization: A Kinetic Study. *Biochemistry* **1997,** *36*, 8504-8513.
269. Minamihata, K.; Goto, M.; Kamiya, N., Site-Specific Protein Cross-Linking by Peroxidase-Catalyzed Activation of a Tyrosine-Containing Peptide Tag. *Bioconjugate Chem.* **2011,** *22*, 74-81.
270. Correia, M.; Neves-Petersen, M. T.; Jeppesen, P. B.; Gregersen, S.; Petersen, S. B., UV-Light Exposure of Insulin: Pharmaceutical Implications upon Covalent Insulin Dityrosine Dimerization and Disulphide Bond Photolysis. *PloS one* **2012,** *7*, e50733.
271. Rocha, J. F.; Pina, A. F.; Sousa, S. F.; Cerqueira, N. M. F. S. A., PLP-dependent enzymes as important biocatalysts for the pharmaceutical, chemical and food industries: a structural and mechanistic perspective. *Catal. Sci. Technol.* **2019,** *9*, 4864-4876.
272. Nestl, B. M.; Nebel, B. A.; Hauer, B., Recent progress in industrial biocatalysis. *Curr. Opin. Chem. Biol.* **2011,** *15*, 187-93.
273. Illanes, A.; Cauerhff, A.; Wilson, L.; Castro, G. R., Recent trends in biocatalysis engineering. *Bioresour. Technol.* **2012,** *115*, 48-57.

274. Mokhtar, N. F.; Abd. Rahman, R. N. Z. R.; Muhd Noor, N. D.; Mohd Shariff, F.; Mohamad Ali, M. S., The Immobilization of Lipases on Porous Support by Adsorption and Hydrophobic Interaction Method. *Catalysts* **2020,** *10*, 744-760.
275. Basso, A.; Serban, S., Industrial applications of immobilized enzymes—A review. *Mol. Catal.* **2019,** *479*, 110607-110626.
276. Li, F.; Li, L.; Tong, L.; Daniel, Q.; Göthelid, M.; Sun, L., Immobilization of a molecular catalyst on carbon nanotubes for highly efficient electro-catalytic water oxidation. *Chem. Commun.* **2014,** *50*, 13948-13951.
277. Sabater, S.; Mata, J. A.; Peris, E., Catalyst Enhancement and Recyclability by Immobilization of Metal Complexes onto Graphene Surface by Noncovalent Interactions. *ACS Catal.* **2014,** *4*, 2038-2047.
278. Yiu, H. H. P.; Wright, P. A., Enzymes supported on ordered mesoporous solids: a special case of an inorganic–organic hybrid. *J. Mater. Chem.* **2005,** *15*, 3690-3700.
279. Wang, P.; Dai, S.; Waezsada, S. D.; Tsao, A. Y.; Davison, B. H., Enzyme stabilization by covalent binding in nanoporous sol-gel glass for nonaqueous biocatalysis. *National Library of Science* **2001,** *74*, 249-255.
280. Pandya, P. H.; Jasra, R. V.; Newalkar, B. L.; Bhatt, P. N., Studies on the activity and stability of immobilized α-amylase in ordered mesoporous silicas. *Microporous Mesoporous Mater.* **2005,** *77*, 67-77.
281. Tortajada, M.; Ramón, D.; Beltrán, D.; Amorós, P., Hierarchical bimodal porous silicas and organosilicas for enzyme immobilization. *J. Mater. Chem.* **2005,** *15*, 3859-3868.
282. Min, K. H.; Yeo, K. B.; Ki, M.-R.; Jun, S. H.; Pack, S. P., Novel silica forming peptide, RSGH, from Equus caballus: Its unique biosilica formation under acidic conditions. *Biochem. Eng. J.* **2020,** *153*, 107389-107395.
283. Borase, T.; Iacono, M.; Ali, S. I.; Thornton, P. D.; Heise, A., Polypeptide core–shell silica nanoparticles with high grafting density by N-carboxyanhydride (NCA) ring opening polymerization as responsive materials and for bioconjugation. *Polym. Chem.* **2012,** *3*, 1267-1275.
284. Federsel, H.-J.; Moody, T. S.; Taylor, S. J. C., Recent Trends in Enzyme Immobilization-Concepts for Expanding the Biocatalysis Toolbox. *Molecules* **2021,** *26*, 2822-2835.
285. Robinson, P. K., Enzymes: principles and biotechnological applications. *Essays Biochem.* **2015,** *59*, 1-41.
286. Breslow, R., Biomimetic Chemistry and Artificial Enzymes: Catalysis by Design. *Acc. Chem. Res.* **1995,** *28*, 146-153.
287. Jiang, L.; Liu, Z.; Liang, Z.; Gao, Y., An artificial aspartic proteinase system. *Bioorg. Med. Chem.* **2005,** *13*, 3673-3680.
288. Dydio, P.; Dzik, W. I.; Lutz, M.; de Bruin, B.; Reek, J. N., Remote supramolecular control of catalyst selectivity in the hydroformylation of alkenes. *Angew. Chem. Int. Ed.* **2011,** *50*, 396-400.
289. Huang, X.; Yin, Y.; Jiang, X.; Tang, Y.; Xu, J.; Liu, J.; Shen, J., Construction of smart glutathione peroxidase mimic based on hydrophilic block copolymer with temperature responsive activity. *Macromol. Biosci.* **2009,** *9*, 1202-1210.
290. Schmittel, M.; De, S.; Pramanik, S., Reversible ON/OFF nanoswitch for organocatalysis: mimicking the locking and unlocking operation of CaMKII. *Angew. Chem. Int. Ed.* **2012,** *51* (16), 3832-3836.
291. Kuwabara, J.; Stern, C. L.; Mirkin, C. A., A coordination chemistry approach to a multieffector enzyme mimic. *J. Am. Chem. Soc.* **2007,** *129*, 10074-10075.
292. Murakami, Y.; Kikuchi, J.-i.; Hisaeda, Y.; Hayashida, O., Artificial Enzymes. *Chem. Rev.* **1996,** *96*, 721-758.

293. Chen, Y.; Yang, Y.; Orr, A. A.; Makam, P.; Redko, B.; Haimov, E.; Wang, Y.; Shimon, L. J. W.; Rencus-Lazar, S.; Ju, M.; Tamamis, P.; Dong, H.; Gazit, E., Self-Assembled Peptide Nano-Superstructure towards Enzyme Mimicking Hydrolysis. *Angew. Chem. Int. Ed.* **2021,** *60*, 17164-17170.
294. List, B.; Lerner, R. A.; Barbas, C. F., Proline-Catalyzed Direct Asymmetric Aldol Reactions. *J. Am. Chem. Soc.* **2000,** *122*, 2395-2396.
295. Zhu, M.; Wang, M.; Qi, W.; Su, R.; He, Z., Constructing peptide-based artificial hydrolases with customized selectivity. *J. Mater. Chem. B* **2019,** *7*, 3804-3810.
296. Davie, E. A.; Mennen, S. M.; Xu, Y.; Miller, S. J., Asymmetric catalysis mediated by synthetic peptides. *Chem. Rev.* **2007,** *107*, 5759-5812.
297. Zozulia, O.; Dolan, M. A.; Korendovych, I. V., Catalytic peptide assemblies. *Chem. Soc. Rev.* **2018,** *47*, 3621-3639.
298. Miller, S. J., In search of peptide-based catalysts for asymmetric organic synthesis. *Acc. Chem. Res.* **2004,** *37*, 601-610.
299. Wang, Q.; Yang, Z.; Zhang, X.; Xiao, X.; Chang, C. K.; Xu, B., A supramolecular-hydrogel-encapsulated hemin as an artificial enzyme to mimic peroxidase. *Angew. Chem. Int. Ed.* **2007,** *46*, 4285-4289.
300. Singh, N.; Conte, M. P.; Ulijn, R. V.; Miravet, J. F.; Escuder, B., Insight into the esterase like activity demonstrated by an imidazole appended self-assembling hydrogelator. *Chem. Commun.* **2015,** *51*, 13213-13216.
301. Guler, M. O.; Stupp, S. I., A self-assembled nanofiber catalyst for ester hydrolysis. *J. Am. Chem. Soc.* **2007,** *129*, 12082-12083.
302. Wong, Y.-M.; Masunaga, H.; Chuah, J.-A.; Sudesh, K.; Numata, K., Enzyme-Mimic Peptide Assembly To Achieve Amidolytic Activity. *Biomacromolecules* **2016,** *17*, 3375-3385.
303. Hamley, I. W., Biocatalysts Based on Peptide and Peptide Conjugate Nanostructures. *Biomacromolecules* **2021,** *22*, 1835-1855.
304. Neurath, H., Proteolytic enzymes, past and future. *Proc. Natl. Acad. Sci.* **1999,** *96*, 10962-10963.
305. Kirk, O.; Borchert, T. V.; Fuglsang, C. C., Industrial enzyme applications. *Curr. Opin. Biotechnol.* **2002,** *13*, 345-351.
306. Nothling, M. D.; Xiao, Z.; Hill, N. S.; Blyth, M. T.; Bhaskaran, A.; Sani, M.-A.; Espinosa-Gomez, A.; Ngov, K.; White, J.; Buscher, T.; Separovic, F.; O'Mara, M. L.; Coote, M. L.; Connal, L. A., A multifunctional surfactant catalyst inspired by hydrolases. *Sci. Adv.* **2020,** *6*, eaaz0404.
307. Hu, L.; Zhao, Y., Molecularly imprinted artificial esterases with highly specific active sites and precisely installed catalytic groups. *Org. Biomol. Chem.* **2018,** *16*, 5580-5584.
308. Buller, A. R.; Townsend, C. A., Intrinsic evolutionary constraints on protease structure, enzyme acylation, and the identity of the catalytic triad. *Proc. Natl. Acad. Sci.* **2013,** *110*, E653-E661.
309. Carter, P.; Wells, J. A., Dissecting the catalytic triad of a serine protease. *Nature* **1988,** *332*, 564-568.
310. Ekici, O. D.; Paetzel, M.; Dalbey, R. E., Unconventional serine proteases: variations on the catalytic Ser/His/Asp triad configuration. *Protein Sci.* **2008,** *17*, 2023-2037.
311. Wieczorek, R.; Adamala, K.; Gasperi, T.; Polticelli, F.; Stano, P., Small and Random Peptides: An Unexplored Reservoir of Potentially Functional Primitive Organocatalysts. The Case of Seryl-Histidine. *Life* **2017,** *7*, 19-42.
312. Plastina, P.; Fazio, A.; Attya, M.; Sindona, G.; Gabriele, B., Synthesis of analogues of ochratoxin A. *Nat. Prod. Res.* **2012,** *26*, 1799-1805.

313. Biraboneye, A. C.; Madonna, S.; Laras, Y.; Krantic, S.; Maher, P.; Kraus, J.-L., Potential Neuroprotective Drugs in Cerebral Ischemia: New Saturated and Polyunsaturated Lipids Coupled to Hydrophilic Moieties: Synthesis and Biological Activity. *J. Med. Chem.* **2009,** *52*, 4358-4369.
314. Zhang, P.; Zhou, Y.; Han, X.; Xu, J.; Liu, H., N-Heterocyclic Carbene Catalyzed Enantioselective [3 + 2] Dearomatizing Annulation of Saturated Carboxylic Esters with N-Iminoisoquinolinium Ylides. *J. Org. Chem.* **2018,** *83*, 3879-3888.
315. Webster, K. L.; Maude, A. B.; O'Donnell, M. E.; Mehrotra, A. P.; Gani, D., Design and preparation of serine–threonine protein phosphatase inhibitors based upon the nodularin and microcystin toxin structures. Part 3. *J. Chem. Soc., Perkin Trans. 1* **2001**, 1673-1695.
316. Oliveira, L.; Karim, B.; Picco, A.; Capeletti, L.; Gonçalves, K.; Santos, J.; Kobarg, J.; Cardoso, M., Tailored Silica Nanoparticles Surface to Increase Drug Load and Enhance Bactericidal Response. *J. Braz. Chem. Soc.* **2017,** *28*, 1715-1724.
317. Schirowski, M.; Hauke, F.; Hirsch, A., Controlling the Degree of Functionalization: In-Depth Quantification and Side-Product Analysis of Diazonium Chemistry on SWCNTs. *Chem. Eur. J.* **2019,** *25*, 12761-12768.
318. Das, S.; Das, D., Rational Design of Peptide-based Smart Hydrogels for Therapeutic Applications. *Front Chem* **2021,** *9*, 770102-770131.
319. Das, D.; Das, P. K., Improving the Lipase Activity Profile in Cationic Water-in-Oil Microemulsions of Hydroxylated Surfactants. *Langmuir* **2003,** *19*, 9114-9119.
320. Das, D.; Dasgupta, A.; Roy, S.; Mitra, R. N.; Debnath, S.; Das, P. K., Water Gelation of an Amino Acid-Based Amphiphile. *Chem. Eur. J.* **2006,** *12*, 5068-5074.
321. Almeida, V. M.; Marana, S. R., Optimum temperature may be a misleading parameter in enzyme characterization and application. *PloS one* **2019,** *14*, e0212977.
322. Peterson, M. E.; Daniel, R. M.; Danson, M. J.; Eisenthal, R., The dependence of enzyme activity on temperature: determination and validation of parameters. *Biochem. J.* **2007,** *402*, 331-337.
323. Mondal, J. H.; Ahmed, S.; Das, D., Physicochemical Analysis of Mixed Micelles of a Viologen Surfactant: Extended to Water-in-Oil (w/o) Microemulsion and Cucurbit[8]uril-Assisted Vesicle Formation. *Langmuir* **2014,** *30*, 8290-8299.
324. Dyson, P. J.; Jessop, P. G., Solvent effects in catalysis: rational improvements of catalysts via manipulation of solvent interactions. *Catal. Sci. Technol.* **2016,** *6*, 3302-3316.
325. Asemave, K.; Anhwange, B.; Ahile, U., Hydrolysis of Fatty Esters in DCM/Methanol. *Fed. Univ. Wukari Trends Sci. Technol. J.* **2017,** *2*, 521-524.
326. De Vylder, A.; Lauwaert, J.; Esquivel, D.; Poelman, D.; De Clercq, J.; Van Der Voort, P.; Thybaut, J. W., The role of water in the reusability of aminated silica catalysts for aldol reactions. *J. Catal.* **2018,** *361*, 51-61.
327. Lechner, C. C.; Becker, C. F., Immobilising proteins on silica with site-specifically attached modified silaffin peptides. *Biomater. Sci.* **2015,** *3*, 288-297.
328. Yu, M.; Gu, Z.; Ottewell, T.; Yu, C., Silica-based nanoparticles for therapeutic protein delivery. *J. Mater. Chem. B* **2017,** *5*, 3241-3252.
329. Oviedo, M. J.; Quester, K.; Hirata, G. A.; Vazquez-Duhalt, R., Determination of conjugated protein on nanoparticles by an adaptation of the Coomassie blue dye method. *MethodsX* **2019,** *6*, 2134-2140.
330. Li, J.; Liu, F.; Shao, Q.; Min, Y.; Costa, M.; Yeow, E. K.; Xing, B., Enzyme-responsive cell-penetrating peptide conjugated mesoporous silica quantum dot nanocarriers for controlled release of nucleus-targeted drug molecules and real-time intracellular fluorescence imaging of tumor cells. *Adv. Healthc. Mater.* **2014,** *3*, 1230-1239.

331. Maeda, Y.; Saito, K.; Akamatsu, N.; Chiba, Y.; Ohno, S.; Okui, Y.; Yamada, M.; Hasegawa, T.; Kako, M.; Akasaka, T., Analysis of Functionalization Degree of Single-Walled Carbon Nanotubes Having Various Substituents. *J. Am. Chem. Soc.* **2012,** *134*, 18101-18108.
332. Krishnan, S.; Chatterjee, S.; Solanki, A.; Guha, N.; Singh, M. K.; Gupta, A. K.; Rai, D. K., Aminotetrazole-Functionalized SiO2 Coated MgO Nanoparticle Composites for Removal of Acid Fuchsin Dye and Detection of Heavy Metal Ions. *ACS Appl. Nano Mater.* **2020,** *3*, 11203-11216.
333. Roy, S.; Das, D.; Dasgupta, A.; Mitra, R. N.; Das, P. K., Amino Acid Based Cationic Surfactants in Aqueous Solution: Physicochemical Study and Application of Supramolecular Chirality in Ketone Reduction. *Langmuir* **2005,** *21*, 10398-10404.
334. Das, D.; Roy, S.; Das, P. K., Efficient and Simple NaBH4 Reduction of Esters at Cationic Micellar Surface. *Org. Lett.* **2004,** *6*, 4133-4136.

7. CHARACTERIZATION FILES

Chapter 2:

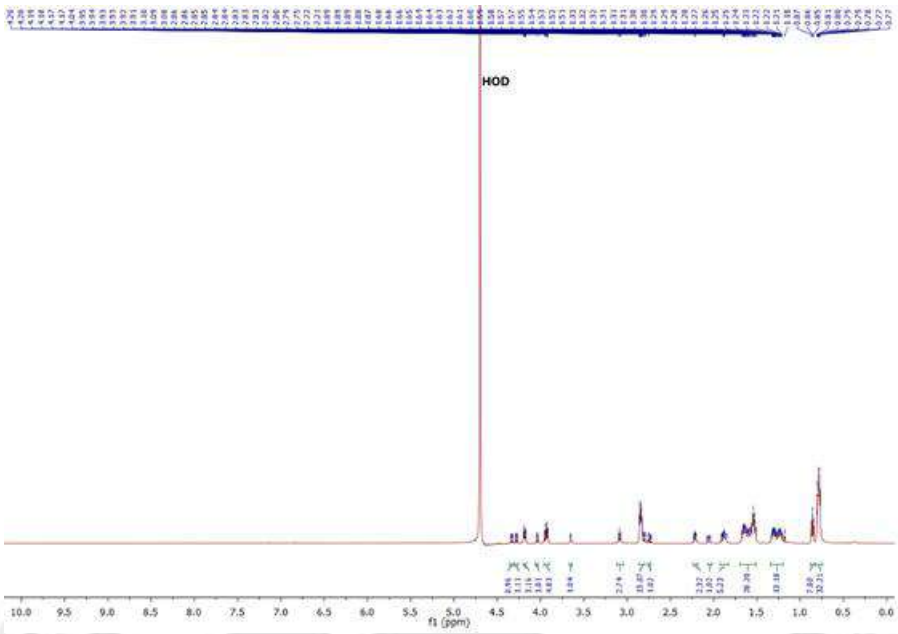

Figure 7.1 ^{1}H NMR spectra of **PA-2.1** in D_2O.

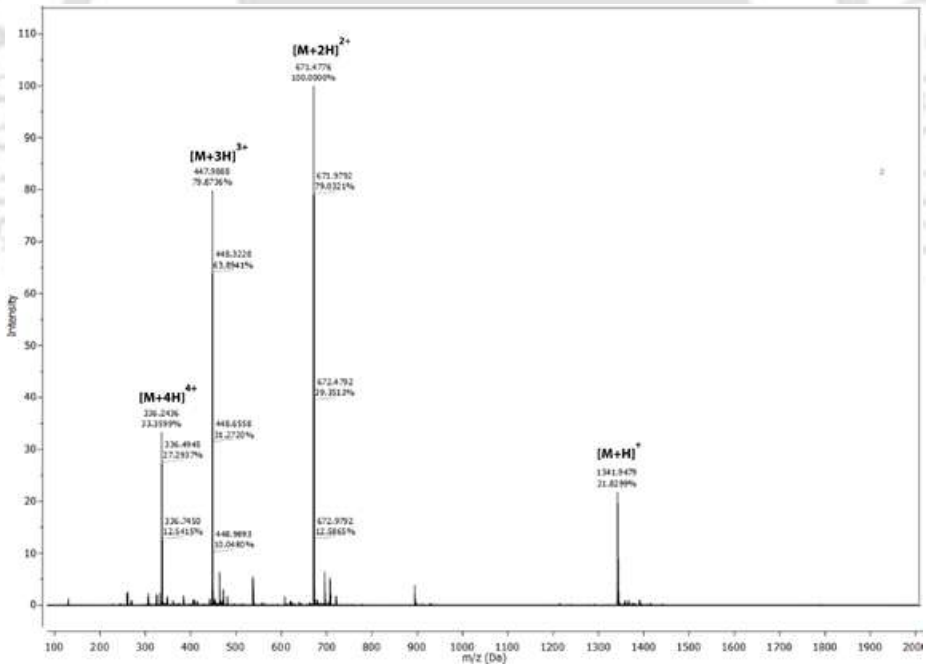

Figure 7.2 ESI-MS of **PA-2.1**.

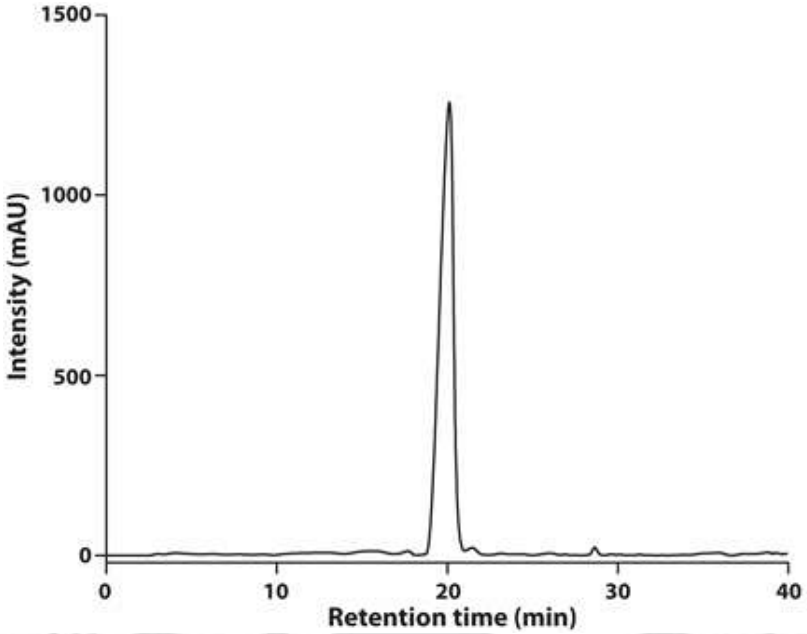

Figure 7.3 Analytical HPLC chromatogram of **PA-2.1**.

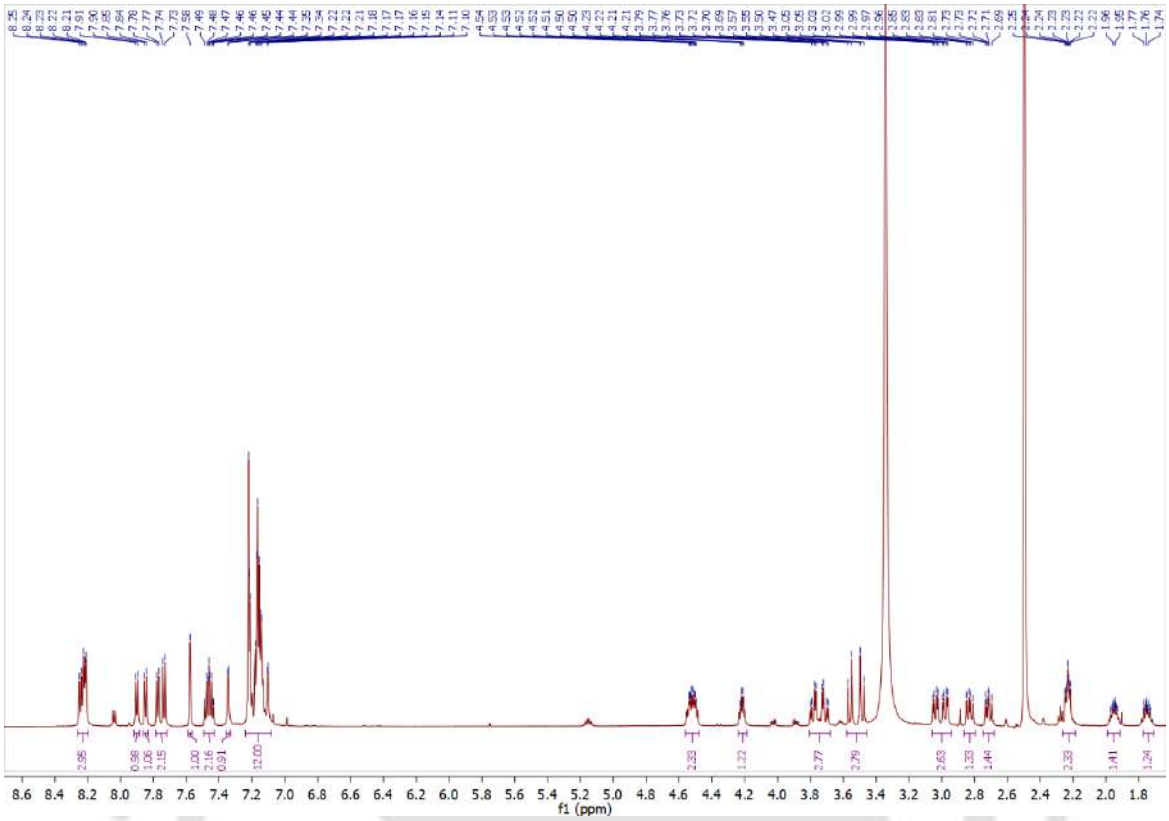

Figure 7.4 ^{1}H NMR spectrum of **Pep-A** in DMSO-d_6.

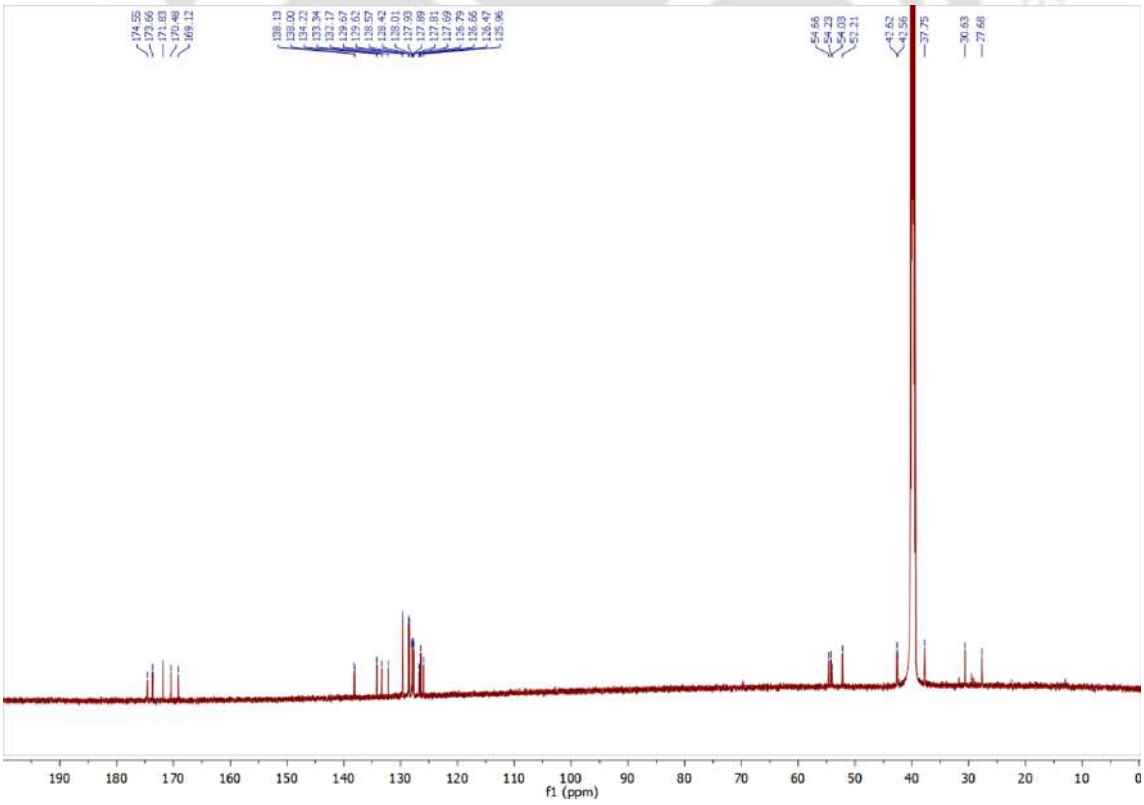

Figure 7.5 ^{13}C NMR spectrum of **Pep-A** in DMSO-d_6.

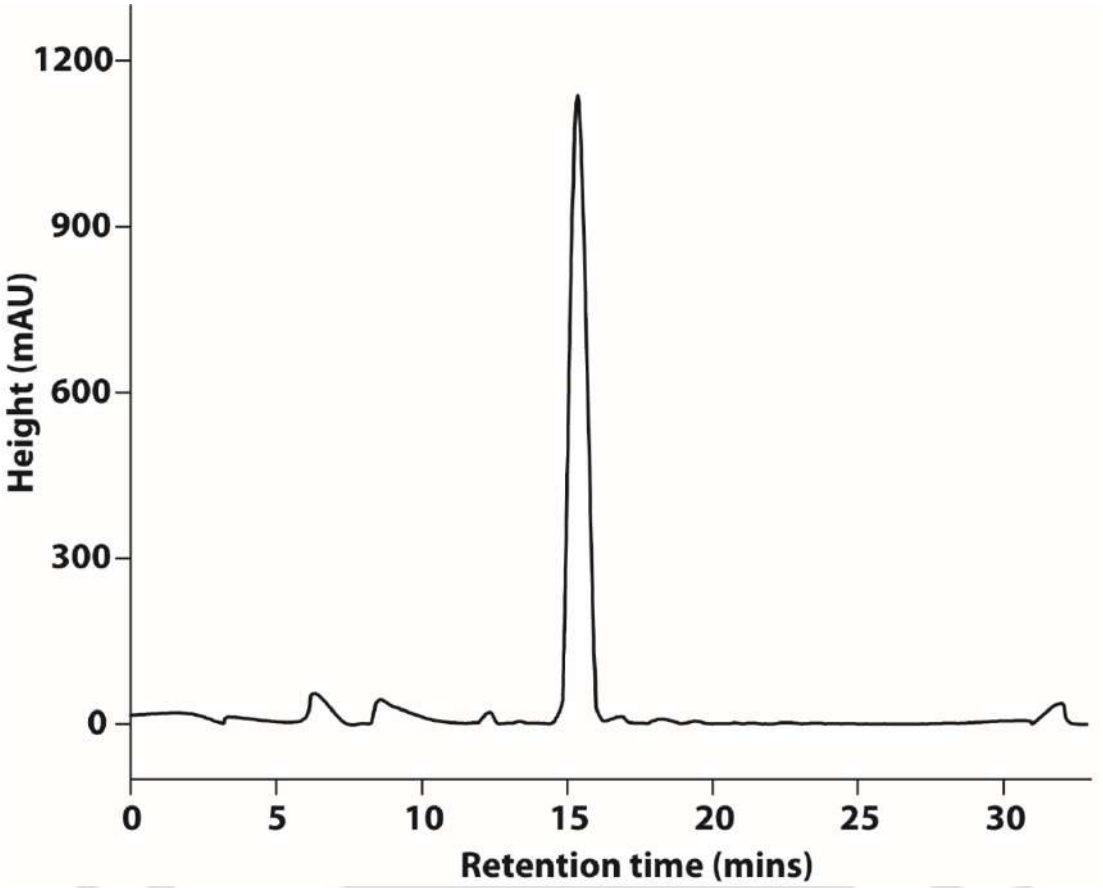

Figure 7.6 Analytical HPLC chromatogram of **Pep-A.**

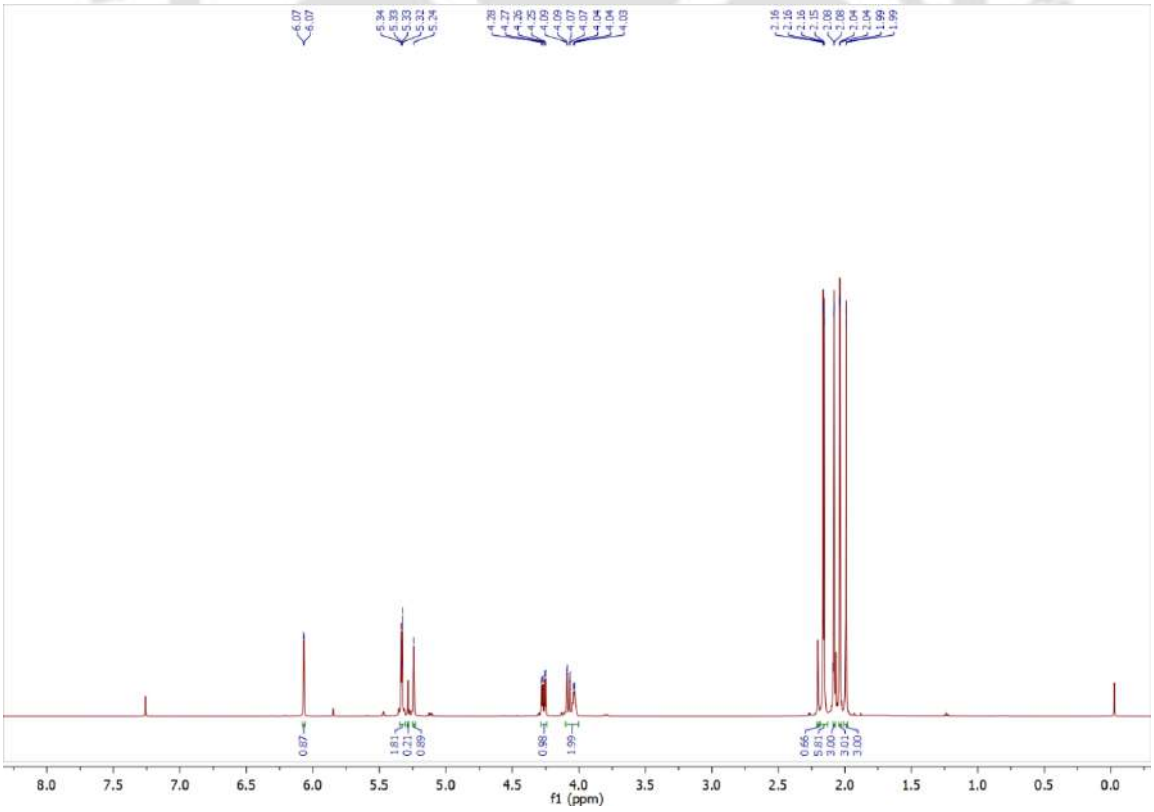

Figure 7.7 ^{1}H NMR spectrum of $Man(OAc)_5$ in $CDCl_3$.

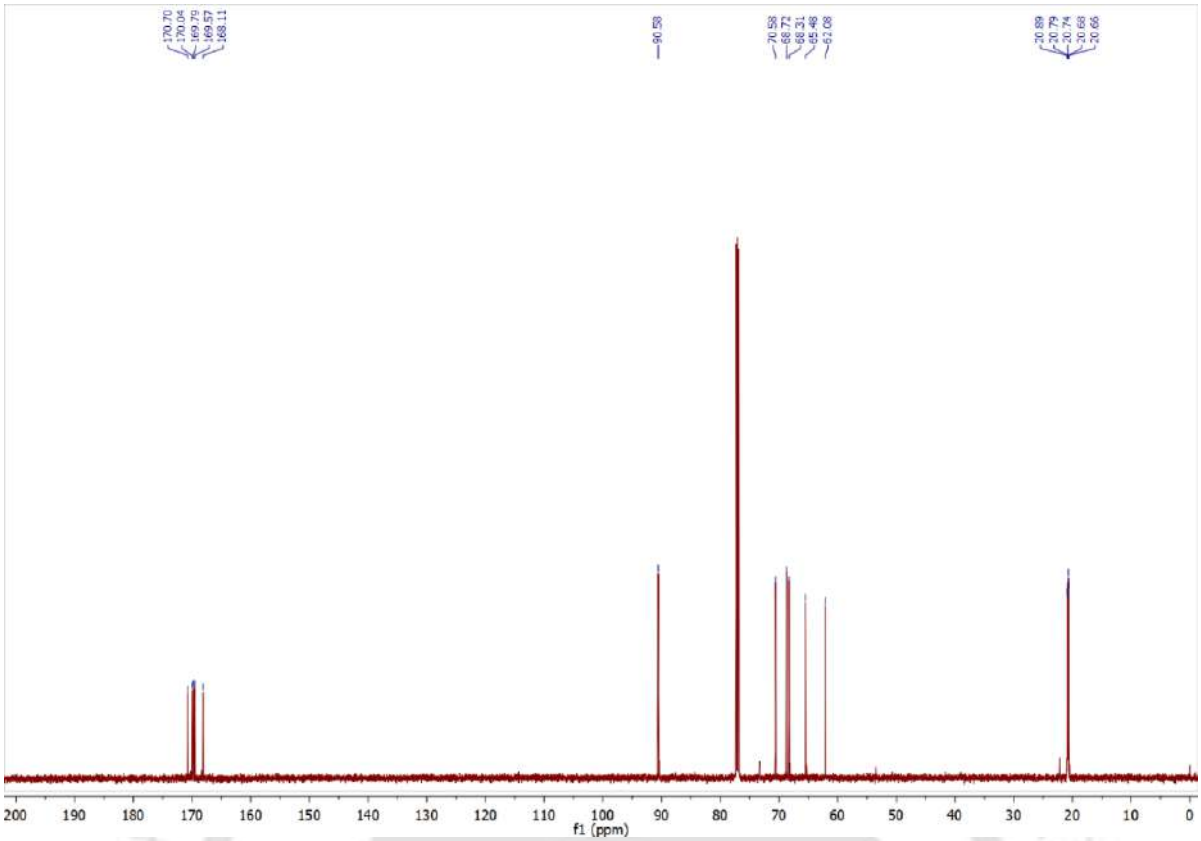

Figure 7.8 ^{13}C NMR spectrum of $Man(OAc)_5$ in $CDCl_3$.

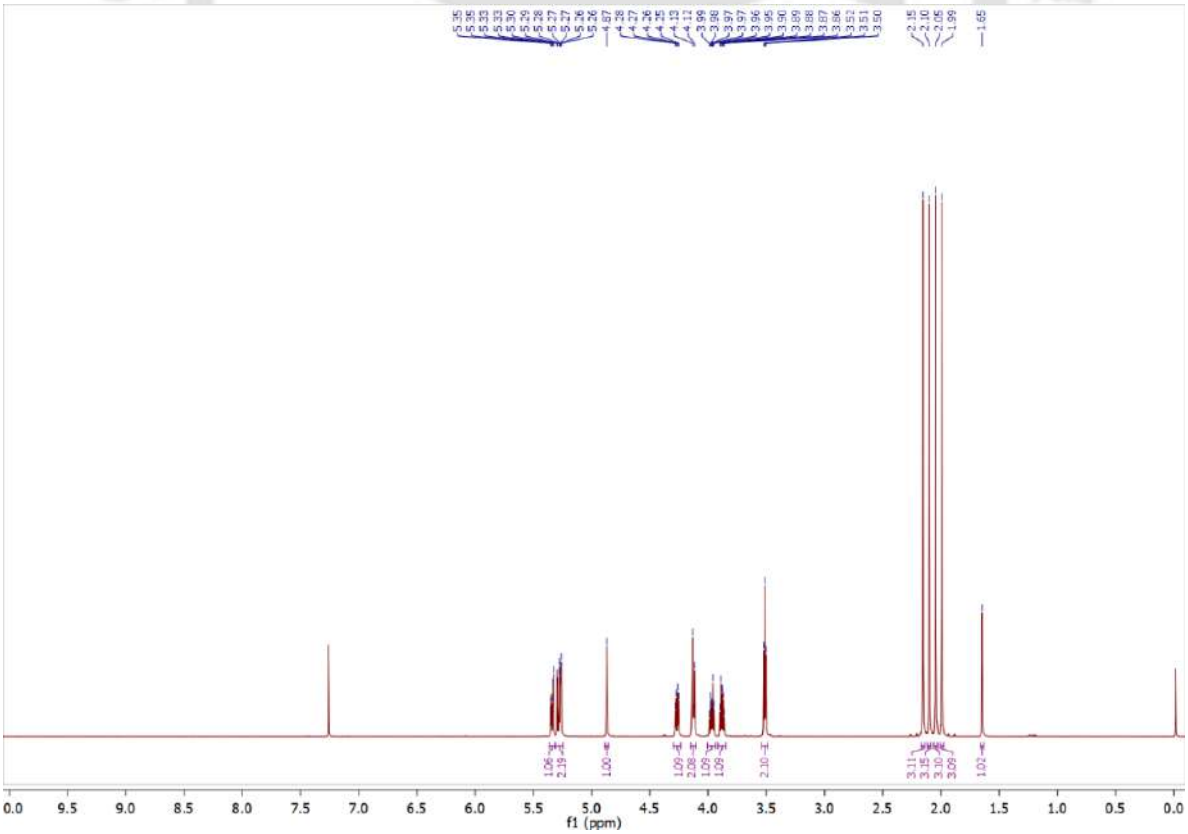

Figure 7.9 ^{1}H NMR spectrum of $Man(OAc)_4$ C_2H_4Br in $CDCl_3$.

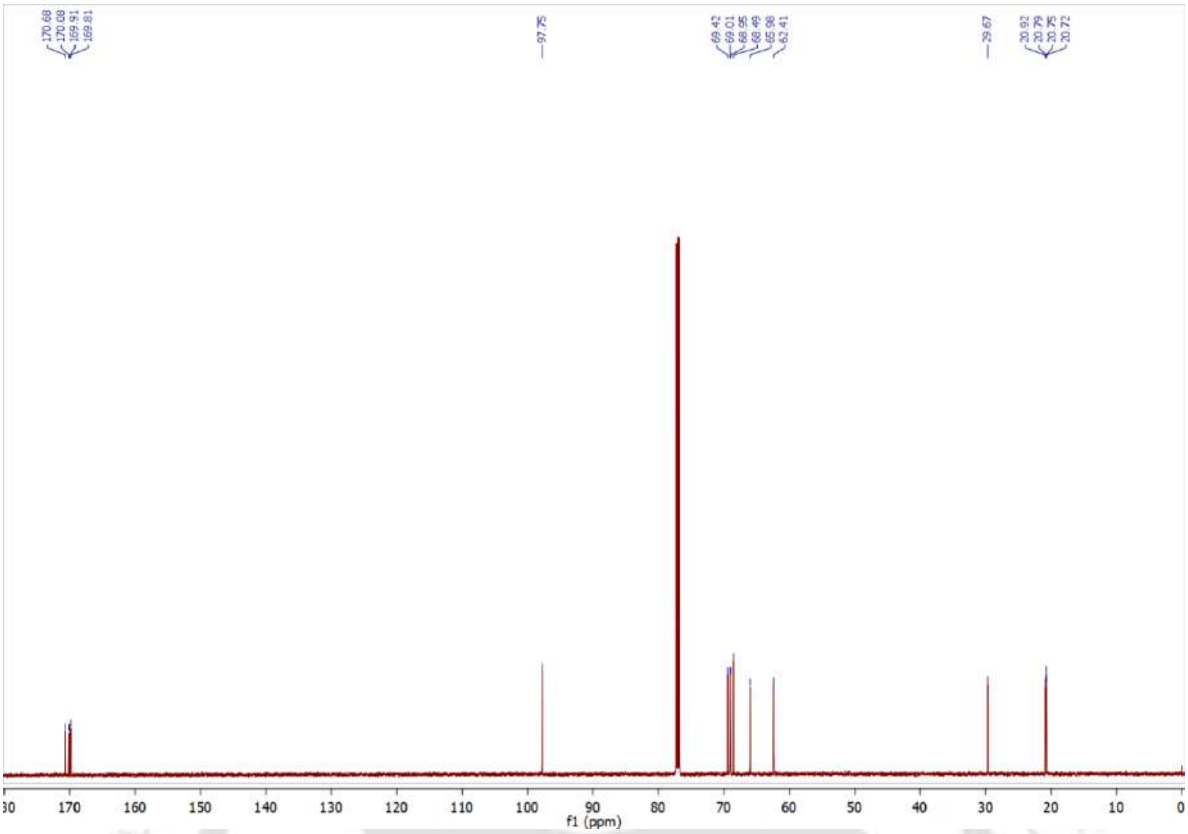

Figure 7.10 ^{13}C NMR spectrum of Man(OAc)$_4$ C_2H_4Br in $CDCl_3$.

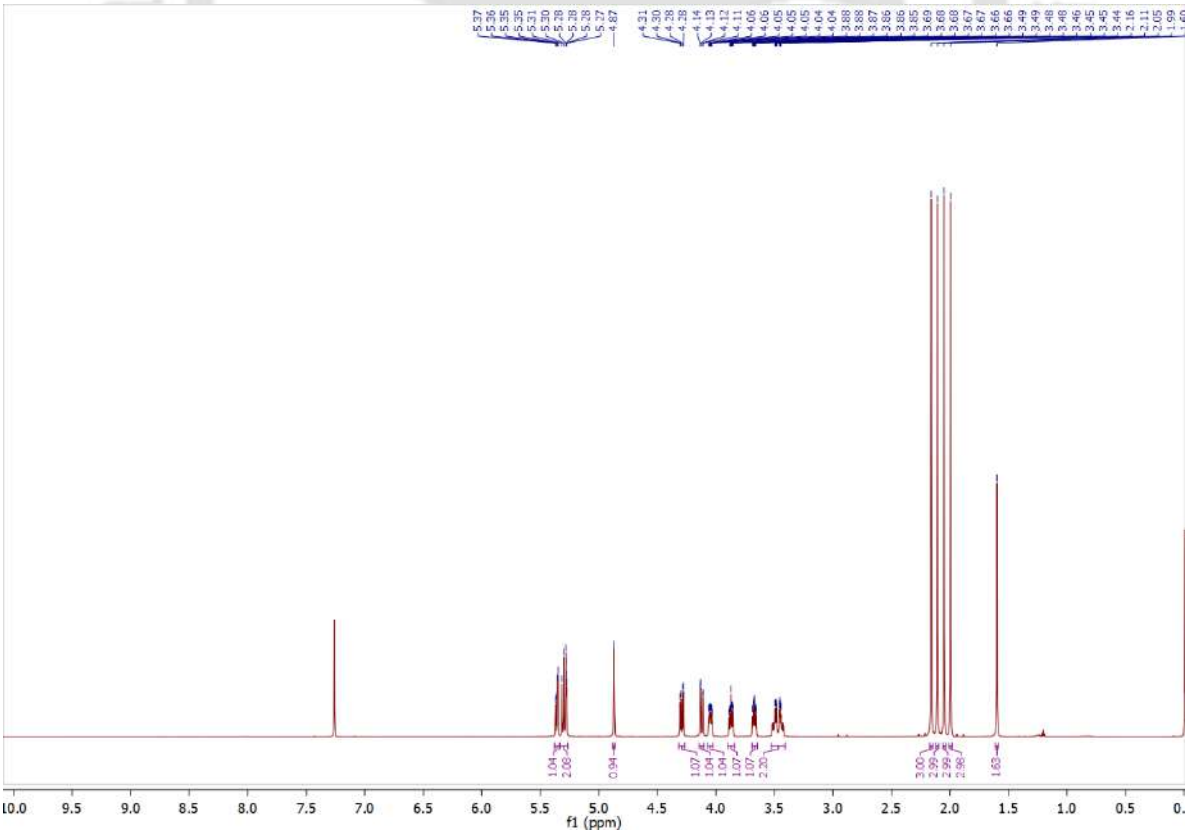

Figure 7.11 ^{1}H NMR spectrum of Man(OAc)$_4C_2H_4N_3$ in $CDCl_3$.

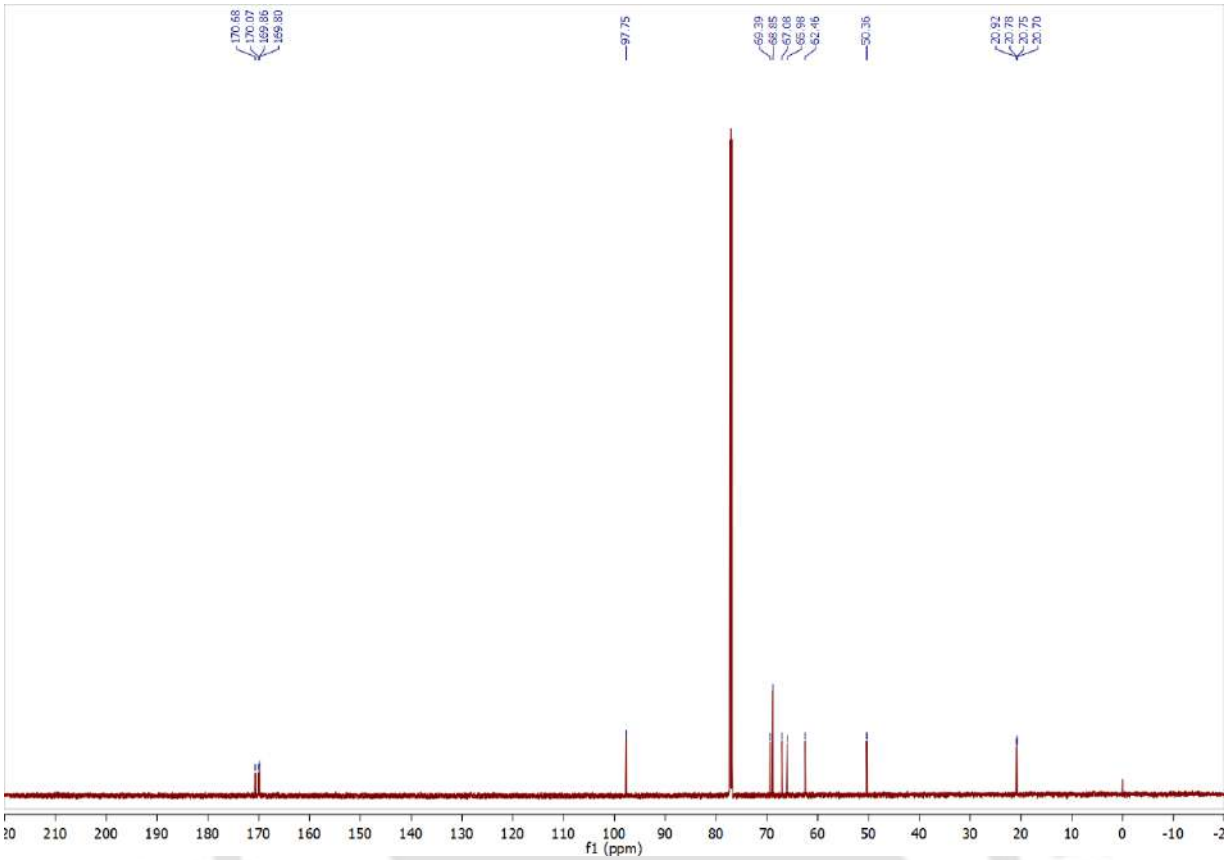

Figure 7.12 ^{13}C NMR spectrum of $Man(OAc)_4C_2H_4N_3$ in $CDCl_3$.

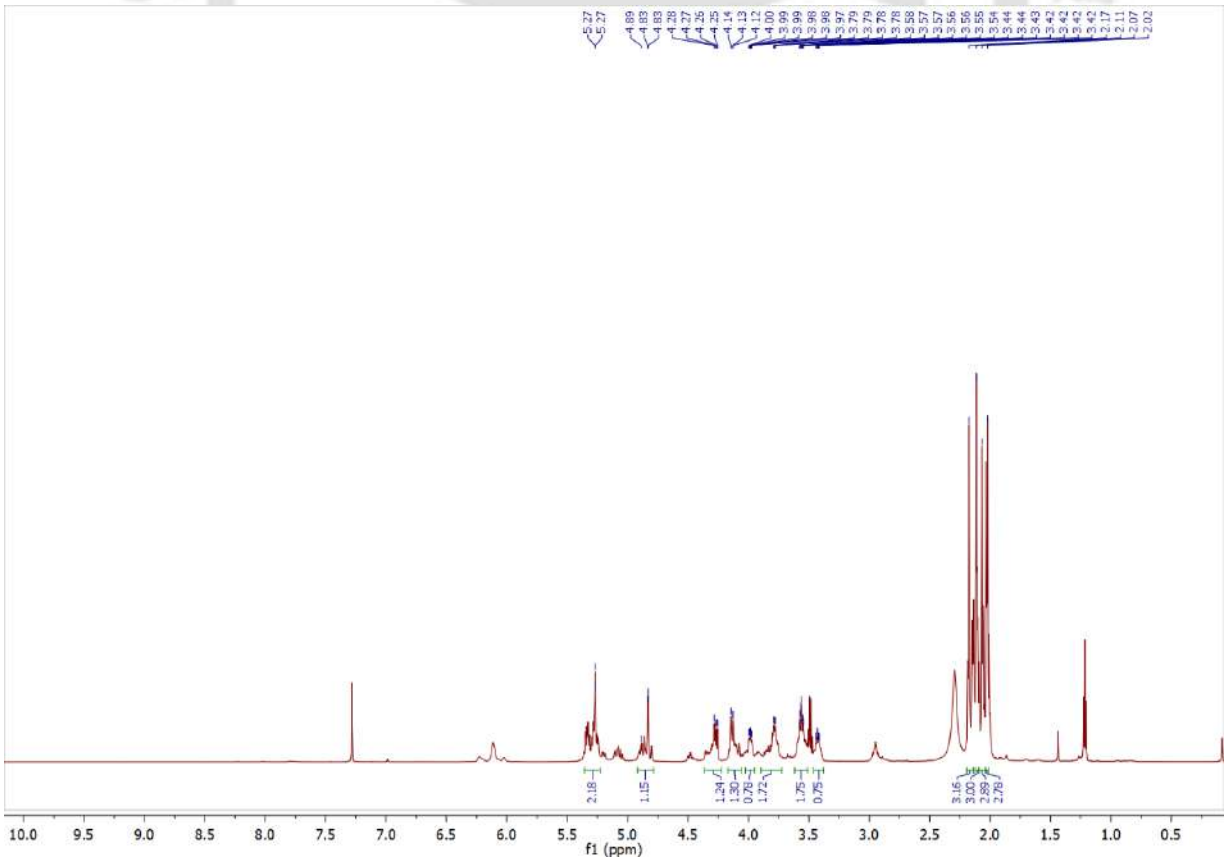

Figure 7.13 ^{1}H NMR spectrum of $Man(OAc)_4C_2H_4NH_2$ in $CDCl_3$.

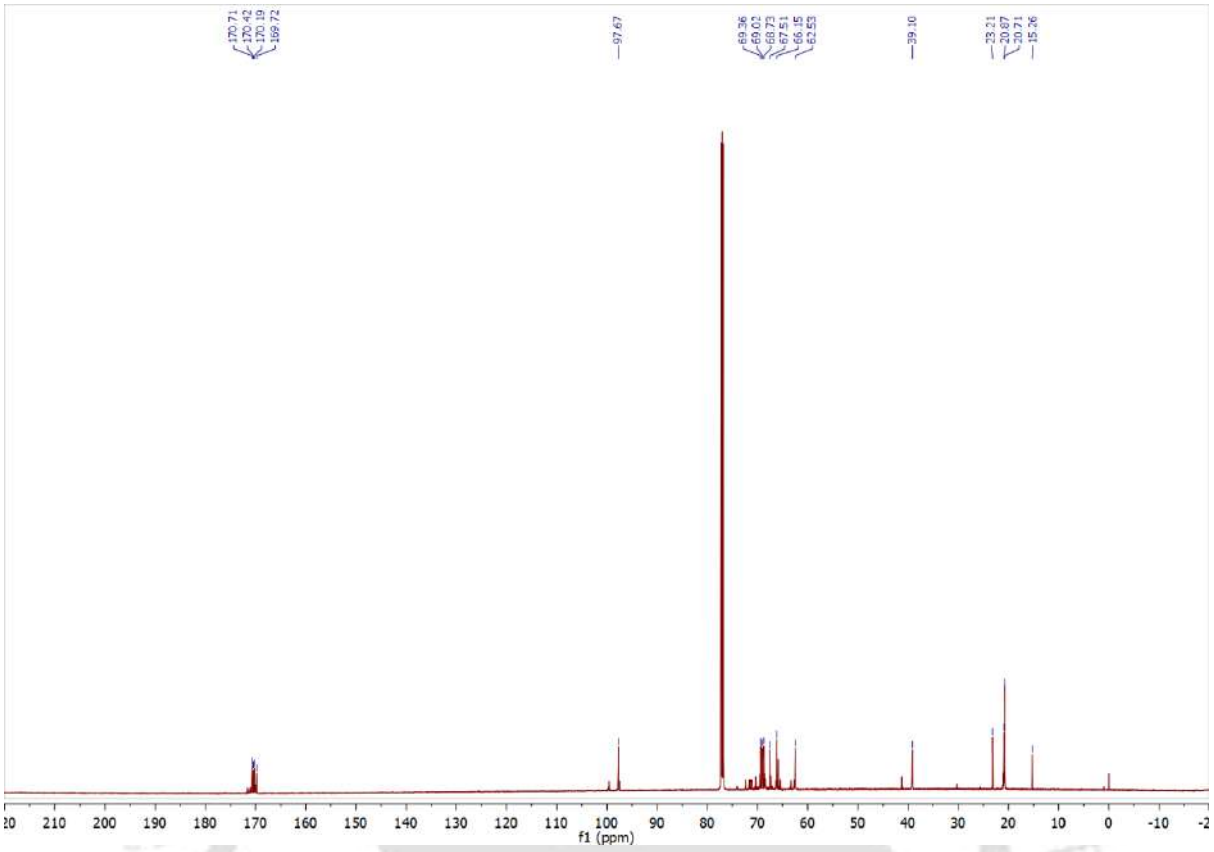

Figure 7.14 ^{13}C NMR spectrum of $Man(OAc)_4C_2H_4NH_2$ in $CDCl_3$.

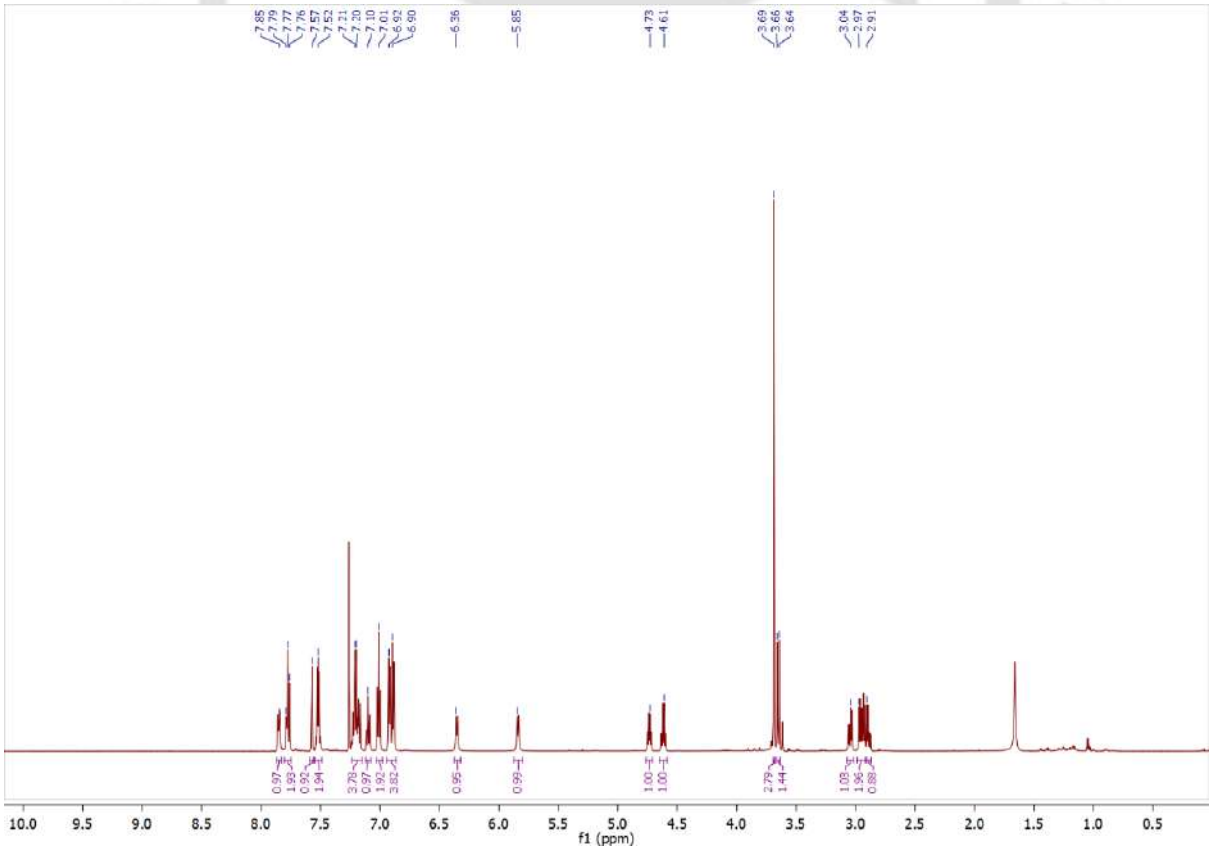

Figure 7.15 ^{1}H NMR spectrum of Nap-FF-OH in $CDCl_3$.

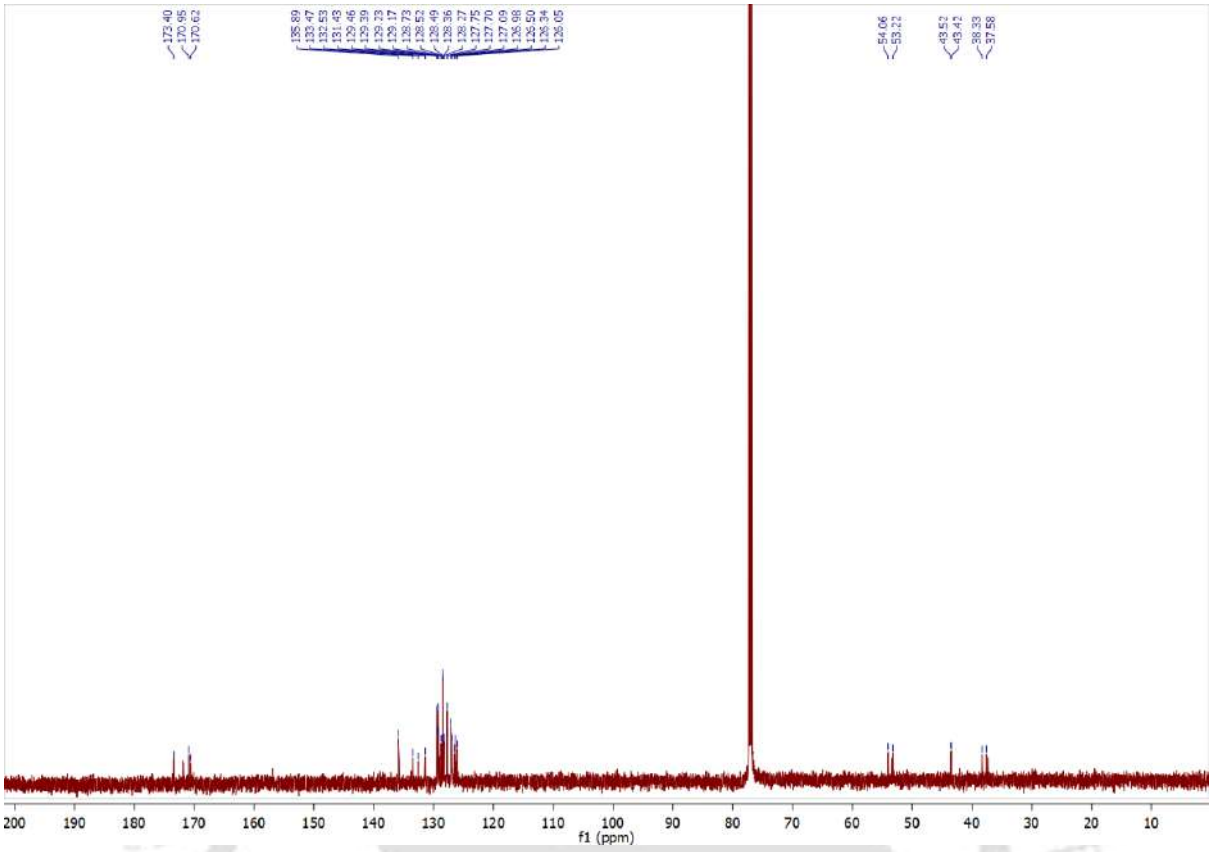

Figure 7.16 ^{13}C NMR spectrum of Nap-FF-OH in $CDCl_3$.

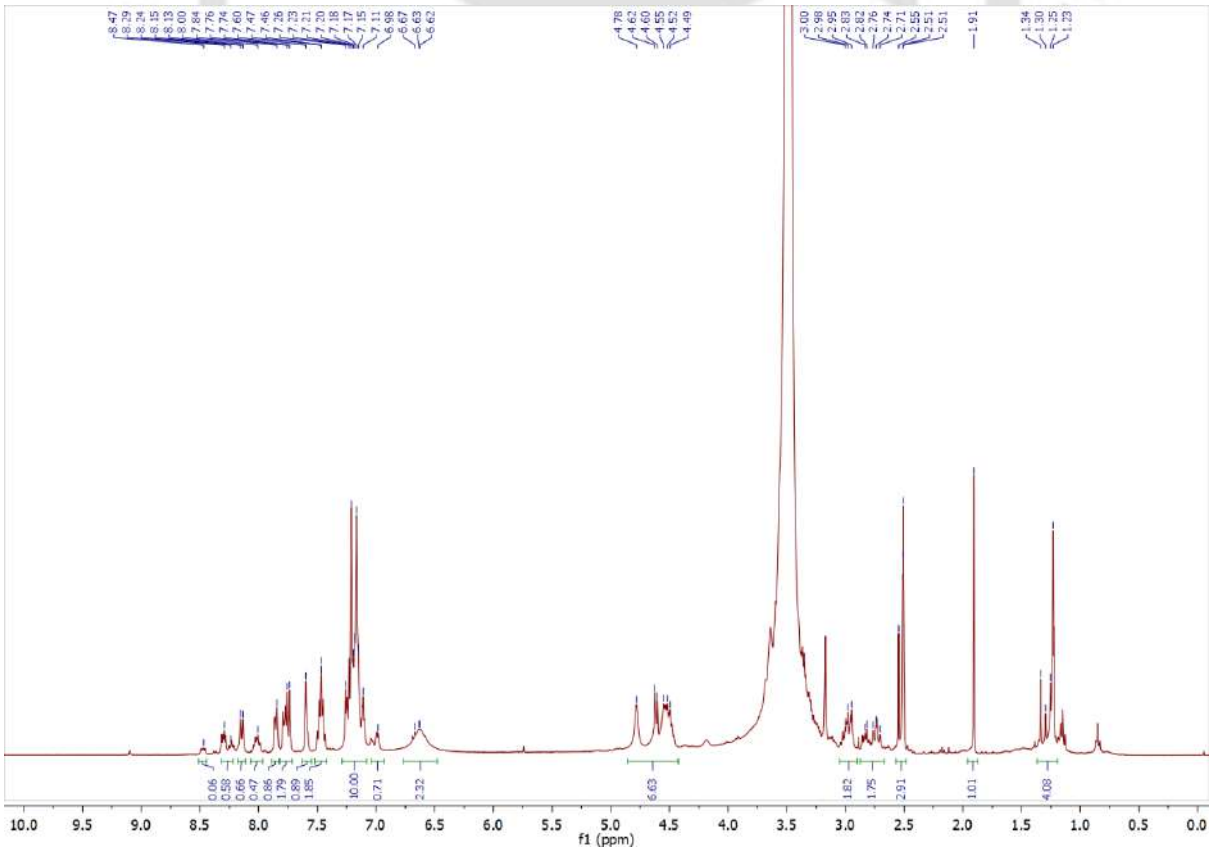

Figure 7.17 ^{1}H NMR spectrum of **Pep-B** in DMSO-d_6.

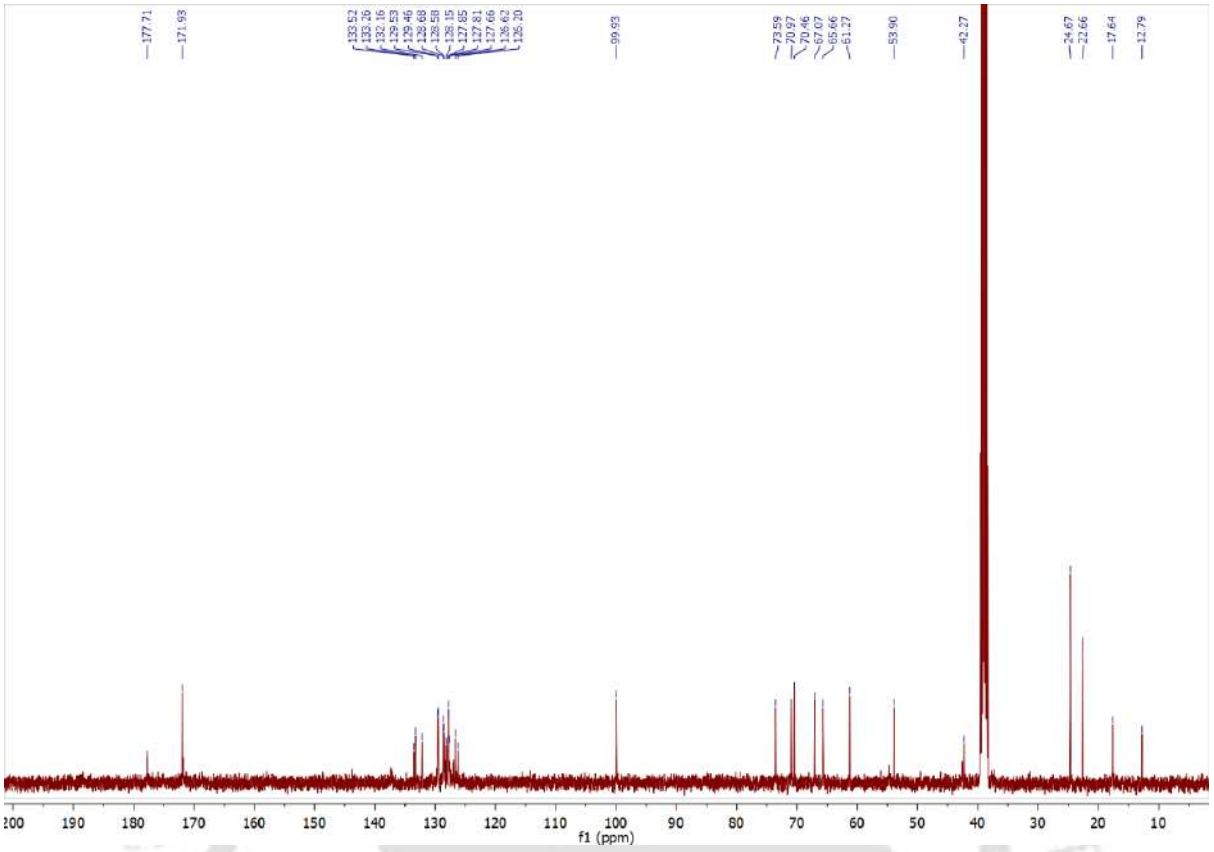

Figure 7.18 ^{13}C NMR spectrum of **Pep-B** in DMSO-d_6.

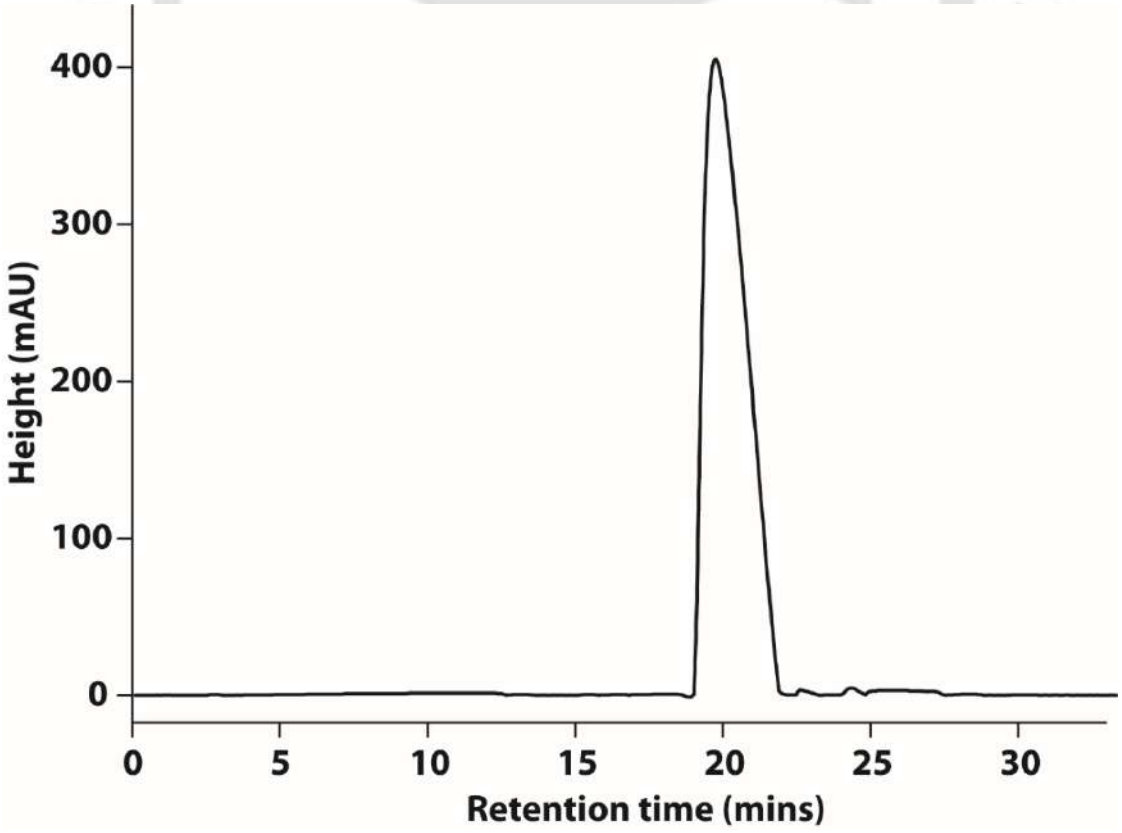

Figure 7.19 Analytical HPLC chromatogram of **Pep-B**.

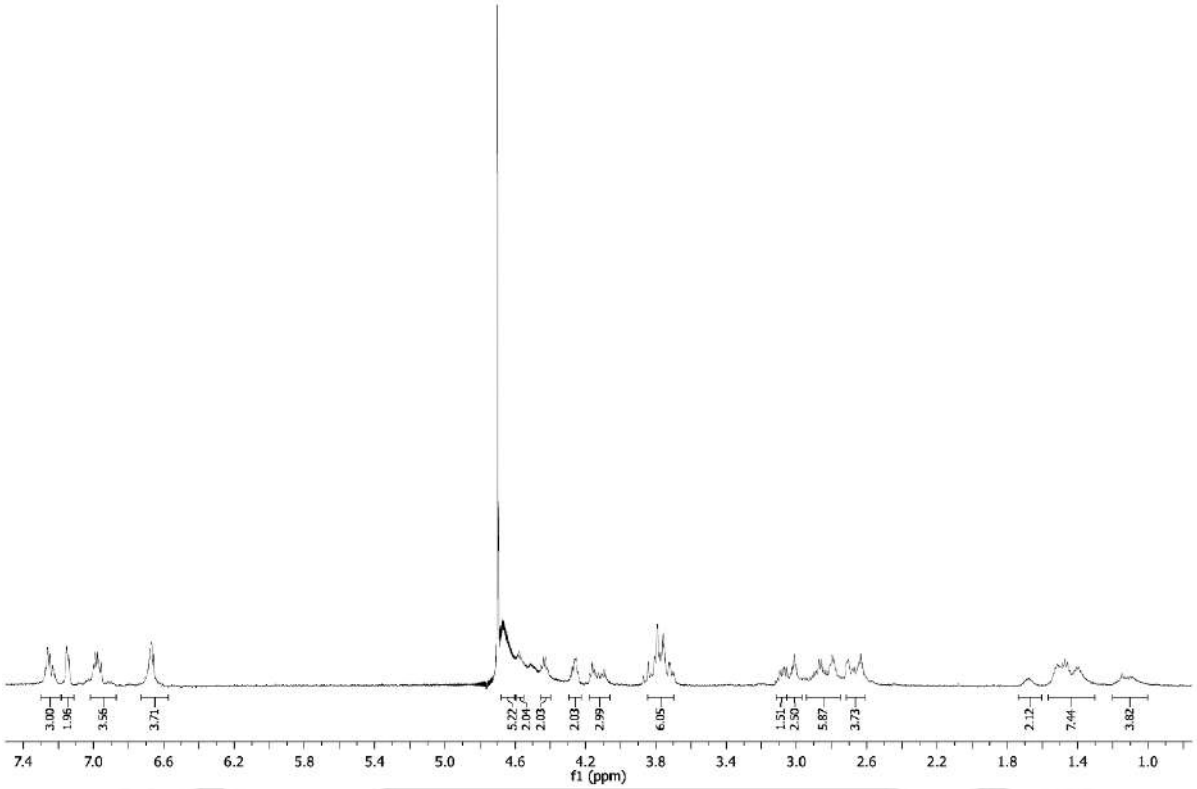

Figure 7.20 ^{1}H NMR spectrum of monomer **4.1**.

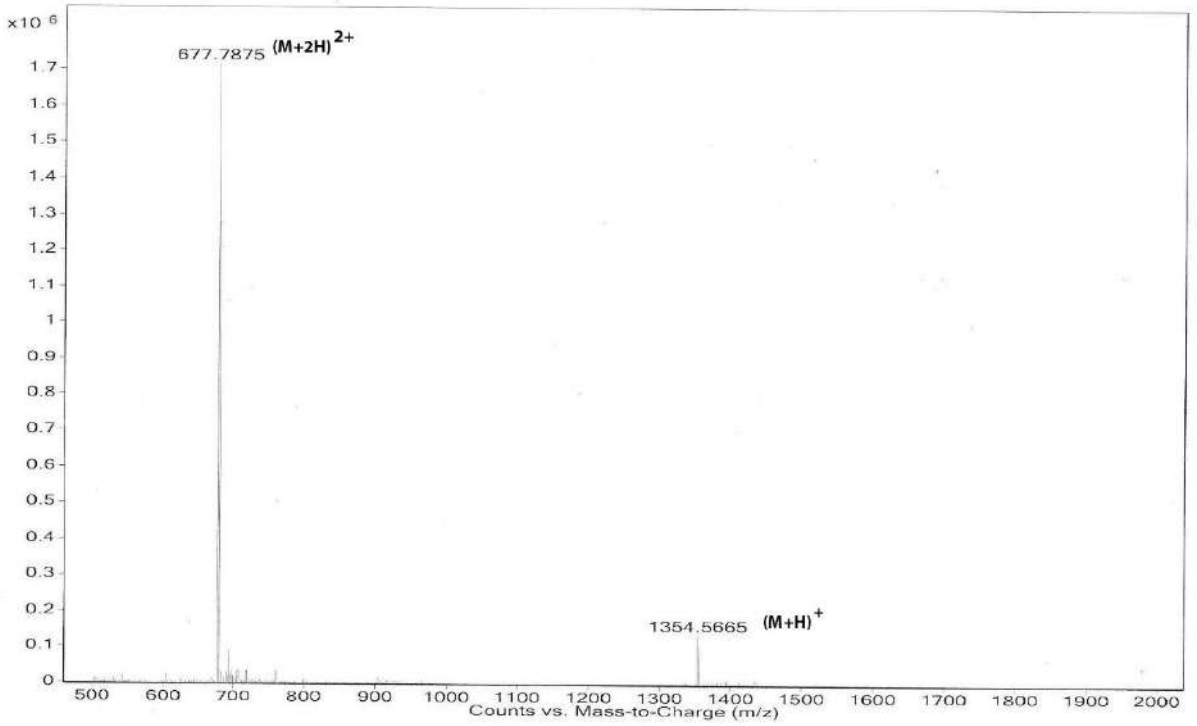

Figure 7.21 ESI-MS of **4.1**.

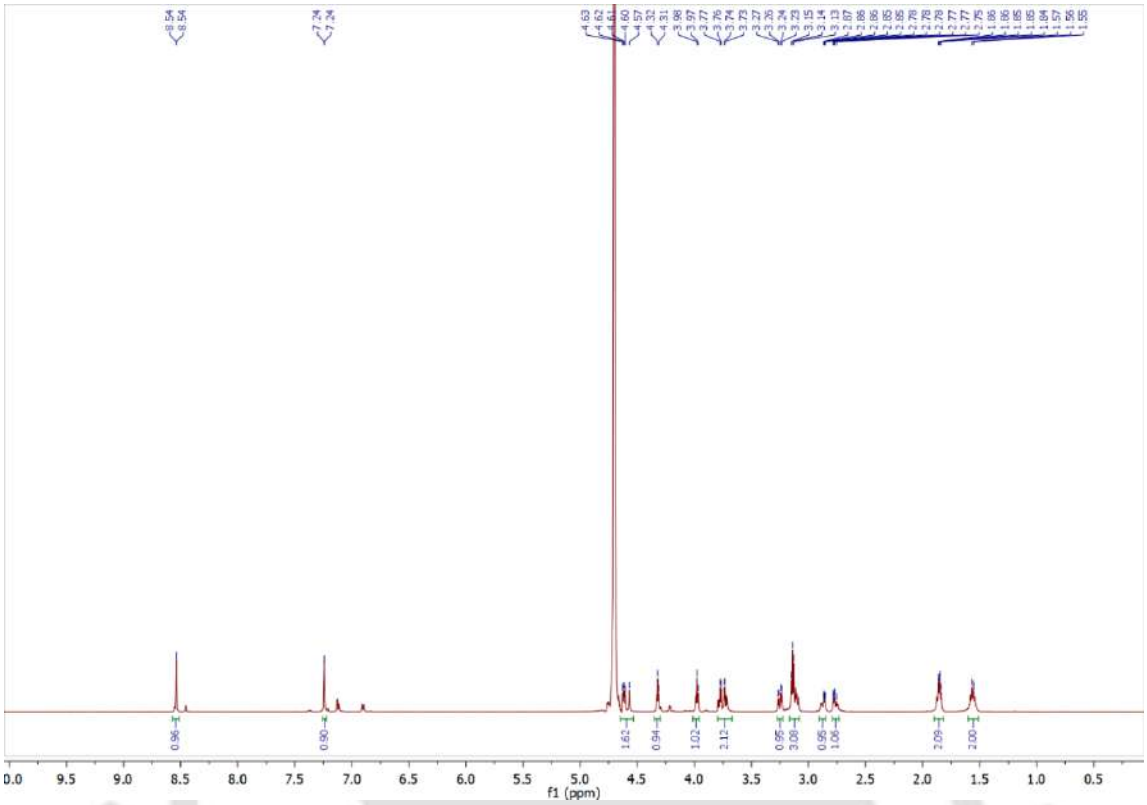

Figure 7.22 ^{1}H NMR spectra of PA **5.1** in D_2O.

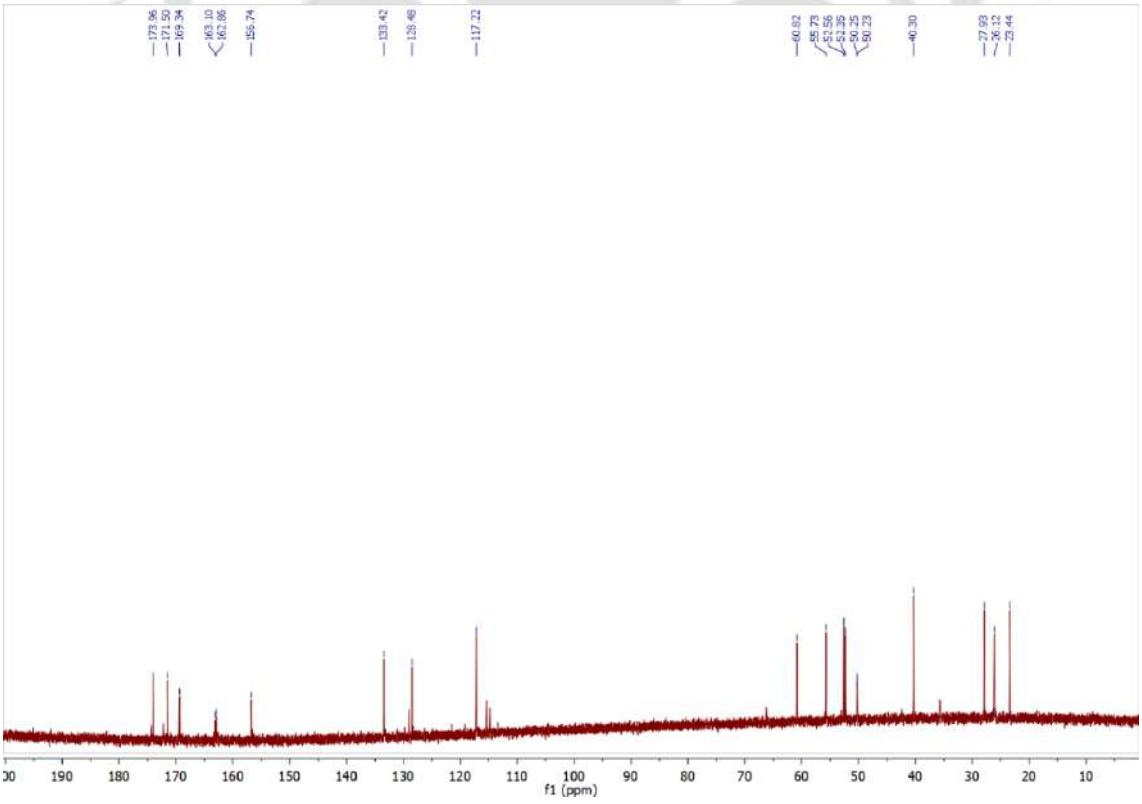

Figure 7.23 ^{13}C NMR spectra of PA **5.1** in D_2O.

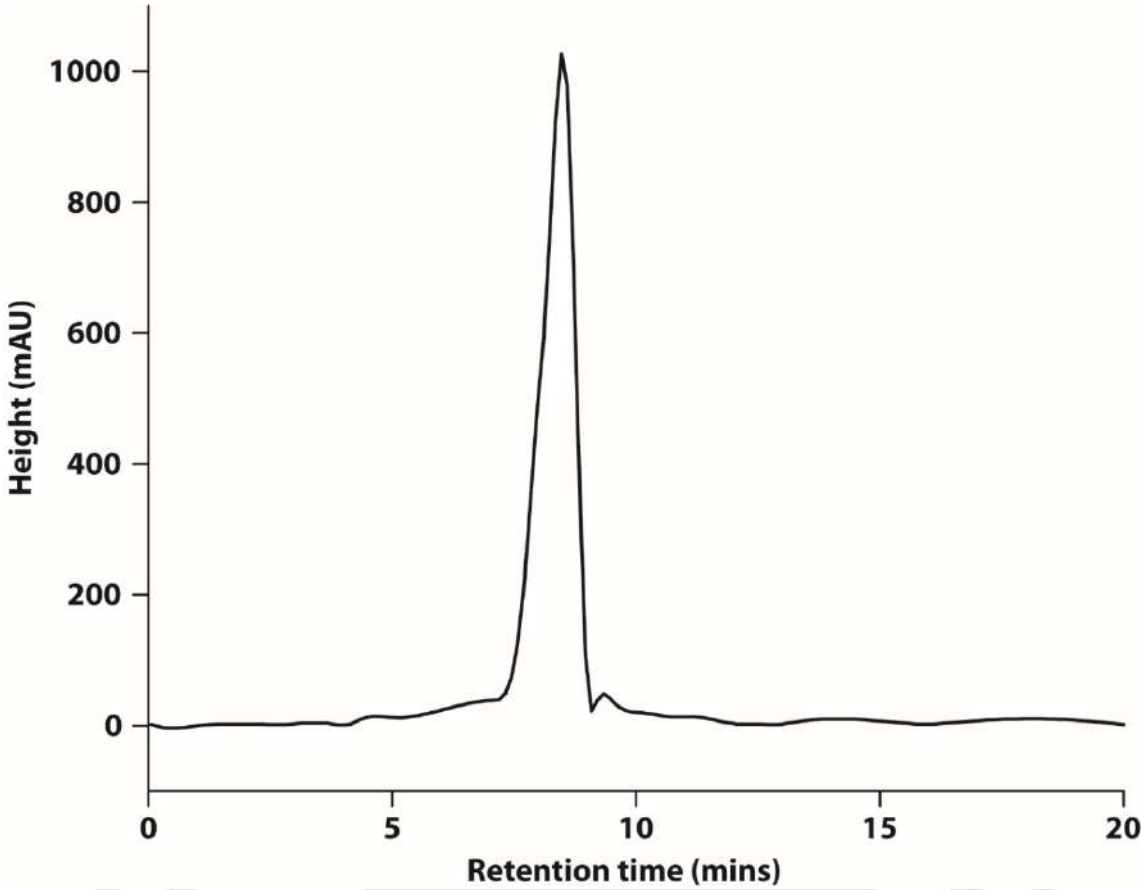

Figure 7.24 Analytical HPLC chromatogram of PA **5.1.**

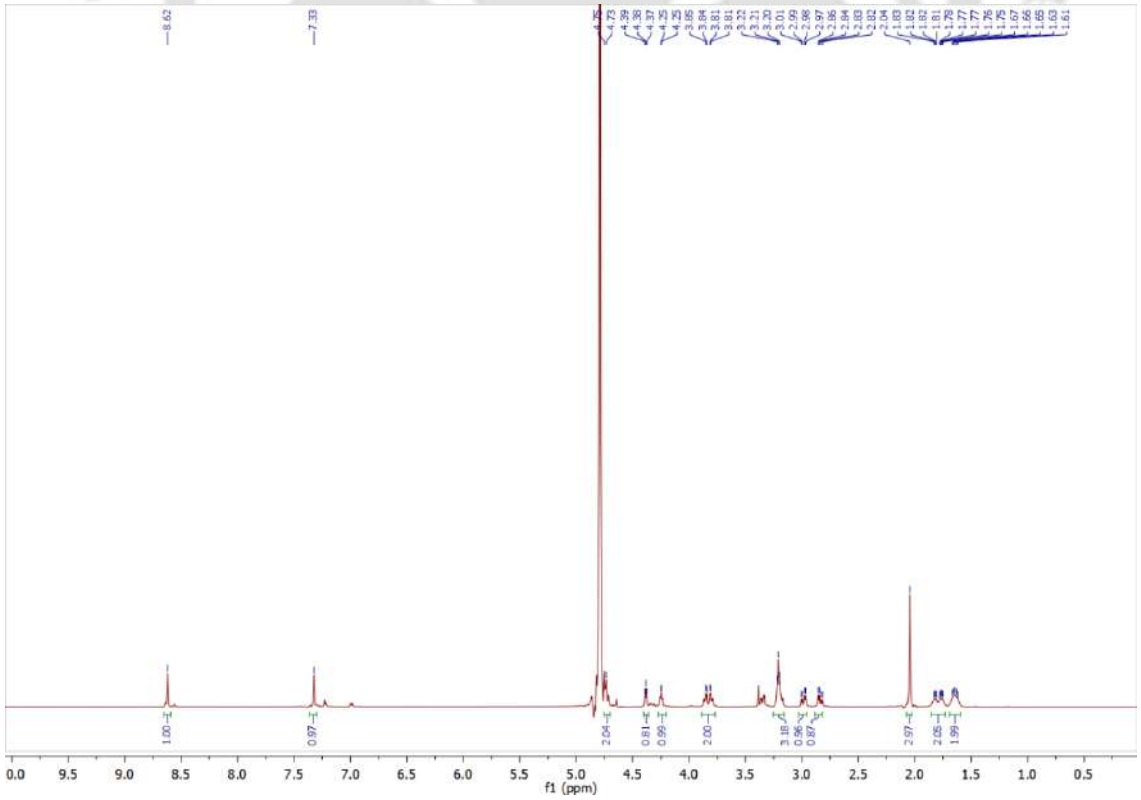

Figure 7.25 ^{1}H NMR spectra of PA **5.2** in D_2O.

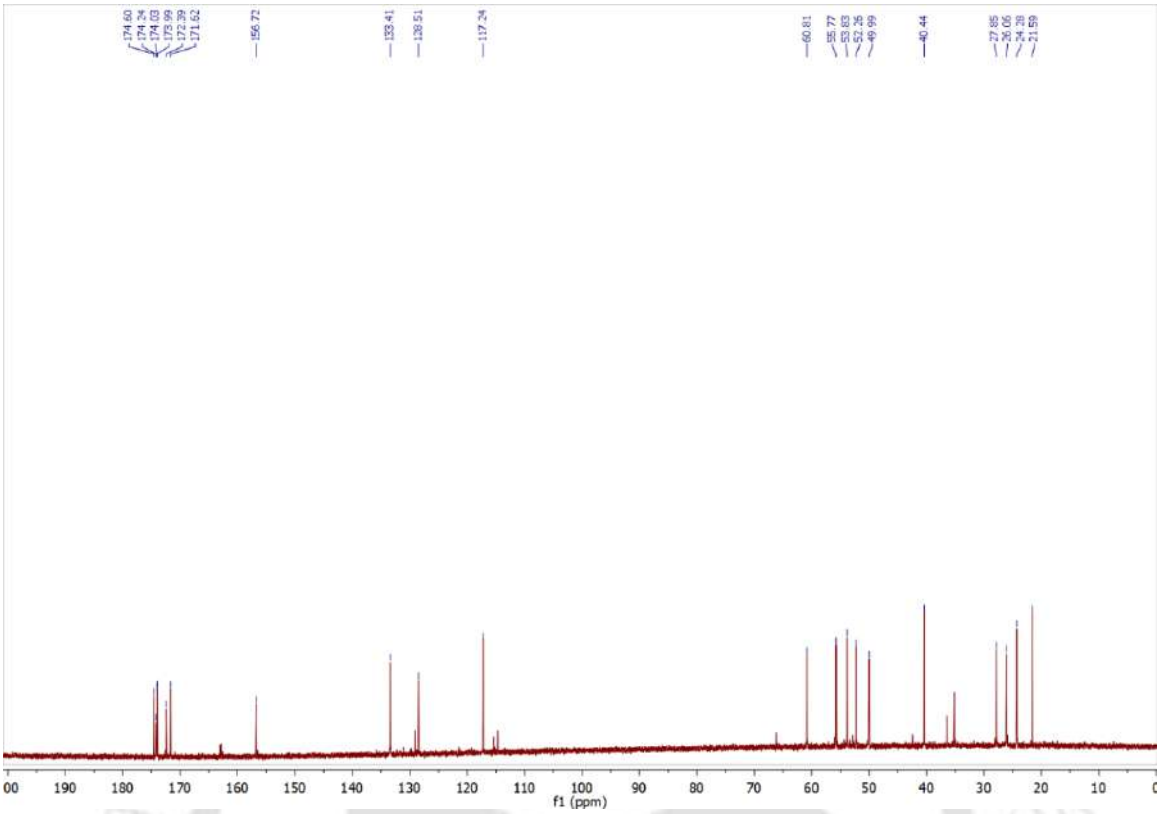

Figure 7.26 ^{13}C NMR spectra of PA **5.2** in D_2O.

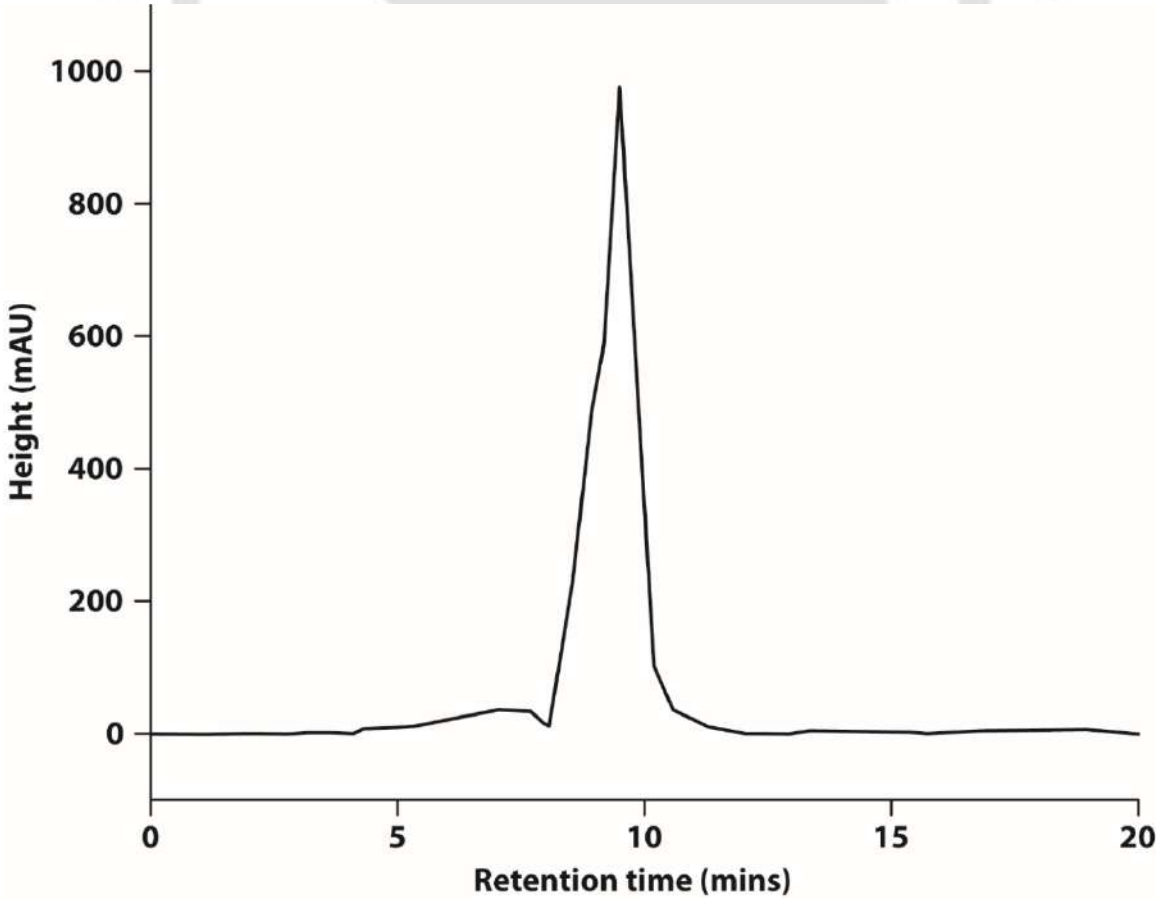

Figure 7.27 Analytical HPLC chromatogram of PA **5.2.**

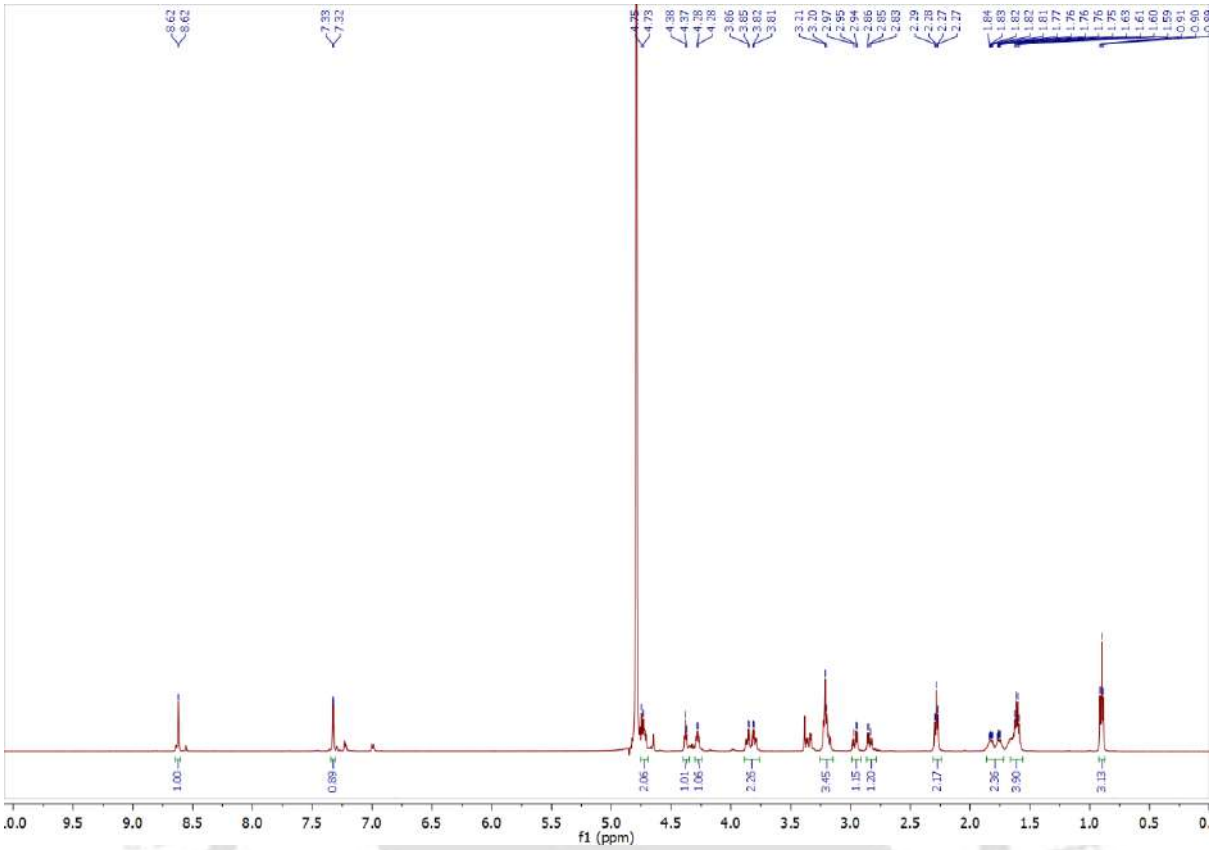

Figure 7.28 ^{1}H NMR spectra of PA **5.3** in D_2O.

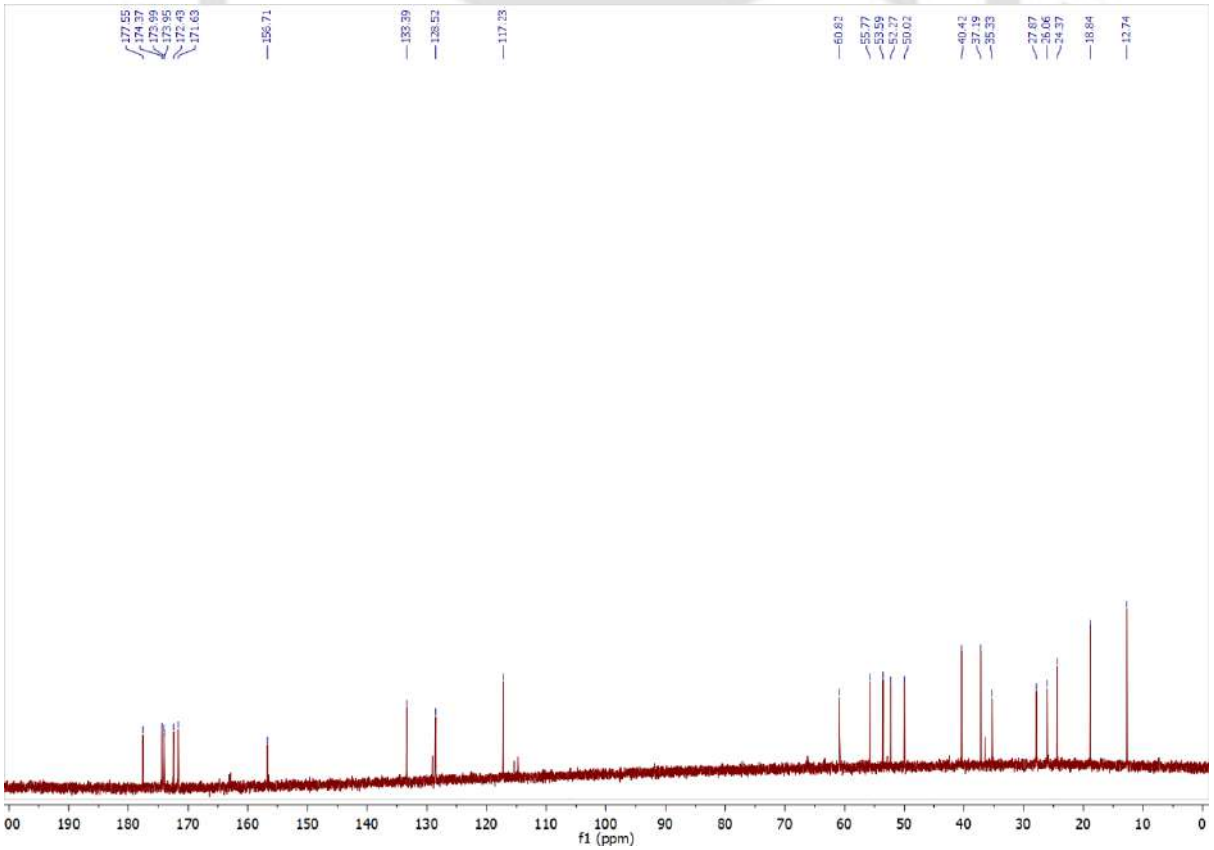

Figure 7.29 ^{13}C NMR spectra of PA **5.3** in D_2O.

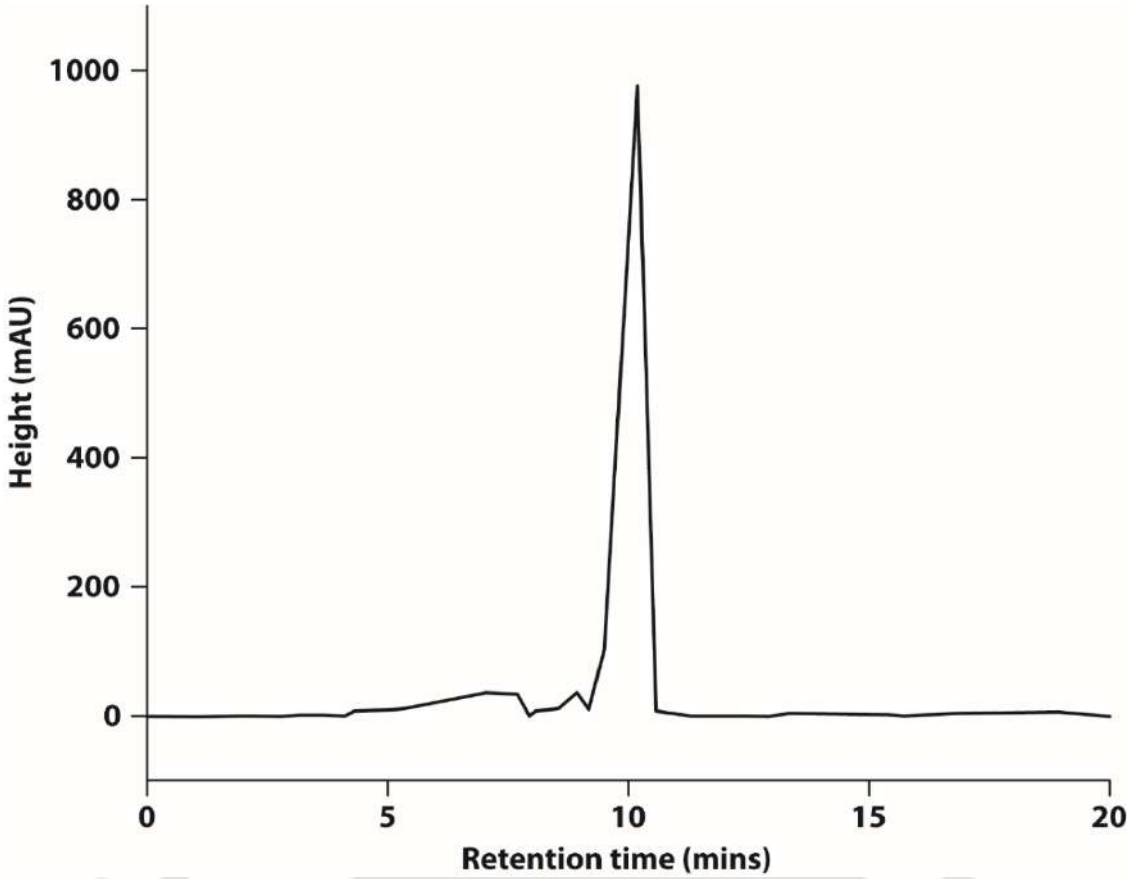

Figure 7.30 Analytical HPLC chromatogram of PA **5.3.**

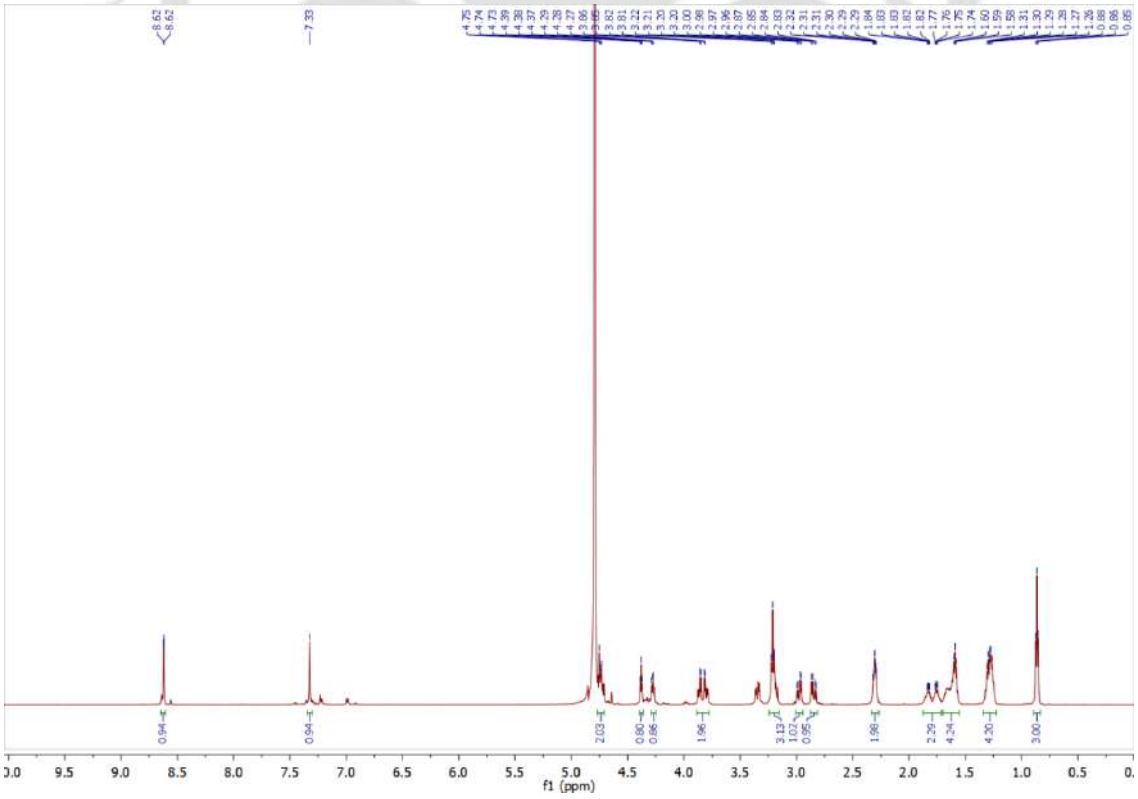

Figure 7.31 ^{1}H NMR spectra of PA **5.4** in D_2O.

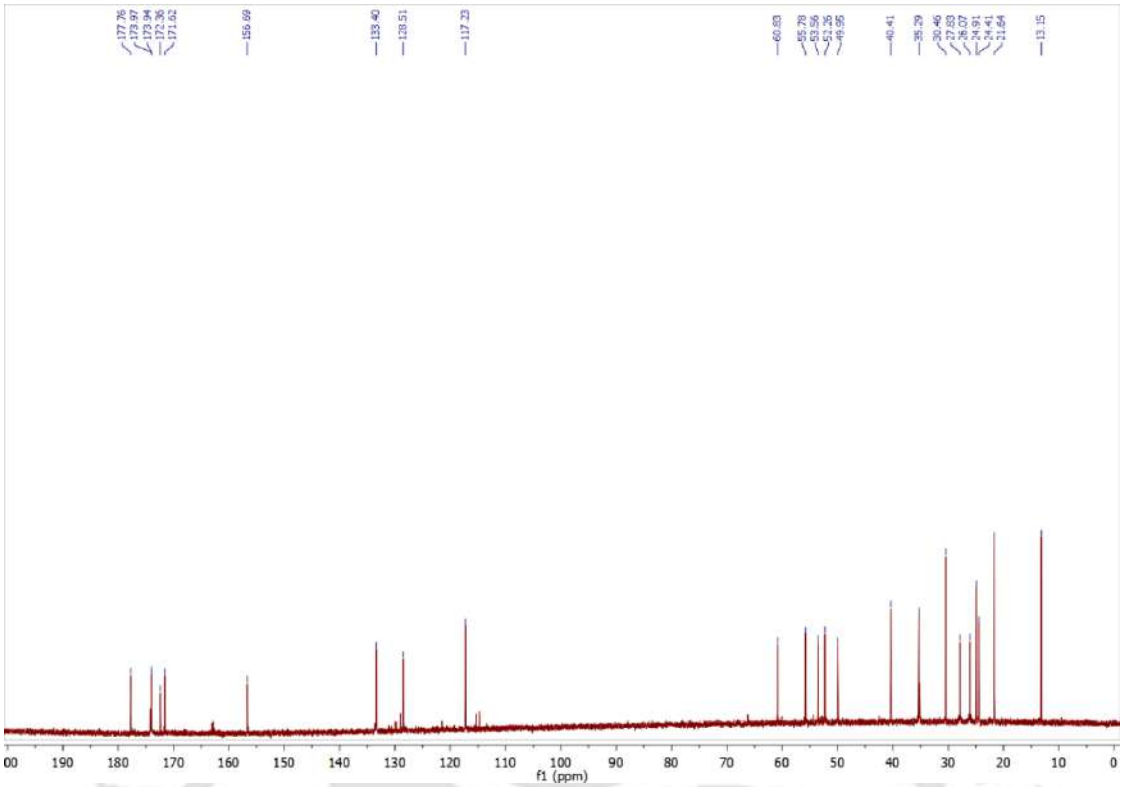

Figure 7.32 ^{13}C NMR spectra of PA **5.4** in D_2O.

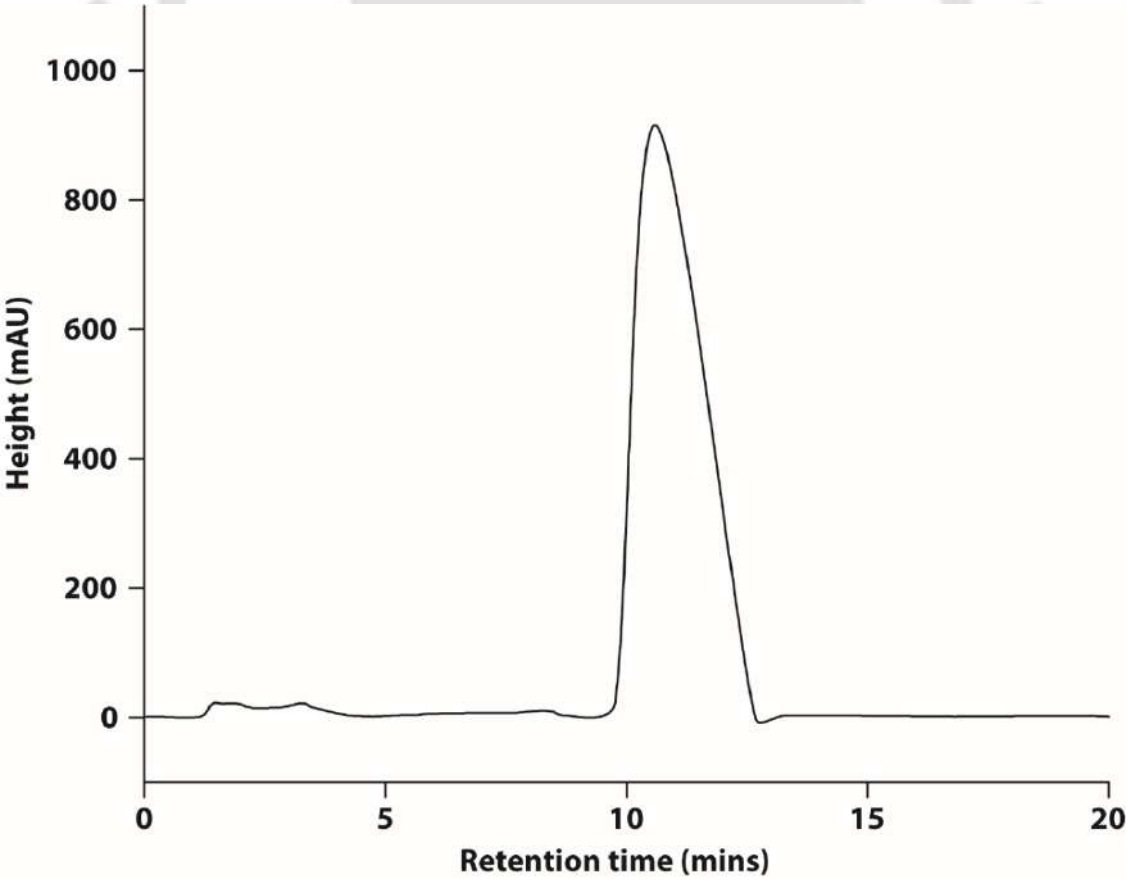

Figure 7.33 Analytical HPLC chromatogram of PA **5.4.**

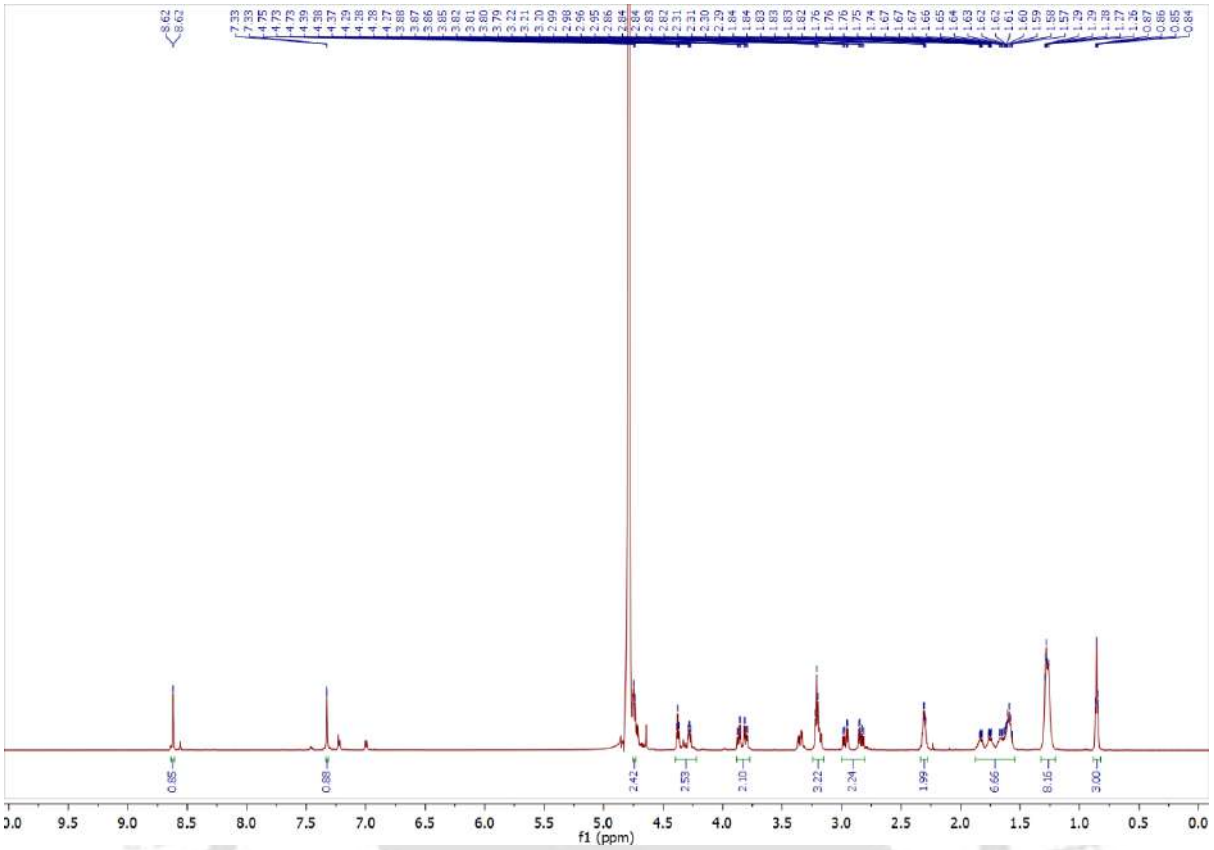

Figure 7.34 ^{1}H NMR spectra of PA **5.5** in D_2O.

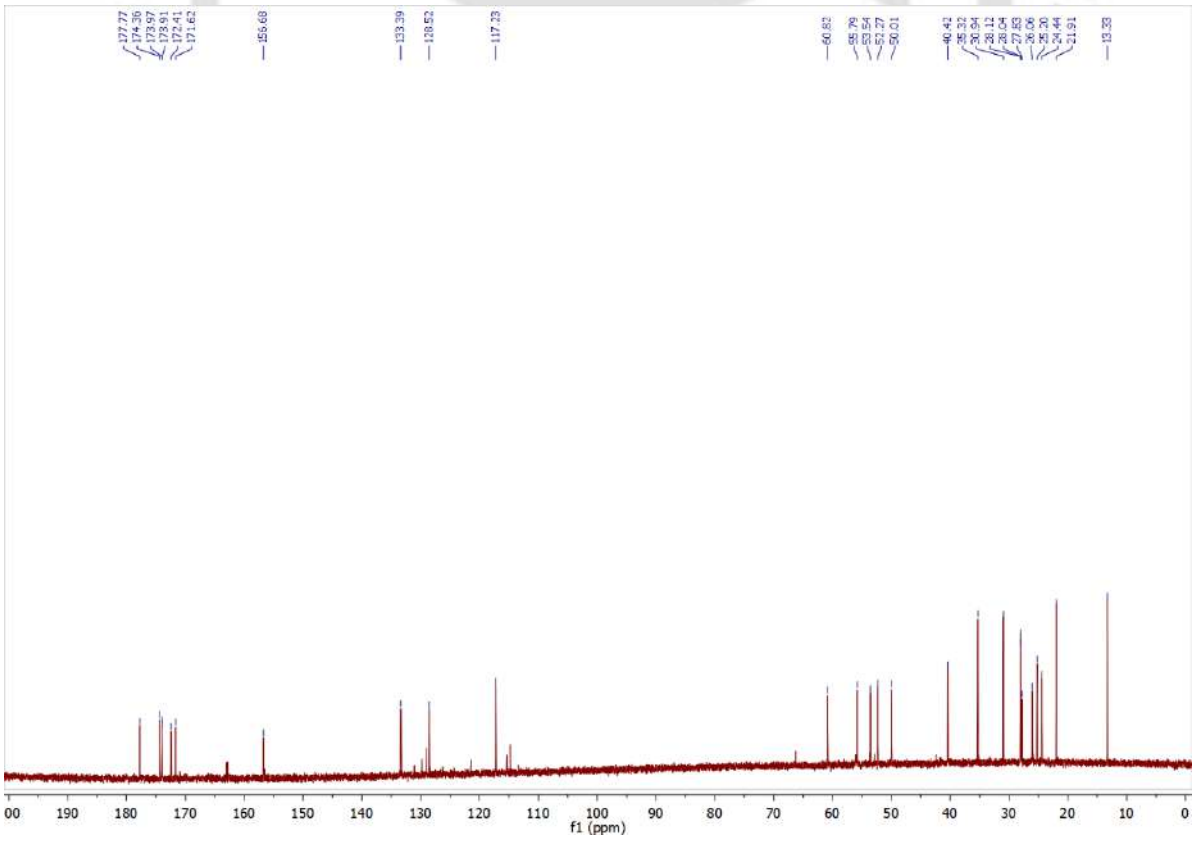

Figure 7.35 ^{13}C NMR spectra of PA **5.5** in D_2O.

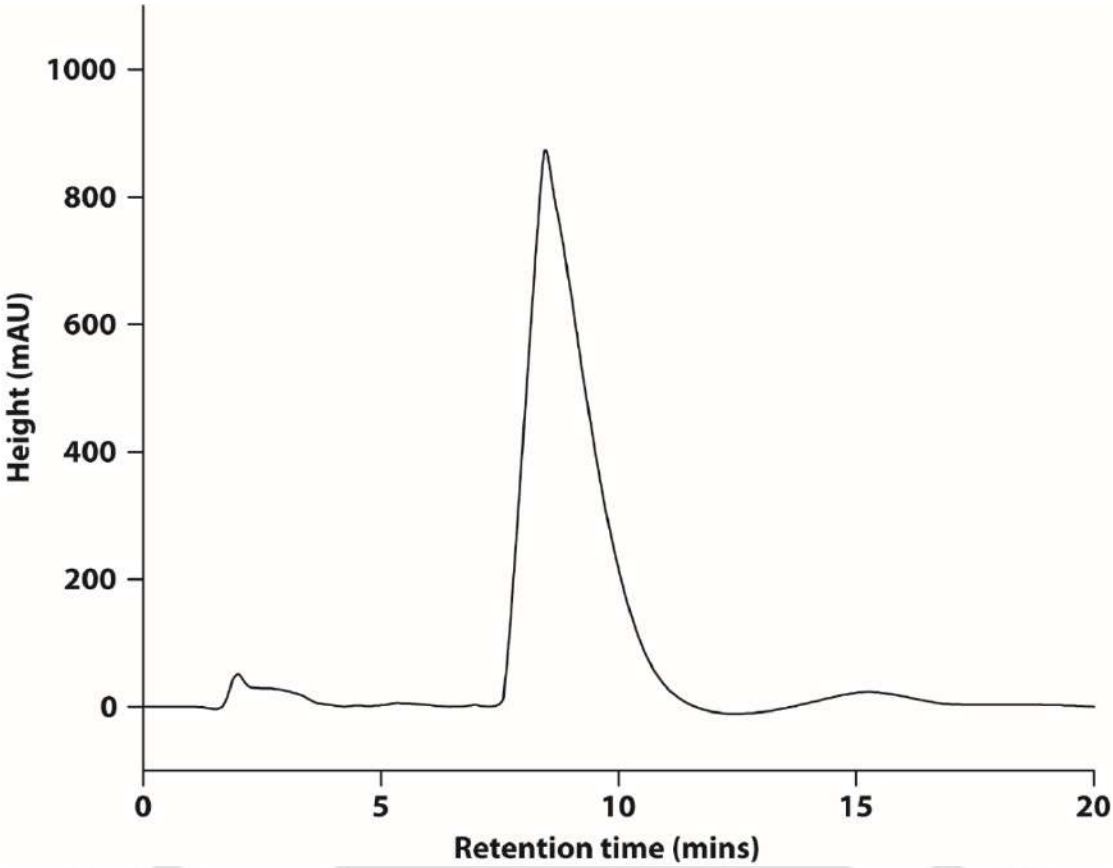

Figure 7.36 Analytical HPLC chromatogram of PA **5.5.**

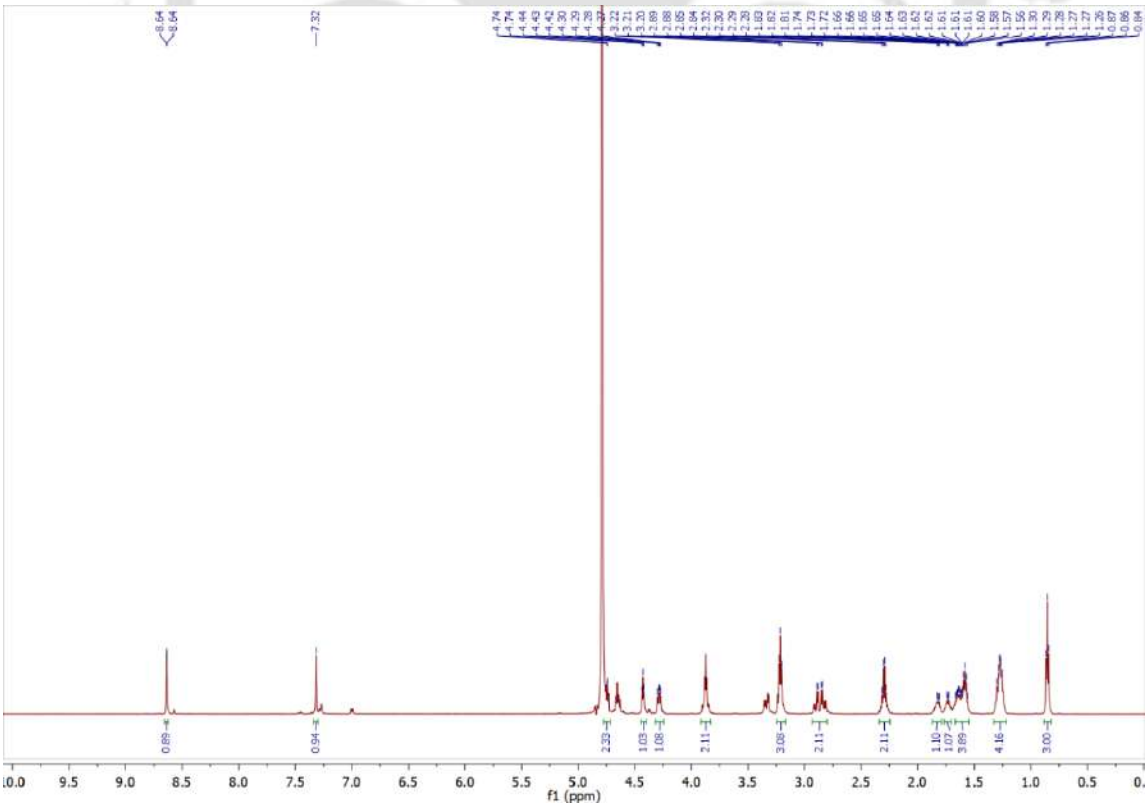

Figure 7.37 ^{1}H NMR spectra of PA **5.7** in D_2O.

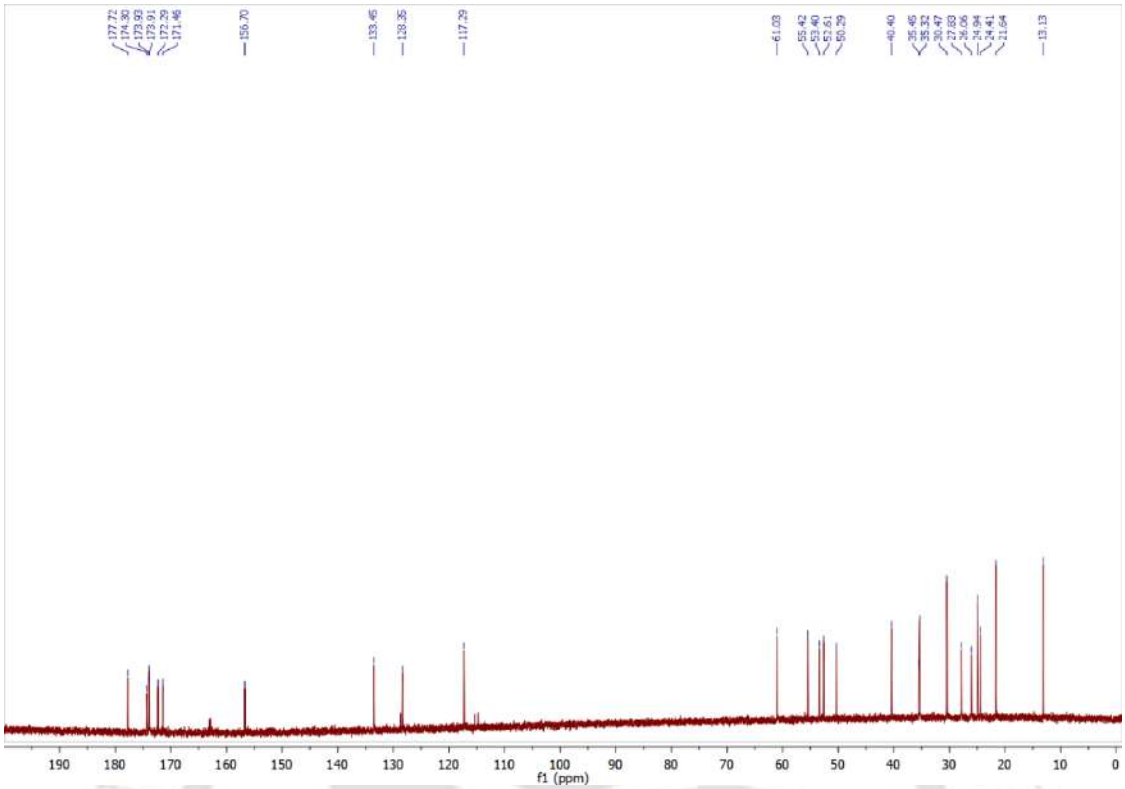

Figure 7.38 ^{13}C NMR spectra of PA **5.7** in D_2O.

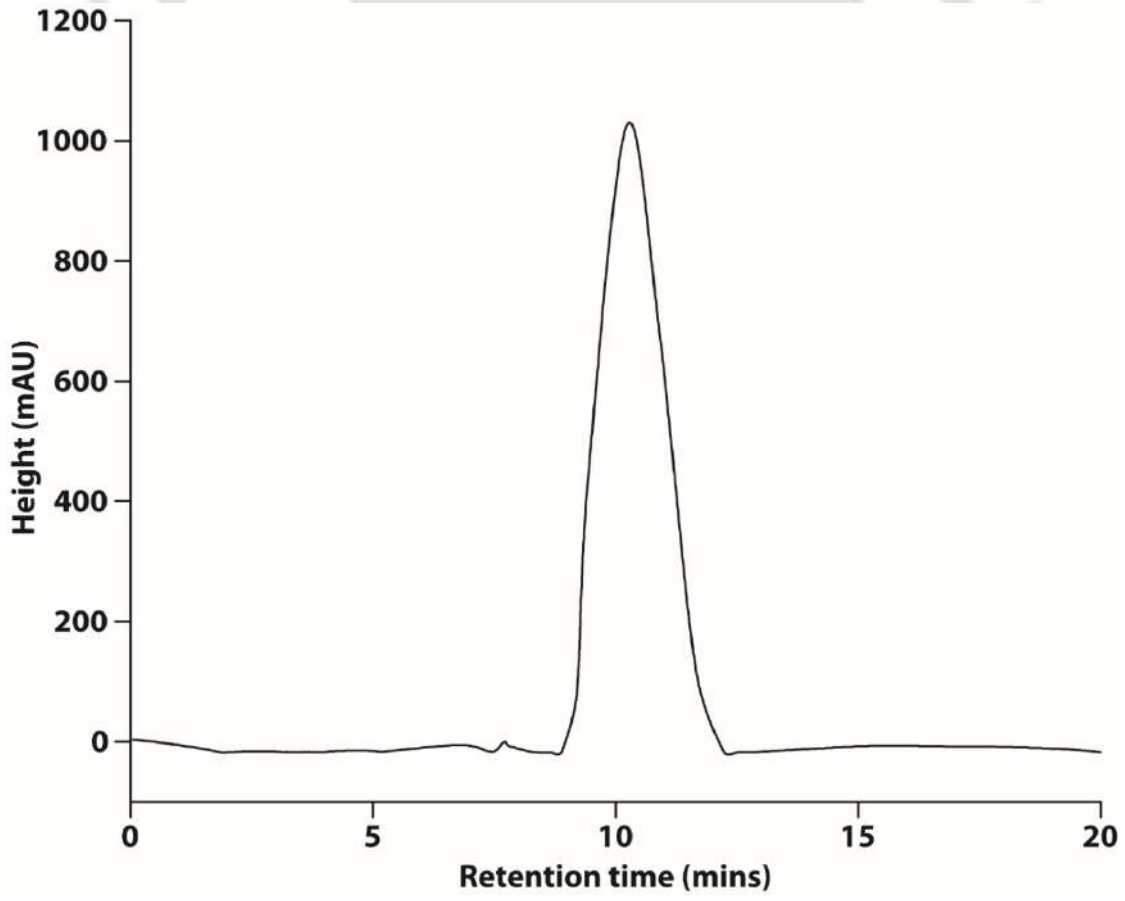

Figure 7.39 Analytical HPLC chromatogram of PA **5.7.**

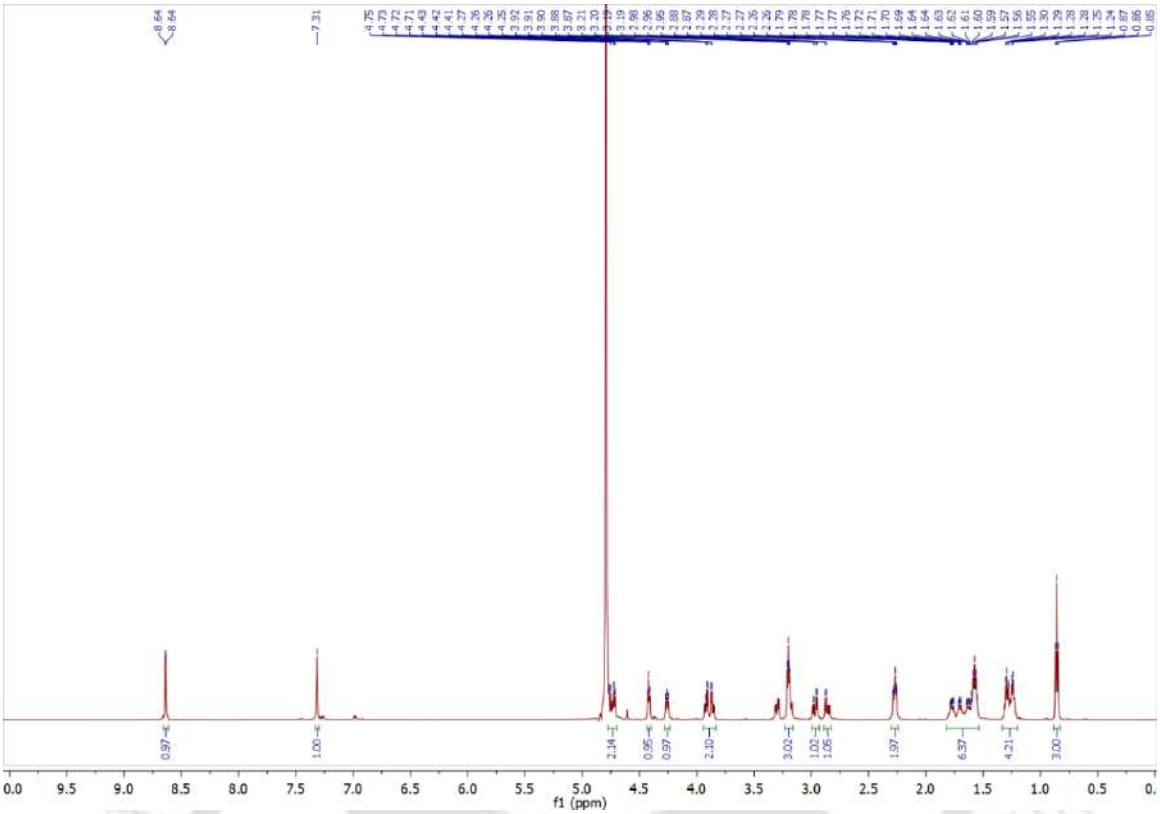

Figure 7.40 ^{1}H NMR spectra of PA **5.8** in D_2O.

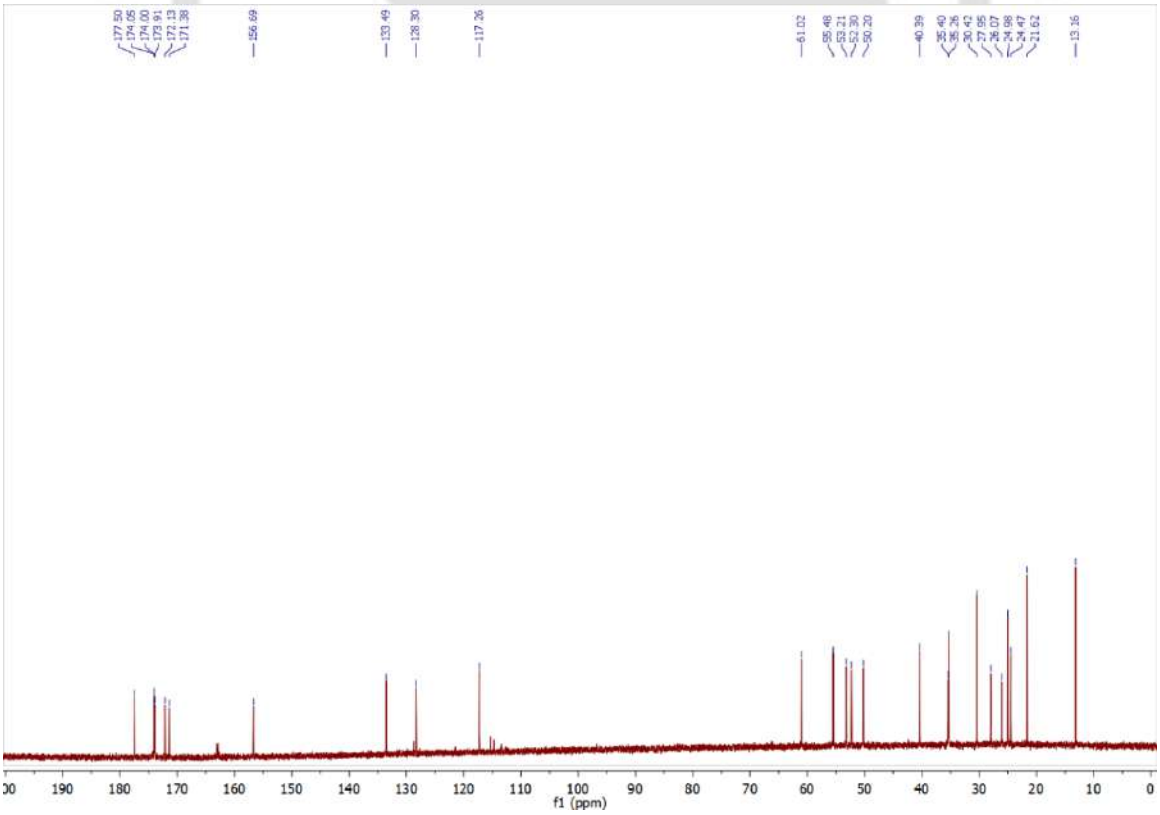

Figure 7.41 ^{13}C NMR spectra of PA **5.8** in D_2O.

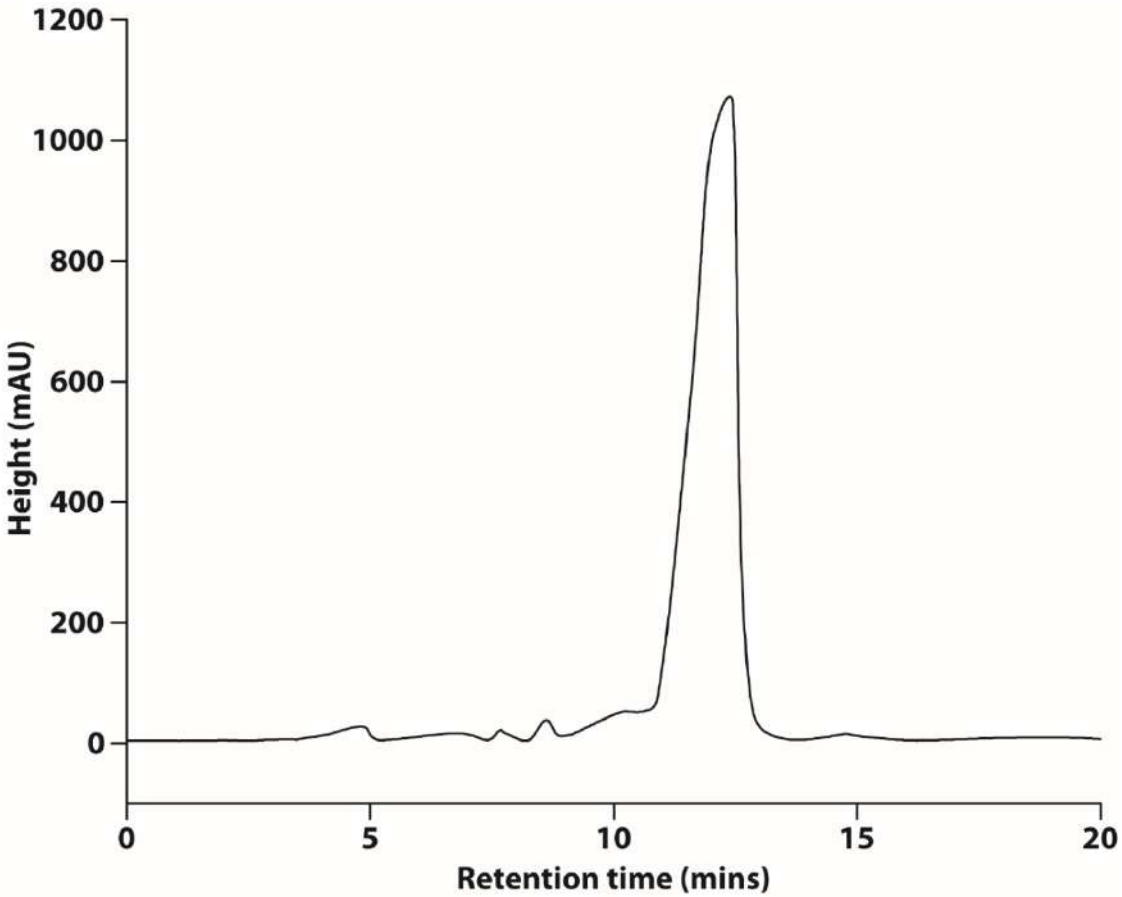

Figure 7.42 Analytical HPLC chromatogram of PA **5.8.**

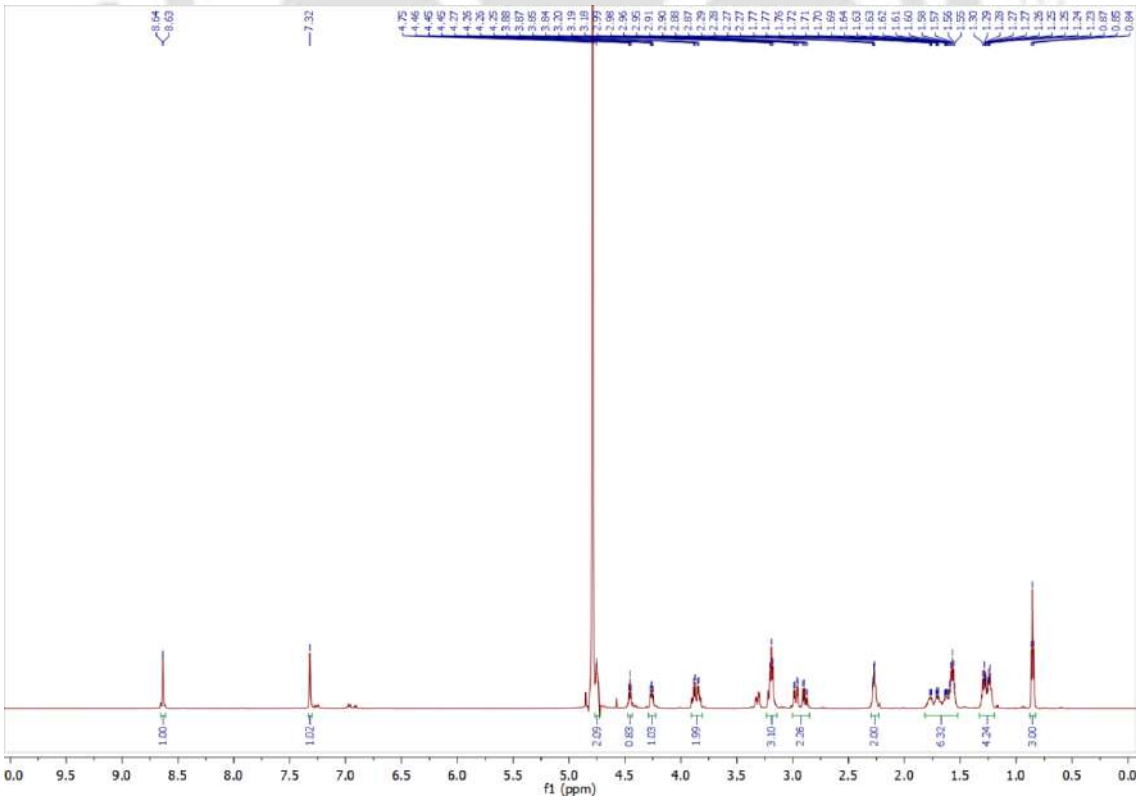

Figure 7.43 ^{1}H NMR spectra of PA **5.9** in D_2O.

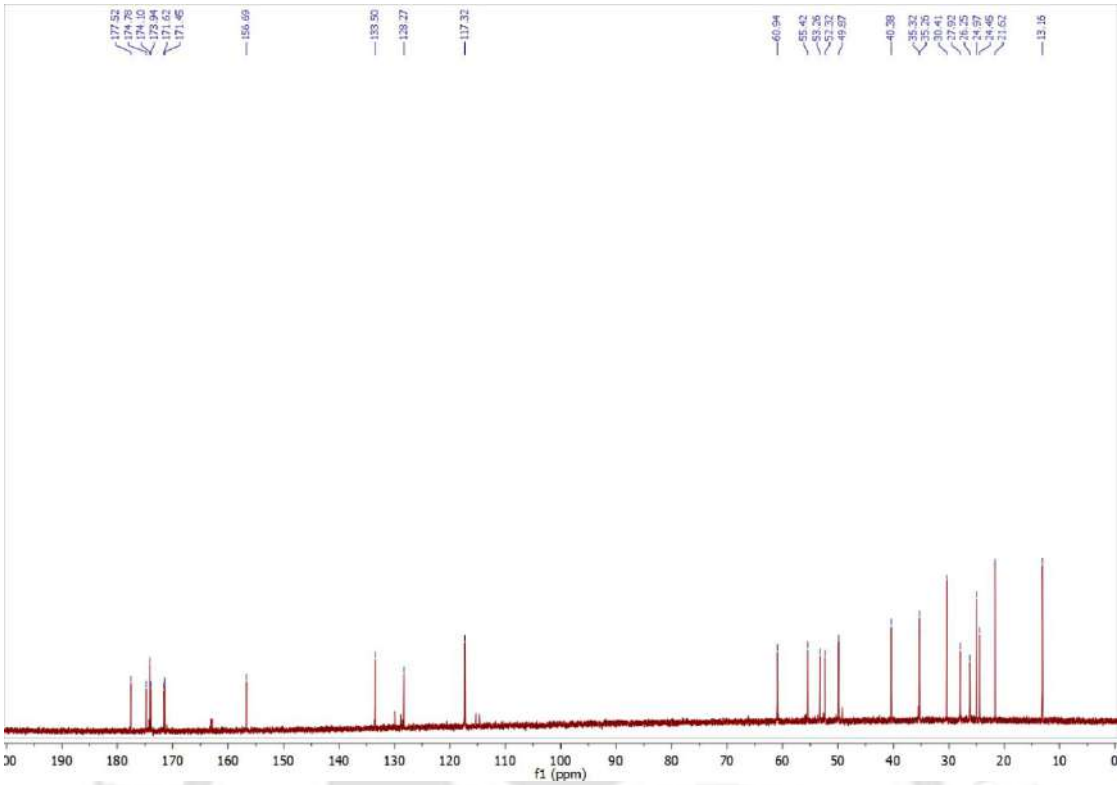

Figure 7.44 ^{13}C NMR spectra of PA **5.9** in D_2O.

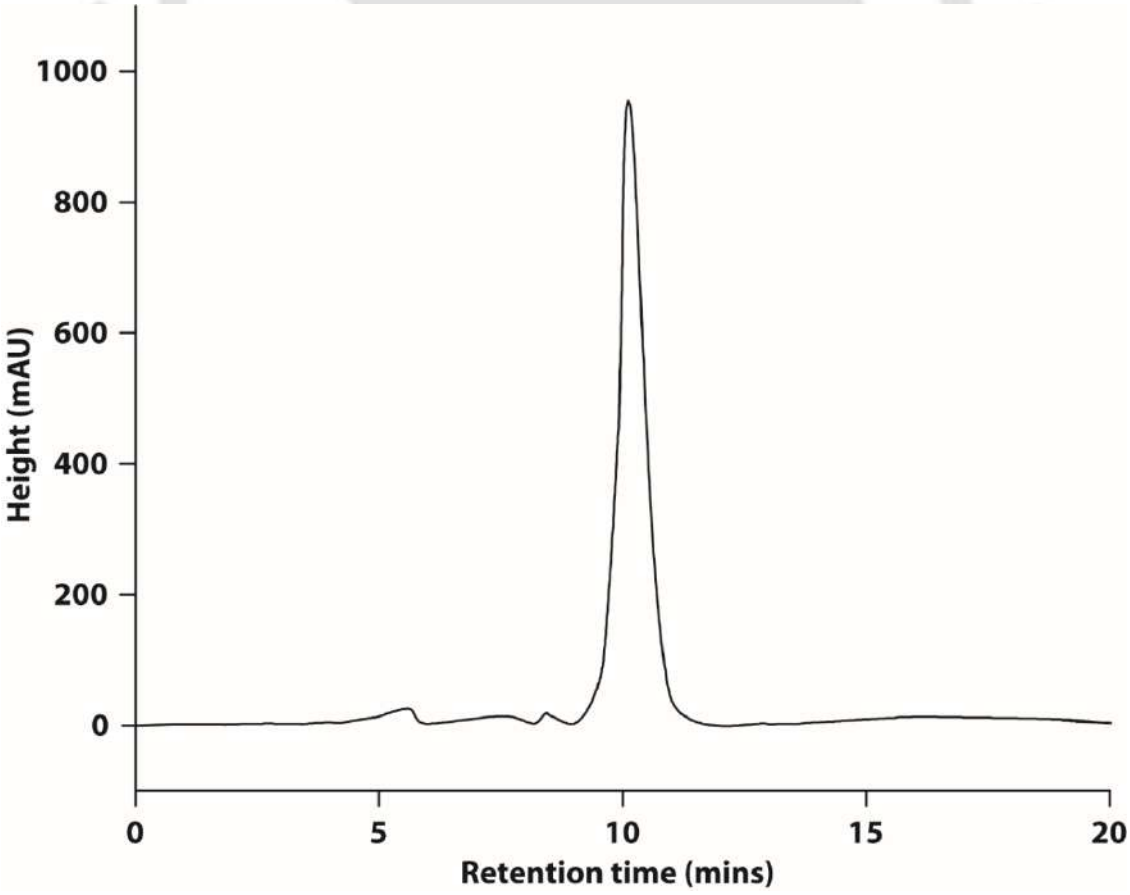

Figure 7.45 Analytical HPLC chromatogram of PA **5.9.**

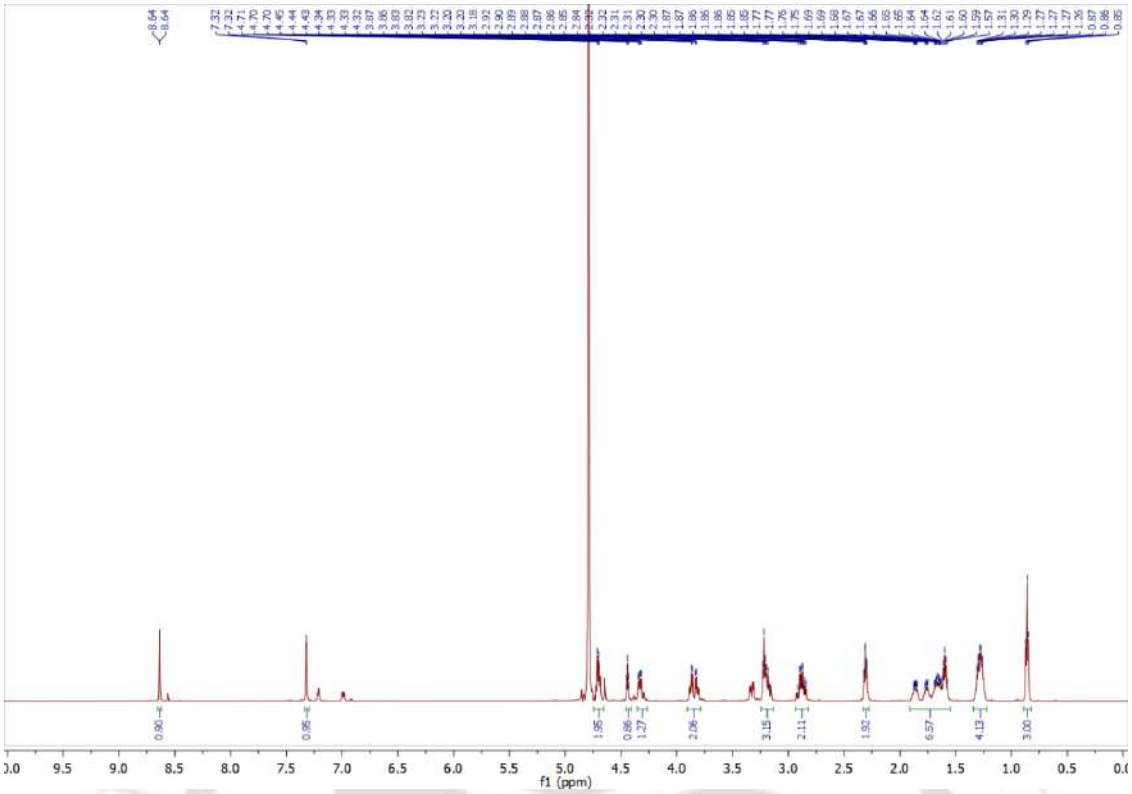

Figure 7.46 ^{1}H NMR spectra of PA **5.10** in D_2O.

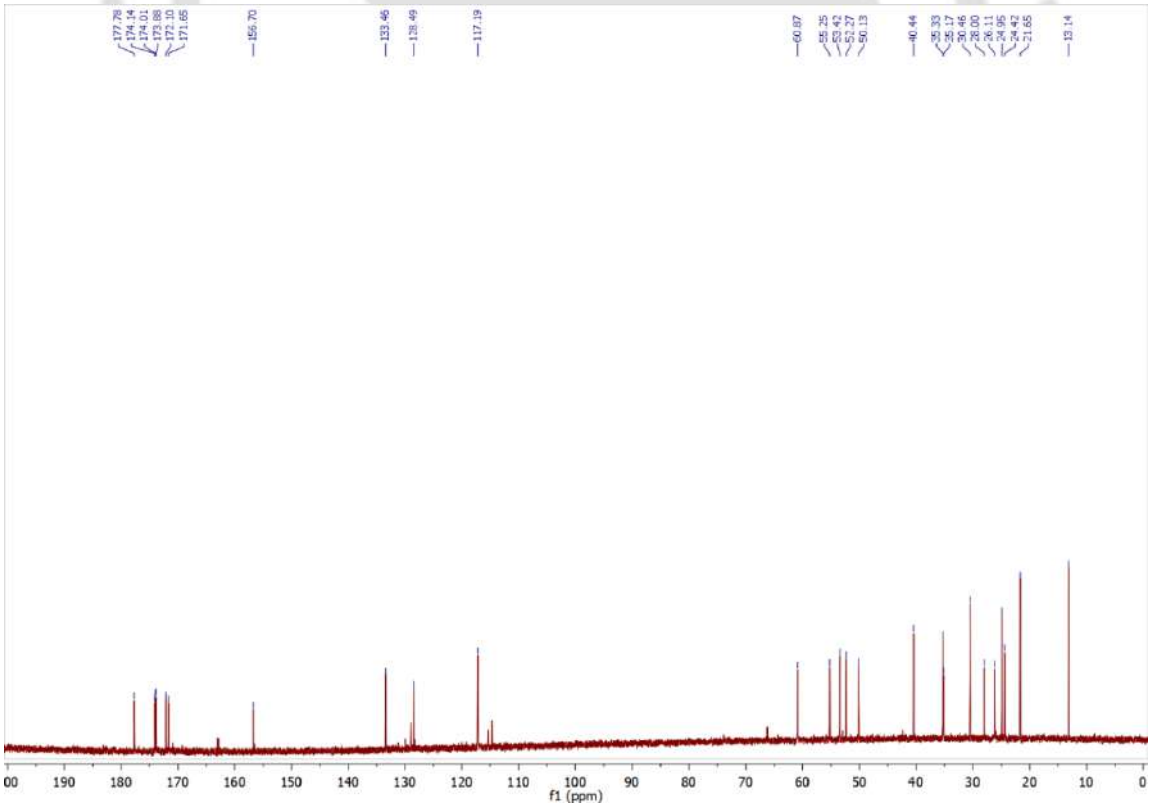

Figure 7.47 ^{13}C NMR spectra of PA **5.10** in D_2O.

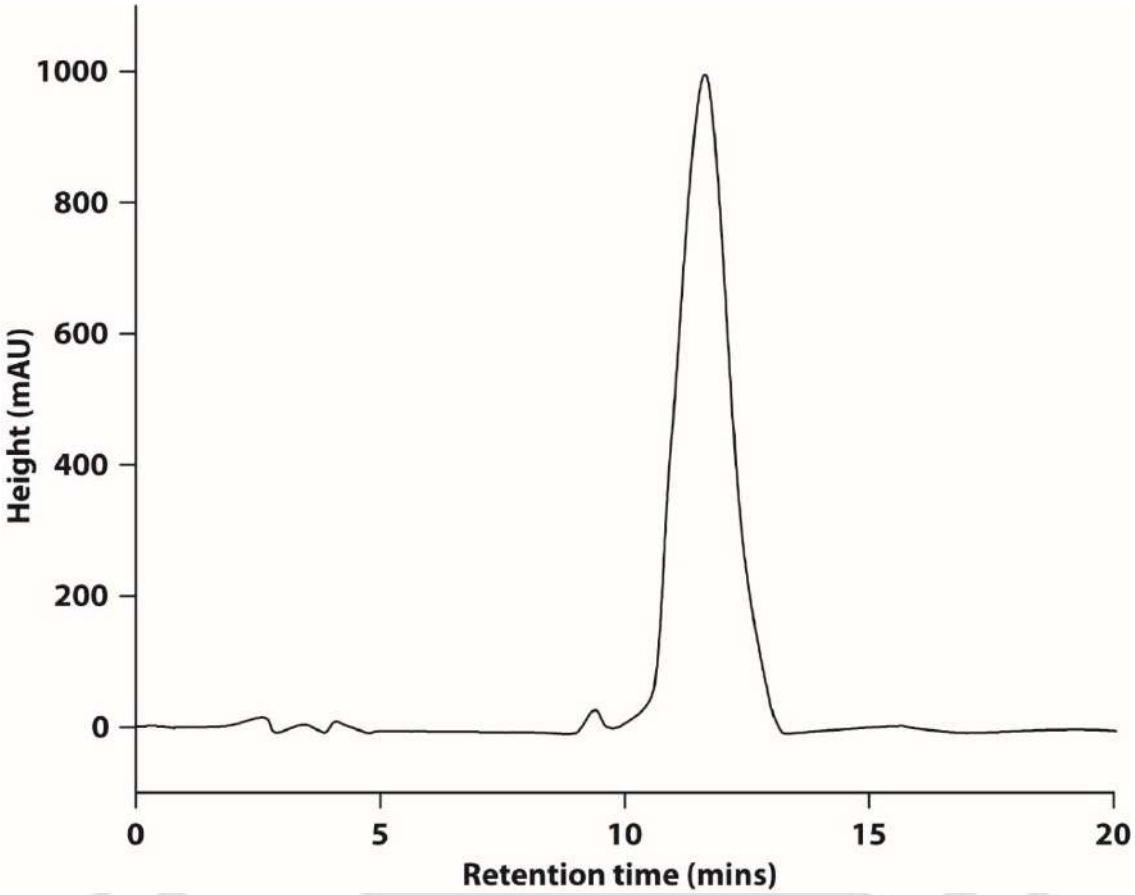

Figure 7.48 Analytical HPLC chromatogram of PA **5.10.**

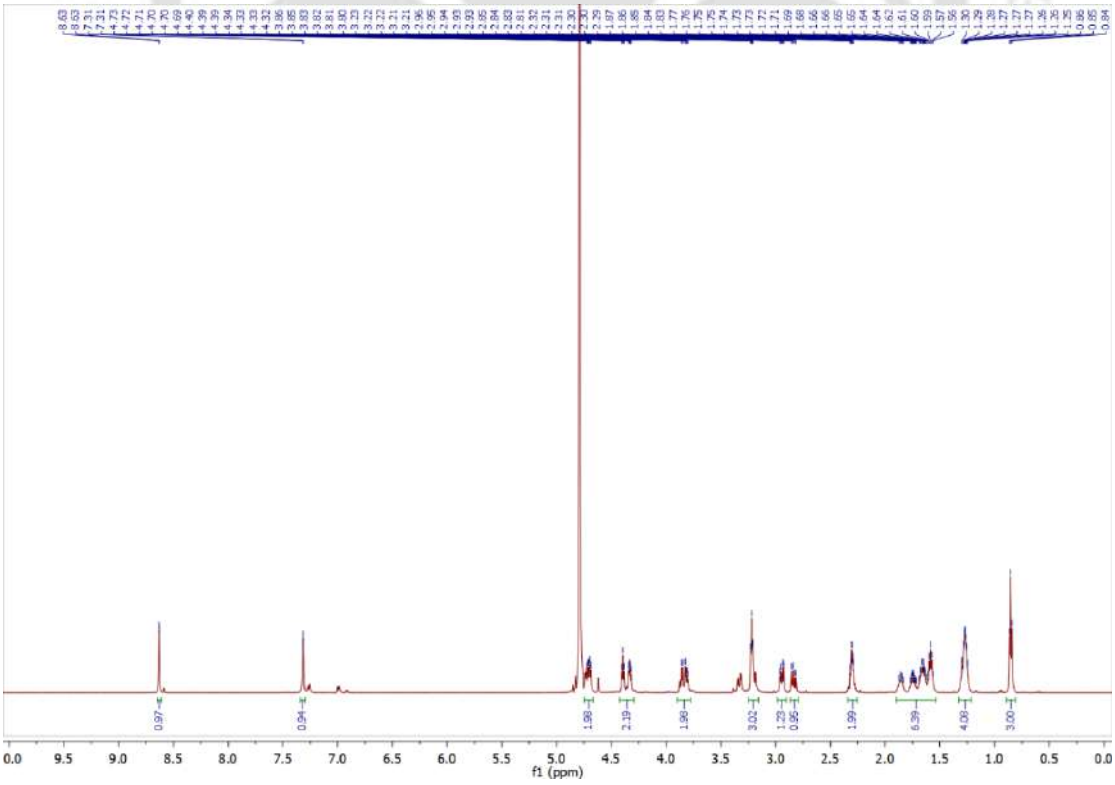

Figure 7.49 ^{1}H NMR spectra of PA **5.11** in D_2O.

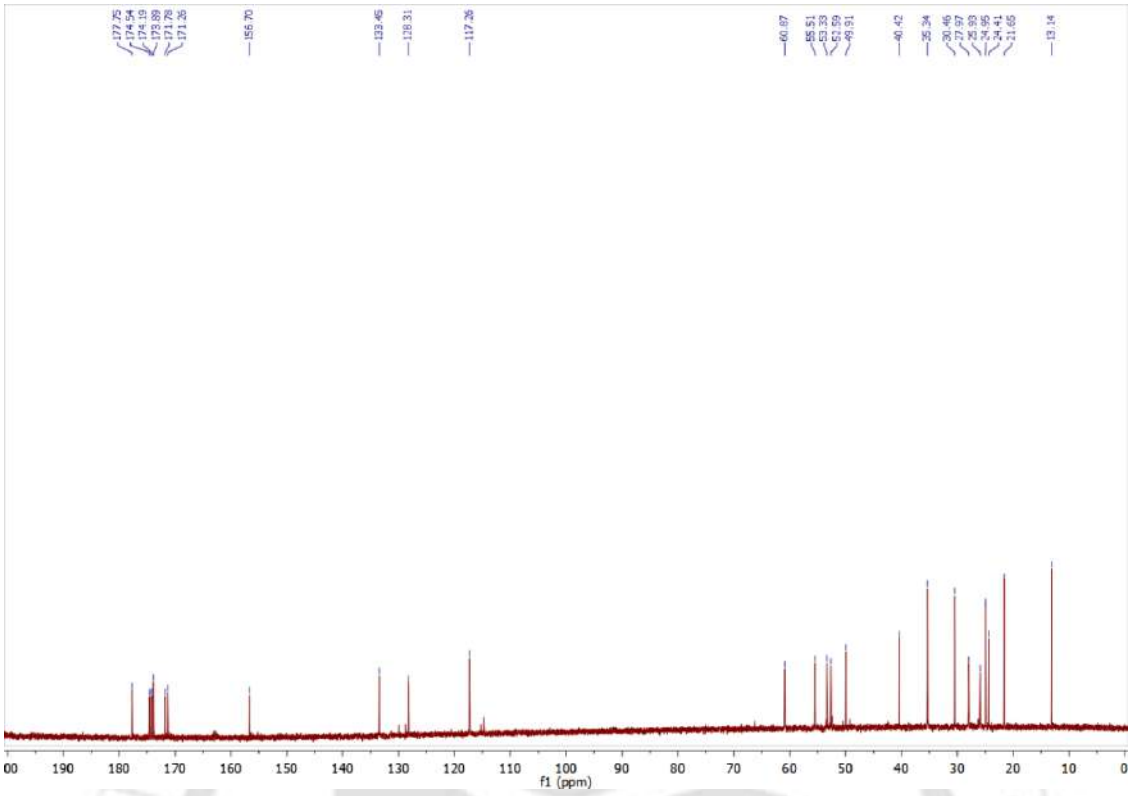

Figure 7.50 ^{13}C NMR spectra of PA **5.11** in D_2O.

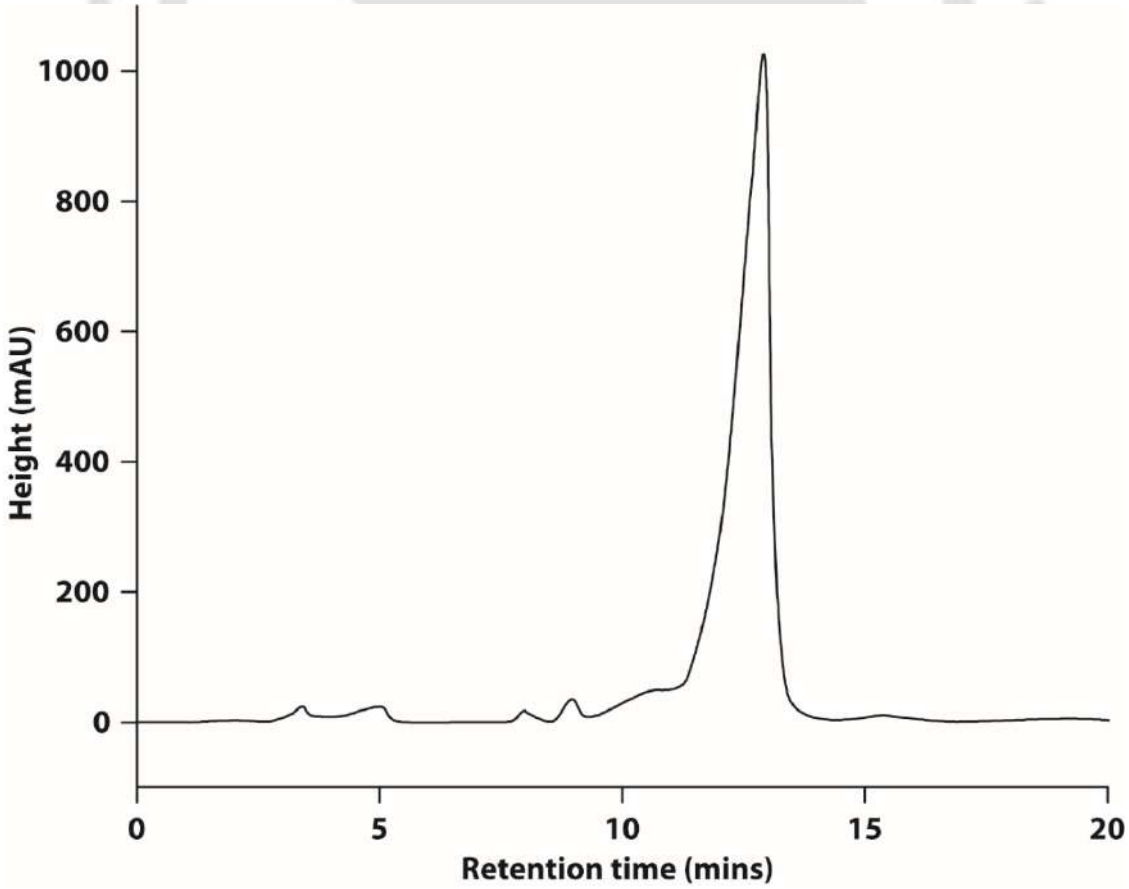

Figure 7.51 Analytical HPLC chromatogram of PA **5.11.**

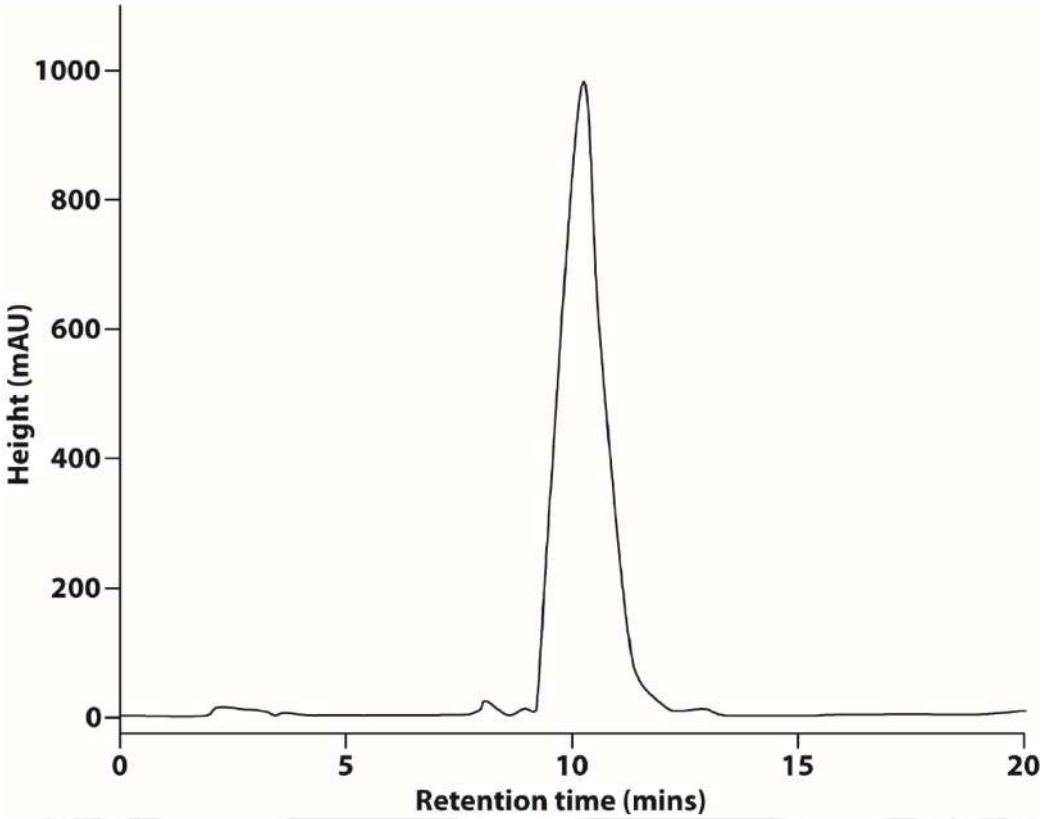

Figure 7.52 Analytical HPLC chromatogram of PA **5.12.**

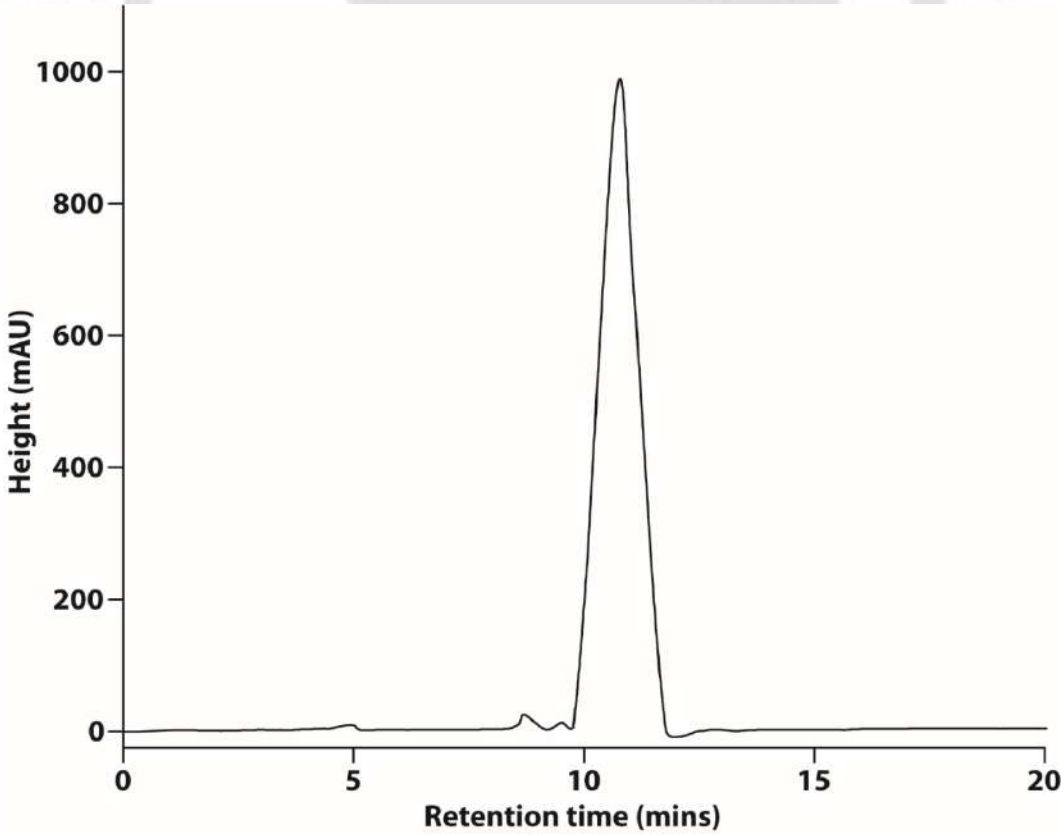

Figure 7.53 Analytical HPLC chromatogram of PA **5.13.**

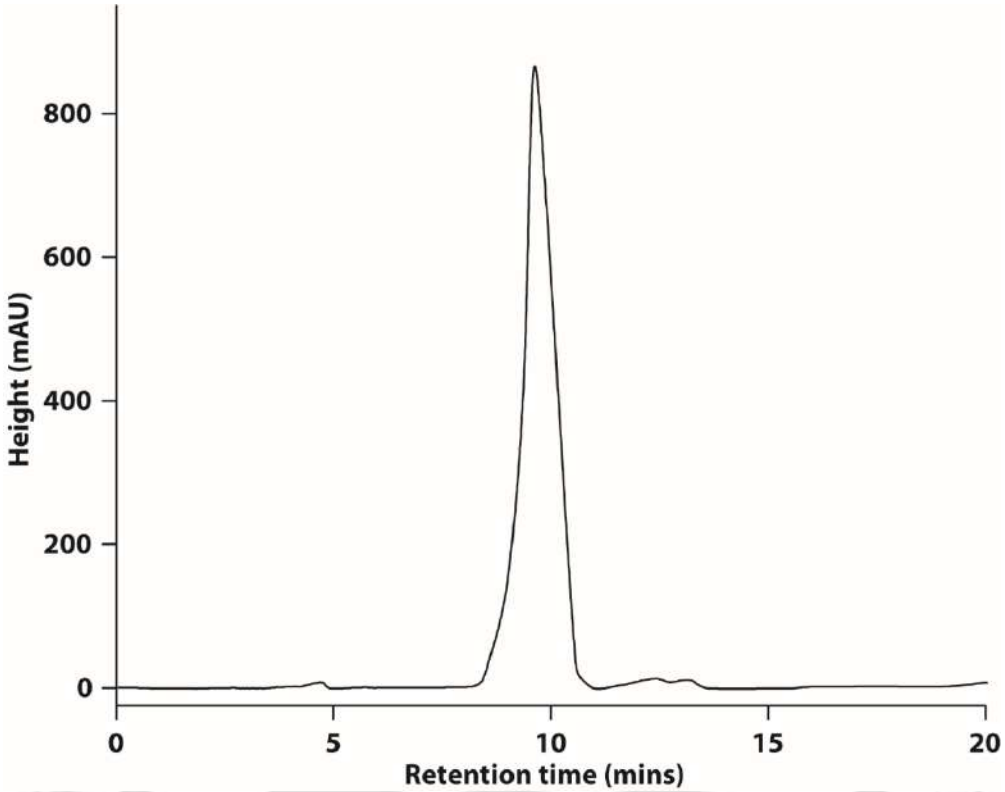

Figure 7.54 Analytical HPLC chromatogram of PA **5.14.**

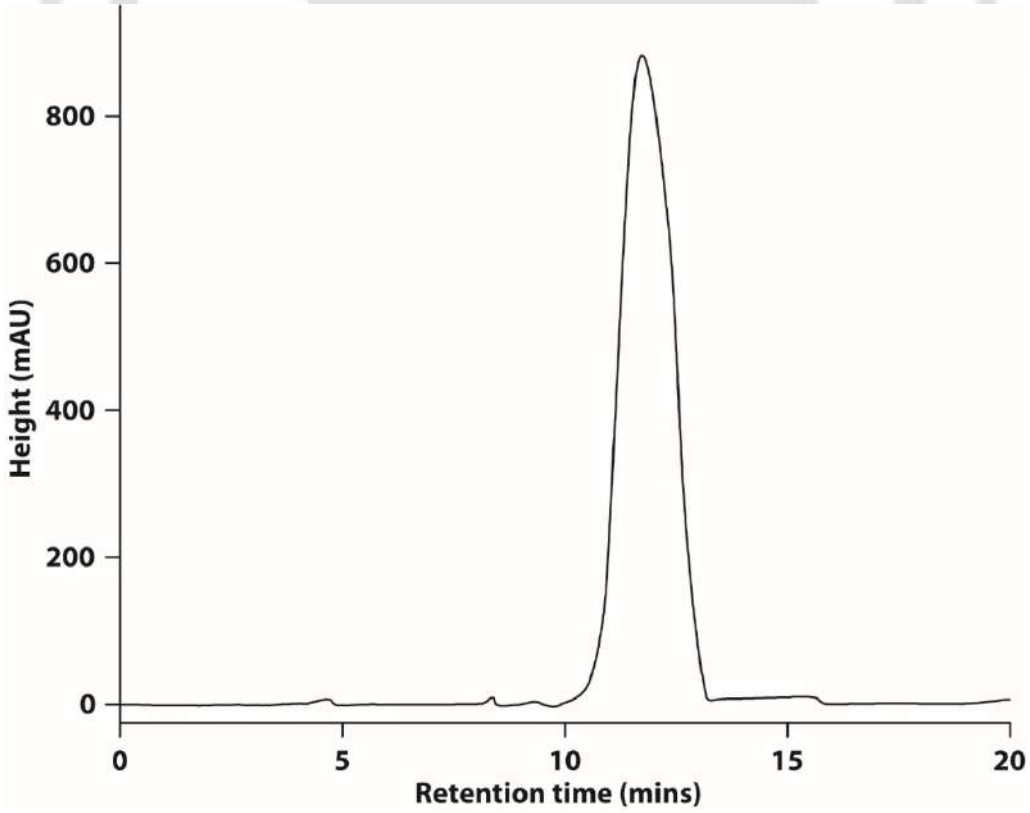

Figure 7.55 Analytical HPLC chromatogram of PA **5.15.**

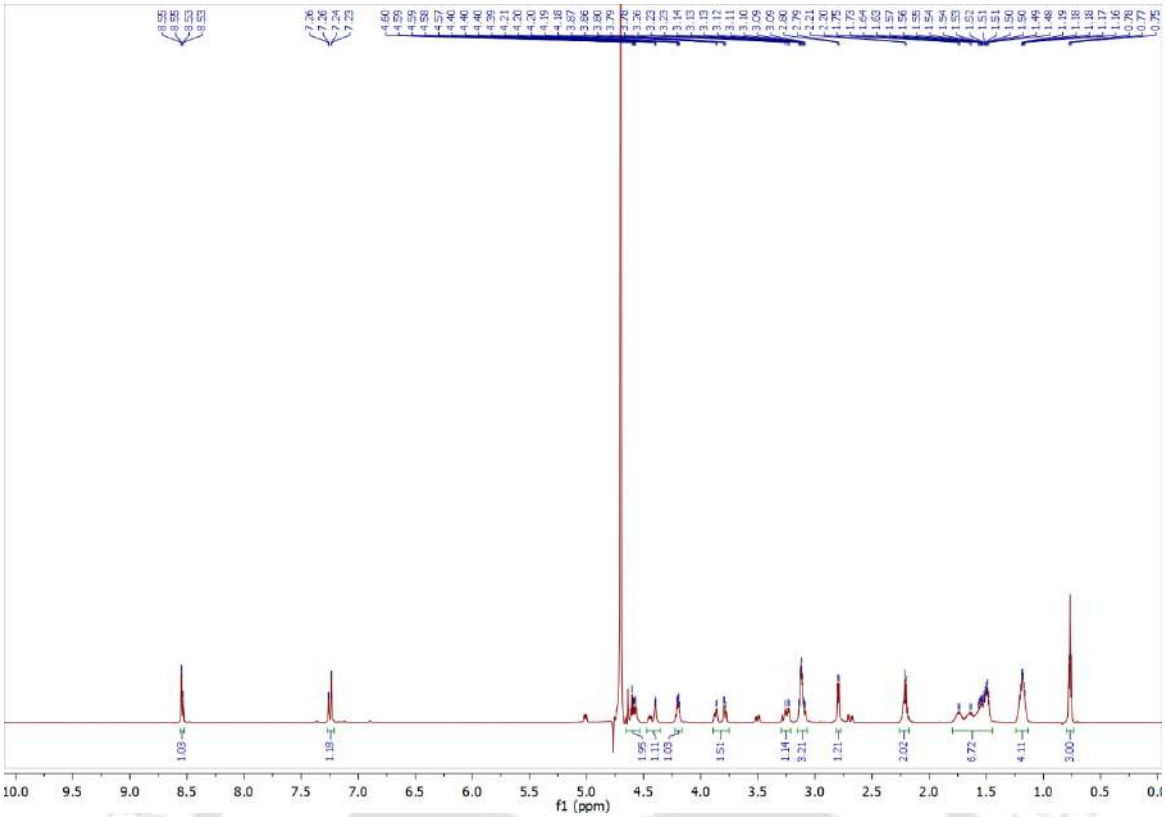

Figure 7.56 ^{1}H NMR spectra of PA **5.16** in D_2O.

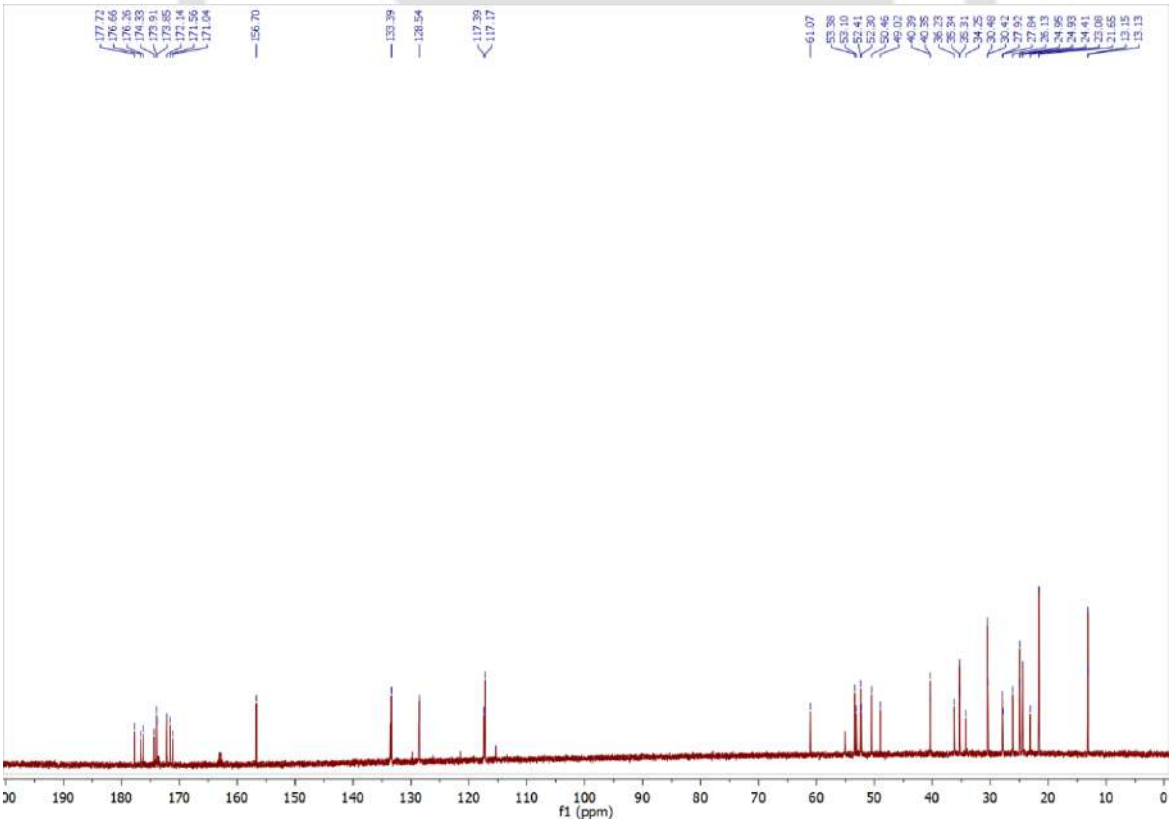

Figure 7.57 ^{13}C NMR spectra of PA **5.16** in D_2O.

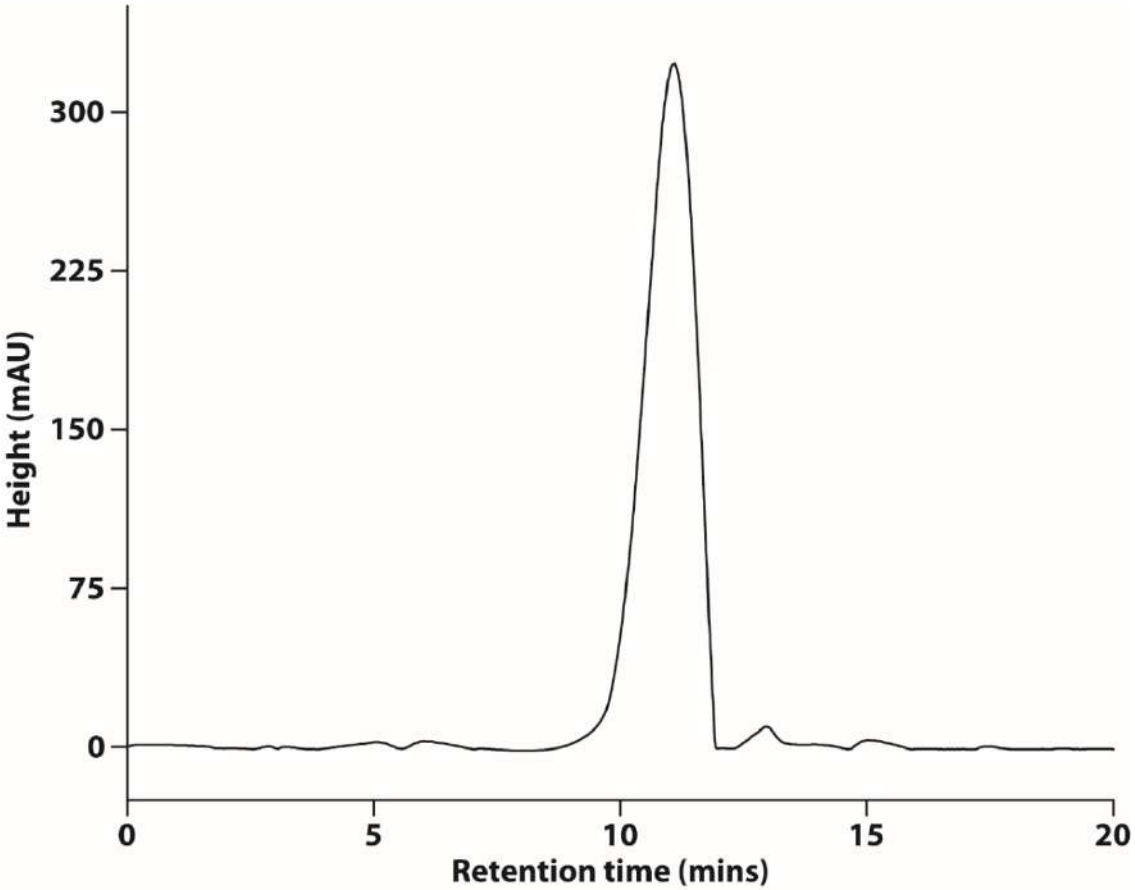

Figure 7.58 Analytical HPLC chromatogram of PA **5.16.**